Stress Corrosion Cracking of Duplex Stainless Steels in Caustic Solutions

A Dissertation
Submitted to
The Academic Faculty

By

Ananya Bhattacharya

In Partial Fulfillment
of the Requirements for the Degree
Doctor of Philosophy in Materials Science and Engineering

Georgia Institute of Technology
Atlanta, GA

December 2008

Stress Corrosion Cracking of Duplex Stainless Steels in Caustic Solutions

Approved by:

Dr. Preet M Singh, Advisor
School of Materials Science and Engineering
Georgia Institute of Technology

Dr. Arun M. Gokhale
School of Materials Science and Engineering
Georgia Institute of Technology

Dr. Thomas H. Sanders, Jr.
School of Materials Science and Engineering
Georgia Institute of Technology

Dr. Richard Neu
School of Materials Science and Engineering and Mechanical Engineering
Georgia Institute of Technology

Dr. W. Brent Carter
School of Materials Science and Engineering
Georgia Institute of Technology

Date approved: October 31, 2008

TO

SHRI SIDDHI VINAYAK

ACKNOWLEDGEMENT

Learning is a journey. And the last four years of my doctoral studies and research work at Georgia Tech have been the most enjoyable one. It is difficult to overstate my gratitude to my Ph.D. advisor, Dr. Preet M. Singh, for his advice and support throughout my research. His constant enthusiasm, inspiration, and great efforts to explain things clearly and simply during the early parts of my graduate studies helped me understand the true values of research and set me on the right path to a smooth and easy journey to graduation. I would like to thank him for being such a great advisor. I would also like to thank my committee members Dr. Thomas H. Sanders, Dr. W. Brent Carter, Dr. Arun M. Gokhale and Dr. Richard Neu for their valuable input and guidance to improve this study.

I greatly appreciate and wish to thank Mr.Jamshad Mahmood for always being there to help me in the laboratory. I would further like to thank my corrosion group members for their support throughout the work.

This research was funded by the PSE Foundation Fellowship Program at Institute of Paper Science and Technology at Georgia Tech and State of Georgia-TIP3 Program.

Lastly, I am indebted to my husband, Dr. Soumendu Bhattacharya, my parents, Mr. Asit K. Haldar and Bharati Haldar and my brother, Dr. Sounick Haldar for their love, support and understanding throughout my work and would like to dedicate my thesis to them.

Table of Contents

List of Tables

List of Figures

CHAPTER 1

CHAPTER 3

CHAPTER 4

CHAPTER 5

CHAPTER 6

CHAPTER 7

SUMMARY

Duplex stainless steels (DSS) with roughly equal amount of austenite and ferrite phases are being used in industries such as petrochemical, nuclear, pulp and paper mills, de-salination plants, marine environments, and others. However, many DSS grades have been reported to undergo corrosion and stress corrosion cracking in some aggressive environments such as chlorides and sulfide-containing caustic solutions. Although stress corrosion c

racking of duplex stainless steels in chloride solution has been investigated and well documented in the literature but the SCC mechanisms for DSS in caustic solutions were not known. Microstructural changes during fabrication processes affect the overall SCC susceptibility of these steels in caustic solutions. Other environmental factors, like pH of the solution, temperature, and resulting electrochemical potential also influence the SCC susceptibility of duplex stainless steels.

In this study, the role of material and environmental parameters on corrosion and stress corrosion cracking of duplex stainless steels in caustic solutions were investigated. Changes in the DSS microstructure by different annealing and aging treatments were characterized in terms of changes in the ratio of austenite and ferrite phases, phase morphology and intermetallic precipitation using optical micrography, SEM, EDS, XRD, nano-indentation and microhardness methods. These samples were then tested for general and localized corrosion susceptibility and SCC to understand the underlying mechanisms of crack initiation and propagation in DSS in the above-mentioned environments.

Results showed that the austenite phase in the DSS is more susceptible to crack initiation and propagation in caustic solutions, which is different from that in the low pH chloride environment where the ferrite phase is the more susceptible phase. This study also showed that microstructural

changes in duplex stainless steels due to different heat treatments could affect their SCC susceptibility. Annealed and water quenched specimens were found to be immune to SCC in caustic environment. Aging treatment at 800°C gave rise to sigma and chi precipitates in the DSS. However, these sigma and chi precipitates, known to initiate cracking in DSS in chloride environment did not cause any cracking of DSS in caustic solutions. Aging of DSS at 475°C had resulted in '475°C embrittlement' and caused cracks to initiate in the ferrite phase. This was in contrast to the cracks initiating in the austenite phase in the as-received DSS. Alloy composition and microstructure of DSS as well as solution composition (dissolved ionic species) was also found to affect the electrochemical behavior and passivation of DSS which in turn plays a major role in stress corrosion crack initiation and propagation. Corrosion rates and SCC susceptibility of DSS was found to increase with addition of sulfide to caustic solutions. Corrosion films on DSS, characterized using XRD and X-ray photoelectron spectroscopy, indicated that the metal sulfide compounds were formed along with oxides at the metal surface in the presence of sulfide containing caustic environments. These metal sulfide containing passive films are unstable and hence breaks down under mechanical straining, leading to SCC initiations. The overall results from this study helped in understanding the mechanism of SCC in caustic solutions. Favorable slip systems in the austenite phase of DSS favors slip-induced local film damage thereby initiating a stress corrosion crack. Repeated film repassivation and breaking, followed by crack tip dissolution results in crack propagation in the austenite phase of DSS alloys. Result from this study will have a significant impact in terms of identifying the alloy compositions, fabrication processes, microstructures, and environmental conditions that may be avoided to mitigate corrosion and stress corrosion cracking of DSS in caustic solutions.

CHAPTER 1

INTRODUCTION

1.1. MOTIVATION

Duplex stainless steels (DSS) have a dual microstructure consisting of roughly equal volume fractions of ferrite and austenite phases. This balanced microstructure contributes to the superior mechanical and corrosion properties of these steels as compared to carbon steels and austenitic stainless steels. However, in spite of the overall better performance of duplex steels, corrosion problems are persistent in the various process streams of chemical industries using DSS. In the pulp and paper industry, pulp mill digesters were previously made of carbon steel. But due to severe stress corrosion cracking (SCC) [1],[2] in sulfide containing caustic solutions and due to changes in the pulping processes, they are being replaced by duplex stainless steels. Today, almost all new pressure vessels in the pulp and paper industry (Kraft digesters and other pulp mill equipments) are made of DSS. Although the frequency of corrosion failures have decreased by the substitution of carbon steel with DSSs, field experience and recent laboratory studies have shown that the aggressive alkaline pulping liquor environment consisting of sodium hydroxide (NaOH) and sodium sulfide (Na_2S) may cause severe stress corrosion cracking at temperatures higher than ~ 120°C [3]-[6]. DSS equipment in different pulp mills have been reported to show stress corrosion cracking in pressure vessels and other high stress components [7][8] as shown in Figure 1.1 to Figure 1.3. SCC failures were found in the weld sections as well as in the base DSS metal.

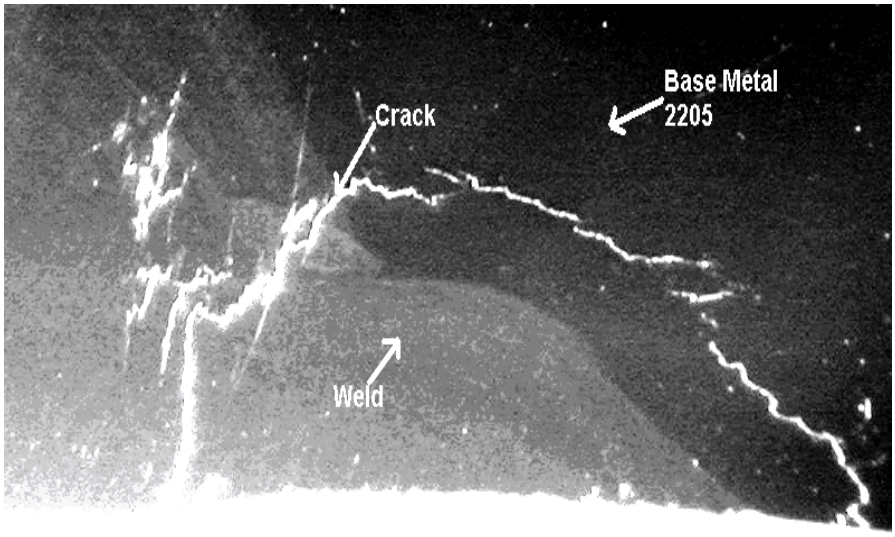

Figure 1.1. Propagation of stress corrosion cracks in the base metal of 2205 DSS white liquor accumulator.

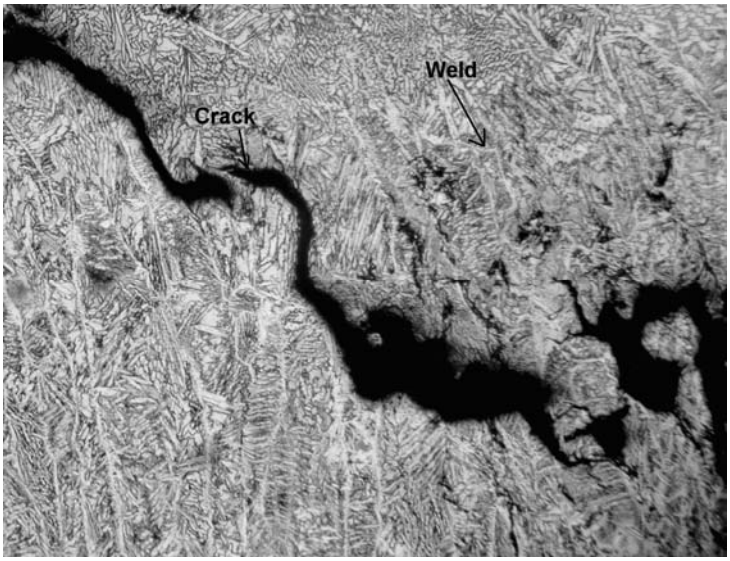

Figure 1.2. Propagation of stress corrosion cracks in weld metal of 2205 DSS white liquor accumulator.

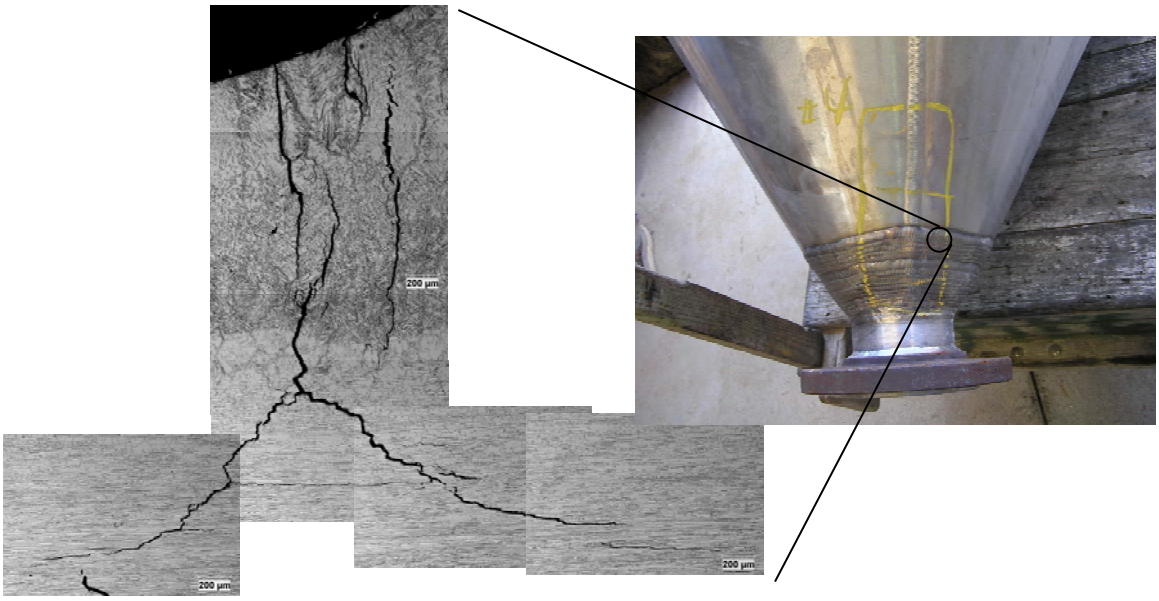

Figure 1.3. Stress corrosion cracking of 2205 DSS sand-separator cone in pulp mill.

Although a number of studies were devoted to the problem of SCC of specific DSS grades in chloride containing environments, especially in sea-water and similar high temperature environments, not much work has been done in studying the SCC mechanisms of DSS in sulfide-containing caustic solutions. Factors affecting SCC in DSS in sulfide-containing caustic solutions, like changes in microstructure (austenite/ferrite phase ratio), intermetallic precipitation due to heat treatment, and environmental conditions such as pH, electrochemical potential, threshold temperatures and caustic concentrations are not known. Heat treatments in field may come from improper welding or other fabrication processes, and may adversely affect the corrosion and SCC susceptibility of DSS. Hence, systematic investigation was required to understand the conditions for stress corrosion cracking of DSS in caustic solutions for effective mitigation and reliable use of these materials in chemical processes where an unexpected failure may cause tremendous harm to life and/or property.

1.2. BACKGROUND AND LITERATURE REVIEW

1.2.1. Duplex Stainless Steels

Duplex stainless steels (DSS) represent a class of stainless steels with dual microstructure consisting of roughly 50% ferrite and 50% austenite (by volume). Figure 1.4 and Figure 1.5 shows typical microstructure of a DSS 2205 plate in longitudinal and transverse directions. The volume fractions of ferrite and austenite in DSS depend upon thermal and mechanical history [9]. Maintaining equal volume fraction of phases involves the simultaneous control of chemical composition and heat treatment. Superior corrosion performance of DSS is due to the alloying elements such as chromium, molybdenum and nitrogen [10]-[12], which increase the pitting corrosion and stress corrosion cracking resistance of these steels in a variety of environments. The austenite phase provides good formability, toughness, and weldability. It also provides good resistance to hydrogen embrittlement. On the other hand, the ferrite phase contributes to the high tensile and fatigue strength and good corrosion resistance of DSS. There are various reasons for strength enhancement in the duplex structure. The element partitioning causes an enrichment of nitrogen and carbon in austenite, causing solution hardening. The mixed structure also causes grain refinement, thus improving the mechanical properties of the steel. Owing to their superior mechanical properties and corrosion resistance, DSS have been employed for the construction of equipments in chemical processing industry, pulp mill digesters, heat exchangers, pressure vessels, seawater systems, and for various other industrial applications where high temperature, corrosive environment and other factors restrict the use of carbon steel and austenitic

stainless steels. A number of duplex stainless steel grades are commercially available. Nominal compositions of some common DSS grades are given in TABLE 1.1. The metallurgical structure of DSS can also be related to its composition by means of Schaeffler diagram, which is shown in Figure 1.6. The figure exhibits a wide composition range in which the stainless steels exhibit a duplex structure and varying the concentration of different alloying elements in this range, a variety of commercial DSS grades can be obtained. Alloying elements are grouped as ferrite stabilizers (Cr, Mo, Si) and austenite stabilizers (Ni, N, C, Cu) which are expressed in terms of chromium equivalence and nickel equivalence respectively and form the two axis of the Schaeffler diagram. These elements in correct proportions give rise to the dual microstructure of DSS.

New grades of lean duplex stainless steels, like grade LDX2101 have been developed where the concentration of Cr and Ni in the alloy is lower than 2205 DSS grade. Since these two elements are important for corrosion resistance, 2101 may have corrosion related problems in certain environments. The role of composition and microstructure on SCC susceptibility of DSS has been studied in acidic chloride media. Whereas their performance limits in terms of SCC susceptibility and general corrosion in other environments, especially caustic solutions, have not been studied to the same extent.

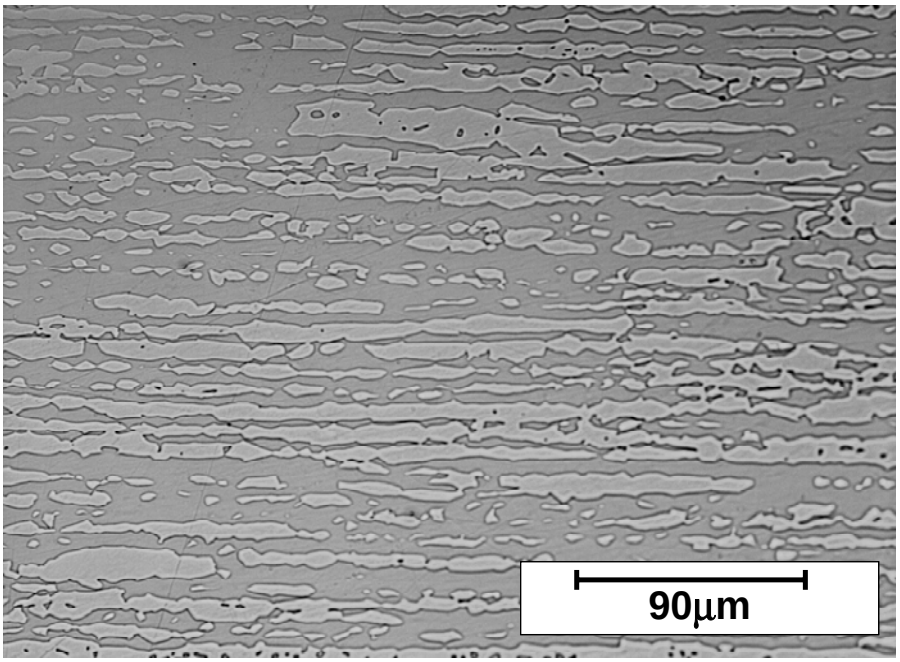

Figure 1.4. Micrograph showing duplex stainless steel 2205 etched in 40% NaOH solution longitudinal section (rolling direction). The darker phase is ferrite and the lighter phase is austenite.

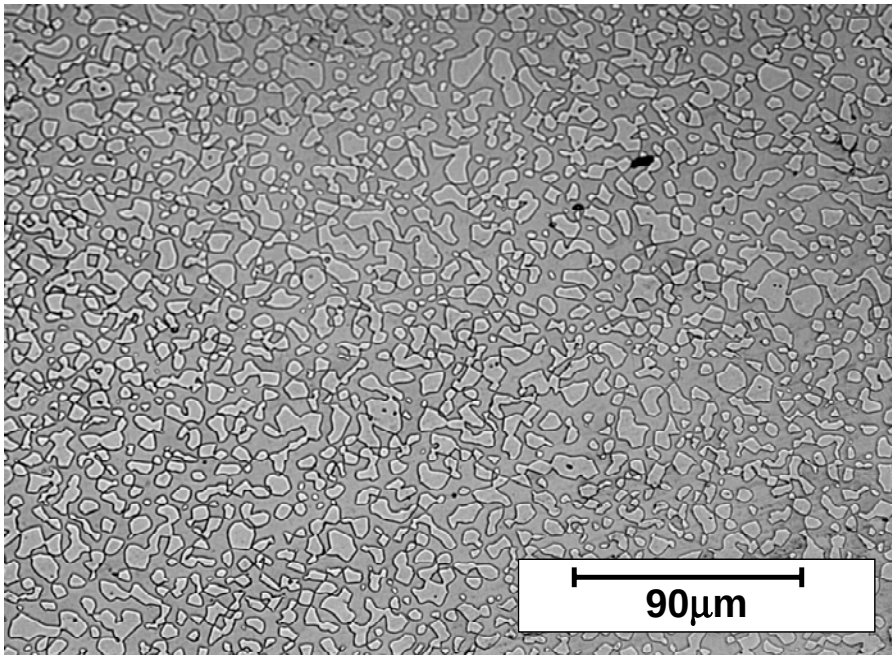

Figure 1.5. Micrograph showing duplex stainless steel 2205 etched in 40% NaOH solution (transverse section).

TABLE 1.1. COMMON GRADES OF DUPLEX STAINLESS STEELS AND THEIR NOMINAL COMPOSITIONS (IN WT %)

UNS Number	Common Name	C	Mn	P	S	Si	Cr	Ni	Mo	N	Cu
S32750	2507	0.03	1.2	0.035	0.02	0.8	24-26	6-8	3-5	0.24-0.32	0.5
S32205	2205	0.03	2.0	0.03	0.02	1.0	22-23	4.5-6.5	3.0-3.5	0.14-0.2	……
S32304	2304	0.03	2.5	0.04	0.03	1.0	21.5-24.5	3-5.5	0.05-0.60	0.05-0.2	0.05-0.6
S32001	2101	0.03	5.0	0	0	0.7	21.5	1.5	0.3	0.22	0.3

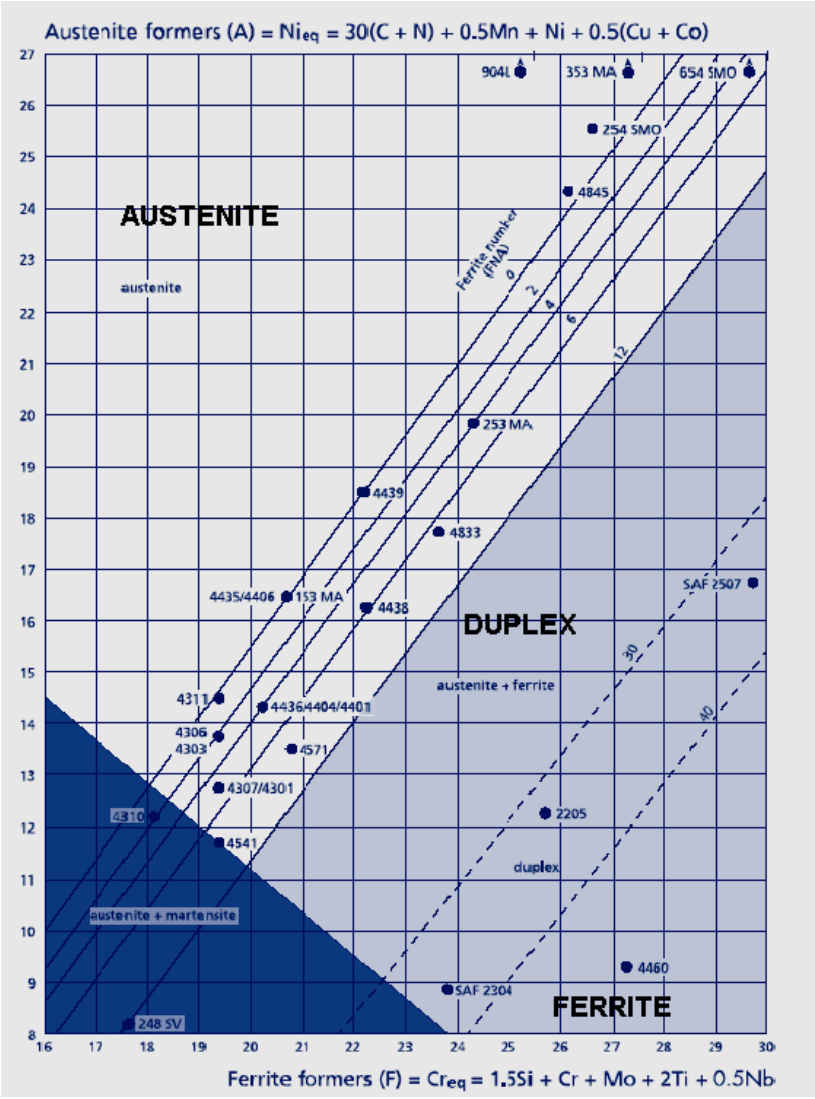

Figure 1.6. Schaeffler diagram showing composition range in which stainless steels exhibit a duplex structure [1]

1.2.2. Stress Corrosion Cracking

Stress Corrosion Cracking is a localized form of corrosion occurring under the simultaneous action of tensile stress and corrosive environment such as chloride and caustic solutions [13]. Alloy composition has a significant effect on its SCC susceptibility. For example, the maximum susceptibility of steels to SCC in chloride containing environments is in the range of 5-35% of nickel [14]. Temperature is an important factor, depending upon the alloy composition and environment, SCC may not occur below a threshold temperature. The tensile stress requirements for the SCC to occur may be fulfilled either by the residual stresses in the alloy due to fabrication processes or by the operational stresses due to equipment being used. In certain alloy/environment systems, stress corrosion cracking can occur at stresses well below the yield strength of the material. The cracks can nucleate at corrosion pits or other pre-existing stress concentrators and propagate into the metal if conditions are suitable. SCC is an insidious form of corrosion and produces a drastic loss of mechanical strength without significant metal loss. It causes a rapid, brittle failure of the steel without any prior indication and hence is considered catastrophic. Several major disasters have been attributed to stress corrosion cracking of steel equipment, including rupture of high-pressure gas transmission pipes, boiler explosions and severe damage in power stations and oil refineries. SCC cracking can be either intergranular (along grain boundaries) or transgranular (through the grains). Figure 1.7 shows intergranular and transgranular stress corrosion cracking. SCC mechanism can be different for different alloy/environment combinations. For example, SCC of sensitized austenitic stainless steels in acidic chloride media is intergranular [15], whereas in absence of sensitized microstructure, SCC in

austenitic stainless steels in the same media nucleates at slip steps and propagates in transgranular mode. On the other hand, ferritic steels are more susceptible to hydrogen assisted stress corrosion cracking.

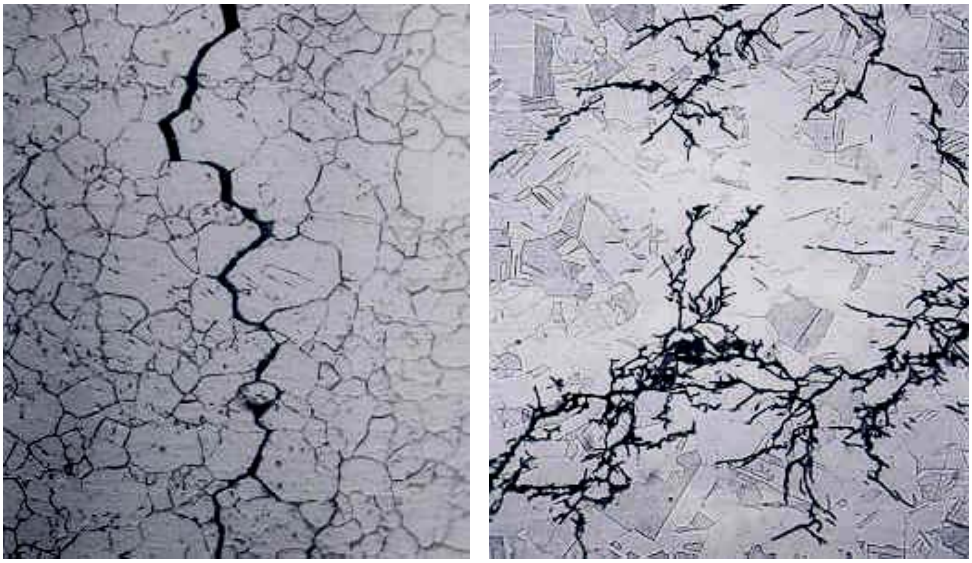

(i) **(ii)**

Figure 1.7. Figures showing (i) intergranular SCC (IGSCC) along grain boundaries and (ii) transgranular stress corrosion cracking (TGSCC) through grains [16]

Stress corrosion cracking phenomenon can be divided into four stages:

- Incubation period
- Crack initiation and stage I propagation
- Stage II or steady state crack propagation
- Stage III crack propagation or final failure

1.2.2.1. Role of Surface Films in SCC

Surface films may include adsorbed layers, films of corrosion product and dealloyed layers [17]. These films may produce brittle medium in which cracks may propagate or

may affect adsorption of hydrogen. These films may also affect local stresses in the surface of the metal.

Protective surface films generally reduce the corrosion rate, but if such film breaks down locally, then local corrosion current density increases, which may lead to dissolution of metal and formation and propagation of cracks. The rate of propagation in this case will depend on the rate of dissolution of metal. On the other hand, if the film is thick and brittle, SCC cracks may propagate into this brittle film and get arrested when it enters the ductile base-metal. In this case, the rate of crack propagation depends on the rate of film formation. In both cases, rate of crack propagation depends on electrochemical processes.

In case of hydrogen embrittlement, especially in case of high strength steels, the film may control hydrogen adsorption.

Finally, surface films may change the mechanical properties of a material on which they are formed by preventing the operations of surface sources of dislocations and thereby leading to strengthening and stiffening of the materials.

The surface film may be ruptured locally due to mechanical stress [17]. This leads to active dissolution of metal, resulting in a groove formation. This groove acts as a stress raiser, due to which the metal at the tip of the groove may rupture again. This is seen in (Figure 1.8). If the tip of the crack remains active with respect to the crack wall, the crack may propagate. However, if the environment leads to rapid repassivation of the film, SCC will not occur, as seen in region (I) illustrated in Figure 1.8. But if the repassivation rate is very slow, crack may blunt and the stress concentration gets reduced as seen in Figure

1.8(III). SCC is more severe where the film is moderately stable and intermediate repassivation occurs (Figure 1.8(II)).

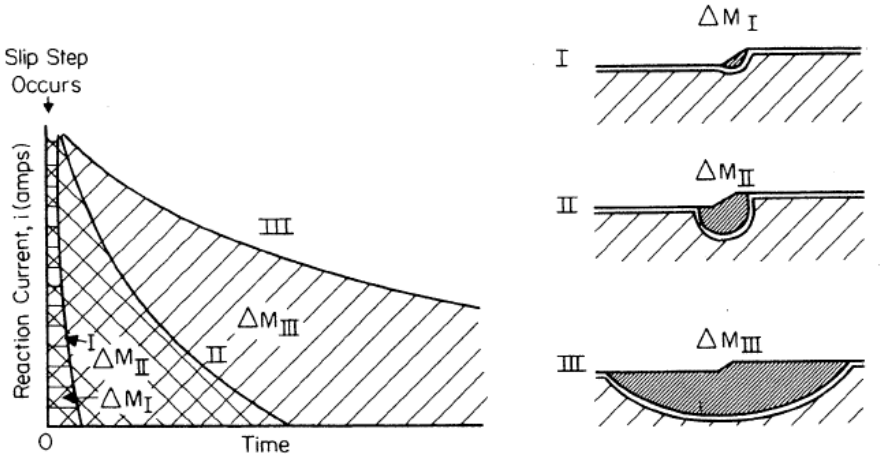

Figure 1.8. Schematic figure showing relationship between current versus time transient. (I) Rapid repassivation. (II) Intermediate repassivation resulting in SCC. (III) Extensive lateral dissolution [17]

Chemical breakdown of the passive film is made easier by mechanical stress. But if deformation is very slow, chemical breakdown of film may occur before mechanical deformation has an effect. The time taken for chemical film breakdown may be related to the incubation time in SCC. Rate of crack propagation depends on rate of metal dissolution.

1.2.2.2. SCC Initiation

SCC initiation is the time required to achieve a local environmental conditions at any pre-existing defects on the specimen surface or to form a defect that may result into a crack. These defects may be from machining, scratches, pits or intergranular corrosion notches. Prior to the initiation process, local chemistry of the environment suitable for crack initiation needs to be established. This stage is very important for active-passive

materials such as austenitic stainless steels because the local environment at the crack tip is different from the bulk environment and this local environment is critical for the crack initiation and propagation. This exposure time is also called the 'induction time' (t_i) or 'incubation time', which is usually a large fraction of the total time to fracture (t_f) [35]. Hence, initiation of SCC can be described in terms of two parameters:

- an incubation or initiation time t_i, prior to crack formation
- a critical mechanical loading threshold, expressed either as threshold stress σ_f (for smooth surfaces), or as a critical concentration factor K_{ISCC} (in the presence of preexisting cracks)

The relationship between crack growth rate and the time at different stages of crack propagation is shown in Figure 1.9.

The incubation time depends on the material/environment combination. For a steady state material/environment combination, there is a specific incubation time, but if this steady-state is upset for some reason, the incubation time may change. Earlier work on SCC of austenitic stainless steels in chloride solution has shown that there is a long incubation period before cracking is initiated.

Once a crack has been initiated, preceded by the incubation time, it propagates under the combined action of corrosive environment and adequate tensile stresses. There are several mechanisms for crack propagation, which are described in the proceeding sections.

Cracks may be initiated by several mechanisms [19],[20]. They may be initiated at scratches, nicks or dents on the metal surface where the stress intensity is high, or at corrosion pits where the passive film is mechanically destroyed [21]. The localized

rupture of passive film at the metal surface may also take place due to plastic deformation. Galvanic corrosion can also initiate SCC, where the selective dissolution of one phase (e.g. matrix, inclusions or precipitates) with respect to another phase, in a specific corrosive environment, results in the concentration of stress at the tip of dissolution. Slip steps emerging at the surface also have a pronounced effect on the initiation of stress corrosion cracks as the passive film may be damaged locally and form local anodes at the sites, which may further initiate transgranular cracks [22].

1.2.2.3. SCC propagation

Once initiated, SCC propagation takes place under the combined action of environment, tensile stresses, and microstructure. Crack geometry is maintained such that the crack tip is typically active while the crack walls have a passive film. The common rate controlling steps in crack propagation mechanisms are mass transport rates in the crack enclave, oxidation and reduction rates at the strained crack tips and the inelastic behavior in that region.

Figure 1.10 shows a schematic representation of the different processes that can be involved in crack propagation. Any of these steps may be the rate controlling step in crack propagation [23].

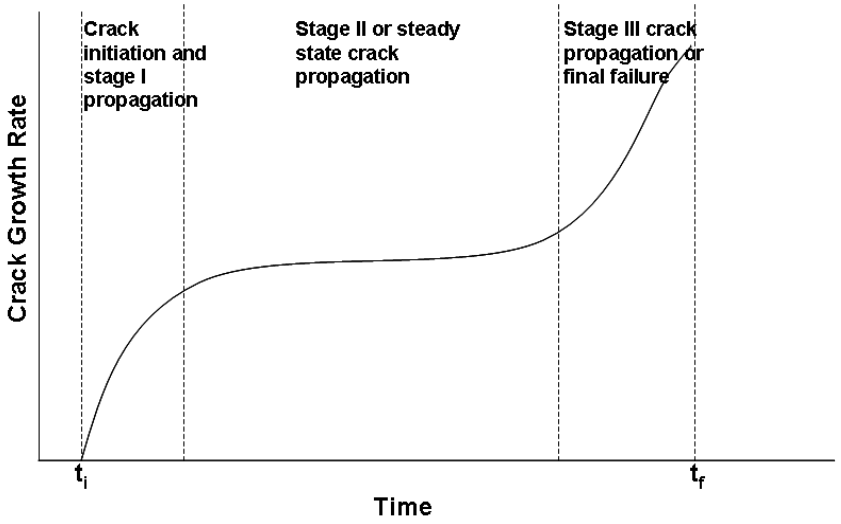

Figure 1.9. Schematic showing different stages of stress corrosion cracking versus time

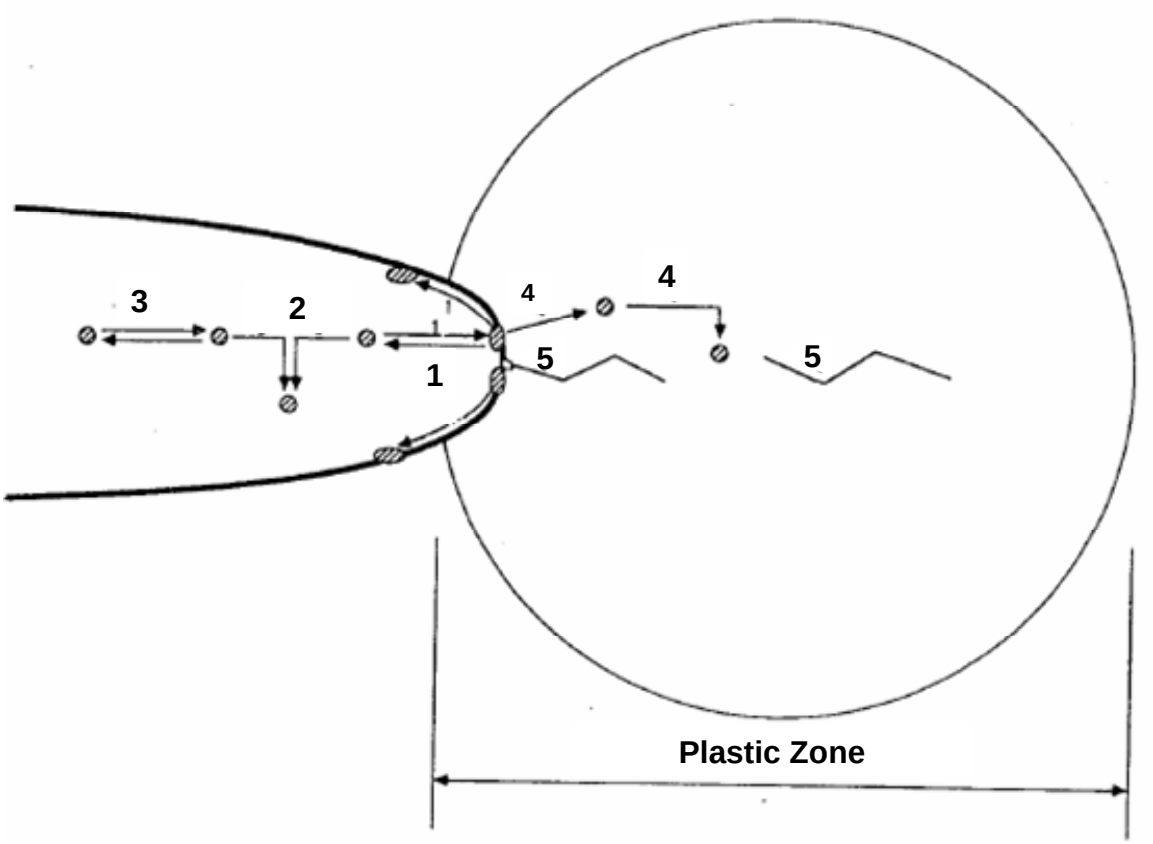

Figure 1.10. Principal types of mechanisms involved in the propagation of stress corrosion cracks: (1) Surface reactions and transport. (2) Reactions in the liquid phase. (3) Transport in the liquid phase (4) Local modification of the properties of the material (5) Mechanical failure [23]

The processes are as follows:

- Surface reactions at the crack tip
  - anodic reactions: oxidation, dissolution, repassivation, formation of salt films
  - cathodic reactions: reduction of water or protons and others
  - adsorption: adsorption of hydrogen produced during cathodic reaction, adsorption of ions containing chlorine, sulfur or inhibitors
  - surface diffusion
- Reactions in the solution near the crack tip such as hydrolysis of the metal cations, precipitation of salts.
- Mass transportation along the crack in the liquid phase:
  - chemical diffusion
  - diffusion in a potential gradient
  - convection
- Local modification of the material at the crack tip:
  - adsorption and diffusion in the material: hydrogen produced by cathodic reactions, vacancy produced by the dissolution reactions
  - formation of porous or depleted layers by selective dissolution

    - modification of the mechanical properties such as plastic strain due to stress concentration, partial relaxation of strain by anodic dissolution and increase in dislocation mobility by hydrogen
    - reactions in the material such as local transformation to martensite in relatively unstable austenitic stainless steels
- Mechanical failures:
    - at the surface such as rupture of the passive film, de-bonding from the material, cleavage, etc.
    - ahead of crack-tip interface due to hydrogen traps

Among all these processes, some contribute directly to crack advance whereas others create local conditions different from the bulk material, suitable for crack propagation.

Hence, during crack propagation, thermodynamic and kinetic conditions are created at the crack tip, which cannot be created at the free surface of the bulk material. Any of these processes can be a rate-determining step in crack propagation.

SCC propagation mechanisms can be divided distinctly into either those which involve embrittlement of metal due to corrosive reactions (mechanical fracture models) or those in which cracks grow by localized dissolution process. There are several proposed mechanisms for crack propagation, which depend on the material/environment combination. The mechanical fracture model assumes that the crack essentially propagates by dissolution, and then the remaining ligaments fail by mechanical fracture (ductile or brittle). There are several proposed models under this broad category. These

are *film induced cleavage model, tarnish rupture model, tunnel model, adsorption model and hydrogen models*.

The dissolution mechanism assumes that crack propagation is due to active dissolution at the crack tip. This may be continuous or may be due the periodic failure of the otherwise thermodynamically stable surface film on a material. The different models under this mechanism are *slip dissolution model or film rupture model and intergranular stress corrosion cracking*.

1.2.2.3.1 Dissolution Mechanisms

This model assumes that crack propagation is due to active dissolution at the crack tip. This may be continuous or may be due the periodic failure of the otherwise thermodynamically stable surface film on a material. This may lead to either intergranular stress corrosion cracking or transgranular stress corrosion cracking. Once a crack has initiated, it undergoes propagation due to the action of specific environment. The crack wall dissolution rates are orders of magnitude slower than the crack tip dissolution rates. Hence, in passive metals, crack walls repassivate behind the active crack tip, leading to dissolution at the crack tip and causing crack propagation. For high rates of crack propagation by crack tip anodic dissolution model, high values of corrosion current are required at the crack tip. The main criteria for the proposed cracking mechanisms in aqueous solutions is that the crack tip must propagate faster than the corrosion rate on the unstrained crack sides, otherwise the crack will degrade into a blunt notch. Based on this criterion, the material-environment condition for SCC may be defined based on thermodynamic and kinetic requirements for the existence of protective films on the crack sides. Hence, cracking susceptibility will depend on specific

potential/pH ranges, where the protective film is thermodynamically stable, but if ruptured, bare surface dissolution is thermodynamically possible. Another requirement for the crack propagation is the electrochemical reaction rate (dissolution or oxidation), which must be significantly higher at the crack tip as compared to those at the crack sides for a sharp crack to propagate. Therefore, SCC can be suppressed by blunting of newly nucleated cracks during early initiation stages by specific material/environment combination if this condition is not satisfied. The crack propagation rates for many ductile alloy/environment systems are in direct proportion to the experimentally determined dissolution rates under the mechanical and chemical conditions expected at the crack tip, as can be seen in Figure 1.11 [24]. In the figure, it can be seen that the crack propagation rate in austenitic stainless steel corresponds to an average current density of ~10^{-1}A/cm^2.

1.2.2.3.2 Intergranular Stress Corrosion Cracking

In intergranular cracking, the segregation of solutes or the precipitation of the discrete phases can occur at grain boundaries, which may result in electrochemical heterogeneity at the grain boundaries, leading to their dissolution [25]. Auger electron spectroscopy was used to determine the segregation effect in the vicinity of intergranular fracture surfaces in type 304 stainless steels [25]. The results showed that depletion of chromium in the grain boundary region resulted in attack by a weakly oxidizing solution, such as, H_2SO_4-$CuSO_4$. This dissolution is due to galvanic effects at grain boundaries, because of the potential difference between the grain boundary regions and the bulk metal. Hence, the driving force for dissolution is related to the potential difference between the matrix and the segregant atoms forming a galvanic cell. Apart from the galvanic effects, modified

film characteristics in the grain boundary regions, where segregants are present, are also responsible for the dissolution and IGSCC. Studies have shown that if enhanced dissolution occurs in grain boundary regions due to the presence of segregants, protective film may be impaired in those regions causing the crack to propagate. Grain boundaries also provide obstacles to dislocation motion where pileups occur at these boundaries, leading to localized deformation in the grain boundary region. This may also cause IGSCC.

1.2.2.3.3 Slip Dissolution Model or Film Rupture Model

In the slip dissolution model, dissolution takes place at or along the slip lines [23], [27]-[29]. The steel is protected by a surface film, which is ruptured due to stress during plastic deformation, causing anodic dissolution of the underlying metal. Localized plastic deformation at the crack tip concentrates stress in this region leading to film rupture only at the crack tip and not at the sides of the crack. This causes anodic dissolution at the tip permitting crack propagation. This mode of propagation is generally found in transgranular SCC of austenitic stainless steels. Film ruptures due to emergence of slip steps through the thin passive film (10 to 50Å) and repassivation proceeds after a stage of transient dissolution. The fundamental parameters that govern the crack propagation are the strain rate at the crack tip ($d\varepsilon/dt_{CT}$), which determines the frequency of film rupture, and the kinetics of active dissolution and repassivation of the exposed metal due to film rupture. The initiation and propagation of cracks by this model is shown in Figure 1.12. A correlation between the dissolution/repassivation kinetics and rates of intergranular/transgranular corrosion can also be obtained from Figure 1.11.

In order for the slip step dissolution model to operate, the slip step height should be more than the thickness of the surface films, if unfilmed metal is to be exposed to the environment. Slip step dissolution model can explain most of SCC failures in austenitic stainless steel in high temperature water, chloride containing solutions and caustic media.

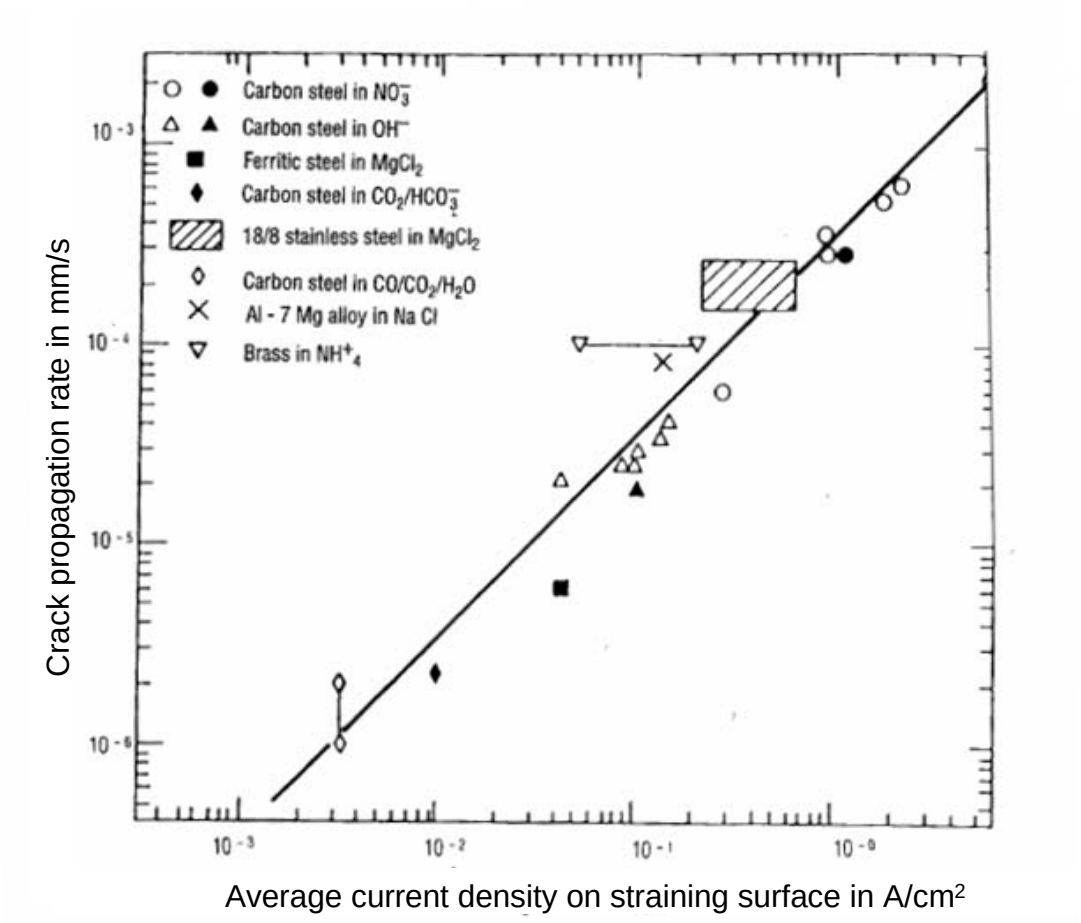

Figure 1.11. Correlation between crack propagation rates and anodic dissolution currents measured during tensile tests under an imposed potential [25]

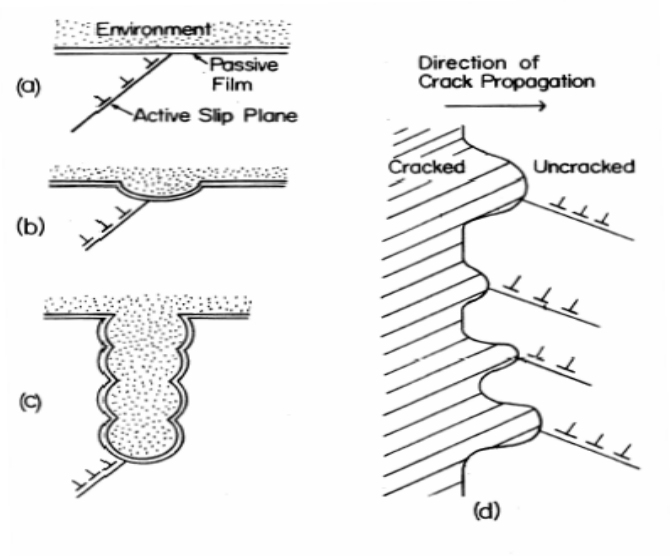

Figure 1.12. Schematic showing various steps (a,b and c) of film rupture model and (d) showing crack tip intersected by several active slip steps [27]

There have been various hypotheses for the precise atomistics at the crack tip that have been proposed considering the effect that environment has on the ductile fracture process. These hypotheses propose an increase in the number of active sites for dissolution due to strain concentration and the preferential dissolution of mobile dislocations due to chemical activity of dislocation core or solute segregation at the dislocations. For crack propagation by slip dissolution model, different types of protective films present, such as oxides, mixed-oxides, salts or noble metals left at the metal surface may be ruptured due to the strain developed in these films, leading to crack initiation [30]. The strain rate at the crack tip, which is necessary for the film to rupture, may increase due to monotonically increasing the stress or cyclic stress, or due to the creep process in the underlying base metal under constant stress. Once the film is ruptured, crack tip propagation is governed by the oxidation on the bare metal surface, depending on the thermodynamics and kinetics of the system as well as the film reformation. The crack propagation will be maintained if the film rupture and reformation

processes occur continuously due to varying strain rates at the crack tip as shown in Figure 1.13. This model also provides a quantitative description of crack propagation. According to this figure, the crack sides have a passive film. The crack tip is active due to the rupture of the passive film and active dissolution occurs at the tip. This film rupture occurs because of the strain rate at the tip. Hence, crack advance will only be maintained if the film rupture process reoccurs. Therefore, according to Faradays law, the average environmentally controlled crack propagation rate (V_t) is related to the oxidation charge density between oxide rupture events (Q_f) and the strain rate at the crack tip ($\dot{\varepsilon}_{ct}$) by:

$$\dot{V}_t = \frac{M}{z\rho F} \times \frac{Q_f}{\varepsilon_f} \times \dot{\varepsilon}_{ct} \qquad (1)$$

where M is the atomic weight and ρ is the atomic density of the crack tip metal, F is the Faraday's constant, z is the number of electrons involved in the oxidation of an atom of metal, and ε_f is the fracture strain of the oxide at the crack tip.

The rate controlling steps that govern the crack propagation by slip dissolution model are:

1). Liquid diffusion of either water molecules or solvated cations to and from the crack tip region.

2). The overall oxidation (dissolution and oxide re-growth) rate or rate of repassivation.

3). Film rupture rate at the crack tip.

These parameters can directly be related to stress, environment, and microstructure, as seen in Figure 1.14.

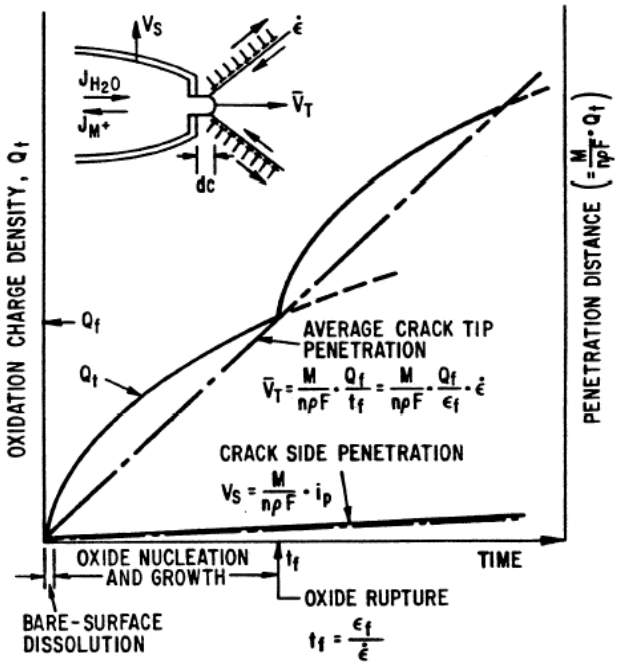

Figure 1.13. Schematic showing oxidation charge density/ time relationships for a strained crack tip and unstrained crack sides [30]

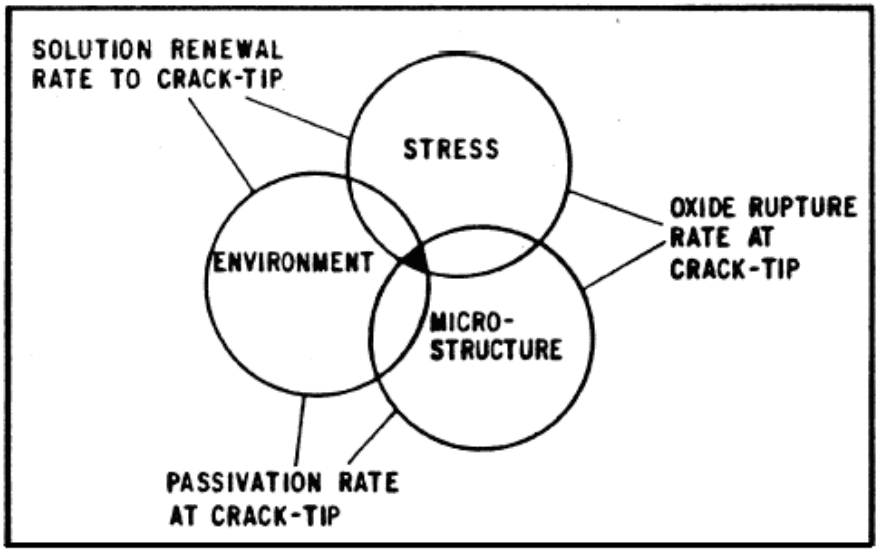

Figure 1.14. Interrelationship between the fundamental controlling parameters (mass transport rate, passivation rate, oxide rupture rate) and the phenomenological parameters (stress, environment, microstructure) known to affect SCC [30]

As the oxidation charge density on the bare metal surface depends on material and environment composition at the crack tip, the crack propagation rate can be expressed as:

$$\overline{V_t} = A\dot{\varepsilon}_{ct}^{n} \quad (2)$$

where, A and n are constants depending on material and environment composition at the crack tip. This equation has limitations at very high and very low crack tip strain rate as seen in Figure 1.15.

At low strain rates, sharp cracks cannot be maintained because the crack tip propagation rate $\overline{V_t}$ becomes equal to the oxidation rate on the crack sides. Hence, repassivation of the crack tip occurs easily and crack propagation due to dissolution of the metal at the tip is inhibited. Under these conditions, crack propagation rates will decrease and crack will be arrested because of blunting. At high crack tip strain rates, a bare surface will be continuously maintained at the crack tip and the crack propagation rate becomes independent of $\dot{\varepsilon}_{ct}^{n}$.

1.2.2.3.4 Mechanical Fracture Models

Mechanical fracture of ductile metal or of the brittle outer layer is involved in these, mechanisms. There are several proposed models under this broad category.

1.2.2.3.4.1 Film-Induced Cleavage Mechanism

Sometimes during transgranular cracking, the faradaic equivalent of the oxidation rate at the strained crack tip is insufficient to explain the observed crack propagation rate [30]. In addition, cleavage like crystallographic features on transgranular fracture surfaces cannot be explained by the dissolution/oxidation model alone. Hence, studies have shown

that transgranular, environmentally controlled, crack propagation can occur by a combination of slip dissolution and brittle fracture mechanisms [31]-[33]. It has been suggested that initially the crack front propagates by oxidation process that is controlled by rate determining steps, similar to those in the slip dissolution model. But when the film rupturs due to strain increment, the crack in the brittle surface film may rapidly penetrate a small amount (a*) into the underlying ductile metal matrix, due to its inability to accommodate the imposed strain rate. This is illustrated in Figure 1.16.

Hence, the crack tip propagation rate equation for the film rupture model is modified as follows:

$$\overline{V_t} = \left(\frac{M}{z\rho F} Q_f + a^*\right) \frac{\dot{\varepsilon}_{ct}}{\varepsilon_f} \tag{3}$$

This film-induced cleavage component, a* is controlled by state of coherency between the surface film and the metal and the fracture toughness of the substrate. The ability of the brittle crack in the surface film to propagate into a ductile matrix depends on the ratio between the rate of propagation of the crack initiated in the surface film and the velocity of the dislocations emitted in the underlying metal. This model is attractive for caustic SCC of non-sensitized austenitic stainless steels [34].

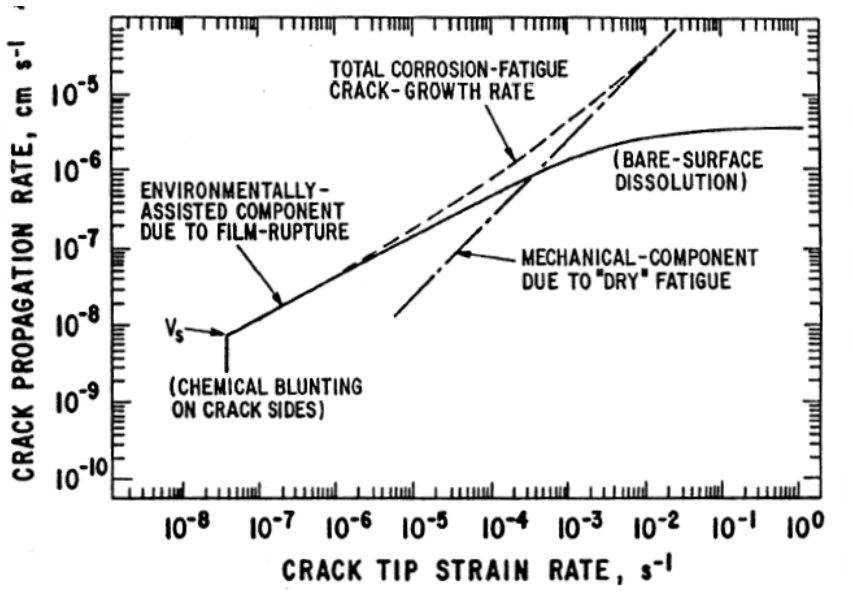

Figure 1.15. Strain-rate dependence of the crack propagation rate in the slip dissolution model [30]

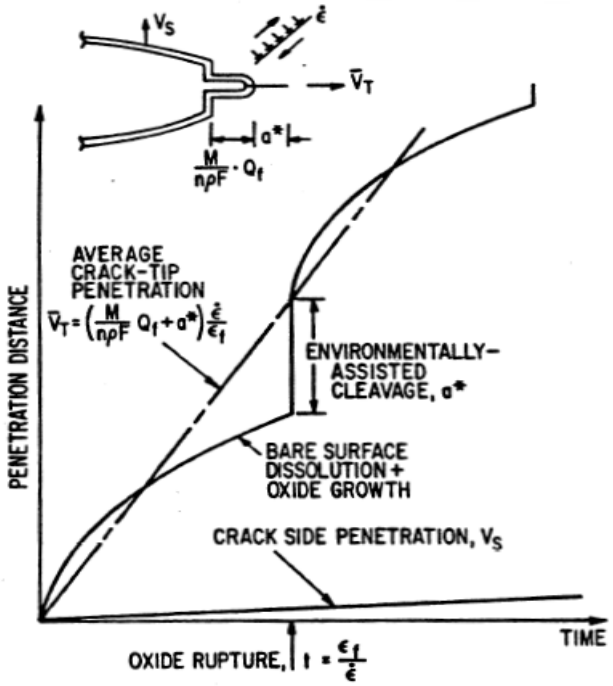

Figure 1.16. Schematic illustration of the elements of the film-induced cleavage mechanism of crack propagation. Similarity of the slip dissolution model (Figure 1.13) during initial stages of propagation cycle can be observed [30]

1.2.2.3.4.2 Tarnish Rupture Model or Brittle Film Model

The tarnish rupture model or sometimes referred to as the brittle film model is relevant to the intergranular stress corrosion cracking of austenitic stainless steels. This model can also be applied to SCC of stainless steels in high temperature water or in polythionate solutions. In this model, a brittle or mechanically weak surface film is produced by the environment [27]. This film grows preferentially along the grain boundaries, as seen in Figure 1.17. In a stressed material, this film undergoes brittle fracture at some critical depth, and enters the substrate, exposing bare metal and leading to its dissolution until the metal repassivates and the brittle film is formed again. This process repeats itself, leading to discontinuous crack propagation. This model is also called stress assisted intergranular corrosion. The difference between this model and the film rupture model is that film rupture model involves thin passive films (~ 50 Å) and rate of repassivation plays an important role in the crack propagation. But tarnish rupture model deals with thick (~ 1000 Å or greater) nonprotective films whose growth is limited by the transportation of ions in the solution.

1.2.2.3.4.3 Tunnel Model

Tunnel model assumes the formation of fine arrays of small corrosion tunnels at emerging slip steps [35]. These tunnels grow in diameter and length until stress in the remaining ligaments of metal are unable to bear the stress and cause ductile fracture leading to crack propagation. This process is repeated and results in a discontinuous crack propagation, as shown in Figure 1.18. Hence, the cracks propagate by alternating tunnel growth and ductile fracture.

The occurrence of corrosion tunnels in austenitic stainless steels was observed in a number of SCC cases as shown in Figure 1.19. The corrosion tunnel model for crack propagation is applicable very rarely as compared to other models.

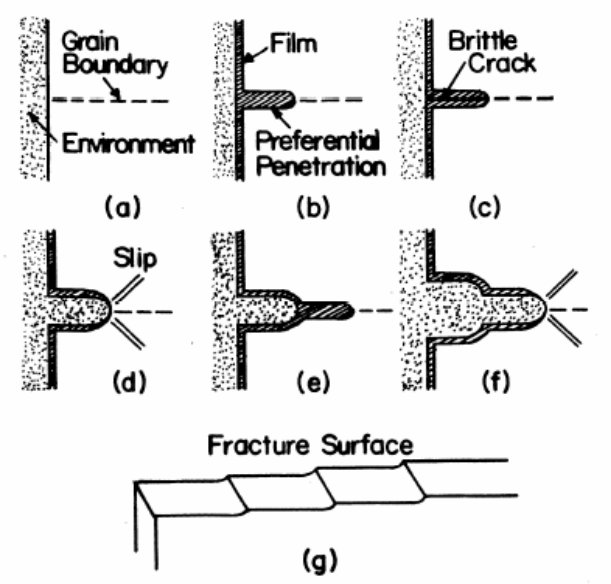

Figure 1.17. Schematic representation of the tarnish rupture model showing the formation of brittle film along the grain boundaries and subsequent rupture of the brittle film under stress leading to crack initiation and propagation [27]

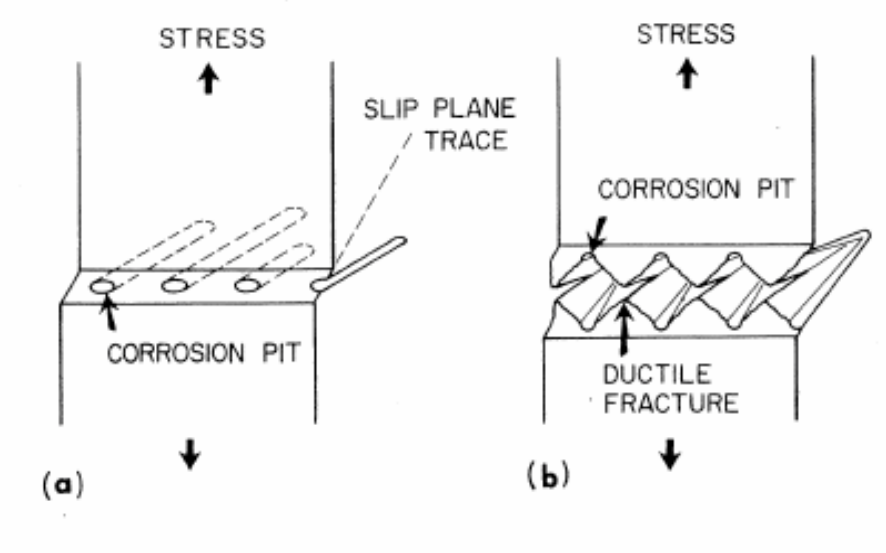

Figure 1.18. Schematic representation of the tunnel model showing (a) the formation of fine arrays of small corrosion tunnels at emerging slip steps (b) ductile fracture in ligaments between tunnels leading to crack propagation [27]

Figure 1.19. Scanning electron micrograph of corrosion tunnels along slip traces in activated surface of 304 austenitic stainless steels [18]

1.2.2.3.4.4 Embrittlement Models

According to this group of mechanisms, SCC cracks propagate in a brittle manner in most cases, and hence the Griffith's approach to brittle fracture can be relevant [25]. Thus, the fracture stress required to cause the propagation of an elliptical crack in a brittle manner can be estimated from the equation:

$$\sigma_c = \left(\frac{2E\gamma_s}{\pi C} \right)^{1/2} \tag{4}$$

where E is the Young's modulus and γ_s is the surface energy. Hence, any process that lowers γ_s will reduce the stress required for brittle fracture. This γ_s may be lowered if some species are adsorbed at the fracture surface. This usually takes place during hydrogen embrittlement of steels. But if plastic deformation is involved in the fracture, then according to Orowan, the surface energy term will be modified to account for the work done during plastic deformation. Hence γ_p (work for plastic strain) is added to the γ_s term. Apart from hydrogen reacting with dislocations, vacancies or larger voids and affecting fracture, it may also form hydrides and affect fracture. These embrittling films may be formed at the exposed surface of the metal and rupture, leading to active dissolution of metal and crack propagation.

1.2.2.3.4.5 Selective Adsorption Model

Selective adsorption model proposes that specific species may be adsorbed at the metal surface thus reducing the surface energy, γ_s term in the Griffith or Petch-Stroh equations, leading to a reduction in the stress required to cause a brittle fracture. According to this model, specificity of species as well as electrochemical dependence of SCC can be explained be the selective corrosive species getting adsorbed at surface of

given metal and interacting with the strained bonds at the crack tip, causing a reduction in the bond strength as shown in Figure 1.20 [24].

Adsorption usually occurs at dislocations or other mobile imperfections at the crack tip. This model involves brittle fracture and is therefore consistent with the cleavage-like transgranular fracture of austenitic stainless steels. However, there are several controversies regarding this theory. One of the main controversies is that crack propagation is controlled by rate of transport of damaging ions to the crack tip, and studies have shown that an atomistically sharp crack cannot remain stable in a ductile FCC alloy at such low crack velocities.

Fuller, Lawn and Thompson [36] considered the atomistic model for adsorption induced fracture. In this model, the atoms are connected by horizontal bonds of spring constant (β) and vertical stretchable (breakable) bonds of spring constant (α). This model is shown in Figure 1.21. When a chemical species (diatomic molecule A_2 in Figure 1.21) is adsorbed at the crack tip, it forms two AB bonds and the failure occurs by the breakage of the weakened AA bond.

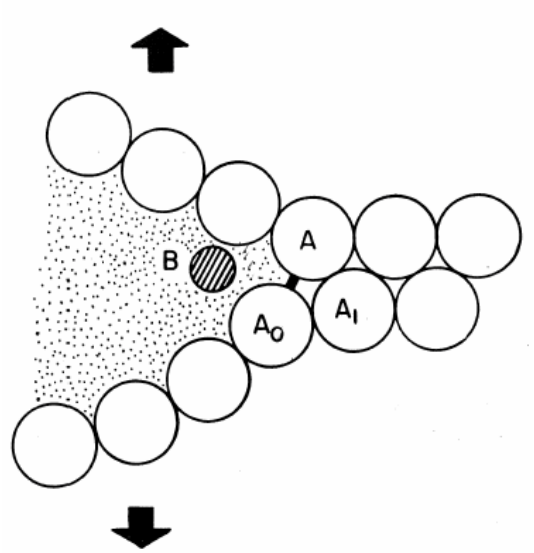

Figure 1.20. Schematic representation of the adsorption model. This model requires that a specific ion from the environment, B, interacts and reduces the cohesive strength of strained bond A-A_0 at the tip of a brittle crack [27]

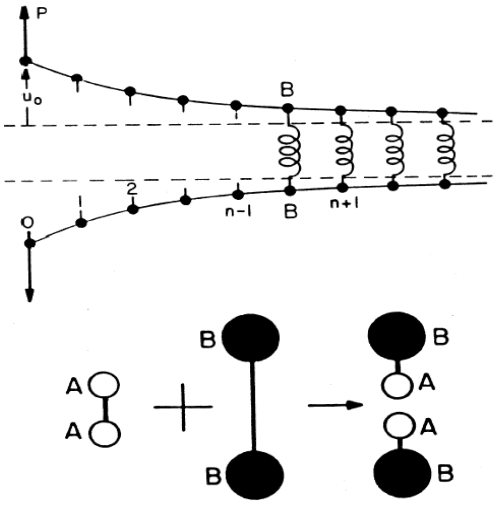

Figure 1.21. Quasi one dimensional model of a crack and schematic showing chemically induced bond rupture. Extraneous molecule AA reacts with crack tip bond BB to produce terminal bonds AB [36]

1.2.2.3.4.6 Hydrogen Embrittlement Models

According to these models, SCC is caused by slow crack growth induced by external sources of hydrogen [27]. There are a number of hydrogen embrittlement models proposed for different alloy/environment systems and they are:

1). Strain-induced martensite model

2). Hydride models

3). Interaction with dislocations

In *strain-induced martensitic* model, formation of strain-induced martensite may be involved in TGSCC of austenitic stainless steels. The observation of martensite on the SCC fracture surface of austenitic 304L stainless steels in many cases suggest the role of strain-induced martensite in the SCC susceptibility of these steels. It was hypothesized that hydrogen entry into the lattice may have promoted the transformation of metastable austenite to martensite.

In hydride models, hydrides are considered to play key role in the SCC of some non-ferrous alloys such as titanium alloys either by acting as barriers to dislocation motion and hence promoting brittle fracture of the matrix or by providing paths for brittle fracture through the hydride phase formed in these alloys.

Dislocations can play a role in the hydrogen embrittlement process. In this model, embrittlement is brought about by hydrogen, which interacts with and pins dislocations, permitting brittle fracture.

Hydrogen embrittlement occurs in metals due to hydrogen adsorption during hydrogen evolution on metal surface [37]. The reactions which precede hydrogen adsorption are:

$$H_2O + 2M = MH + MOH \quad (5)$$

$$H_2O + MH = MOH + H_2 \quad (6)$$

These reactions can only occur at active sites, i.e. free of O_2 and passive films at the bottom of growing pits and cracks. This hydrogen may precipitate at non-metallic inclusions, carbides, grain boundaries, etc. Nucleation of micro cleavage cracks or voids occur due to piling up and coalesce of dislocation group in the vicinity of any obstacle. These obstacles are formed due to diffusion of lattice-dissolved hydrogen to the point of maximum triaxiality of stress. Fracture occurs due to lowering of the cohesion energy of the bonds.

In DSS, depending upon the environmental conditions, either austenite or ferrite phases can be preferentially susceptible to SCC. Therefore, SCC growth in DSS will depend upon the volume fraction and morphology of austenitic and ferritic phases. Thorough understanding of SCC mechanisms in caustic solutions may lead to tailored duplex microstructure or eliminate environmental parameters which may make the steel susceptible to SCC in these systems.

1.2.3. Effect of Heat Treatment on Microstructure and Stress Corrosion Cracking Susceptibility of Duplex Stainless Steels

1.2.3.1. Heat Treatment and Microstructure

Different alloying elements in duplex stainless steel alloys are partitioned in the austenite and ferrite phases as a function of temperature [38]. Except for nitrogen, the partition coefficients of other elements vary very little in different duplex stainless steel

grades. The partitioning coefficient of nitrogen (ratio of mole fraction of nitrogen in the austenite phase to that in the ferrite phase) varies manifestly with its total concentration in the alloy and was reported to be 7.0 at temperatures around 1300°C. Hence, the ferrite becomes saturated with nitrogen faster than the austenite and the remaining nitrogen goes into solution in the austenite. Therefore, a slight increase in the proportion of nitrogen produces a corresponding enrichment of this element in the austenite phase.

Ferrite is a body centered cubic (BCC) structure, whereas austenite is face centered cubic (FCC).. As a consequence, the rate of diffusion of alloying elements in ferrite is generally faster than that in austenite, resulting in transformations, mainly in the ferrite phase, during various isothermal and anisothermal heat treatments of duplex stainless steels. Ferrite stabilizers such as chromium and molybdenum also promote the precipitation of intermetallic phases which adversely effect the mechanical properties and corrosion resistance.

When DSS are heated above 1300°C, the austenite phase dissolves completely in the ferrite [39]. On cooling, austenite is nucleated at ferrite grain boundaries and grows in a “blocky” manner, which is generally known as grain boundary allotriomorphs. These allotriomorphs may have incoherent α/γ interfaces or semicoherent interfaces. On further cooling, the austenite grows into the ferrite grains from the allotriomorphs in a plate like manner known as Widmanstatten side plates. The austenite is further recrystallized as intergranular precipitates in the ferrite matrix [40].

During various fabrication processes, when duplex stainless steel is exposed to isothermal heat treatments in the temperature range of 300°C to 1000°C, solid-state phase

transformations occur, resulting in the precipitation of different intermetallic phases, as shown schematically in Figure 1.22 [41]-[44].

In the temperature range of 500°C to 1000°C, sigma phase, chromium nitride and chromium carbide precipitation takes place. The chromium rich sigma phase has the most severe deleterious effect on the corrosion resistance and mechanical properties of duplex stainless steels. The kinetics of sigma formation are rapid and contains ferrite stabilizing elements such as Fe-Cr-Mo with traces of Si and W, which lead to the depletion of these elements in the matrix [45][46]. Prior investigations have shown that eutectoid decomposition of ferrite phase results in the formation of sigma and secondary austenite [46]. The sigma phase nucleates at the ferrite-austenite interface and then grows towards the ferrite. Hence the depletion of Cr and Mo is more pronounced in the ferrite phase due to higher diffusion rates, making it more prone to pitting corrosion in chloride containing environment. The size and amount of this intermetallic phase increases with aging time at 900°C [48]. The sigma phase is hard and brittle; hence, prolonged aging causes loss of toughness and corrosion resistance in the steel. Chemical analysis of secondary austenite lamellae has shown that it has low amount of Cr and no Mo at all. These Cr and Mo depleted zones around the sigma phase have low pitting potentials, making the passive film breakdown at these sites easier [49].As a result, the passive film of these austenite lamellae can break down locally in chloride containing corrosive environments making the steel susceptible to pitting and stress corrosion cracking. Similarly other intermetallic precipitates also affect corrosion and SCC behavior of DSS and can make the steel less resistant to pitting corrosion and stress corrosion cracking.

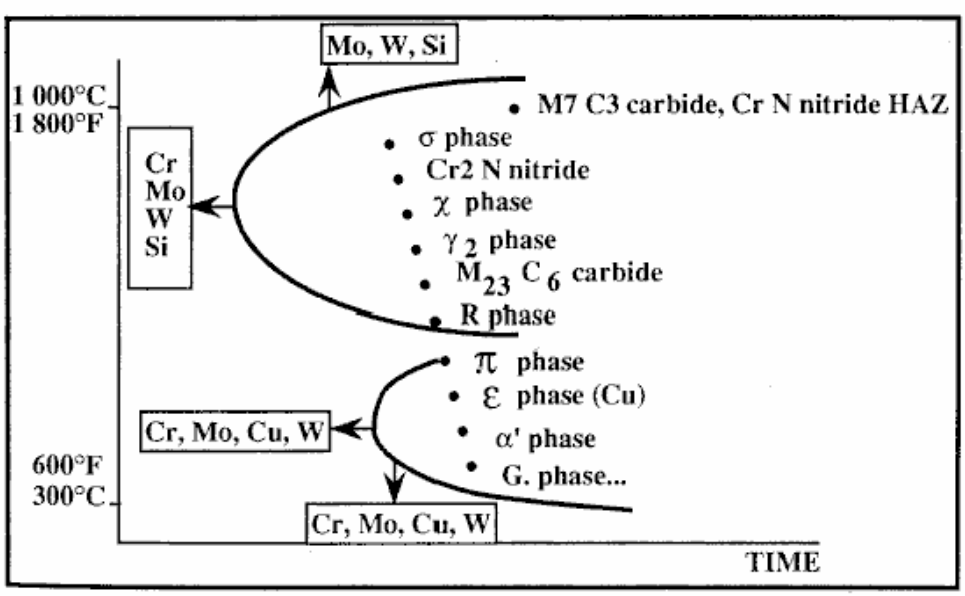

Figure 1.22. Isothermal cooling curve showing possible precipitations in DSS [9]

Carbide ($M_{23}C_6$) and Nitride (CrN and Cr_2N) precipitates form between ~500° and 1000°C in duplex stainless steels [50]. These precipitates generally nucleate along grain boundaries and ferritic-austenitic interfaces (higher energy regions) causing depletion of ferrite and austenite stabilizing elements along the boundaries. This has been shown to cause intergranular stress corrosion cracking in chloride media.

Aging at about 750°C produces χ precipitates discretely distributed along ferrite-austenite grain boundaries. This phase is rich in Mo and is unstable, hence it transforms into sigma phase with prolonged aging time, depleting the matrix of Cr and Mo and effecting pitting corrosion resistance and subsequently stress corrosion cracking resistance. Studies have shown that molybdenum is one of the most important alloying elements for pitting and crevice corrosion resistance in oxidizing and low pH environments. However, it also enhances the precipitation tendency of sigma phase at high temperature. In tungsten substituted 2205 duplex stainless steel, the ferrite and χ

phases contain large amount of tungsten, and hence they decompose into sigma phase at a much lower rate than the duplex steels containing only molybdenum [51][52].

Another deleterious effect of heat treatment in duplex stainless steel is the thermal embrittlement at 475°C [53][54]. In the temperature range of 300°-600°C, the ferrite phase decomposes spinodally into Cr-rich α' phase and a Fe-rich α phase. Spinodal decomposition takes place when alloys between the spinodal points are unstable and decomposes into two coherent phases. In this case, the ferrite phase decomposes into two coherent phases α' and α. Studies have shown that the α' phase is a body centered cubic (bcc) structure with its lattice constants being almost same as that of the ferrite matrix. Since this reaction takes place more rapidly at 475°C, this process is known as "475°C embrittlement." When duplex stainless steel is exposed to this temperature for a longer time period, the steel hardens and looses its toughness. This is the main reason why DSS are not used in high temperature process equipments operating above ~350°C - 400°C.

1.2.3.2. Thermal Effect on Microstructure of DSS during Welding

Field data have shown that some pulp mill equipments have experienced stress corrosion cracking in the welded and heat affected zone. SCC susceptibility of DSS has been attributed to the changes in the steel microstructure in the fusion zone and heat affected zone (HAZ), when the steel is subjected to certain welding operations [55]-[58] During welding, the austenitic – ferritic phase balance can be affected and can deviate from the 1:1 ratio. In the fusion zone and HAZ the base metal may experience temperatures above 1100°C where the austenite phase tends to dissolve partially or completely, depending upon the chemical composition of the alloy [59]-[61]. If the welded section undergoes rapid cooling thereby slow diffusion at lower temperatures will

favor lesser amount of austenite and more ferritic phase in DSS whereas multiple passes or resulting lower cooling rates may favor higher austenite locally in DSS.

Nitrogen has more solubility in austenite phase compared to ferrite phase. Hence, during cooling of weldments, the ferrite phase becomes supersaturated with nitrogen due to the dissolution of the austenite phase. This excess nitrogen combines with chromium to form chromium nitride precipitate [62]-[64], which nucleates at dislocations, inclusions and grain boundaries. This can result in chromium depletion in the ferrite matrix. Prior investigations have shown that Cr_2N precipitation from ferrite can induce pitting in chloride environments.

Previous work on the composition of weld metals has shown that the addition of nickel to the weld metal shifts the thermodynamic equilibrium towards a higher austenitic fraction, maintaining the phase balance of duplex stainless steel. It also raises the $(\alpha+\gamma)/\alpha$ solvus and hence the ferrite to austenite transformation during cooling of welds take place at a higher temperature [65]. Restoring the phase balance helps in improving the corrosion resistance of duplex stainless steel in chloride and acidic solutions. However, because the role of DSS microstructure on their SCC susceptibility in caustic solution was not known, it was difficult to control the heat treatment, welding process or weld metal composition to avoid fabrication related failures in caustic solutions.

1.2.4. Effect of Environment on Stress Corrosion Cracking Susceptibility of Duplex Stainless Steels

Corrosive environments play a vital role in crack initiation and growth of SCC. Generally SCC in a given environment/steel combination occurs in a specific electrochemical potential range, so the redox potential of the environment also has an

important role in overall SCC. Redox potential of the solution will change with the composition of the solution as well as by the temperature, thereby influencing SCC susceptibility. Numerous studies have been carried out to investigate stress corrosion cracking of duplex stainless steel in chloride solutions [66]-[71].

The stress corrosion cracking susceptibility of duplex stainless steel in 26wt% NaCl solution at 90°C was tested by slow strain rate tests under open circuit potential and different anodic potentials. It was observed that the critical potential for SCC coincided with the pitting potential in this environment [72]. Hence pitting was considered to be the precursor to stress corrosion cracking in chloride environments. Examination of the fractured surfaces showed selective dissolution of the ferrite phase signifying that crack propagation was due to the galvanic effect between ferrite and austenite. Selective dissolution of either austenite or ferrite phase depended on the corrosive medium to which the duplex steel is exposed and the potential of the solution.

Stress corrosion cracking susceptibility was tested in high temperature caustic solutions (30% sodium hydroxide solution at 200°C) at different strain rates [73]. It was seen that the stress corrosion susceptibility of DSS specimens increased with decreasing strain rates, while other test conditions remained identical. The addition of hydrogen sulfide to the caustic solution also increased the susceptibility of DSS to stress corrosion cracking.

The behavior of austenitic stainless steels in 300g/L of sodium hydroxide at 200°C was studied [74]. Susceptibility of austenitic stainless steels increased with the addition of sulfide ions to the caustic solution. Further, the resistance of this steel to SCC increased with increasing chromium content. The susceptibility of stress corrosion

cracking of type 304LSS in caustic solutions was found to be above 100°C, but in the presence of sulfide, SCC occurred at temperatures as low as 50°C [75]. In some studies, the mechanism of stress corrosion cracking of austenitic stainless steels in caustics and chlorides was found to be associated with dealloying of elements, selective dissolution of elements or film induced cleavage [76]-[79]. Ferritic steels, on the other hand, showed greater resistance to general corrosion and SCC in caustic environments. Open circuit potential for austenitic stainless steels moves to more cathodic potentials with an increase in temperature, and concentration of sulfides and hydroxides [80]. These changes may stabilize potential in cracking zone, making steels susceptible to SCC.

Caustic stress corrosion cracking is a major concern in the pulp and paper industry [81], where the pulp mill equipments are exposed to white liquor used in Kraft pulping process containing high concentrations of sodium hydroxide (NaOH) and sodium sulfide (Na_2S) [82]. Other pulp mill liquors also contain hydroxide and sulfides but white liquor contains the highest concentrations of caustic and sulfur containing species and hence is considered to be the most aggressive of all pulping liquors. Sulfide in high pH solutions exists mainly in hydrated form (HS^-) but also in the forms of sulfide (S^{2-}) and polysulfides [83]. In addition to this, other sulfur anions like thiosulfate ($S_2O_3^{2-}$), sulfite (SO_3^{2-}), and sulfate (SO_4^{2-}) may also be present in pulping liquors. Some of the oxidized sulfur species in white liquor such as thiosulfates and polysulfides are known to accelerate the corrosion of mild steel [84]. Wensley et al., have reported that increasing the amount of polysulfides caused an increase in the corrosion potential of mild steel in white liquor [85]. This could either lead to accelerated active corrosion of the steel over that in polysulfide free solution or cause passivation of the mild steel with a subsequent

decrease in corrosion rate depending on the amount of polysulfide present. However, thiosulfate concentration was found to enhance the magnitude of the anodic current maxima in sodium hydroxide solution [85]. Sulfite and sulfate were reported to have no effect on the corrosion rate of mild steel [85]. These species are not added intentionally to the white liquor but are formed as impurity due to air oxidation of the sulfides.

However, range of potentials and effect of environmental parameters on stress corrosion cracking of DSSs in sulfide-containing caustic solutions are not known.

1.2.5. Effect of Alloy Composition on Stress Corrosion Cracking Susceptibility of DSS

Alloy composition of DSS may affect localized corrosion as well as SCC susceptibility [86]. These effects may be either due to stability of passive film or due to microstructural changes like precipitation and phase ratios, and in turn may affect corrosion resistance. One way to quantify effect of alloy composition to localized corrosion in oxidizing chloride environments is by calculation of pitting resistance equivalent number (PREN), which takes beneficial and detrimental effects of alloying elements into account. Higher PREN suggests greater resistance to pitting corrosion. It was shown that by changing the composition of alloying elements with respect to standard duplex stainless steels, the corrosion properties could be changed. Alloying elements also affect phase ratios. It was reported that an increase in manganese content of cast steel decreased the volume fraction of austenite [87]. For example, the increase of manganese content from 0% to 0.8% decreased the volume fraction of austenite from 44% to 40%. The shape of the austenite phase also changed from round to needle shaped. On further increasing Mn content to 2%, the volume fraction of austenite was reduced to

35%, and size of austenite phase became larger and rounder than that with 0.8% Mn. There was an increase in the yield strength of the steels pertaining to the increase in the volume fraction of ferrite from 56 to 65%. The change in shape of the austenite phase also affected elongation and pitting resistance of the steel. With the evolution of needle shaped phase, the contact area between the noble austenite and the less noble ferrite increased, which led to the selective dissolution of ferrite and subsequently pitting started in chloride medium (3.5% NaCl + 5% H_2SO_4). The increase in the contact area of the ferrite and austenite phase in the alloy containing 0.8% Mn also decreased the stress corrosion cracking susceptibility of the steel. The general corrosion properties of the alloy containing 2% Mn was also inferior to that containing 0% Mn in chloride solution due to the higher volume fraction of ferrite phase. However, similar effects on corrosion and SCC in caustic solutions and sulfide containing caustic solutions are not known.

1.2.6. Residual stress and elastic-plastic behavior of duplex stainless steels

Commercially produced DSS have an inhomogeneous microstructure, hence each phase in the material will have a different response to the applied stress. Moreover, since the two phases have different coefficients of thermal expansion, thermal microstresses are introduced in DSS during cooling from an elevated temperature. In a study performed by Johansson et al. [88], the evolution of the triaxial residual stress state in commercially produced 2304 DSS was measured in-situ during uniaxial loading. The microstresses within the material may arise in various ways such as by deformation of a two-phase material with different yield points or due to difference in thermal expansion. Crystallographic texture of both phases determined from X-Ray diffraction measurements showed that the austenite phase had a more complex type of texture as

compared with the ferrite phase. To determine triaxial stress, it is necessary that the unstressed lattice parameter be accurately determined. The unstressed lattice parameters in this study were found to be a_0=3.59694 ± 0.00020 Å for austenite and a_0=2.87355 ± 0.00018 Å for the ferrite phase. The typical coefficients of thermal expansion (CTE) for the two phases as a function of temperature are shown in TABLE 1.2 [88]. Since the two phases have significantly different coefficients of thermal expansion, phase specific residual stresses are introduced because of quenching from the solution annealing temperature. The higher value of CTE of the austenite phase indicates that tensile stresses could be expected in the austenite phase and compressive stresses in the ferrite phase. The results of this study indicated that the microstresses are tensile in the austenite phase and compressive in the ferrite phase, which is in agreement with the above theory. Microstresses were also found to be higher in the transverse direction compared to the rolling direction. Highest stresses were always found in the austenite phase and the microstresses increased with an increase in the load in the macroscopic elastic regime. These microstresses became saturated when plastic deformation started to occur, and even after 2.5% of total plastic deformation, stresses were still higher in the austenite phase.

Due to the complex microstructure of DSS, a heterogeneous stress distribution is generated in the two phases. The presence of surface stress gradients may also affect the corrosion resistance of the steel [89]. The surface macrostresses are same in both the phases and vary on a scale that is large compared to the material microstructure. On the other hand, surface microstresses vary on the scale of the material microstructure and must be balanced between phases [89]. The average total stress is the sum of the surface

macrostresses and the average value of the surface microstresses. This total stress can be determined by measurements using neuron, X-ray and synchrotron X-ray. Mary et al. have performed texture analysis and surface stress analysis on 2205 (UNS S31803) duplex stainless steel using XRD measurements and compared the results with the surface stresses determined by finite-element method [89]. It is evident from their results that the stress amplitude depends on the surface preparation. Both phases were found to be under compression after polishing. However, the ferrite phase, which has lower atomic packing factor of 68% as compared to that of austenite (74%) had undergone more compression as compared to the austenite phase.

Elastic-plastic behavior of both phases was also studied by Mary et al. [89] by determining the load partitioning between the two phases under straining condition. Results showed that the austenite phase had developed tensile surface stresses under straining above 160MPa, whereas the ferrite phase was still under compression. Above 300MPa, the austenite phase was found to deform plastically, indicated by the emergence of slip steps in some grains of austenite. Surface observation of the DSS specimen (Figure 1.23) strained to 400MPa showed the presence of numerous slip bands in the austenite phase, indicating that it deforms plastically while the ferrite deforms elastically. The plastic deformation of the ferrite phase was noticed above 425MPa (Figure 1.24). The Schmid's factors for the possible deformation modes (among 48 potentially active slip systems for a body-centered cubic structure and 12 potentially active slip systems for a face-centered cubic structure) were calculated in the above study. The results indicated that the $(1\bar{1}1)\ [\bar{1}01]$ slip first operates in the austenite phase and $(10\bar{1})\ [1\bar{1}1]$ and $(01\bar{1})\ [\bar{1}11]$ first operates in the ferrite phase. According to the values of the Schmid's factor

associated with these systems, both phases are likely to undergo plasticity at roughly the same surface stress value. But as the ferrite is in a highly compressive state and the terms of the stiffness tensor are of the same order of magnitude in both phases, the applied stress necessary to reach micro-plasticity in the ferrite phase is much larger than that in the austenite phase. Hence, the austenite phase undergoes plastic deformation at an applied stress far below the yield strength of the material (at about 54% of $R_{p0.2}$) whereas the ferrite phase plastically deform at about 76% of $R_{p0.2}$.

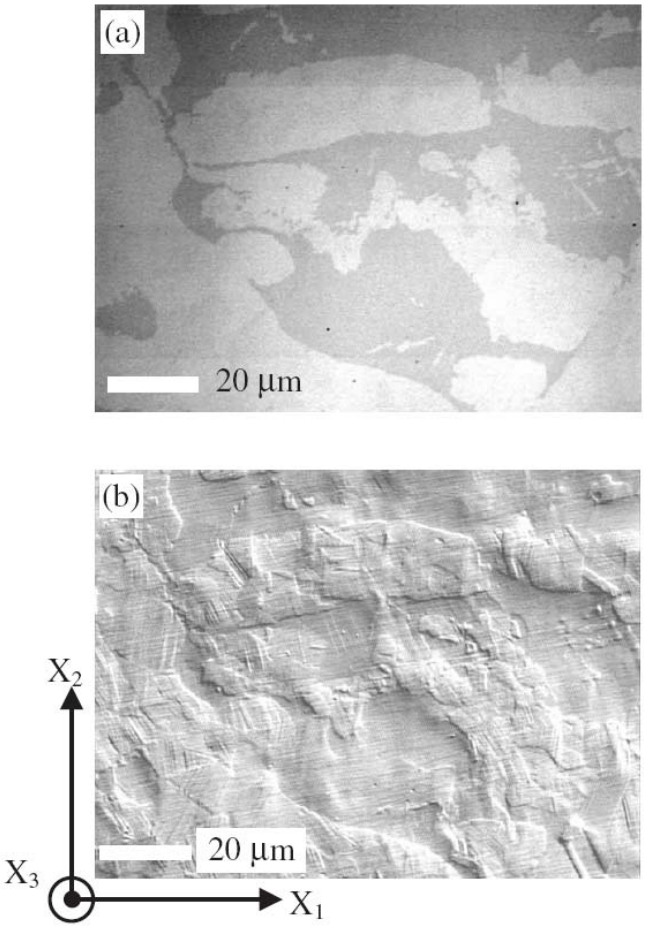

Figure 1.23. Lamellar microstructure of 2205 DSS obtained from a classical optical microscope after tensile test at 400MPa (a) bright field image (b) Differential interface contrast image showing numerous slip bands in the austenite phase which deformed plastically while the ferrite deformed elastically [89]

TABLE 1.2. TYPICAL COEFFICIENTS OF THERMAL EXPANSION (CTE)

Grades	Alloy Type	Mean CTE from 0ºC to :		
		100 ºC	315 ºC	538 ºC
Ferritic phase	445	10.4	10.8	11.2
Austenitic phase	303	17.2	17.8	18.4

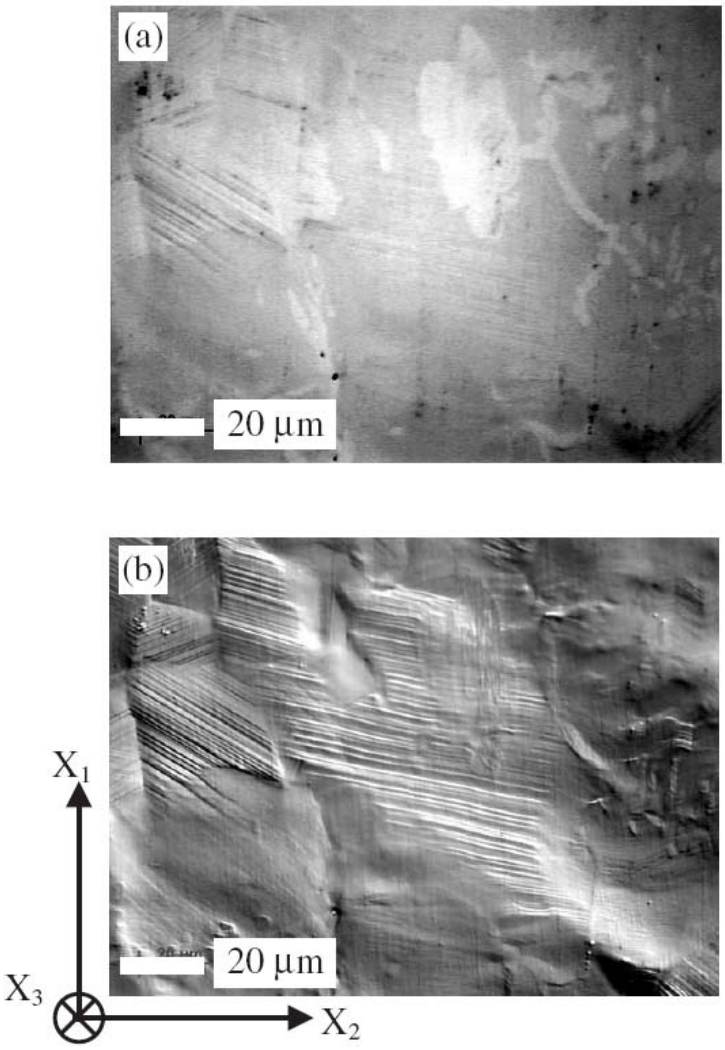

Figure 1.24. Lamellar microstructure of 2205 DSS obtained from a classical optical microscope after tensile test at 450MPa (a) bright field image (b) Differential interface contrast image showing numerous slip bands visible in both the austenite an ferrite phases [89]

The effect of residual stresses on the individual phase mechanical properties of duplex stainless steel was studied by Dakhlaoui et al. [90]. The material was UR45N containing 22.4 % chromium and 5.4% nickel. Elastic phase strains were measured axially and transversely to the applied load. The results showed a large anisotropy of the elastic and plastic properties in both austenite and ferrite phases. At the beginning of the tests, the axial elastic strains for tensile loading showed that upto about 250MPa, both the phases were below the yield point and linear elastic deformation occurred. At the threshold stress of 250MPa, a deviation from linearity appeared in the axial strain data indicating the beginning of plastic deformation in the austenite phase. Beyond 250MPa, the elastic strains of austenite reflections increased more slowly with increasing applied stress than in the elastic regime, whereas the elastic strains of the ferrite increased more rapidly. This continued upto a loading of about 500MPa, beyond which the plastic deformation of the ferrite phase occurred. The ferrite phase was found to work harden more slowly than the austenite phase. The two threshold stresses of 250MPa and 500MPa indicate the yield points of the austenite and ferrite phase respectively. In this study, it was found that the austenite phase is initially the softer phase and the critical resolved stress of ferrite is higher than that of austenite. Nevertheless, the yield stresses of the phases within duplex stainless steel are affected by both the critical resolved stresses within the crystallites and initial residual stresses present within the material. The austenite phase exhibits stronger hardening than ferrite phase [90].

In situ tensile tests were carried out with an atomic force microscope (AFM) to study the plastic deformation of an austenitic-ferritic duplex stainless steel Uranus 50® by Frechard et al [91]. The tensile tests consisted of nine deformation steps of 0.1mm

separated by pauses. Electron backscattered diffraction (EBSD) method was used to determine the crystallographic orientations of the austenite and ferrite grains in the deformed samples. After a 0.5mm elongation of the specimens, the AFM image showed that some austenite grains exhibited nearly equidistant lines, which corresponded to the intersection of active slip planes with the grain surface. After 0.6mm elongation, the slip systems in the austenite phase became well developed in all the austenite grains. Moreover, secondary slip system was found to be activated in some grains. Many austenite grains exhibited two or three kinds of slip planes and at this point, no sign of plastic deformation was detected in the ferrite grains. The global deformation corresponding to 0.6mm elongation was estimated to be about 45%. EBSD measurements at the end of the tensile test with 0.9mm elongation revealed slip lines distributed in the majority of the austenite grains and no slip lines in the ferrite phase. The activated slip planes in the austenite phase were determined from a comparison between the calculated angles and the measured angles. The active slip directions were then determined from the highest values of the Schmid factor (μ). Thus the activated slip systems for the austenite grains were identified as $(\bar{1}\bar{1}1)\,[1\bar{1}0]$ and $(111)\,[1\bar{1}0]$. Detailed AFM study, with smaller scanned areas near the phase boundaries, revealed slip traces in some ferrite grains. The existence of slip steps in the ferrite near the phase boundaries was attributed to two deformation mechanisms. The accumulation of dislocations in austenite at the austenite/ferrite grain boundary had generated dislocations in the ferrite. The slip system corresponding to this was identified as $(01\bar{1})\,[111]$ in the ferrite grain. In the other mechanism, dislocations in the austenite grains were found to shear a ferrite grain, producing slip traces in the ferrite grain.

The residual stress state of the heat affected zones (HAZ) of welded duplex stainless steel U-bend specimens was studied by Heikki et al [4]. These stresses were determined by X-ray diffraction. The entire stress state of the U-bend specimens consisted of residual and bending stresses. From the measured stresses, the macro and micro stresses in austenite and ferrite were calculated in this study. Results showed that by increasing austenite content in the HAZ, the macro residual stresses increased and the micro residual stresses in austenite and ferrite decreased and increased respectively. The variation of the austenite/ferrite phase ratio in HAZ of the U-bend welded specimens modified the macro and micro stresses. Moreover, microstresses in the austenite phase of DSS SCC specimens were high in tension and were found to decrease when the percentage of austenite in DSS increased.

1.3. SUMMARY

Stress corrosion cracking occurs under the conjoint action of tensile stresses, aggressive environment and susceptible microstructure. Microstructures of DSS may change during fabrication processes such as welding, or due to changes in the alloy composition of the steel. Microstructures may also change during different thermo-mechanical processes or due to isothermal heat treatments of localized areas of DSS equipments. In Chapter 3 of the present work, effect of welding related parameters such as different heat input, cooling rates and filler metal composition on the microstructural changes and SCC susceptibility of DSS in caustic environment has been discussed. Chapter 4 discusses the effect of different alloy composition, thermo-mechanical treatments and isothermal heat treatments on the corrosion and SCC susceptibility of DSS. Environmental conditions such as concentration of dissolved ionic species,

temperature and pH under which SCC may occur in DSS in caustic solutions has been investigated in Chapter 5. Corrosion is an electrochemical process hence knowledge of the electrochemical behavior of materials in environment is necessary for the proper understanding the corrosion and SCC mechanism. Electrochemical behavior of DSS and their alloying elements in caustic environment has been discussed in Chapter 6. In Chapter 7, the results of the above work have been used to propose a mechanism which might be responsible for the SCC of DSS in high pH caustic environment.

REFERENCES

[1] A.L.SCHAEFFLER, Metals Progress, Volume 77, Issue 2, pp. 100B, 1960.

[2] D.C.BENNETT, "Continuous Digester Cracking Task Group Reports on Past Year's Efforts," TAPPI, Volume 64, Issue 9, pp. 75-77, September 1981.

[3] H.T.LEINONEN, "Corrosion Resistance of Duplex Stainless Steel and its Welds in Modern Kraft Batch Cooking," 11th International Symposium on Corrosion in Pulp and Paper Industry, pp. 55-66, June 2004.

[4] H.T.LEINONEN, P.POHJANNE, "Stress Corrosion Cracking Susceptibility of Duplex Stainless Steels and Their Welds in simulated Cooking Environments," NACE Corrosion, Paper No.06244, March 2006.

[5] A.HARRISON, "Corrosion control offers paper mills a method of cost control," Pulp & Paper, Volume 68, Issue 10, pp. 135-137, October 2005.

[6] K.C.BENDALL, "Duplex stainless steel in the pulp and paper industry," Anti-Corrosion Methods and Material, Volume 44, Issue 3, pp. 170-173, 1997.

[7] R.BHASKARAN, N.PALANISWAMY, M.JAYACHANDRAN, M.RAGHAVAN, "Cost of corrosion/wear in indian pulp and paper industry-a case study," Corrosion Engineering, Science and Technology, Volume 40, Issue 1, pp. 75-80, 2005.

[8] P.M.SINGH, J.J.PERDOMO, J.E.OTENG, J.MAHMOOD, "Stress Corrosion Cracking and Corrosion Fatigue Cracking of a Duplex Stainless Steel in White Water Environments," Corrosion, pp. 852-861, September 2004.

[9] J.CHARLES, “The Duplex Stainless Steels: Materials to Meet Your Needs”, Duplex Stainless Steels, Vol. 1, pp. 3-48, 1991.

[10] J.E.TRUMAN, K.R.PIRT, "Properties of a Duplex (Austenitic - Ferritic) Stainless Steel and Effects of Thermal History".

[11] H.J.GRABKE, "The Role of Nitrogen in the Corrosion of Iron and Steels," ISIJ International, Volume 36, Issue 7, pp. 777-786, 1996.

[12] J.FOCT, T.MAGNIN, P.PERROT, J.B.VOGT, “Nitrogen Alloying of Duplex Stainless Steels”, Duplex Stainless Steels, Vol. 1, pp. 49-66, 1991.

[13] T.SOURMAIL, H.K.D.H.BHADESHIA, "Stainless Steels," http://www.msm.cam.ac.uk/phase-trans/2005/Stainless_steels/stainless.html, (accessed May 2005).

[14] JOHN.C.TVERBERG, "A Stainless Steel Primer:Part II," http://www.flowcontrolnetwork.com/PastIssues/sep2000/2.asp (accessed June 2006).

[15] "Intergranular Stress Corrosion Cracking," http://www.structint.com/tekbrefs/sib96139 (accessed March 2005).

[16] PIERRE R. ROBERGE, http://www.corrosion-doctors.org/Forms/scc.htm (accessed January 2005).

[17] J.S.LEWELYN LEACH, "The Possible Role of Surface Films in Stress Corrosion Cracking," NACE-5, pp. 16-20, 1977.

[18] HUGH.L.LOGAN, "The Stress Corrosion of Metals".

[19] B.D.CRAIG, R.A.LANE, "Environmentally Assisted Cracking," Amptiac Quarterly, Volume 9, Issue 1, pp. 17-24, 2005.

[20] "Stress Involved Corrosion Mechanisms," http://www.egr.uri.edu/che/course/CHE534w/chapter6stressCorrosionCracking.htm (accessed April 2006).

[21] G.S.FRANKEL, "Pitting Corrosion Of Metals, A Summary of the Critical Factors," http://www.er6.eng.ohio-state.edu/~frankel/fcc/pitreview.html (accessed July 2006).

[22] R.NISHIMURA, Y.MAEDA, "SCC Evaluation of Type 304 and 316 Austenitic Stainless Steels in Acidic Chloride Solutions Using the Slow Strain Rate Technique," Corrosion Science, Volume 46, pp. 769-785, 2004.

[23] P.Combrade, "Stainless Steels," (1993).

[24] R.N.Parkins, "Corrosion Processes," (1982).

[25] R.N.Parkins, "Stress Corrosion Cracking," NACE 10, EICM Proccedings, pp.1-19.

[26] A. Joshie, D.F.Stein, Corrosion 28(1972), p.321.

[27] E.N.PUGH, "A Post Conference Evaluation Of Our Understanding Of The Failure Mechanisms," NACE-5, pp. 37-51, 1977.

[28] L.L.Shreir,R.A.Jarman,G.T.Burstein, "Corrosion 1, Metal/Environment Reactions," Third Edition, 1994.

[29] "Metals Handbook, Ninth Edition, Volume 13, Corrosion," ASTM International Handbook Committee, 1987.

[30] F.P.FORD, “The Crack-Tip System and Its relevance to the Prediction of Cracking in Aqueous Environments”, NACE 10, EICM Proccedings, pp.139-165.

[31] K.Sieradzki, R.C.Newman, Phil. Mag. A51, pp.95-132 (1985).

[32] C.Edeleanu, A.J.Forty, Phil. Mag. 5, p.1029 (1960).

[33] R.C.Newman, K. Sieradzki, Scripta Metall. 17(1983): p.621.

[34] R.C.NEWMAN, A.MEHTA, " Stress Corrosion Cracking of Austenitic Stainless Steels,", NACE 10, EICM Proccedings, pp.489-509.

[35] Russell H. Jones, "Stress Corrosion Cracking," ASM International, Materials Park, Ohio 44073.1992.

[36] K.SIERADZKI, "Atomistic and Micromechanical Modeling Aspects of Environment Induced Cracking of Metals ," NACE 10, EICM Proccedings, pp.125-137.

[37] Z.SZKLARSKA-SMIALOWSKA, "Various forms of localized corrosion common features and differences," NACE-5, pp. 30-36, 1977.

[38] S.ATAMERT, J.E.KING, "Elemental Partitioning and Microstructural Development in Duplex Stainless Steel Weld Metal," Acta Metallica, Volume 39, Issue 3, pp. 273-285, 1991.

[39] G.S.REIS, A.M.JORGE JR., O.BALANCIN, "Influence of the Microstructure of Duplex Stainless Steels on their Failure Characteristics During Hot deformation," Materials Research, Volume 3, Issue 2, April 2000.

[40] H.Y.LIOU, R.I.HSIEH, W.T.TSAI, "Microstructure and Stress Corrosion Cracking in Simulated Heat-affected Zones of Duplex Stainless Steels," Corrosion Science, Volume 44, 2002, pp. 2841-2856.

[41] T.AMADOU, A.BEN RHOUMA, H.SIDHOM, C.BRAHAM, J.LEDION, "Influence of Thermal Aging on the Reactivity of Duplex Stainless Steel Surfaces," Metallurgical and Materials Transactions A, Volume 31A, pp. 2000-2015.

[42] T.H.CHEN, K.L.WENG, J.R.YANG, "The Effect of High-temperature Exposure on the Microstructural Stability and Toughness Property in a 2205 Duplex Stainless Steel," Materials Science and Engineering A, Volume 338, pp. 259-270, 2002.

[43] K.L.WENG, T.H.CHEN, J.R.YANG, "The High-Temperature and Low-Temperature Aging Embrittlement in a 2205 Duplex Stainless Steel," Bulletin of the College of Engineering, Issue 89, October 2003.

[44] B.JOSEFSSON, J.O.NILSSON, A.WILSON, " Phase Transformations in Duplex Stainless Steels and the relation Between Continuous Cooling and Isothermal Heat Treatment ",Duplex Stainless Steels, Vol. 1, pp. 67-78, 1991.

[45] Y.S.SATO, H.KOKAWA, "Preferential Precipitation Site of Sigma Phase in Duplex Stainless Steel Weld Metal," Scripta Materialia, Volume 40, Issue 6, pp. 659-663, 1999.

[46] I.ZUCATO, M.C.MOREIRA, I.F.MACHADO, S.M.G.LEBRAO, "Microstructural Characterization and the Effect of Phase Transformations on Toughness of UNS

31803 Duplex Stainless Steel Aged Treated at 850C," Materials Research, Volume 5, Issue 3, July/September 2002.

[47] D.Y.KOBAYASHI, S.WOLYNEC, "Evaluation of the Low Corrosion Resistant Phase Formed During the Sigma Phase Precipitation in Duplex Stainless Steels," Materials Research, Volume 2, Issue 4, October 1999.

[48] C.S.HUANG, C.C.SHIH, ""Effects of Nitrogen and High Temperature Aging on "σ" phase Precipitation of Duplex Stainless Steels"," Materials Science and Engineering A, Volume 402, pp. 66-75, 2005.

[49] S.S.M. TAVARES, M.R.DA SILVA, J.M.NETO: Journal of Alloys and Compounds, 2000, vol. 313, pp.168-173.

[50] A.J.RAMIREZ, J.C.LIPPOLD, S.D.BRANDI, “The Relationship Between Chromium Nitride and Secondary Austenite Precipitation in Duplex Stainless Steels,” Metallurgical and Materials Transactions A, Volume 34, pp. 1575-1598, 2003.

[51] Y.S.AHN, J.P.KANG, “Effect of Aging Treatments on Microstructure and Impact Properties of Tungsten Substituted 2205 Duplex Stainless Steel,” Materials Science and Technology, Volume 16, pp. 382-388, April 2000.

[52] K.Y.Kim, P.Q.Zhang, T.H.Ha, Y.H.Lee, “Electrochemical and Stress Corrosion Properties of Duplex Stainless Steels Modified with Tungsten Addition,” NACE Corrosion, (1998).

[53] F.IACOVIELLO, F.CASARI, S.GIALANELLA, “Effect of ‘475C Embrittlement’ on Duplex Stainless Steels Localized Corrosion Resistance”, Corrosion Science, 2004.

[54] S.S.M.TAVARES, R.F.DE NORONHA, M.R.DA SILVA, J.M.NETO, S.PAIRIS, “475C Embrittlement in a Duplex Stainless Steel UNS S31803,” Materials Research, Volume 4, Issue 4, October 2001.

[55] C.A.CLARK, P.GUHA, "Welding Characteristics of Duplex Steels,” pp. 631-648.

[56] J.D.KORDATOS, G.FOURLARIS, G.PAPADIMITRIOU, "The Effect of Cooling Rate on the Mechanical and Corrosion Properties of SAF 2205 (UNS 31803) Duplex Stainless Steel Welds," Scripta Materialia, Volume 44, pp. 401-408, 2001.

[57] RALPH DAVISON, "Duplex stainless steels-fabrication and welding," TAPPI journal, Volume 83, Issue 9.

[58] T.A.PALMER, J.W.ELMER, JOE WONG, "In-Situ Observations of Phase Transformations in HAZ of 2205 Duplex Stainless Steel Weldments,” pp. 1-10, August 2005.

[59] D.E.NELSON, W.A.BAESLACK III, J.C.LIPPOLD, "Characterization of the Weld Structure in a Duplex Stainless Steel Using Color Metallography," Materials Characterization, Volume 39, pp. 467-477, 1997.

[60] V.MUTHUPANDI, P.BALA SRINIVASAN, V.SHANKAR, S.K.SESHADRI, S.SUNDARESAN, "Effects Nickel and Nitrogen Addition on the Microstructure and Mechanical Properties of Power Beam Processed Duplex Stainless Steel (UNS 31803) Weld Metals," Materials Letters, Volume 59, pp. 2305-2309, 2005.

[61] D.E.NELSON, W.A.BAESLACK III, J.C.LIPPOLD, "Characterization of the Weld Structure in a Duplex Stainless Steel Using Color Metallography," Metallography, Volume 18, pp. 215-225, 1985.

[62] H.Y.LIOU, R.I.HSIEH, W.T.TSAI, "Microstructure and Pitting Corrosion in Simulated Heat-affected Zones of Duplex Stainless Steels," Materials Chemistry and Physics, Volume 74, pp. 33-42, 2002.

[63] T.H.CHEN, J.R.YANG, "Microstructural Characterization of Simulated Heat Affected Zone in a Nitrogen-containing 2205 Duplex Stainless Steel," Materials Science and Engineering A, Volume 338, pp. 166-181, 2002.

[64] T.G.GOOCH, " Corrosion Resistance of Welds in Duplex Stainless Steels", Duplex Stainless Steels, Vol. 1, pp. 325-346, 1991.

[65] V.MUTHUPANDI, P.BALA SRINIVASAN, S.K.SESHADRI, S.SUNDARESAN, "Effect of Weld Metal Chemistry and Heat Input on the Structure and Properties of Duplex Stainless Steel Welds," Materials Science and Engineering A, Volume 358, pp. 9-16, 2003.

[66] H.S.KWON, H.S.KIM, "Investigation of Stress Corrosion Susceptibility of Duplex (a+g) Stainless Steel in a Hot Chloride Solution," Materials Science and Engineering A, Volume 172, pp. 159-166, 1993.

[67] R.OLTRA, A.DESESTRET, E.MIRABAL, J.P.BIZOUARD, "The Stress Corrosion Cracking of Duplex Stainless Steels in Environments Containing Chlorides and H2S. Study of the Ferrite Phase Behavior," Corrosion Science, Volume 27, Issue 10-11, pp. 1251-1269, 1987.

[68] M.PUIGGALI, D.DESJARDINS, L.AJANA, "A Critical Study of Stress Corrosion Craking Testing Method for Stainless Steels in Hot Chloride Media," Corrosion Science, Volume 27, Issue 6, pp. 585-594, 1987.

[69] C.M.TSENG, W.T.TSAI, "Environmentally Assisted Cracking Behavior of Single and Dual Phase Stainless Steels in Hot Chloride Solutions," Materials Chemistry and Physics, Volume 84, pp. 162-170, 2004.

[70] C.M.TSENG, H.Y.LIOU, W.T.TSAI, "The Influence of Nitrogen Content on Corrosion Fatigue Crack Growth Behavior of Duplex Stainless Steel," Materials Science and Engineering A, Volume 344, pp. 190-200, 2003.

[71] W.T.TSAI, S.L.CHOU, "Environmentally Assisted Cracking Behavior of Duplex Stainless Steel in Concentrated Sodium Chloride Solution," Corrosion Science, Volume 42, pp. 1741-1762, 2000.

[72] W.T.TSAI, M.S.CHEN, "Stress Corrosion Cracking Behavior of 2205 Duplex Stainless Steel in a Concentrated NaCl Solution," Corrosion Science, Volume 42, pp. 545-559, 2000.

[73] G.RONDELLI, B.VINCENTINI, E.SIVIERI, "Stress Corrosion Cracking of Stainless Steels in High Temperature Caustic Solutions," Corrosion Science, Volume 39, Issue 6, pp. 1037-1049, 1997.

[74] G.RONDELLI, B.VINCENTINI, "Susceptibility of Highly Alloyed Austenitic Stainless Steels to Caustic Stress Corrosion Cracking," Materials and Corrosion, Volume 53, pp. 813-819, 2002.

[75] P.M.SINGH, O.IGE, J.MAHMOOD, "Stress Corrosion Cracking of Type 304L Stainless Steel in Sodium sulfide-Containing Caustic solutions," Corrosion, Volume 59, Issue 10, pp. 843-850, 2003.

[76] W.J.NISBET, G.W.LORIMER, R.C.NEWMAN, "A Transmission Electron Microscopy Study of Stress Corrosion Cracking in Stainless Steel," Corrosion Science, Volume 35, Issue 1-4, pp. 457-469, 1993.

[77] J.DEAKIN, Z.DONG, B.LYNCH, R.C.NEWMAN, "De-alloying of Type 316 Stainless Steel in Hot Concentrated Sodium Hydroxide Solution," Corrosion Science, Volume 46, pp. 2117-2133, 2004.

[78] J.X.LI, W.Y.CHU, Y.B.WANG, L.J.QIAO, "In Situ TEM Study of Stress Corrosion Cracking of Austenitic Stainless Steel," Corrosion Science, Volume 45, pp. 1355-1365, 2003.

[79] R.NISHIMURA, Y.MAEDA, "Metal Dissolution and Maximum Stress During SCC Process of Ferritic (type 430) and austenitic (type 304 and type 316) Stainless Steels in Acidic Chloride Solutions Under Constant Applied Stress," Corrosion Science, Volume 46, pp. 755-768, 2004.

[80] P.M.SINGH, J.MAHMOOD, P.CONDE, "Stress Corrosion Cracking and Corrosion Susceptibility of Duplex Stainless Steels in Caustic Solutions," Corrosion, 2005.

[81] CASIMIR SVENSSON, MARTTI PULLIAINEN, MARTTI HUTTUNEN, PASI NIEMELAINEN, “Corrosion and corrosion prevention of digesters operating with modern cooking processes”, 2005 TAPPI Engineering, Pulping, Environmental Conference, Philadelphia, PA, USA, August 28-31, (2005).

[82] D.L.SINGBEIL, A.GARNER, “Electrochemical and stress corrosion cracking behavior of digester steels in kraft white liquors”, NACE Corrosion 84, New Orleans, Louisiana, USA, April 2-6, (1984).

[83] J.RAMO, M.SILLANPAA, A.KUJALA, O.HYOKYVIRTA, S.PELTONEN, "Interactions of sulphur anions and stainless steels at kraft pulp digesting temperature," Materials and Corrosion, Volume 52, pp. 531-539, 2001.

[84] LEE PETERMAN, RONALD A.YESKE, “Thiosulfate effects on corrosion in kraft white liquor”, IPC technical paper series; no.205, Appleton, Wisconsin: the Institute, Georgia Institute of Technology, (1986).

[85] D.A.WENSLEY, R.S.CHARLTON, "Corrosion studies in kraft white liquor: Potentiostatic polarization of mild steel in caustic solutions containing sulfur species," Corrosion, Volume 36, 8, pp. 385-389, (1980).

[86] R.MERELLO, F.J.BOTANA, J.BOTELLA, M.V.MATRES, M.MARCOS, "Influence of Chemical Composition on the Pitting Corrosion Resistance of Non-standard Low-Ni High-Mn-N Duplex Stainless Steels," Corrosion Science, Volume 45, pp. 909-921, 2003.

[87] Y.H.JANG, S.S.KIM, J.H.LEE, "Effect of Different Mn Contents on Tensile and Corrosion Behavior of CD4MCU Cast Duplex Stainless Steels," Materials Science and Engineering A, Volume 396, pp. 302-310, 2005.

[88] J.JOHANSSON, M.ODEN, X.H.ZENG, Acta Mater. Volume 47, 9, pp. 2669-2684, 1999.

[89] N.MARY, V.VIGNAL, R.OLTRA, L.COUDREUSE, Philosophical Magazine, Volume 85, pp. 1227-1242, 2005.

[90] R.DAKHLAOUI, A.BACZMANSKI, C.BRAHAM, S.WRONSKI, K.WIERZBANOWSKI, E.C.OLIVER, Acta Materialia, Volume 54, pp.5027-5039, 2006.

[91] S.FRECHARD, F.MARTIN, C.CLEMENT, J.COUSTY, Materials Science and Engineering A. Volume 418, pp. 312-319, 2006.

CHAPTER 2

PROJECT DESCRIPTION

2.1 RESEARCH OBJECTIVE

Microstructure of alloys plays a vital role in the corrosion behavior and stress corrosion cracking (SCC) susceptibility in a given environment. Significant amount of research has been published on the corrosion and SCC behavior of duplex stainless steels (DSS) in chloride environments and to relate the DSS microstructure (or composition and heat treatment effects) and environmental effects to these degradation mechanisms. A recent report described failure of DSS (2205) equipment in high temperature caustic environments due to stress corrosion cracking. However, SCC mechanism for DSS in caustic solutions, especially the sulfide containing caustic solutions, in the absence of chlorides is not known. So the primary objective of this project was:

1. To determine the effect of DSS microstructure on SCC susceptibility in sulfide containing caustic solutions: Different grades of DSSs with varying alloy compositions may have different microstructure (ferrite/austenite ratio, grain morphology and intermetallic precipitation). Differences in the composition and microstructure may influence their resistance to localized corrosion and SCC. Therefore, this objective addressed the effect of alloy composition on microstructure and on SCC susceptibility of DSS alloys in sulfide-containing caustic solutions. Different heat-treatment parameters (annealing temperatures,

cooling rates and aging temperatures) also affect the DSS microstructure (i.e.ferrite/austenite ratio, grain morphology and intermetallic precipitation). Hence, the effect of heat treatment on SCC susceptibility of DSS in sulfide-containing caustic solutions was studied.

2. To study the effect of environmental parameters on SCC susceptibility of DSSs: Temperature effects on SCC susceptibility of DSS were studied. Stress corrosion cracking susceptibility is also affected by the pH and concentration of caustic solutions. Hence, the effects of these parameters on SCC susceptibility of DSS were also explored.

3. To determine the electrochemical conditions for SCC initiation and propagation in DSS in sulfide-containing caustic solutions: Depending on the underlying mechanism, SCC occurs in a certain, relatively narrow, potential range [1]-[2]. This range is generally associated with unstable passivity or the potential range where active-passive transition takes place. The aim of the present work was to study the electrochemical behavior of DSS in sulfide-containing caustic solutions and relate it to the conditions under which SCC is possible in these environments.

4. To investigate the SCC mechanism for DSS in caustic environments and validate it: Specific DSS phases have selective SCC susceptibility in different environments. Therefore, DSS microstructure with continuous susceptible

phase may aid in crack propagation, whereas, the crack growth may be arrested by the continuous non-susceptible phase in DSS. Prior work suggests that austenitic stainless steels are more susceptible to caustic stress corrosion cracking than ferritic steels with equivalent chromium content [3]-[10]. Based on this, a hypothesis was proposed which states that:

a. Duplex stainless steels may have different mechanisms of crack initiation and propagation in the two different environments, caustic solutions, and chlorides.
b. The austenite phase in DSS specimens will be more susceptible to stress corrosion crack initiation and propagation in caustic solutions.

Effect of heat treatment and composition on microstructure and SCC susceptibility of DSS and environmental effects on electrochemical condition of SCC were used to propose an overall mechanism.

2.2 EXPERIMENTAL PROCEDURES

To study stress corrosion cracking susceptibility of DSSs in sulfide-containing caustic solutions, the following experimental procedures were carried out:

2.2.1. Heat Treatment of DSS

Austenite to ferrite ratio in DSSs depends on the alloy composition, annealing temperatures, and cooling rates. Slower cooling rates promote higher austenite fraction and faster cooling rates promote higher ferrite fraction. Intermetallic precipitates with different composition can also form in DSS at different aging temperatures. Selected grades of DSSs (S32205 and S32101), with compositions listed in TABLE 2.1 were

machined out of rolled plates into small sections measuring 12 mm × 10 mm × 10 mm. These samples were subjected to different heat treatments to see the effect resulting microstructure (ferrite/austenite ratio, intermetallic precipitation and grain morphology) on the general and localized corrosion behavior in caustic and chloride solutions. Heat treatments were carried out in a horizontal tube furnace. All heat treatments were performed in an inert environment of argon to prevent oxidation.

The annealing temperatures for S32101 were 1000°C or 1100°C and for S32205 were 1000°C or 1150°C respectively. Annealing treatment included exposing the sample to the annealing temperature for one hour followed by water quenching. After annealing treatments, aging treatments were given to the annealed specimens either at 475°C (for 4 hrs) or 600°C (for 4 hrs) or 800°C (for 1hr, 4hrs, or 8hrs) followed by water quenching. TABLE 2.2 summarizes the different heat treatments given to the S32101 and S32205 samples and the specimen codes for each heat-treated sample used throughout this thesis. In each specimen-code, D1 and D5 represent 2101 and 2205 DSS respectively. First number, 1000°C, 1100°C and 1150°C represents annealing temperatures. Whereas, second number 475°C, 600°C and 800°C refers to aging temperatures.

TABLE 2.1. NOMINAL COMPOSITION OF DIFFERENT DSS GRADES USED IN THIS STUDY

Steel Grade	Composition (wt. Percent)									
Common Trade Name	UNS Number	C	Mn	S	Ni	Cr	Mo	N	Cu	Fe
2205	S32205	0.02	—	—	5.7	22	3.1	0.17	—	Balance
LDX-2101®	S32101	0.03	5	—	1.5	21.5	0.3	0.22	—	Balance
2304	S32304	0.029	1.3	0.001	4.1	22.5	0.2	0.12	0.2	Balance
AL-2003®	S32003	0.03	2.00	0.02	3.00	19.5	1.5	0.14	—	Balance
Iron			_	_	_	_	_	_	_	99.9
Chromium			_	_	_	99.97	_	_	_	_
Nickel			_	_	99.6	_	_	_	_	_
Molybdenum			_	_	_	_	99.9	_	_	_

TABLE 2.2. S32205 and S32101 WITH DIFFERENT HEAT TREATMENTS

Code for 2205 Samples	Code for 2101 Samples	Annealing Temperature °C	Cooling	Aging Temperature °C	Aging time (hrs)
D5-1000-WQ	D1-1000-WQ	1000	water quench	-	-
D5-1000-WQ-475	D1-1000-WQ-475	1000	water quench	475	4
D5-1000-WQ-600	D1-1000-WQ-600	1000	water quench	600	4
D5-1000-WQ-800	D1-1000-WQ-800	1000	water quench	800	1
	D1-1100-WQ	1100	water quench	-	-
	D1-1100-WQ-475	1100	water quench	475	4
	D1-1100-WQ-600	1100	water quench	600	4
	D1-1100-WQ-800	1100	water quench	800	4
D5-1150-WQ		1150	water quench	-	-
D5-1150-WQ-475		1150	water quench	475	4
D5-1150-WQ-600		1150	water quench	600	4
D5-1150-WQ-800		1150	water quench	800	1

Percentage ferrite content in the heat-treated DSS samples was quantified in terms of ferrite number, measured using a Feritscope.

2.2.1.1. Metallography and XRD

Heat-treated samples were polished and etched in 40% NaOH solution to reveal the ferrite/austenite phases. Area fraction of the ferrite and the austenite phases was quantified using image analysis. Differently heat treated DSS samples were also etched in Groesbeck test solution [11] to reveal the precipitates formed due to aging treatments at 800°C and 600°C. Micrographs were taken using an optical microscope. Etched samples were further characterized using a scanning electron microscope (SEM) equipped with an energy dispersive x-ray spectroscope (EDS). The incoming energy of the EDS electron beam was 15 KV. Groesbeck solution does not affect the austenite and ferrite phases but the sigma phase was revealed as grey and black areas [11].

Phases present in the heat-treated DSS specimens were also characterized by using X-Ray Diffraction (PW 1800 X-ray diffractometer, Philips, USA) with Cu-Kα radiation and X'Pert PRO MRD X-ray diffractometer, PANalytical with Cu-Kα radiation.

2.2.1.2. Mechanical Testing Using Nanoindentation and Vicker's Hardness Method

Heat treatment changes the microstructure of DSS as well as the mechanical properties of each phase. Hence nanoindentation technique was employed to evaluate the effect of various heat treatments on the nano-hardness (H) of the ferrite and austenite phase. MTS Nanoindenter XP (MTS Nano Instruments, Oak Ridge, TN) equipped with a Berkovich shaped diamond tip was used to get the load-displacement curves from which the mechanical properties could be extracted. The tests were conducted by displacement

control method on metallographycally mounted and polished heat treated samples with a depth limit of 1000nm. The samples were etched prior to testing to reveal the ferrite and austenite phases. The poissons ratio of each phase was assumed to be 0.3 and the surface approach velocity was 10nm/sec.

Vicker's hardness measurements were used to find the relative micro-hardness of the ferrite and austenite phases in the heat treated DSS samples. The results were further compared with the relative nano-hardness values of the ferrite and austenite phases. A Buehler micro-hardness tester was used to measure the vicker's hardness of the austenite and the ferrite phases. A force of 25gf was used for the experiments.

2.2.2. Testing for General Corrosion and Pitting Corrosion Susceptibility

2.2.2.1. General and Pitting Corrosion Tests of Heat Treated DSS

The heat-treated DSS samples were subjected to corrosion tests to study the effect of microstructure on the general and localized corrosion susceptibility of 2101and 2205 DSS samples. Samples were weighed and their initial surface areas were measured. After cleaning with acetone, the samples were exposed to a sulfide-containing caustic solution (white liquor used in the pulping process) with composition of 150g/L NaOH + 50g/L $Na_2S.9H_2O$, in an autoclave at 170 °C for 15 days. Precautions were taken to avoid any contact between the test samples and the autoclave to avoid any galvanic effects. The samples were placed on a Polytetrafluoroethylene (PTFE) plate and the side facing the bottom of the autoclave was marked to keep track of possible crevice conditions. At the completion of test, the samples were washed, and examined for any visual signs of corrosion. The samples were then cleaned with the Clarke's solution to remove corrosion products. Final weight of each sample was measured and used to calculate the rate of

general corrosion for each sample. It was confirmed that the Clarke's solution did not attack the base DSS metal during cleaning time or affect the final weight measurements.

Another set of heat-treated samples were subjected to exposure tests in a chloride solution. This was done to compare the relative corrosion resistance of DSSs in the two environments (high pH and low pH). Exposure tests in the chloride solution were performed according to the ASTM G48 standard where the chloride solution was prepared by dissolving 100gm of reagent grade ferric chloride, $FeCl_3.6H_2O$ in 900ml of water (about 6% $FeCl_3$ by mass). The samples were exposed in the chloride solution at room temperature (27°C) for 96hours. After the test, the samples were cleaned, weighed and the surface of these samples was analyzed for pitting or crevice corrosion.

2.2.3. Testing for Stress Corrosion Cracking Susceptibility

2.2.3.1. Slow Strain Rate Test

Stress corrosion cracking susceptibility of different DSS samples was tested by slow strain rate tests (SSRT). These tests are also known as constant extension rate tests (CERT). Dimensions of a typical tensile sample used for SSRT are shown in Figure 2.1. All the work was carried out with tensile samples parallel to the rolling direction of plate.

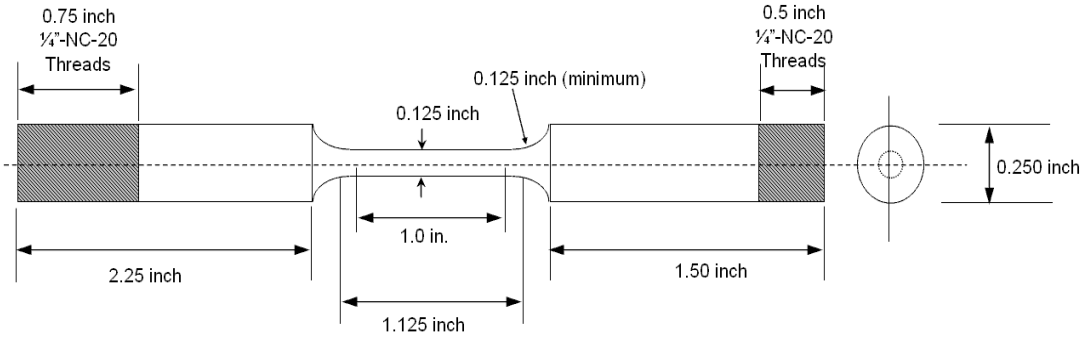

Figure 2.1. A typical slow strain rate specimen showing the gage length and the gage diameter.

The gage length of each tensile specimen was polished to 1000 grit paper finish and cleaned with acetone before using them for SSRT. These specimens were then uniaxially loaded in a modified slow strain rate testing machine with autoclave in an environment containing sulfide-containing caustic solution at 170°C and 200°C under high pressure. Figure 2.2 shows the schematic of the slow strain rate test rig equipped with the autoclave. Figure 2.3 shows the slow strain rate test setup used for the tensile tests. Constant temperature was maintained inside the autoclave throughout these tests. The specimens were then subjected to an initial strain rate of $2x10^{-6}$ s^{-1} and loaded until fracture occurred. Samples were electrically isolated from the test rig by use of ceramic washers. All slow strain rate tests in this study were carried out under open circuit potential. Identical specimens were also subjected to slow strain rate tests in the absence of environment (white liquor) for comparison. Stress-strain curves were obtained from each test. The percentage elongation, the percentage reduction in gage area, the maximum load achieved during SSRT, and the area under the stress strain curve were calculated. This helped to quantify the decrease in ductility and the change in mechanical properties of DSS in the presence of environment and stresses.

Electrochemical potential under open circuit conditions was measured by using an external reference electrode (mostly a saturated calomel electrode). Open circuit potential of SSRT samples was compared with the potentiodynamic polarization data to understand the electrochemical reactions and overall mechanisms involved in SCC of DSS in caustic solutions.

After the test was over, one half of the fractured tensile sample were mounted, polished and electroetched in 40% NaOH solution and examined under an optical

microscope to see the crack morphology and to measure the crack length. Optical microscope was used to study the microstructure and to identify the mode of cracking (intergranular or transgranular or mixed mode) and the point of initiation of cracks (ferrite/austenite phase, grain boundaries). The length of the deepest crack in each specimen was measured and was used to calculate the maximum crack velocity in mm/sec. Fractured surfaces were examined using Scanning Electron Microscope (SEM) to examine the mode of fracture while EDS was used to obtain chemical composition of local areas of the fractured surface and phase composition.

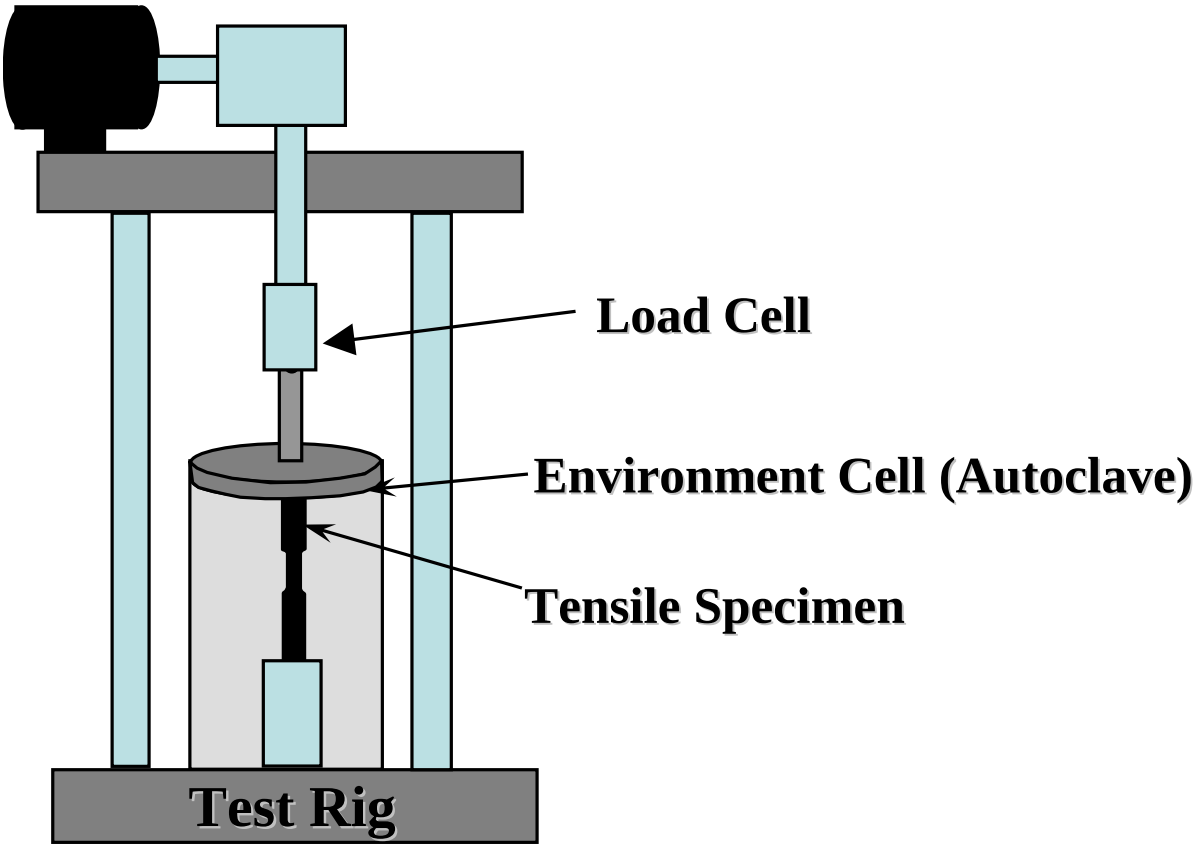

Figure 2.2. Schematic of slow strain rate test setup for high temperature tensile tests (≥ 120ºC)

Figure 2.3. Slow strain test rig with autoclave for high temperature SSRT

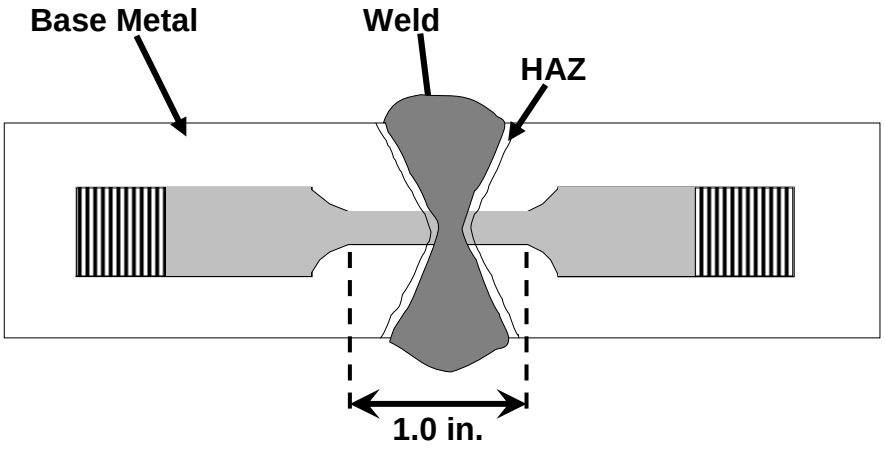

Figure 2.4. Schematic showing welded DSS bar and tensile specimens made out of the welded bar

2.2.3.2. Slow Strain Rate Tests for SCC Susceptibility of Simulated Welded DSS

The susceptibility of DSS grades to SCC can be mainly attributed to the various heating processes involved during the manufacturing of industrial equipments, especially welding. During welding, the heating cycles may affect the dual microstructure (ferrite/austenite ratio) of the steel, making it more prone to cracking in aggressive environments. Hence, the effect of welding on DSS microstructure and the effect of this microstructure on the SCC susceptibility of the steel in caustic environment was investigated through slow strain rate tests of welded specimens.

To investigate the effect of welding parameters on SCC of DSS under simulated pulp mill conditions, welded duplex stainless steel bars with different compositions and filler materials were used in the lab study. The welding procedure used to prepare these test samples was done in accordance to standard EN1011-1. Flux cored arc welding (FCAW) and submerged arc welding (SAW) procedures used in this standard were in accordance with the process numbers 136 and 121, respectively. These welding methods were chosen as they are commonly used in manufacturing process of pulping equipments. SAW procedure was chosen to imitate the welding procedure used for the manufacturing of the white liquor accumulator.

Tensile test samples for slow strain rate test (SSRT) were machined out of the welded DSS bars. The chemical composition (in wt %) of the base material and weld consumables of the white liquor accumulator are presented in TABLE 2.3. Specimens were made such that the composition of the weld metal and base metal were very similar to that of the white liquor accumulator. The tensile samples had a gage length of 25.4mm and a gage diameter of ~3.175mm. Samples were machined such that at least one edge of

the weld was in the middle of the gage (Figure 2.4). The welding methods and chemical compositions of the tensile specimens and the specimen codes are presented in TABLE 2.4. L and H in the specimen codes represent low chromium and high chromium filler metal respectively. Whereas, h and u denote welding in horizontal and upright positions respectively.

TABLE 2.3. CHEMICAL COMPOSITION (IN WT %) OF WELDED WHITE LIQUOR ACCUMILATOR SHELL PLATE

Steel Grade	Specimen Code	Composition				
		Mn	Ni	Cr	Mo	Fe
S31803 DSS	Base Metal	1.8	5.4	22.8	3.0	67
	Weld Metal	1.00	9.75	22.54	3.21	63.46

TABLE 2.4. CHEMICAL COMPOSITION (IN WT %) OF EXPERIMENTAL WELDED BARS USED TO PREPARE TENSILE SAMPLES USED IN THIS STUDY

Steel Grade	Welding Method	Specimen Code	Composition							
			C	Mn	S	Ni	Cr	Mo	N	Cu
S31803 DSS Base Metal			0.027	1.8	0.001	5.1	22.6	2.5	0.16	0.2
DSS Filler	FCAW	2205-Lh	0.04	0.9	0.015	9.0	22.0	3.0	0.15	
DSS Filler	FCAW	2205-Lu	0.04	0.9	0.015	9.0	22.0	3.0	0.15	
DSS Filler	FCAW	2205-Hh	0.04	0.9		9.0	25.0	4.0	0.24	
DSS Filler	FCAW	2205-Hu	0.04	0.9		9.0	25.0	4.0	0.24	
DSS Filler	SAW	2205-SAW	0.02	1.5		9.0	23.0	3.0	0.15	

The effect of different heating and cooling cycles on the phase balance of welded DSS was studied by measuring the Ferrite numbers for each weld, heat affected zone and base metal. This was done using Feritscope®. Ferrite numbers gave the volume fraction of ferrite and austenite in each welded specimen. To verify the phase ratio differences, measurements were also done by image analysis, where the ferrite to austenite area ratios was quantified. Subsequent to this, small samples of the weld and heat affected zones were cut from the bars. These samples were mounted, polished and etched to reveal their microstructure, austenite-ferrite phase distribution and grain size in differently heat treated parts of welded samples. Image analysis was also used to measure the area fraction of ferrite and austenite in weld and HAZ of each specimen.

After quantifying phase ratios and performing metallography, specimens were prepared for slow strain rate tests to study their SCC susceptibility. The slow strain rate tests were performed according to procedure mentioned in Section 2.2.3.1.

2.2.3.3. Slow Strain Rate Tests for SCC Susceptibility of Heat Treated DSS

Tensile samples were machined out of S32205 rolled plates. These tensile samples had a gage length of 25.4mm and a gage diameter of ~3.175mm, as shown in Figure 2.1. S32205 tensile specimens were differently heat-treated to change their microstructure. A summary of the heat treatments given to tensile specimens are provided in TABLE 2.2. Slow strain rate tests of the heat-treated 2205 DSS samples were carried out according to procedure mentioned in Section 2.2.3.1.

2.2.4. Tests to Evaluate Role of Alloy Composition and Environment (Ionic Species, Temperature) on General Corrosion and SCC Susceptibility of DSS

Alloy composition plays an important role in corrosion and SCC. Different grades of DSS with varying alloy composition may be susceptible to general corrosion and stress corrosion cracking to different extent. In addition, varying the temperature and concentration of caustics and sulfides may affect the susceptibility of these steels to SCC differently. Hence to study the effect of alloy composition, temperature and varying ionic species, tests were performed with different grades of DSS (S32205, S32304, S32101, and S32003) varying in composition. The nominal compositions of the material tested in this study are shown in TABLE 2.1.

2.2.4.1. Coupon Exposure Tests for General Corrosion Susceptibility

Samples for the corrosion tests were machined from rolled plates. Corrosion exposure specimens were machined into coupons measuring (2.5 cm x 5.1 cm). The initial weight and surface area of each coupon was recorded after polishing to 1000 grit finish and cleaning with acetone and alcohol. The coupons were then arranged in a coupon rack, separated by crevice washers as shown in Figure 2.5. These samples were exposed to the various test solutions in a duplex stainless steel autoclave (Figure 2.6). The compositions of the simulated white liquors used for this study are shown in TABLE 2.5. Tests for general and localized corrosion in white liquors were carried out at different temperatures, starting at 140^{o}C. Precaution was taken to avoid any contact between these samples and the autoclave to avoid galvanic corrosion. After each exposure test, the specimens were removed, washed, and visually examined for any signs of localized

corrosion (pits or crevices). The samples were then cleaned with Clarke's solution to remove the surface oxide scale without affecting the base metal. The final weight of each sample was measured and used to calculate the rate of general corrosion for each specimen.

TABLE 2.5. COMPOSITION OF SULFIDE-CONTAINING CAUSTIC SOLUTIONS USED IN THIS STUDY

Environment	Composition (per liter)
Environment 1	NaOH 150gm + Na2S 50gm
Environment 3	NaOH 100gm + Na2S 55gm
Environment 2	NaOH 125gm + Na2S 75gm

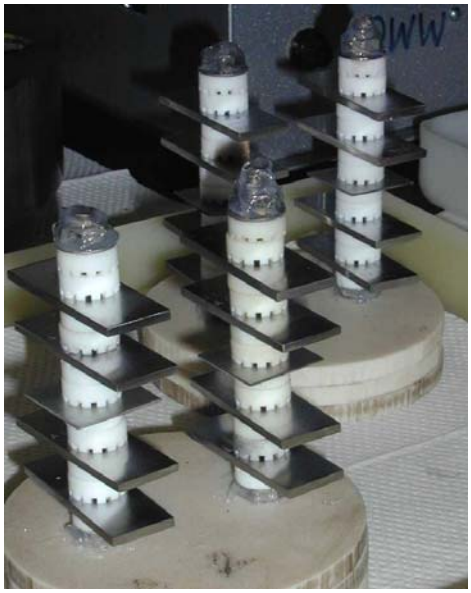

Figure 2.5. Arrangement for coupon exposure tests showing DSS specimens and crevice washers

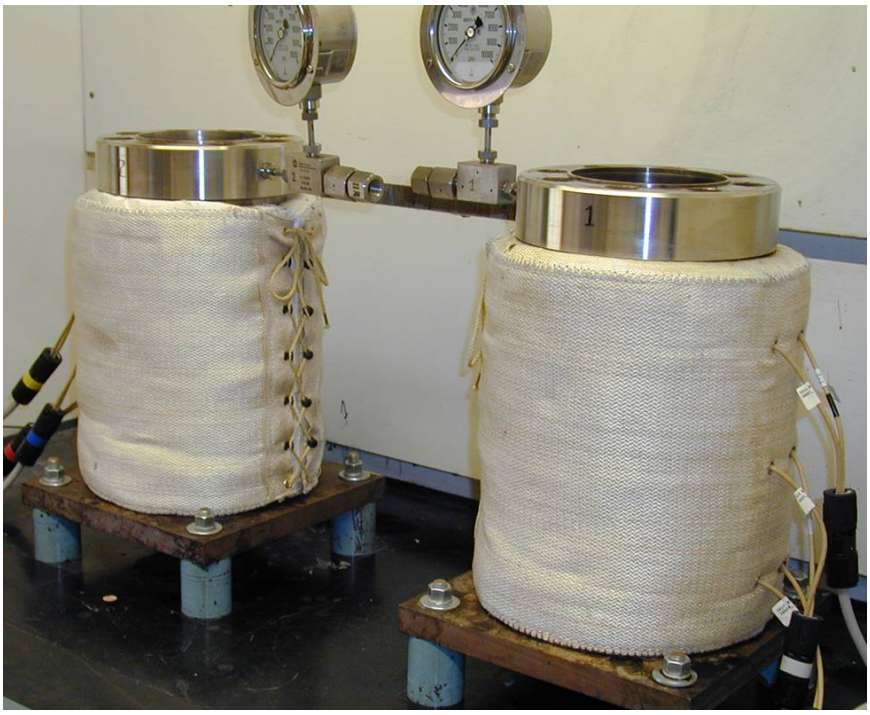

Figure 2.6. Autoclave used for exposure tests at temperatures > 100°C

2.2.4.2. Slow Strain Rate Tests for SCC Susceptibility

Slow strain rate tests were performed to evaluate the effect of different alloy composition and environmental parameters on the SCC susceptibility of different grades of DSS in caustic environment. Slow strain rate tests were performed according to procedure mentioned in Section 2.2.3.1 of this chapter. The DSS grades used were S32205, S32304, S32101, and S32003. The test temperatures were 120°C, 140°C and 170°C and the environment used was sulfide-containing caustic solution with composition shown in TABLE 2.5.

2.2.5. Electrochemical Tests for Corrosion and Stress Corrosion Cracking Susceptibility

2.2.5.1. Potentiodynamic Polarization Tests

Stress corrosion cracking mechanisms typically involve specific electrochemical reactions, which occur at specific potential ranges. To understand the role of composition and microstructure on the corrosion and passivation behavior of different grades of DSS (S32205, S32304 and S32101) potentiodynamic polarization tests were carried out in caustic and sulfide containing caustic solutions at different temperatures (up to 170^{o}C). In potentiodynamic polarization tests, potential is varied at a predetermined rate in a selected range of applied potentials while the current response is monitored continuously. The nominal compositions of materials tested in this study are shown in TABLE 2.1. Potentiodynamic polarization tests were used to evaluate the relative electrochemical behavior of S32205, S32101 and S32304 in 3.75M NaOH solution at 40 ºC, 60 ºC, 90 ºC and 170 ºC. Similar tests were also conducted on the duplex stainless steel specimens in sulfide-containing caustic solution or synthetic white liquor containing 3.75M NaOH + 0.64M Na_2S at 40ºC, 60ºC, 90ºC and 170 ºC.

S32205, S32304 and S32101 samples for the electrochemical tests were machined from rolled plates. Commercially pure samples of Fe, Cr, Ni and Mo were also tested in electrochemical studies to understand the behavior of each major alloying element of DSS in tested environments. All the electrodes were cut in the shape of cylinders with a total surface area of ~5cm^2. The exposed surfaces of the specimens were mechanically polished with 1000 grit SiC paper before testing. The polished specimens were then degreased with acetone and washed with deionized water.

Potentiodynamic polarization tests were used to study the anodic polarization behavior of DSSs and individual alloying elements. The caustic solution was prepared by dissolving 150g of NaOH in 1000ml of water. Sulfide-containing caustic solution or synthetic white liquor was prepared using 150g/L of NaOH and 153.8 g/L of $Na_2S.9H_2O$. pH of the NaOH solution and white liquor was measured prior to the tests and were found to be 12.5 and 12.3 respectively.

A Gamry potentiostat was used for electrochemical measurements. Electrochemical experiments at lower temperatures (40ºC, 60ºC, 90ºC) were performed in a conventional three-electrode PTFE cell as shown in Figure 2.7. The reference electrode used for these tests was a saturated calomel electrode (SCE) with luggin capillary and platinum was used as a counter electrode. An autoclave was used for tests at 170ºC. Pressure balanced Ag/AgCl external reference electrode was used for electrochemical measurements at higher temperature (170ºC). Initially the open circuit potential was measured for each sample, after which the anodic polarization scan was started at a potential 300mV below the corrosion potential measured. The potential scan rate for these tests was $2mVs^{-1}$.

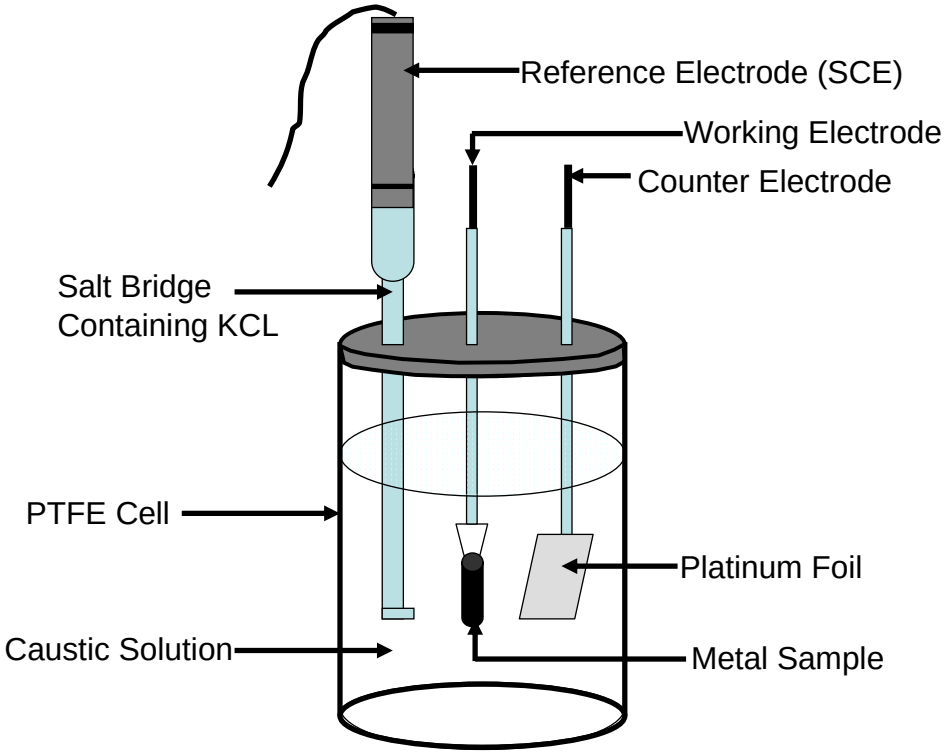

Figure 2.7. PTFE electrochemical polarization cell showing working, reference and counter electrodes

2.2.5.2. Surface Characterization of Passive Films on DSS Using XRD

Corrosion products formed on the S32205, S32101 and S32304 samples exposed to the caustic and sulfide-containing caustic solution at 170ºC for 15 days were characterized by using X- Ray Diffraction (PW 1800 X-ray diffractometer, Philips, USA) with Cu-Kα radiation. X-Ray Diffraction (XRD) of the unexposed DSS metals was also

carried out to identify the austenite and ferrite peaks in the S32205, S32101 and S32304 samples and compare with those of the samples exposed to the tests environments.

2.2.5.3. Surface Characterization of Passive Films on DSS Using X-ray Photoelectron Spectroscopy (XPS)

One of the important means to determine the mechanism of stress corrosion cracking of DSS in sulfide-containing caustic environment is to find out the composition of the passive films formed on the steel surface exposed to environment. XRD technique was used to find the composition of the films on DSS exposed to caustic environment at 170°C as described in Section 2.2.5.2 of this Chapter. Surface analytical method using XPS was also used to find the chemical composition of the passive film formed on 2205 DSS exposed to sulfide-containing caustic solution at 170°C. The equipment used for this study was XPS-SSX-100 with Al K-alpha radiation (1486.6 eV). It was equipped with an electron flood gun to neutralize charge build up. ESCA 25G XPS analysis software was used for data analysis.

The overall experimental approach to achieve the main objectives of this project is shown schematically in Figure 2.8.

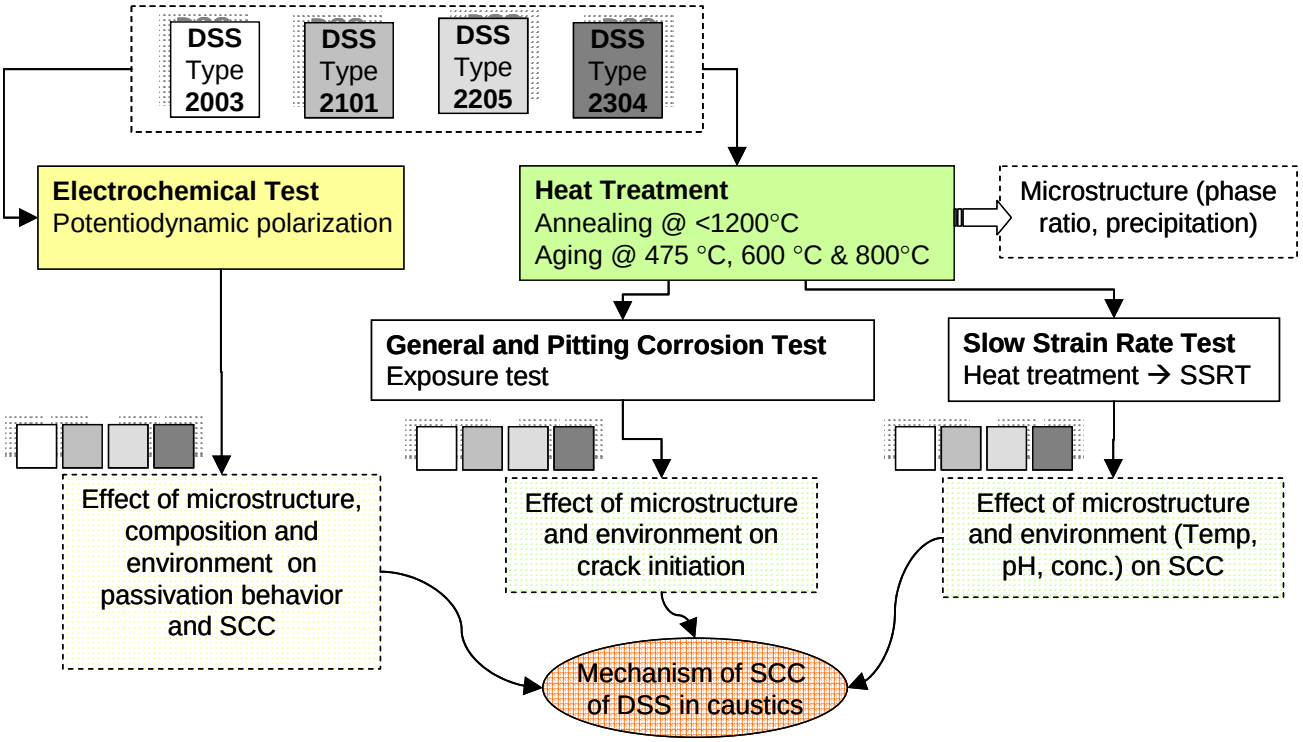

Figure 2.8. Overall approach to study SCC in DSS in caustic environment

REFERENCES

[1] P.E.THOMAS, D.M.WHYTE, "Stress Corrosion Cracking in a Kraft Continuous Digester - Two Important Factors Electrochemical Potential and Residual Stress Level," Appita, Volume 37, Issue 9, pp. 748-752, November 1984.

[2] R.A.YESKE, C.E.GUZI, "In-Situ Studies of Stress Corrosion Cracking in Continuous Digesters," TAPPI journal, pp. 1-11, 1985.

[3] P.P.SNOWDEN, "Comparative Stress-Corrosion Behaviour of Some High-Alloy Steels," Journal of the Iron and Steel Institute, London, Volume 197, pp. 136-141, 1961.

[4] E.M.HORN, S.SAVAKIS, G.SCHMITT, I.LEWANDOWSKI, "Performance of Duplex Stainless Steels in Caustic Solutions," Duplex Stainless Steels, Volume 2, pp. 1111-1119, 1991.

[5] DENNY A. JONES, "Principles and Prevention of Corrosion," Macmillan Publishing Company, 866 Third Avenue, New York, NY 10022.

[6] RUSSELL H. JONES, "Stress Corrosion Cracking," ASM International, Materials Park, Ohio 44073.

[7] JOHN SEDRIKS, "Corrosion of Stainless Steels," John Wiley and Sons, 605 Third Avenue, New York, NY 10158.

[8] PIERRE R. ROBERGE, http://www.corrosion-doctors.org/Forms/scc.htm (Accessed August 2006).

[9] CRAIG .S. TEDMON, JR., "Caustic cracking in hot aqueous and superheated steam environments," Pap. Symp. , pp. 397-409, 1974.

[10] P HURST, H. C.COWEN, RISLEY NUCL., "The stress corrosion cracking of 2 1/4 Cr-Mo ferritic steel in caustic environments," Nuclear Technology, Volume 55, Issue 2 pp. 449-459, 1981.

[11] C. S. HUANG, C. C. SHIH, Materials Science and Engineering A, 402 (2005) 66.

CHAPTER 3

EFFECT OF WELDING RELATED MICROSTRUCTURE ON SCC SUSCEPTIBILITY OF DSS

3.1. INTRODUCTION

Ferritic-austenitic stainless steels have been employed for corrosion resistant applications for many years. Recently, duplex stainless steels (DSS), instead of carbon steel, have been used to construct most of new kraft digesters and other equipment in the pulp and paper industry. This is due to the superior mechanical properties and corrosion resistance of DSS in sulfide containing caustic solutions under pulping temperatures of up to 170°C. However, current field experience and laboratory studies have shown that some pulp mill equipments have experienced stress corrosion cracking (SCC) in the welded and heat affected zones [1]-[4]. The susceptibility of DSS grades to SCC can be mainly attributed to the various heating processes involved during the manufacturing of industrial equipments, especially during welding operations. The ferrite/austenite balance in DSS welds may vary significantly from that of the base metal, since the thermal conditions experienced by the weld metal and heat affected zone (HAZ) are more difficult to control [5], [6]. This shift in phase balance has been shown to favor higher ferrite contents. Prior work has shown that DSS weld metal occurs as delta ferrite and that the structure is fully ferritic at the completion of solidification. The structure remains ferritic until cooling below the ferrite solvus, after which partial transformation from ferrite to austenite occurs. The extent of this transformation is a function of weld metal

composition and cooling rate. Faster cooling rate favors lower retransformation of austenite, resulting in higher ferrite content in the weld and HAZ of DSS. Welding can also result in the precipitation of undesirable intermetallic phases like sigma phase, chromium nitride and secondary austenite in the ferrite phase of the HAZ [8]-[9]. These phases may cause reduced corrosion resistance and impact strength of the steel. Studies have shown that stress corrosion cracking of welded DSS takes place mainly by two mechanisms, namely chloride cracking and cracking in sour H_2S media [10]. In both the chloride and H_2S environments, high ferrite levels in DSS have been shown to have an adverse effect on the SCC resistance of the steel.

Most of the prior research has been carried out to study the effect of microstructure and environmental conditions on chloride SCC of welded DSS. However, recent failure of DSS equipments in pulping environments has generated a need to investigate conditions under which welded DSS may undergo SCC in sulfide-containing caustic environment. In this chapter, effect of microstructure and effect of environmental parameters on the SCC susceptibility of 2205 welded DSS in caustic environment has been investigated. 2205 DSS equipment failed in white liquor (mainly NaOH + Na_2S) was examined for SCC crack morphology and microstructure. Differently welded 2205 DSS samples were tested in simulated white liquor to see the effect of microstructure on SCC susceptibility.

3.2. ANALYSIS OF FAILED 2205 DSS PLATE

White liquor accumulator shell showed weld related leaks within three months of installation. The accumulator vessel had suffered severe cracking, mainly in the circumferential welds of its shell. Figure 3.1 shows a section of the white liquor accumulator shell plate with a large crack in the weld region. Sections of the plate near

the crack and away from this crack were prepared for metallography. Relative ferrite to austenite volume fraction was quantified by measuring the ferrite number in the weld and the heat affected zone (HAZ) and compared with the ferrite numbers of the lab-welded 2205 DSS bars. The ferrite numbers measured by the ferritescope, listed in TABLE 3.1, have an uncertainty of ±16% of the ferrite number measurement. Therefore, to verify the phase ratio differences, measurements were also done by image analysis, where the ferrite to austenite area ratios on etched surfaces was quantified. The ferrite/ austenite of the laboratory welded bar samples were also measured in a similar manner and are listed in TABLE 3.1. “L” and “H” in the specimen codes represent low chromium and high chromium filler metal respectively. Whereas, “h” and “u” denote welding in horizontal and upright positions respectively. It is evident from the table that the ferrite/austenite ratio in the weld and heat affected zone of differently processed laboratory welded bar samples was very similar to that for the equivalent areas of the failed white liquor accumulator plate. Chromium stabilizes the ferrite phase. Hence, welded DSS specimens with higher chromium in the filler material are shown to exhibits higher ferrite content in the weld region (TABLE 3.1).

The micrograph of the weld-bead and HAZ of the white liquor accumulator is shown in **Figure 3.2**. Heat affected zone, which appears as a clouded area near the weld, contains lesser amount of retransformed austenite due to the low heat input and faster cooling rate in this region. Hence, the resulting microstructure in this region shows mostly ferrite phase due to the dissolution of austenite.

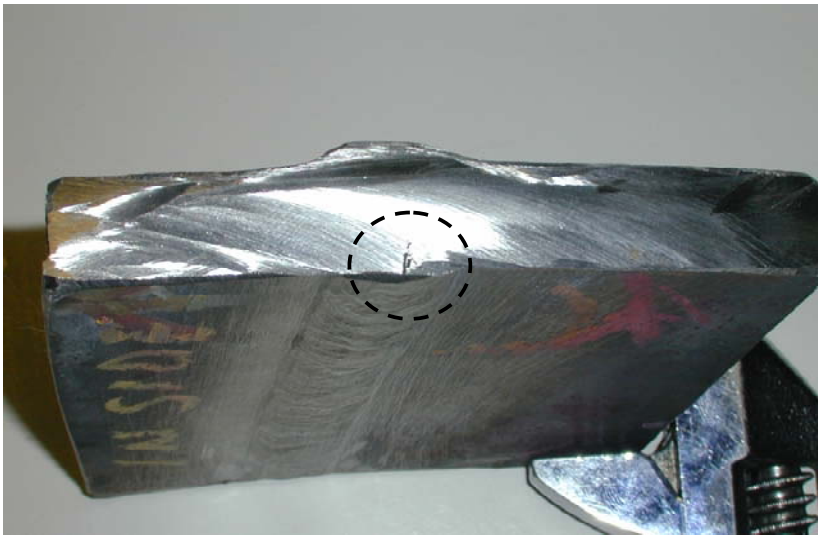

Figure 3.1. A section of the hot white liquor accumulator shell plate showing stress corrosion cracks in the weld region

TABLE 3.1
FERRITE CONTENT IN DIFFERENT WELDED SPECIMENS OF 2205 DSS

Specimen Code	% Ferrite (Using Feritscope)		% Ferrite (Image Analysis)	
	Weld	HAZ	Weld	HAZ
White Liquor Accumulator	36	56	45	64
2205-Lh	41	46	45	63
2205-Hh	47	55	59	57
2205-Lu	45	61	49	66
2205-Hu	48	56	45	65
2205-SAW	45	49	45	54

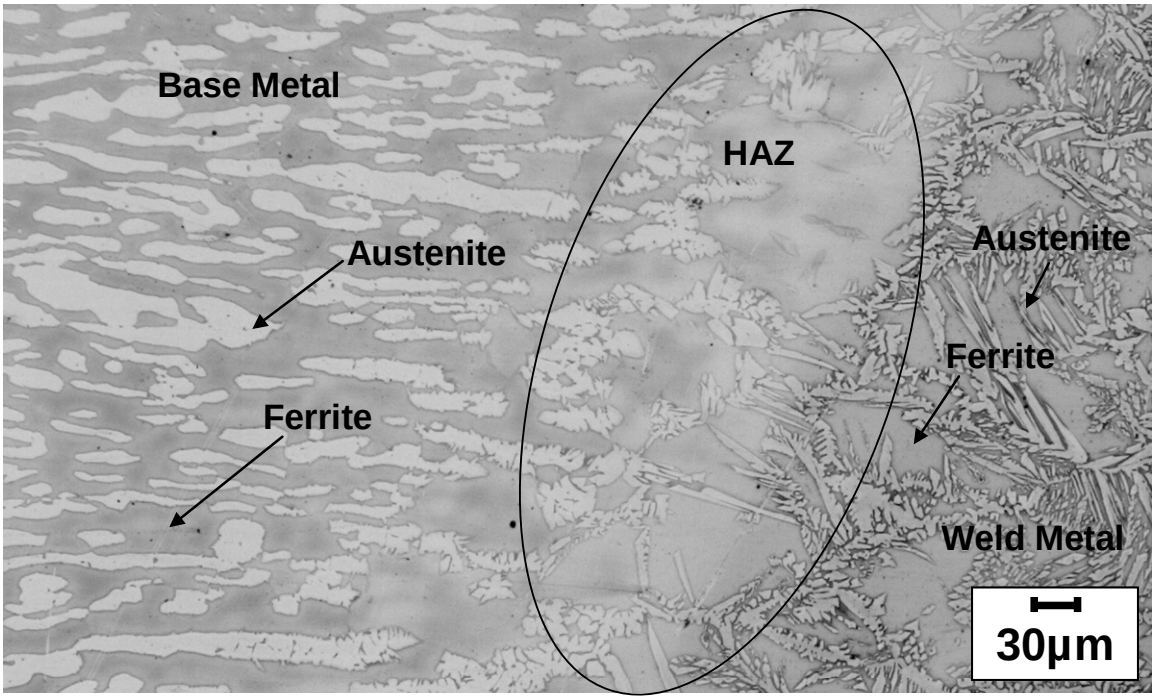

Figure 3.2. Weld and HAZ of the white liquor accumulator showing relatively smaller percentage of austenite in the HAZ

Examination of the failed plate section revealed that the white liquor accumulator failure was due to stress corrosion cracking in hot caustic solution, as suggested by the branched cracks shown in Figures 4-6. The cracks had started in the weld region and had propagated through the HAZ into the base metal, as is evident from Figure 3.3, Figure 3.4 and **Figure 3.5**. It was further evident from the micrographs that in all three regions, i.e. the weld region, HAZ, and the base metal, the cracks seem to preferentially follow the austenite phase. This is clearly visible in Figure 3.6, **Figure 3.7**, Figure 3.8 and **Figure 3.9** where the cracks are following the lighter (austenite) phase. This indicates that the austenite phase is more susceptible to stress corrosion cracking and embrittlement in sulfide-containing caustic solutions.

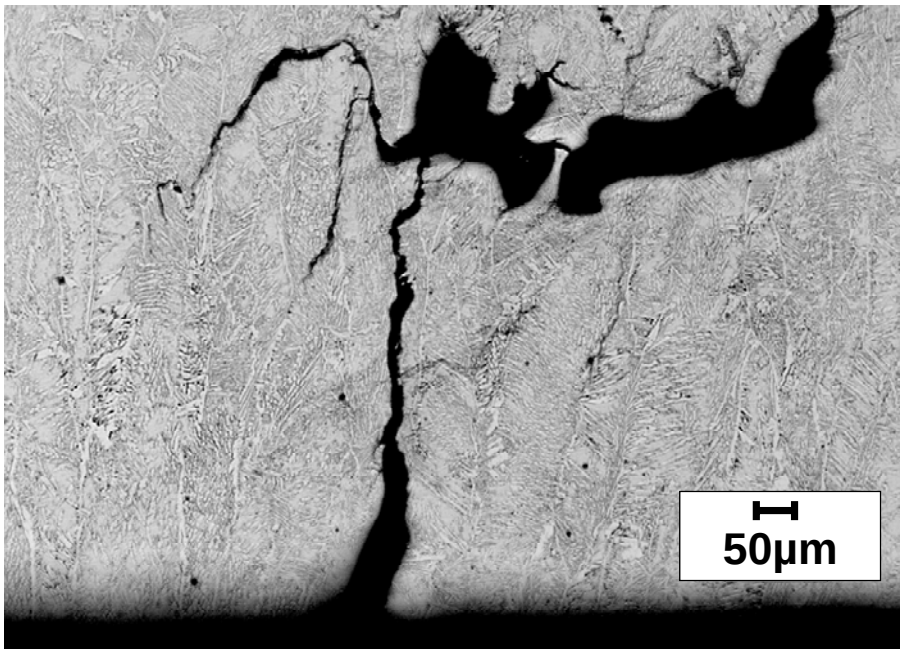

Figure 3.3. Stress corrosion cracks in the hot white liquor accumulator starting in the weld region

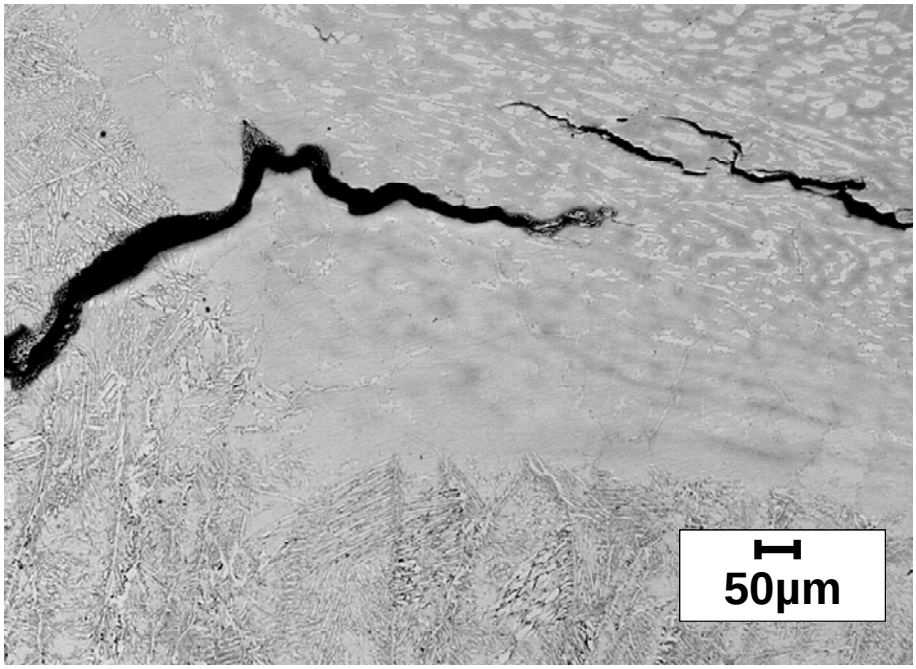

Figure 3.4. Stress corrosion cracks in the hot white liquor accumulator continuing into the HAZ from the weld region

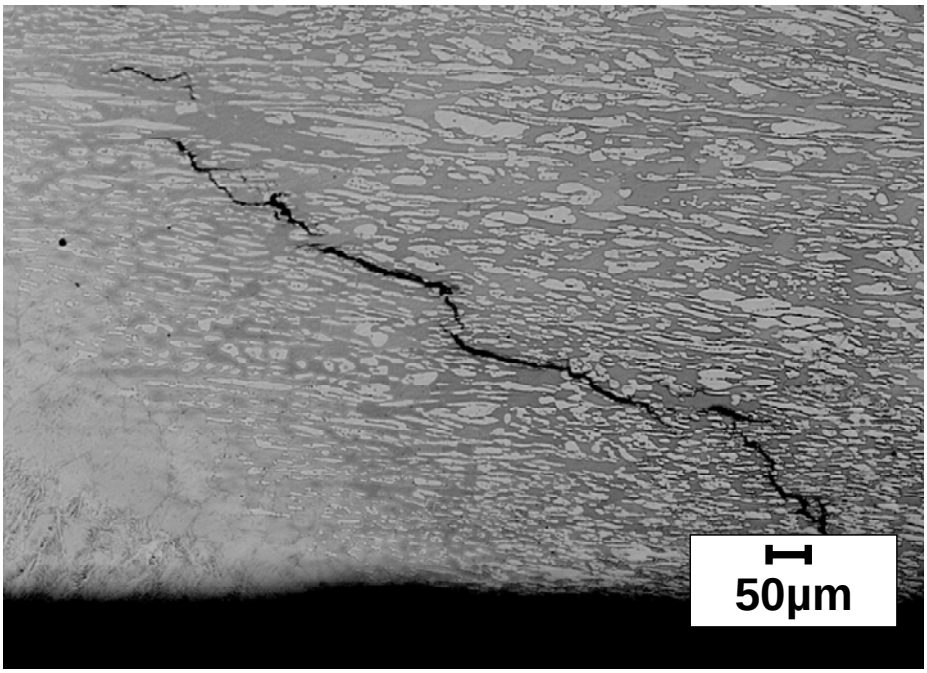

Figure 3.5. Stress corrosion cracks in the hot white liquor accumulator continuing into the base metal from the weld and HAZ

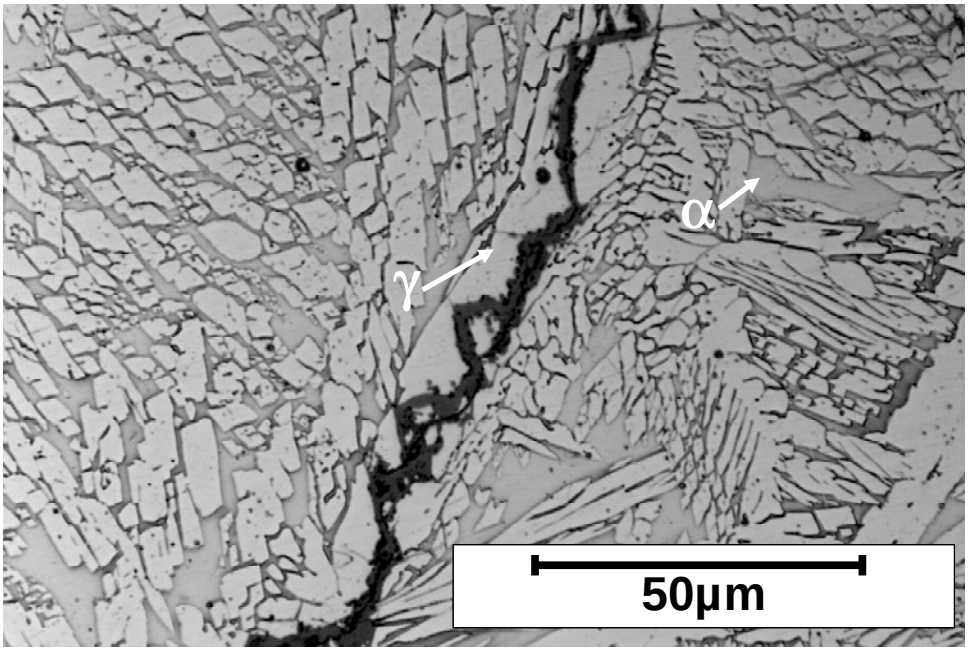

Figure 3.6. Stress corrosion cracks in the weld region of hot white liquor accumulator showing cracks propagating in the austenite phase.

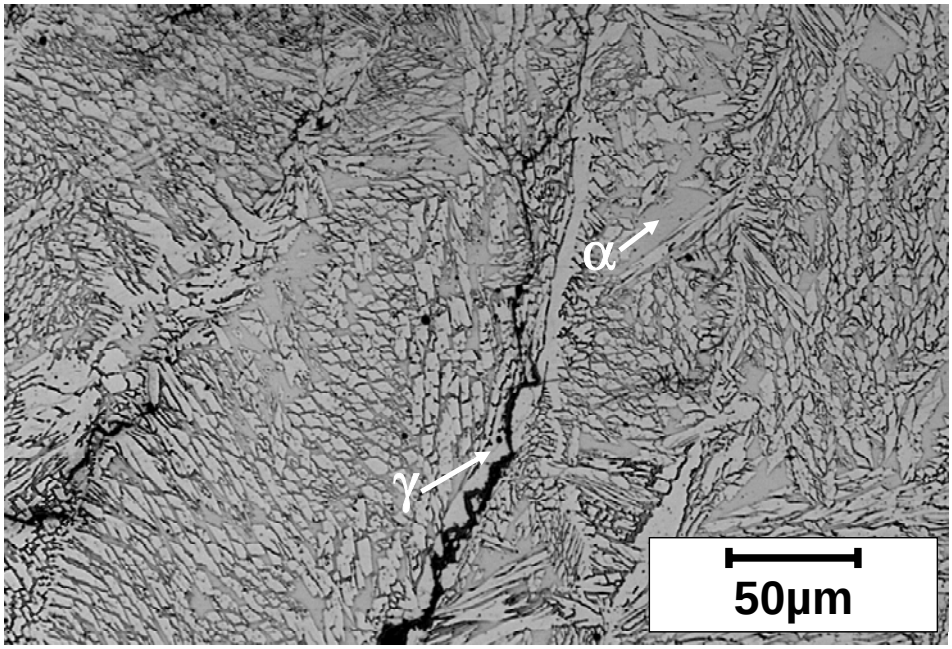

Figure 3.7. Stress corrosion cracks in the weld region of hot white liquor accumulator showing cracks propagating in the austenite phase.

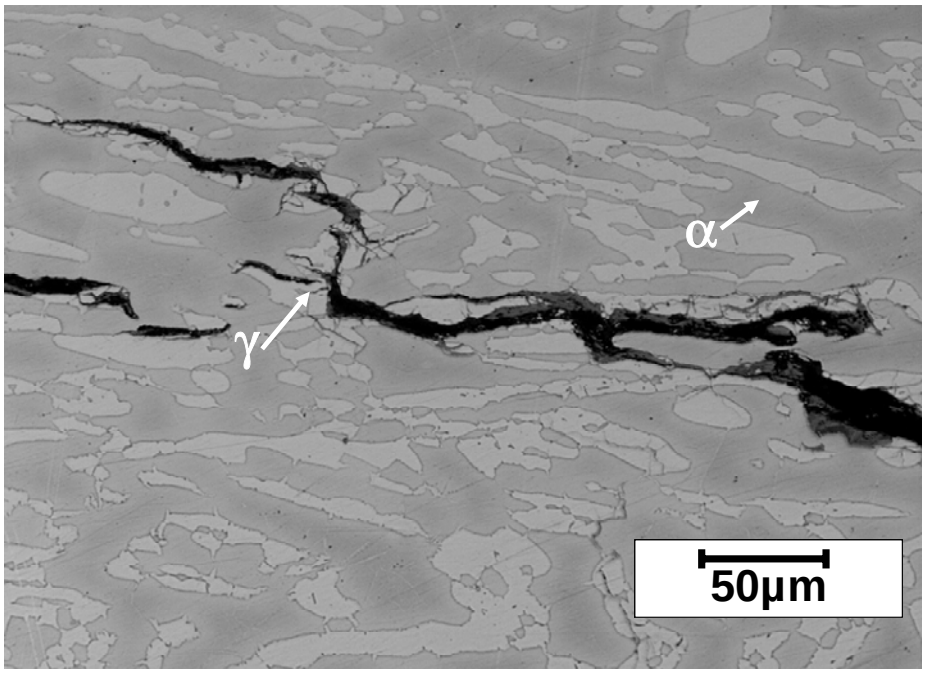

Figure 3.8. Stress corrosion cracks in the HAZ of hot white liquor accumulator showing cracks propagating in the austenite phase

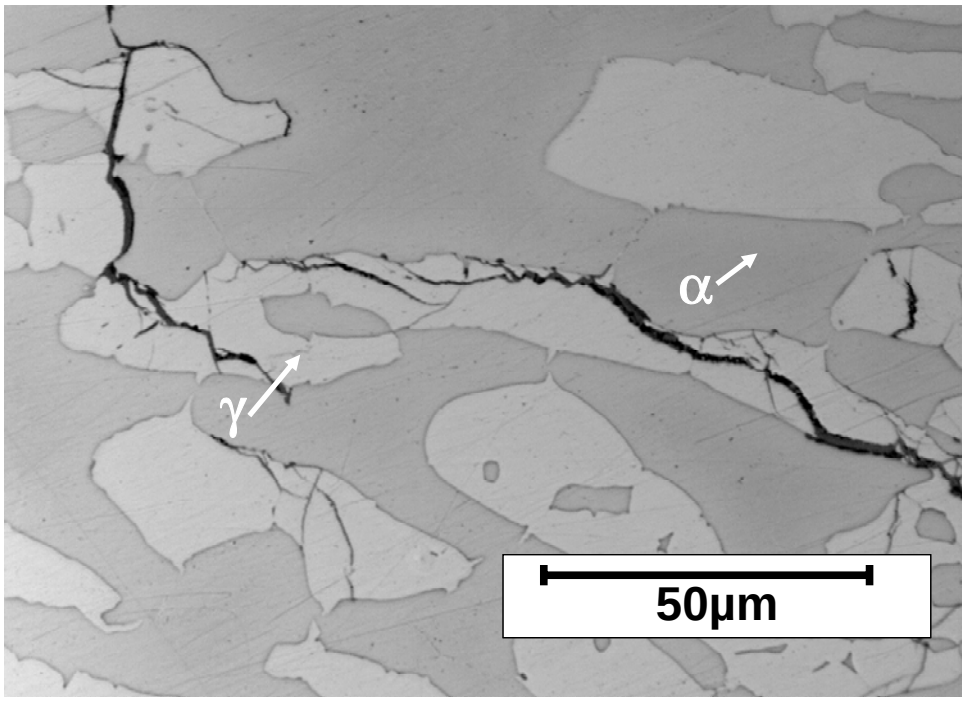

Figure 3.9. Stress corrosion cracks in the base metal of hot white liquor accumulator showing cracks propagating in the austenite phase

3.2.1. Slow Strain Rate Testing of Simulated Welded DSS Specimens

To understand the effect of weld-related microstructure on stress corrosion cracking susceptibility of 2205 DSS, welded tensile samples were used in slow strain rate tests (SSRT) both in inert environment and sulfide-containing caustic environment. Welding condition simulated and composition of materials used are listed in TABLE 2.4 of Chapter 2. Results indicate that most of the welded DSS samples tested in the caustic environment fractured at a lower % fracture strain compared to equivalent samples tested in sand at the same test temperature as shown by results in TABLE 3.2. Figure 3.10 and Figure 3.11 shows the percentage strain to fracture for five differently welded duplex stainless steel samples tested in the sulfide-containing caustic solution at 170°C and 200°C respectively. The %-strain to fracture was lower for the specimens tested at 200 ºC in the sulfide-containing caustic environment as compared to equivalent specimens tested

at 170 ºC. These results clearly show that the sulfide containing caustic solution (white liquor) has an adverse effect on the mechanical properties of the welded duplex stainless steel samples and this effect is more pronounced at higher temperatures (200 ºC). It is also evident from the results that the welding procedure and the environment has significant effect on the overall ductility of these samples. Specimens welded in the upright position (2205-Hu and 2205-Lu) showed a remarkable loss in ductility with an increase in the temperature as compared to the horizontally welded specimens. These specimens were subjected to a slower cooling rate as compared to the horizontally welded specimens, which may have resulted in the precipitation of intermetallic phases and a loss in ductility. It was also observed that the submerged arc welded (SAW) specimens (2205-SAW) showed only 14% fracture strain compared to above 25% for the flux cored arc welded (FCAW) samples in sand (TABLE 3.1). The percentage fracture strain for (SAW) specimens in sulfide-containing caustic environment at 170°C and 200°C were also much lower as compared to (FCAW) specimens. These results indicate that the submerged arc welded samples in general have lower mechanical properties and higher SCC susceptibility as compared to the flux core arc welded duplex stainless steel samples. Clear indication of large stress corrosion cracks were seen on all tested duplex stainless steel samples at 170°C and 200°C.

The adverse effect of environment on the mechanical property and SCC susceptibility of DSS is further evident from Figure 3.12 and Figure 3.13. Figure 3.12 shows the fractured region of specimen 2205-Lh in inert environment (sand). The mode of cracking in the inert environment was ductile with no evidence of SCC on the specimen. On the other hand, the specimen tested in sulfide-containing caustic environment had undergone

brittle failure and severe SCC (Figure 3.13). This severity in cracking increases with an increase in temperature from 170ºC to 200 ºC (Figure 3.14) which further indicates that with the rise in temperature, the SCC susceptibility of DSS increases and the steel becomes more prone to cracking.

TABLE 3.2
% STRAIN TO FRACTURE FOR WELDED DSS IN SAND AND SULFIDE-CONTAINING CAUSTIC SOLUTION AT 170ºC AND 200ºC

Specimen Code	% Fracture Strain (170ºC in Sand)	% Fracture Strain (170ºC in sulfide-containing caustic solution)	% Fracture Strain (200ºC in sulfide-containing caustic solution)
2205-Lh	25	16	11
2205-Hh	33	25	13
2205-Lu	30	31	6
2205-Hu	25	19	6
2205-SAW	14	12	4

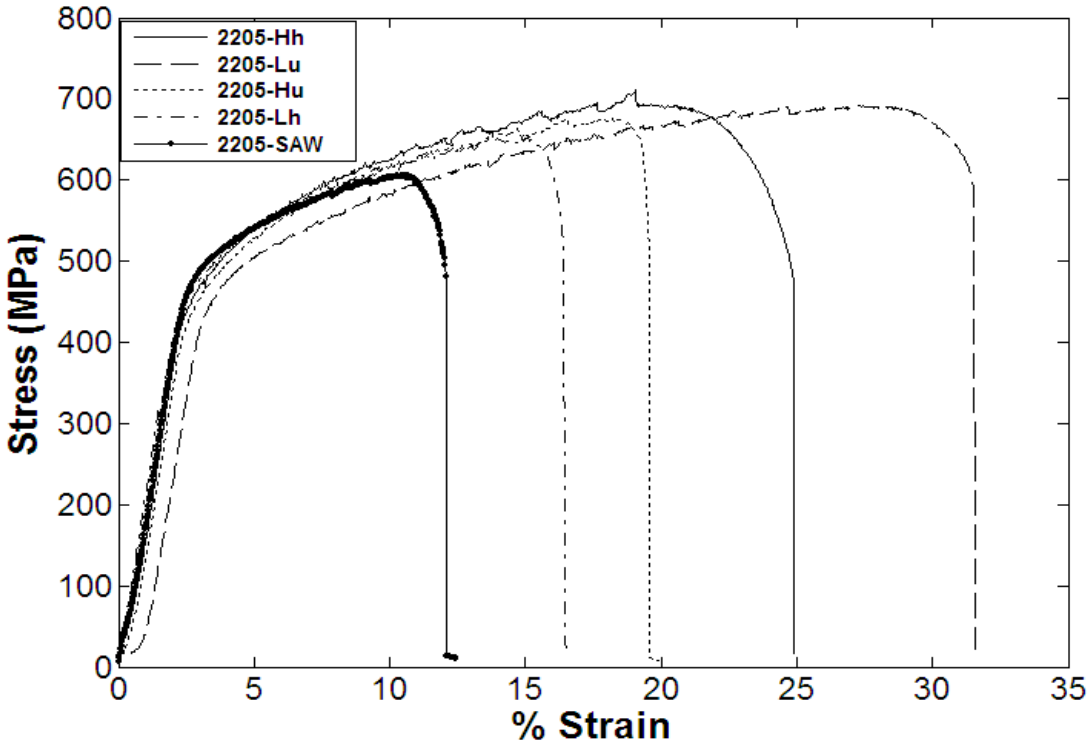

Figure 3.10. Stress-strain curves for different welded specimens tested by SSRT at 170°C in sulfide-containing caustic solution

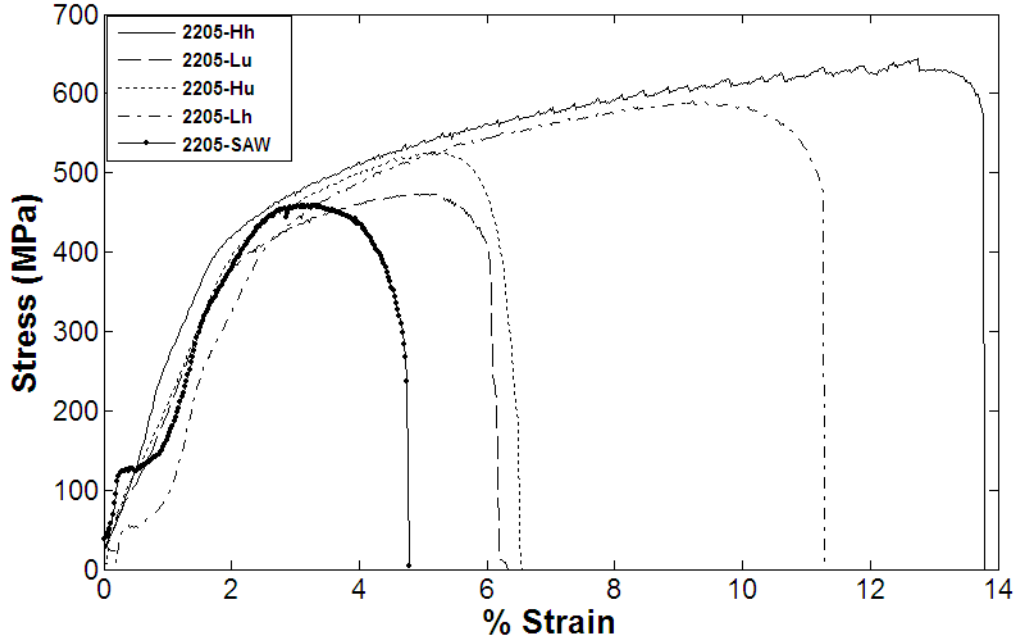

Figure 3.11. Stress-strain curves for different welded specimens tested by SSRT at 200°C in sulfide-containing caustic solution

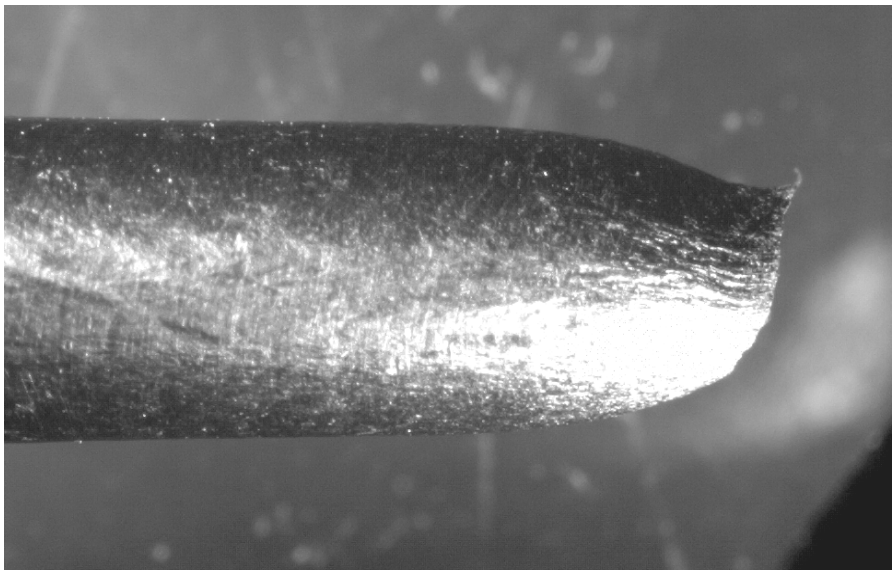

Figure 3.12. Fractured region of 2205-Lh showing no cracks in the absence of environment (6X)

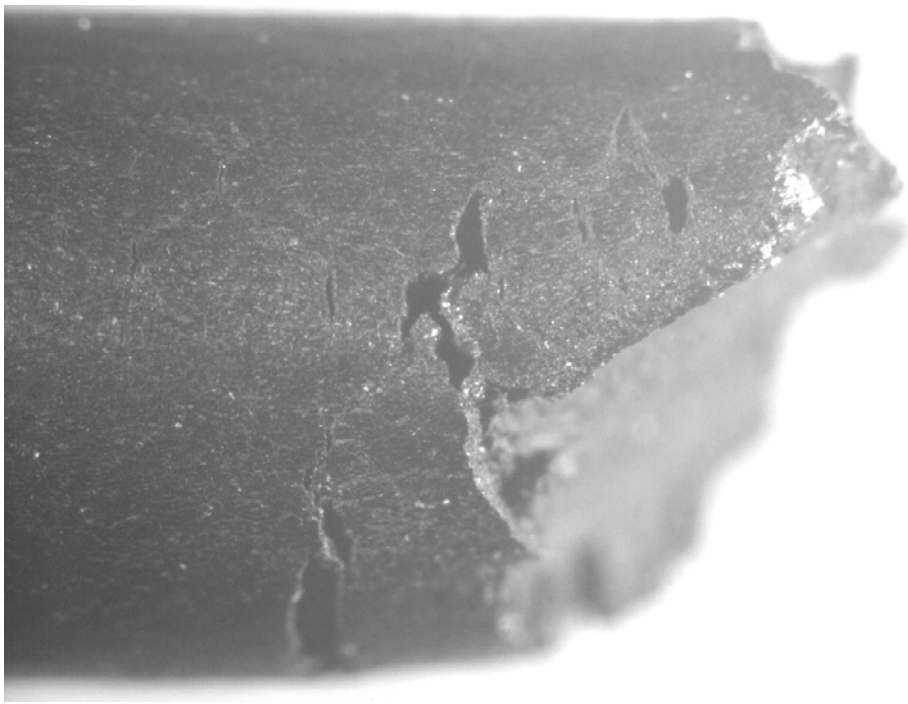

Figure 3.13. Fractured region of 2205-Lh showing presence of stress corrosion cracks when exposed to environment at 170°C (18X)

Figure 3.14. Fractured region of 2205-Lh showing presence of stress corrosion cracks when exposed to environment at 200°C (12X)

TABLE 3.3
CRACK VELOCITY, CRACK DENSITY AND THE REGION OF FRACTURE FOR DIFFERENT WELD SPECIMENS AT 170°C AND 200°C

Specimen Code	Maximum Crack Velocity at 170°C (mm/s)	Maximum Crack Velocity at 200°C (mm/s)	Region of Fracture	
			170°C	200°C
2205-Lh	3.6×10^{-6}	9.0×10^{-6}	Base metal (crack in base metal, weld, and HAZ)	Weld (cracks in weld)
2205-Hh	3.0×10^{-7}	8.5×10^{-6}	Base metal (crack in HAZ)	Base metal (cracks in base metal)
2205-Lu	3.0×10^{-7}	8.9×10^{-6}	Base metal (cracks in base metal, fusion line, and HAZ)	Base metal (base metal, weld)
2205-Hu	1.1×10^{-6}	2.2×10^{-5}	Base metal (cracks in base metal)	Base metal (cracks in base metal)
2205- SAW	4.5×10^{-6}	5.1×10^{-5}	Weld (cracks in weld)	Base metal (cracks in weld, base metal)

The crack velocity and the region of fracture for welded specimens at 170°C and 200°C are summarized in TABLE 3.3. As can be seen from the table, at 170°C the crack velocity was lower compared to the equivalent tests at 200°C. In addition, at both tested temperatures, the submerged arc welded (SAW) specimen, 2205-SAW, showed the highest crack velocity among the tested samples, compared to the samples, which were welded by FCAW process. Weld metal of 2205-SAW samples had more Mn (which leads to higher volume fraction of austenite after similar heat treatment), as compared to the weld metal of other specimens tested in this study. Differences in the chemical composition of the filler metal may also be responsible for the higher SCC susceptibility of 2205-SAW weld. In all cases, cracks were transgranular in nature, both in the base metal as well as in the weld metal, as shown in Figure 3.15 and Figure 3.16 respectively.

All welded DSS samples tested in white liquor had stress corrosion cracks in the base metal S31803. SCC cracks were also found in the weld-bead and the heat affected zone of some specimens, as summarized in TABLE 3.3. Susceptibility of weld-bead and HAZ to SCC was significantly different for differently welded specimens. Weld and the HAZ region of the specimens (2205-Hh) and (2205-Hu) was more resistant to SCC and had fewer cracks in the weld and HAZ as compared to the base metal. Filler metal used for the 2205-Hh and 2205-Hu samples was richer in chromium, which may have contributed to their resistance to SCC in the weld region of these specimens.

A tensile sample machined out of base metal DSS (without welding) was also tested in same environment, the white liquor. The 2205 DSS base metal sample was found to be susceptible to stress corrosion cracking in the white liquor, with crack velocity of 1.8×10^{-6} mm/s. Figure 3.17 shows the transgranular SCC of as-received 2205 DSS with

numerous small crack initiations. Hence, comparing the results of a welded 2205 DSS with an unwelded 2205 base metal sample, it can be said that the welded DSS as well as DSS base metal are susceptible to SCC in sulfide-containing caustic solution.

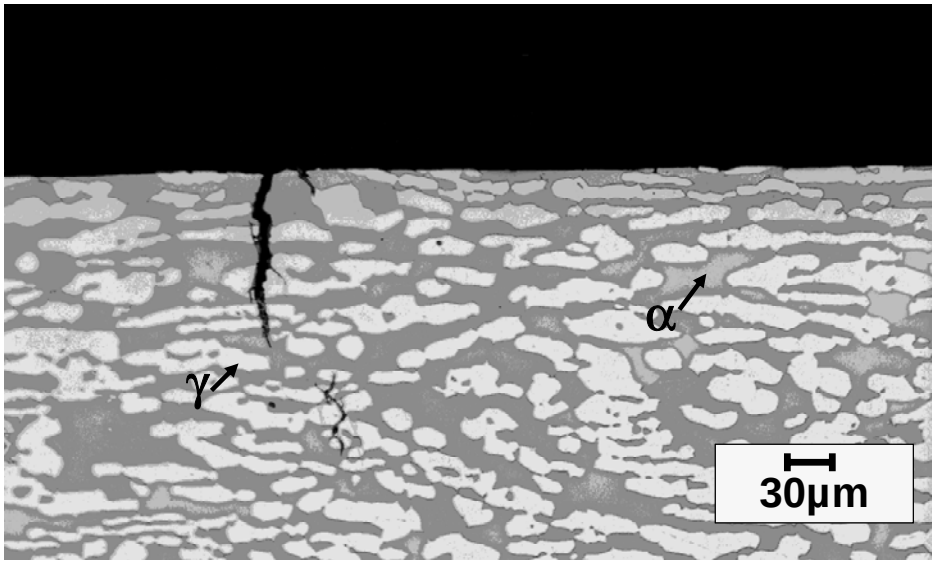

Figure 3.15. Micrograph showing transgranular stress corrosion cracking in the base metal of 2205-SAW at 170°C in caustic environment

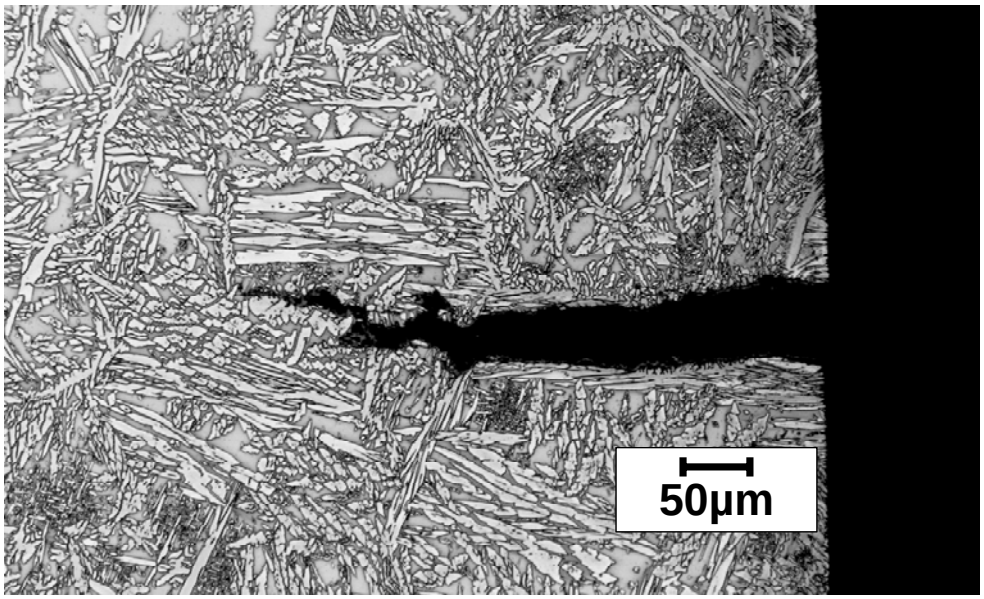

Figure 3.16. Micrograph showing transgranular stress corrosion cracking in the weld metal of 2205-SAW at 170^{o}C in caustic environment

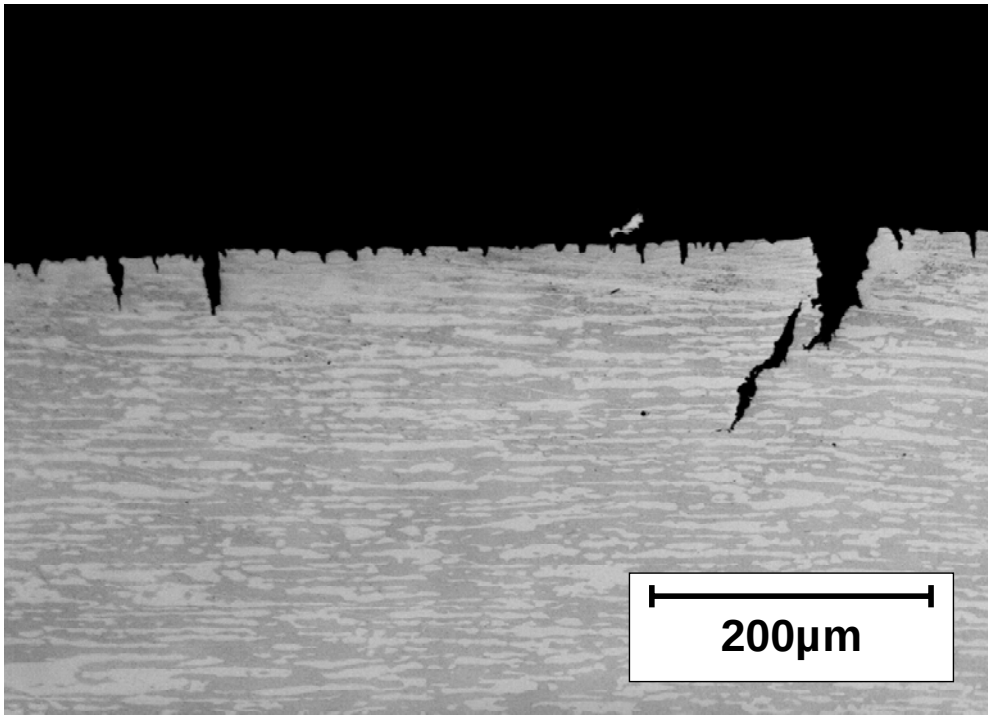

Figure 3.17. Micrograph showing transgranular stress corrosion cracking in as-received 2205 DSS at 170^{o}C in caustic environment

Fractography of samples, tested in sand, revealed microvoid coalescence and ductile mode of failure on the fracture surface (Figure 3.18), whereas specimens tested in the white liquor showed stress corrosion cracking fracture and brittle mode of failure on the surface (Figure 3.19), with transgranular crack morphology.

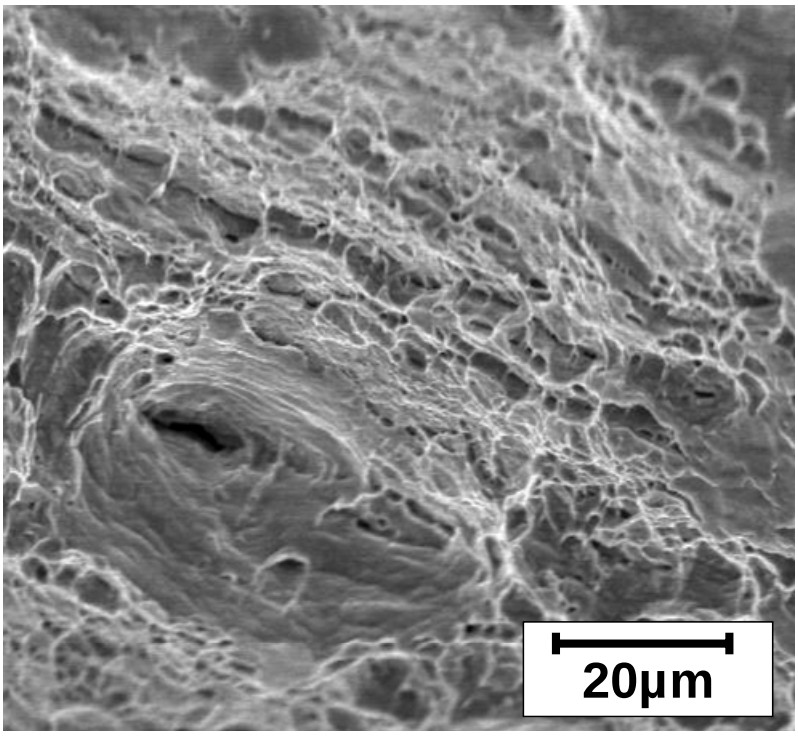

Figure 3.18. SEM image of welded specimen showing microvoids and ductile failure in inert environment

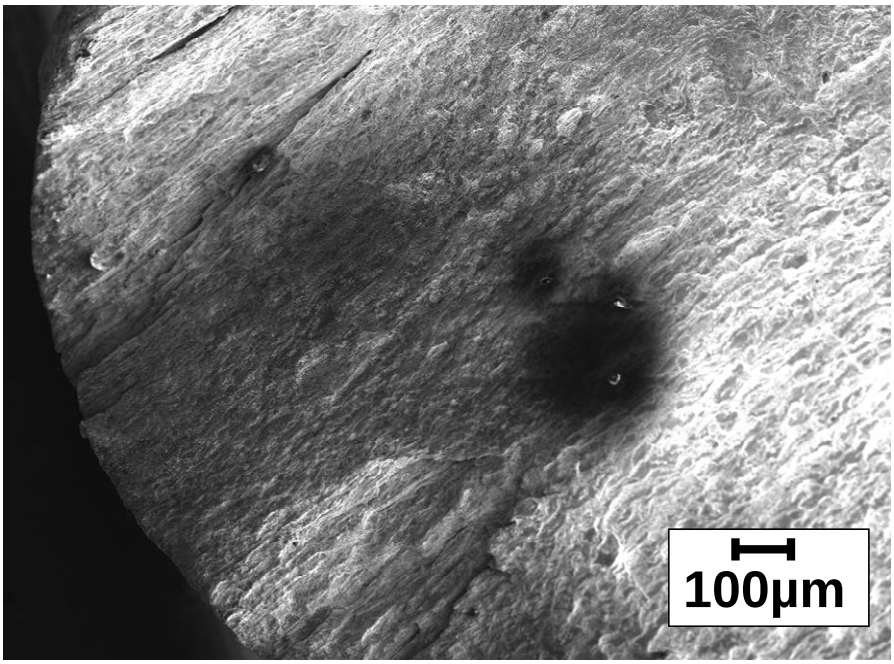

Figure 3.19. SEM image of welded specimen showing stress corrosion cracks and brittle mode of failure in presence of sulfide-containing caustic solutions

Examination of tested tensile sample under scanning electron microscope (SEM) revealed that the crack initiation in the as-received DSS and welded DSS was preferentially in the austenitic phase. Phases were identified by energy dispersive spectroscopy (EDS) analysis of local areas in the SEM. Figure 3.20 and Figure 3.21 shows crack initiation sites in the as received DSS and welded specimen 2205-Hu base metal respectively. Composition of the austenite and ferrite phases in the fractured specimens was found out by EDS. The results are given in TABLE 3.4. The EDS results from these samples confirmed that the SCC crack initiation prefers the austenite phase.

2205-Lh sample had the final fracture in the weld region. Micrograph of this specimen in Figure 3.22 and EDS of this fracture surface also revealed that the small SCC cracks initiated and propagated in the austenitic phase. Crack initiation both in the weld region and in the base metal was found to be in the austenite phase. Previous study has shown that the austenite phase is in tension whereas the ferrite phase is in compression [3].

Preferential susceptibility of ausenite phase in the DSS to SCC in caustic solutions may partially be due to the residual tensile stresses in this phase, which is due to the differences in the coefficient of thermal expansion in the two phases.

TABLE 3.4
COMPOSITION (IN WT%.) OF FERRITE AND AUSTENITE PHASES IN 2205-HH WELDED SPECIMEN

Phases	Elements (wt. %)				
	Cr	Mo	Fe	Ni	Mn
Austenite	22.41	2.04	66.67	6.08	2.8
Ferrite	25.65	3.72	65.15	3.64	1.85

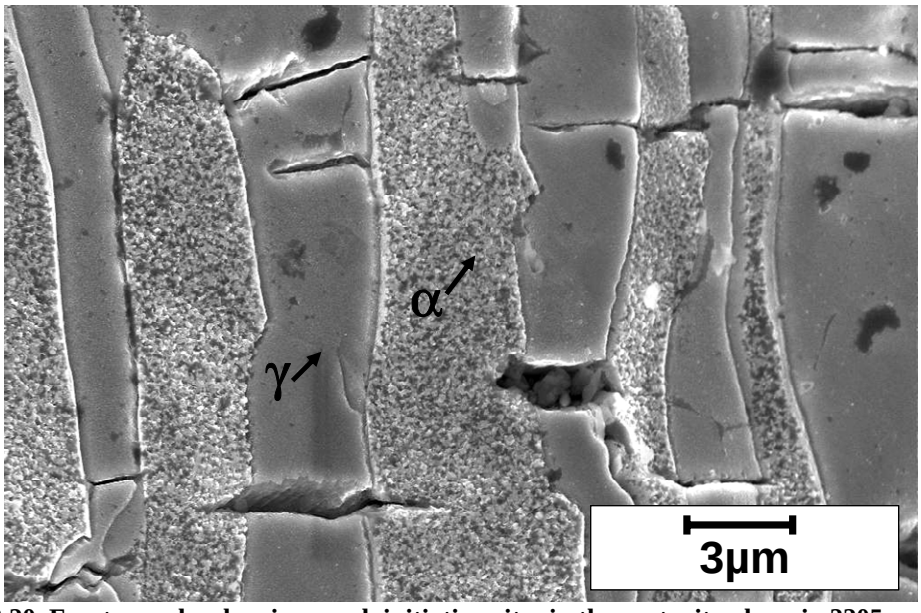

Figure 3.20. Fractography showing crack initiation sites in the austenite phase in 2205 as received DSS tested in sulfide-containing caustic solution at 170°C

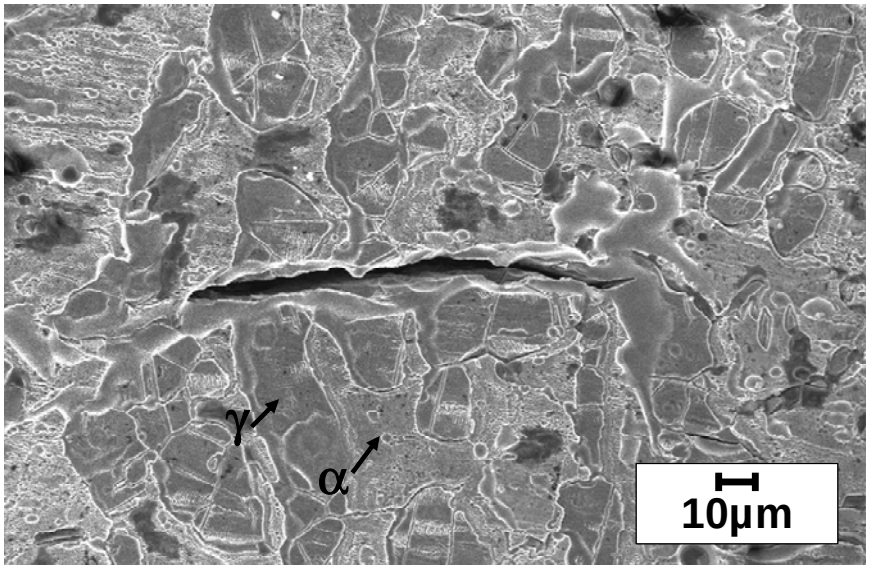

Figure 3.21. Fractography showing crack initiation sites in the austenite phase in 2205-Hu welded specimen tested in sulfide-containing caustic solution at 200°C

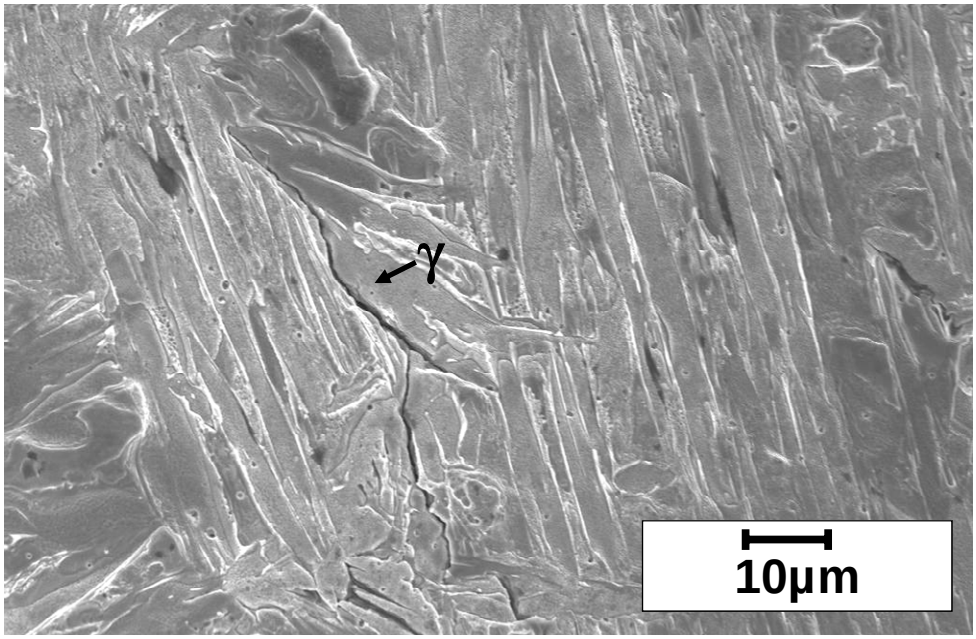

Figure 3.22. SEM micrograph of weld region of 2205-Lh tested in sulfide-containing caustic solution showing crack initiation in the austenite phase at 200°C

3.3. CONCLUSION

Simulated welded 2205 DSS specimens were tested in sulfide-containing caustic environment to find the effect of weld microstructure and environmental parameters on the SCC susceptibility of these steels. From the results, the following conclusions could be made:

1. Welded 2205 specimens were found to have stress corrosion cracks not only in the weld and HAZ but also in the base metal of the samples. Unwelded 2205 DSS as received specimens were also found to undergo severe stress corrosion cracking in sulfide-containing caustic solutions. This indicates that DSS weld as well as base metal is susceptible to SCC in sulfide-containing caustic environments.
2. Flux core arc welds with highly alloyed weld metal (higher chromium) was found to be the most resistant to stress corrosion cracking. These specimens had fewer cracks in the weld and HAZ as compared to the base metal. This shows that high chromium content in DSS will make it more resistant to SCC.
3. The severity of stress corrosion cracking and degradation of mechanical properties was found to increase with increase in temperature. This could explain the failure of the accumulator. Since the upper part of the accumulator was exposed to temperatures higher than 140ºC, it had become more susceptible to stress corrosion cracking.
4. SEM and EDS studies of slow strain rate test specimens showed that crack initiation was mostly in the austenite phase. Moreover, metallographic examinations of 2205 DSS white liquor accumulator showed crack propagation in

the austenite phase. This suggests that the austenite phase in DSS is more susceptible to embrittlement and SCC in sulfide-containing caustic solutions.

3.4. SUMMARY

Failure analysis of failed DSS white liquor accumulator shell plate revealed that the failure was due to SCC in the weld region. Cracks were also found in the base metal in this section. Our lab results from welded samples tested in sulfide-containing caustic solution (white liquor) showed that weld region as well as base metal may be susceptible to SCC in this environment. Austenite phase was found to be more susceptible to cracking than the ferrite phase in all tested samples and in the failed accumulator shell plate. However, SCC susceptibility depends upon the composition of alloy used and environmental conditions.

REFERENCES

[1] H.T.LEINONEN, "Corrosion resistance of duplex stainless steel and its welds in modern kraft batch cooking," *11TH INTERNATIONAL Symposium on Corrosion in the Pulp and Paper Industry*, Charleston, SC, USA, 7-11 June, 2004, pp.55-66.

[2] MARGARET GOROG, "Digester outlet device scraper arm cracking," *2006 Engineering, Pulping and Environmental Conference,* Atlanta, GA, USA, November 5-8, 2006.

[3] H.T.LEINONEN, P.POHJANNE, " Stress corrosion cracking susceptibility of duplex stainless steels and their welds in simulated cooking environments," *NACE Corrosion 2006,* Paper No. 06244, March 12-16, San Diego, CA, USA, 2006.

[4] CRAIG REID, “Stress corrosion cracking of austenitic and duplex stainless steels in the kraft pulp mill,” *1999 TAPPI Engineering/Process and Product Quality Conference*, Anaheim, CA, USA, September 12-16, 1999.

[5] D.E.NELSON, W.A.BAESLACK III, J.C.LIPPOLD, “Characterization of the weld structure in a duplex stainless steel using color metallography,” *Materials Characterization, 39*, pp.467-477, 1997.

[6] J.C.LIPPOLD, I.VAROL, W.A.BAESLACK III, “Microstructural evolution in duplex stainless steel weldments”, Duplex stainless steels ’91, Volume 1, Edited by J.Charles, October (1991).

[7] T.H.CHEN, J.R.YANG, “Microstructural characterization of simulated heat affected zone in a nitrogen-containing 2205 duplex stainless steel,” *Materials Science and Engineering A338*, pp.166-181, 2002.

[8] V.MUTHUPANDI, P.BALA SRINIVASAN, S.K.SESHADRI, S.SUNDARESAN, “Effect of weld metal chemistry and heat input on the structure and properties of duplex stainless steel welds,” *Materials Science and Engineering A358*, pp. 9-16, 2003.

[9] S.-Å. FAGER, “Design of consumables for the welding of superduplex stainless steel,” Duplex stainless steels ’91, Volume 1, Edited by J.Charles, October (1991).

[10] T.G.GOOCH, “Corrosion resistance of welds in duplex stainless steels”, Duplex stainless steels ’91, Volume 1, Edited by J.Charles, October (1991).

[11] H.Y.LIU, R.I.HSIEH, W.T.TSAI, “Microstructure and pitting corrosion in simulated heat-affected zones of duplex stainless steels,” *Corrosion Science*, *44*, pp.2841-2856, 2002.

CHAPTER 4

EFFECT OF MICROSTRUCTURE ON CORROSION AND STRESS CORROSION CRACKING OF DUPLEX STAINLESS STEEL IN CAUSTIC SOLUTIONS

4.1. INTRODUCTION

The duplex microstructure of different ferritic-austenitic stainless steel grades such as S32205, S32304, S32101 and S32003 are manufactured by optimizing the chemical composition and the annealing temperatures of the steel to meet the mechanical properties and corrosion resistance requirements for various applications [1]. The dual phase is usually established by either hot working in a two-phase region or by producing a single phase structure and then age hardening the alloy by precipitation of an additional phase or phases [2]. Annealing above the solvus temperature of austenite (γ) results in a structure, which is completely ferritic (α). The ferrite structure obtained by water quenching from the solvus temperature is unstable with respect to austenite precipitation. Hence reheating into the $\alpha+\gamma$ stability region results in strengthening of the alloy due to the formation of austenite precipitates. Ferrite/austenite ratio in DSS plays an important role in mechanical and corrosion properties of the steel. Apart from the ratio of phases, the distribution of phases as well as partitioning of alloying elements in the two phases is also important [3]. Composition of the two phases in the DSS alloys is not the same. Partitioning of alloying elements in each phase can induce a difference in the electrochemical potential between the ferrite and austenite phases, which may lead to preferential attack on one of the phases. Selective local corrosion attack can also

influence the initiation of SCC for a particular DSS alloy and environment combination [1]. Hence, understanding and control of the DSS microstructure allows us to study the effect of alloy composition and phase ratio on the corrosion susceptibility in a given environment.

High and low temperature aging of duplex stainless steels may give rise to undesirable precipitates such as sigma, chi, chromium carbides and nitrides or '475 embrittlement'. Previous studies have also shown that the presence of sigma phase precipitates makes the DSS alloys susceptible to localized corrosion in chloride environments [4]-[5]. Moreover, pitting corrosion was found to assist in the SCC initiation while selective dissolution of ferrite phase assisted in the propagation of stress corrosion cracks of DSS in chloride solution [6]. Hence, the formation of these intermetallic precipitates may affect the mechanical and corrosion properties of the steel adversely. During welding or other fabrication processes, localized areas of DSS may be exposed to high temperatures and different cooling rates, which may lead to changes in the balanced microstructure of DSS alloys [7]. This change in the microstructure, in-turn, will affect the general and localized corrosion or SCC susceptibility of the affected area as compared to the rest of the metal. This makes it important to understand the effect of heat treatment parameters like annealing temperature, aging temperature, and cooling rates on the DSS microstructure and resulting corrosion behavior in caustic environment.

In this chapter, the effect of composition and microstructure of the as-received DSS grades on their SCC susceptibilities in sulfide-containing caustic environment has been discussed. The affect of different heat treatments on the microstructure of two grades of DSS (S32205 and S32101) has also been studied. S32101 is a relatively new grade of

DSS and very little is known about the affect of heat treatment on its microstructure. Hence, the two grades of DSS with varying alloy composition has been selected to do a comparative study of the effect of similar annealing and aging temperatures on the changes in their microstructure and to find out more about the microstructural properties of 2101 DSS. Moreover, the effect of these annealing and aging temperatures on the corrosion and stress corrosion susceptibility of 2101 and 2205 DSS has further been investigated.

4.2. MICROSTRUCTURE OF AS-RECEIVED DSS

Stress corrosion cracking failures of DSS equipments employing caustic environments have shown that DSS alloys are susceptible to crack initiation and propagation in sulfide-containing caustic solutions at high temperatures. Most of the reported failures were related to the weld region but SCC of the base alloy has also been reported in these environments [8]. To find out the role of DSS alloy composition and microstructure on the SCC susceptibility of these steels in sulfide-containing caustic environment, as-received DSS tensile samples were machined out of different grades of rolled DSS plates. The annealing temperatures, cooling procedures and the measured % ferrite for the as-received DSS are listed in TABLE 4.1. The % ferrite of the DSS samples was determined using a Ferritscope. The heat treatment procedures for the DSS grades were according to ASTM A 480/A 480M – 06b [9]. As can be seen in TABLE 4.1, different alloy compositions as well as heat treatment procedures have resulted in different ferrite/austenite ratios for DSS alloy. Micrographs of S32205, S32304, S32101 and S32003 DSS as-received samples are shown in Figure 4.1 to 4 respectively. These micrographs show that the microstructure (phase size and morphology) differs from one

DSS grade to another depending upon the thermo-mechanical treatments of the as-received samples. From these results it is evident that compositions as well as thermo-mechanical treatments play a role in the microstructure (ferrite/austenite ratio, phase morphology) of duplex stainless steels, which in turn affects its corrosion and SCC properties.

TABLE 4.1. HEAT TREATMENT PROCEDURES AND % FERRITE FOR THE AS-RECEIVED S32205, S32304, S32101 AND S32003 DSS GRADES

DSS grade	Annealing Temperature ºC	Cooling	% Ferrite
S32205	1040	Quenched in water	58
S32304	980	Quenched in water or rapidly cooled by other means	50
S32101	1020	Quenched in water or rapidly cooled by other means	54
S32003	1010	Quenched in water or rapidly cooled by other means	43

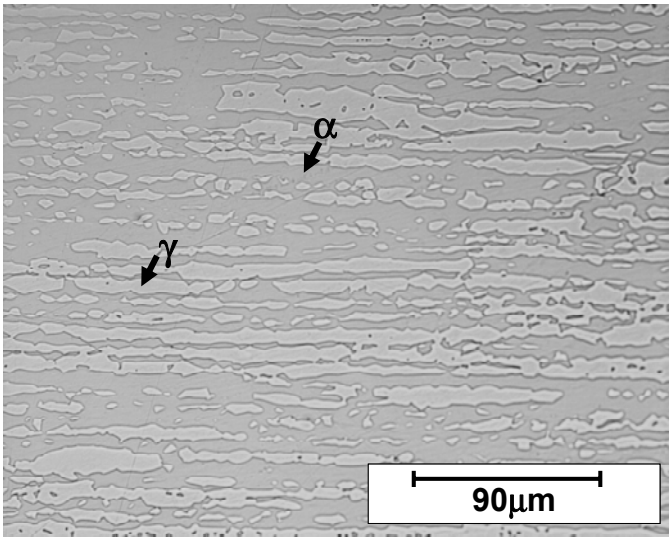

Figure 4.1. Longitudinal section of 2205 DSS polished to 0.05micron finish and etched with 40% NaOH solution

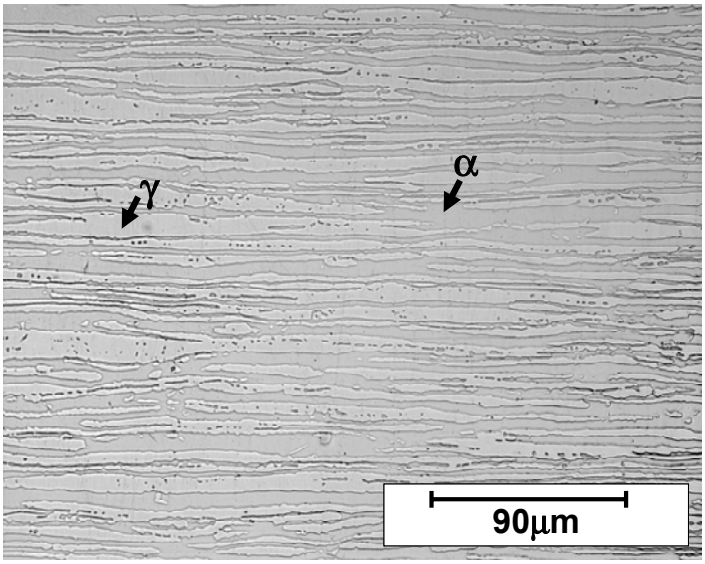

Figure 4.2. Longitudinal section of 2304 DSS polished to 0.05micron finish and etched with 40% NaOH solution

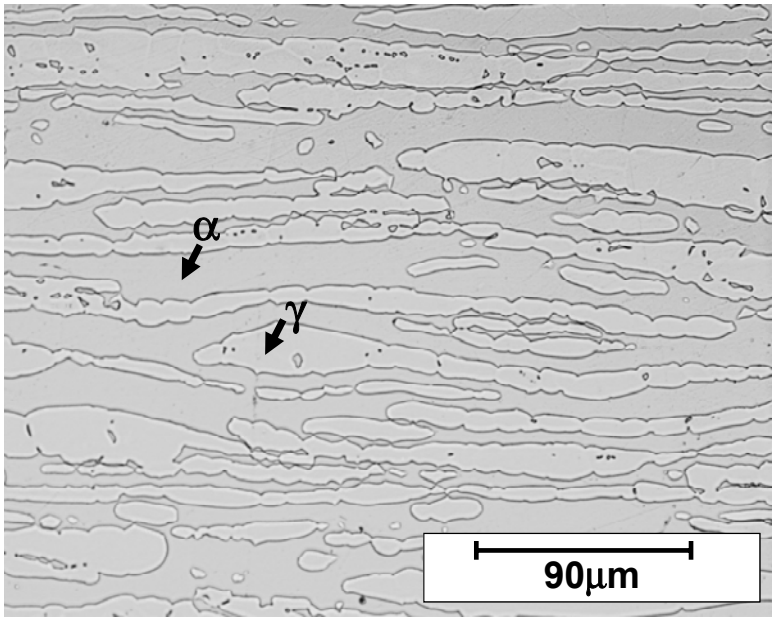

Figure 4.3. Longitudinal section of 2101 DSS polished to 0.05micron finish and etched with 40% NaOH solution

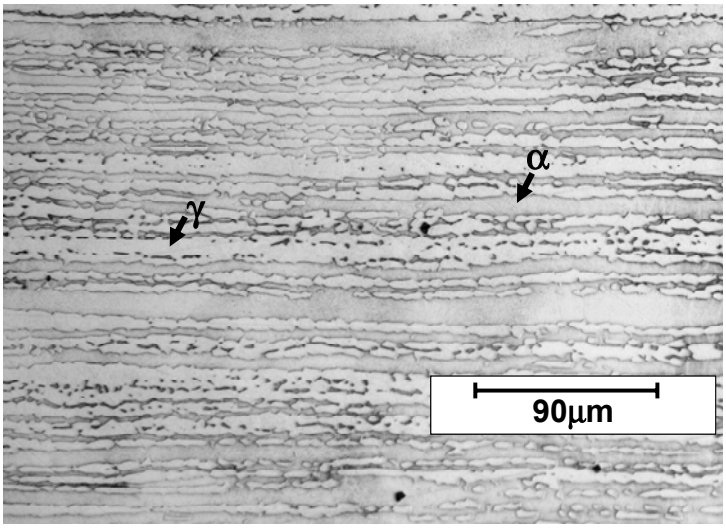

Figure 4.4. Longitudinal section of 2003 DSS polished to 0.05micron finish and etched with 40% NaOH solution

The tensile specimens of S32205, S32304, S32101 and S32003 were subjected to slow strain rate tests in a solution containing 150gm per liter of NaOH + 50 gm per liter of Na_2S at 170^oC. S32205, S32101 and S32003 DSS grades showed SCC susceptibility in sulfide-containing caustic solutions, but the S32304 DSS sample was found to be immune to cracking. Corresponding crack velocities for the samples showing SCC are listed in TABLE 4.2. Although the crack velocities were almost an order of magnitude different for different DSS grades, the cracks were mostly transgranular with a tendency to favor the austenite phase for initiation as well as propagation in all tested DSS grades. Stress-strain curves for the four DSS steels tested in 150gm per liter of NaOH + 50 gm per liter of Na_2S are shown in Figure 4.5. From the figure, it is evident that the mechanical behavior of different DSS grades varies in the same environment depending upon their microstructure and thermo-mechanical treatments. S32205 DSS samples had higher strength but had higher crack velocity in sulfide-containing caustic environment. Results from these tests have shown that the duplex stainless steels can be susceptible to stress corrosion cracking in sulfide-containing caustic solution, depending upon the environmental parameters and alloy composition. Representative micrographs of stress corrosion cracks are shown in Figure 4.6 to Figure 4.9.

TABLE 4.2. CRACK VELOCITIES OF DSS GRADES TESTED IN 150GM/L OF NAOH + 50GM/L OF NA_2S AT 170°C

DSS Grade	Environment	Temp (°C)	Crack Velocity mm/sec	Stress Corrosion Susceptibility
S32205	NaOH 150gm/l + Na_2S 50gm/l	170	1.8E-6	SCC
S32101		170	2.73E-7	SCC
S32304		170	0	No SCC
S32003		170	6.6E-7	SCC

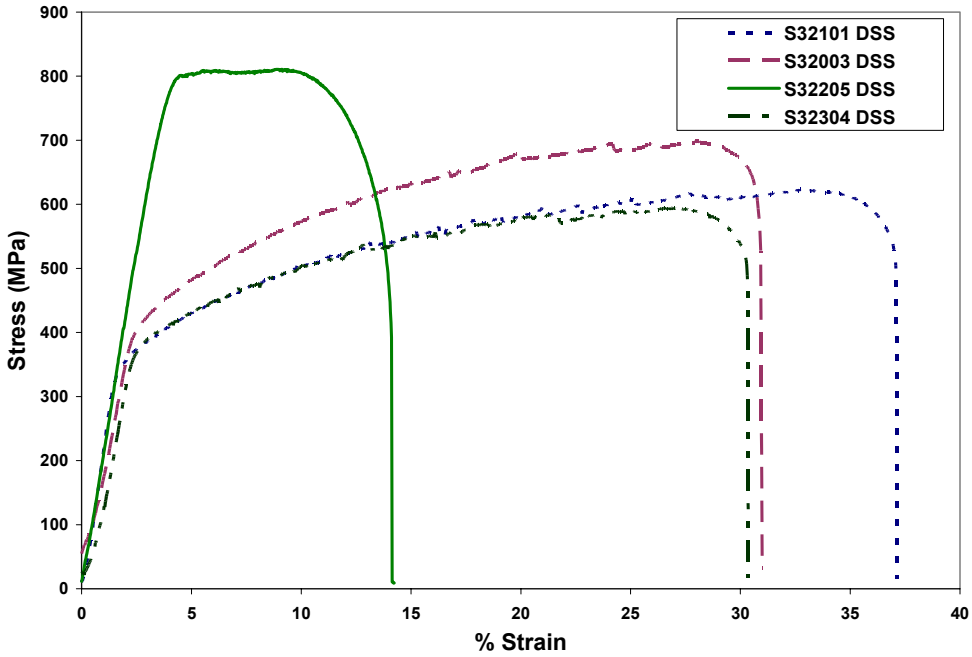

Figure 4.5. Stress strain curve of various DSS grades in150gm/L NaOH + 50gm/L Na_2S at 170°C.

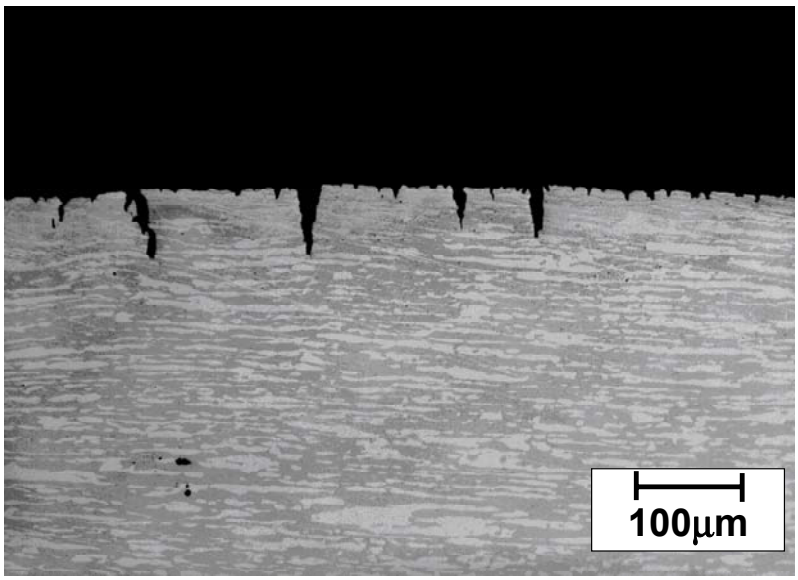

Figure 4.6. Stress corrosion cracks in S32205 DSS tested in 150gm/L NaOH + 50gm/L Na_2S at 170°C

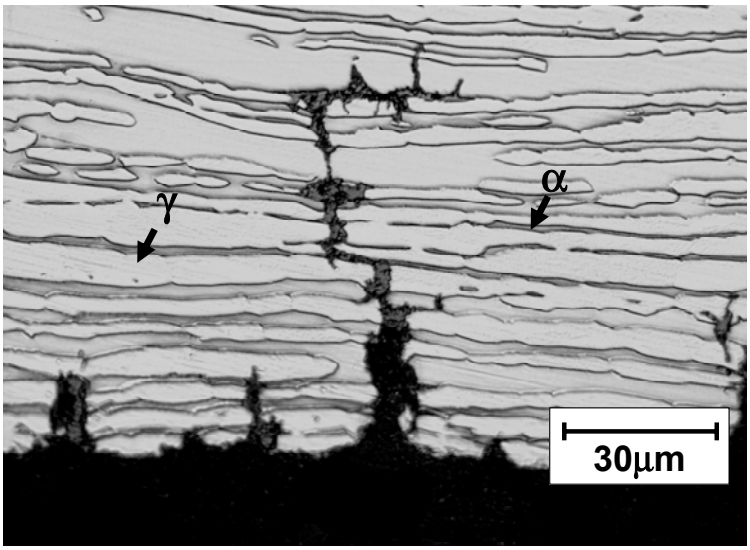

Figure 4.7. Stress corrosion cracks in S32003 DSS tested in 150gm/L NaOH + 50gm/L Na_2S at 170ºC

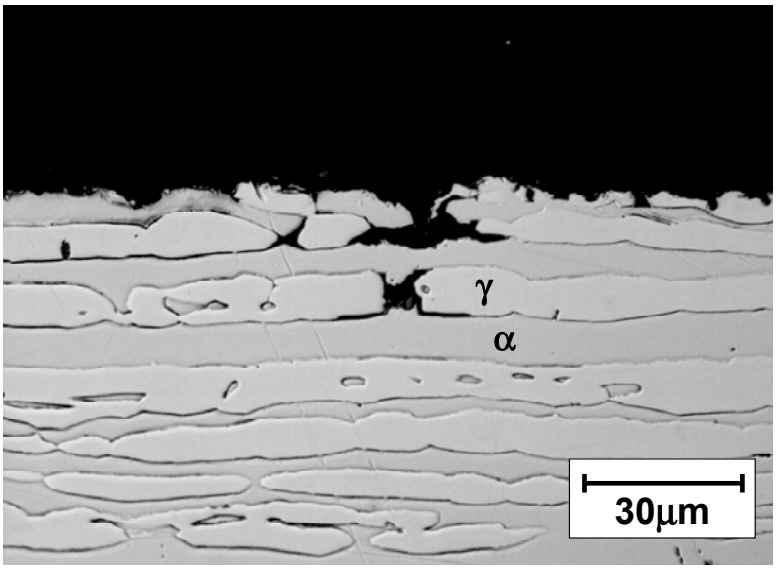

Figure 4.8. Stress corrosion cracks in S32101 DSS tested in 150gm/L NaOH + 50gm/L Na_2S at 170ºC. Notice the crack propagation through austenite phase (light phase)

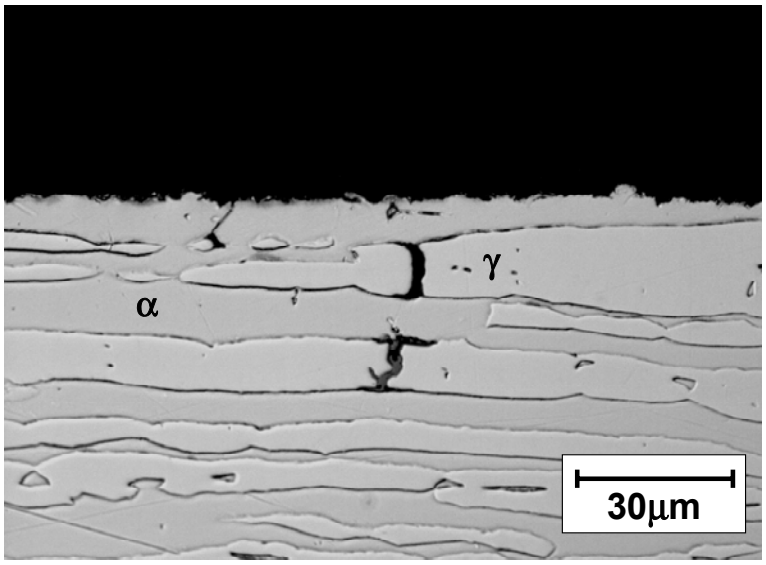

Figure 4.9. Stress corrosion cracks in S32101 DSS tested in 150gm/L NaOH + 50gm/L Na_2S at 170ºC. Notice the crack propagation through austenite phase (light phase)

The 2205 DSS sample tested in 150gm/L NaOH + 50gm/L Na_2S at 170^oC, shown in Figure 4.6, had numerous stress corrosion cracks initiated at the surface. Some of these cracks had propagated many grains deep into the sample while some cracks remained dormant and did not grow beyond the first austenite grain at the surface of the tensile sample. Although the microstructures of S32205 and S32003 were different, but samples of both DSS grades showed similar transgranular cracks (Figure 4.7). Cracks were found to preferentially propagate through the austenite phase and get arrested at ferrite phase boundaries in 2003 DSS. Crack propagation was also found to favor the austenite phase in the S32101 sample (Figure 4.8 and Figure 4.9), whereas the ferrite ligaments typically failed by overload. This effect was more apparent in the lean duplex grades S32101 and S32003 compared to the S32205 grade with higher chromium and nickel content. In some cases, the cracks initiated at the surface but did not grow beyond the first austenite grain. These micrographs clearly indicate that the austenite phase in DSS is more

susceptible to stress corrosion cracks in sulfide-containing caustic solutions. This is different from the susceptibility of DSS in acidic chloride environments, where our work and previous work has shown that the ferrite phase is more susceptible to the SCC initiation and propagation [6]. The crack morphology was different for different grades of DSS. The thin lamellar ferrite phase between the thicker lamellae of austenite made it easier for the cracks to propagate in S32003 (Figure 4.7). On the contrary, the discontinuous austenite phase in S32101 did not provide a continuous path for crack propagation and the cracks were limited to the austenite phase and were arrested at ferrite/austenite phase boundaries. Highly alloyed 2304 DSS did not show any cracking which shows that the chemical composition along with the microstructure (ferrite/austenite ratio and phase morphology) of the steel has a significant effect on the susceptibility of DSS to SCC in caustic solutions. X-ray diffraction studies were performed by Leinonen et al. on S31803 to study stress state of the austenite and ferrite phases. The ferrite/austenite ratio in the above study was assumed to be 50%/50% by volume [10]. The results have shown that the microstresses (σ^{γ}_{mi}) in the austenite phase were of the order of almost +209MPa and hence the austenite phase was in tension. The microstress in the ferrite phase was -209MPa and balanced out the tensile stress of the austenite. Therefore the ferrite phase was in compression. This difference in the stress states is mainly due to the differences in the coefficient of thermal expansions between the two phases (Chapter 1, Table 1.2). Hence, due to the more active slip system and the residual tensile stress in the austenite phase of DSS, this phase undergoes plastic deformation more easily and at an applied stress far below the ferrite phase. This makes the austenite phase more susceptible to crack initiation and propagation.

4.3. EFFECT OF HEAT TREATMENT ON THE MICROSTRUCTURE OF S32205 AND S32101 DSS

Two grades of DSS (S32205 and S32101), with compositions listed in Table 2.1 (Chapter 2) were selected as they represent a commonly used grade (2205) and a relatively new lean DSS alloy (2101). Phase ratio and precipitation of intermetallic phases in DSS depends on both alloy composition and heat treatment. Different grades of DSS were selected to study how similar heat treatments could affect microstructure of alloys differing in composition. Microstructure of the steel samples was changed to obtain different ferrite/austenite ratio and grain morphology and to produce intermetallic precipitation so as to see their effect on the general and localized corrosion behavior in caustic and chloride solutions.

The annealing temperatures used for S32101 were 1000°C or 1100°C and for S32205 were 1000°C or 1150°C respectively. Samples were held at the annealing temperatures for one hour followed by water quenching. After annealing treatments, samples were aged either at 475°C (for 4 hrs) or 600°C (for 4 hrs) or 800°C (for 1hr, 4hrs, or 8hrs) followed by water quenching. TABLE 4.3 and TABLE 4.6 summarizes the different heat treatments given to the S32101 and S32205 samples respectively and the specimen codes for each heat-treated sample used in this study. In each specimen-code, D1 and D5 represent 2101 and 2205 DSS respectively. 1000°C, 1100°C and 1150°C represents the annealing temperatures. 475°C, 600°C and 800°C refers to aging temperatures.

4.3.1. Microstructure of Heat treated S32101 DSS

4.3.1.1. Metallography

Lean 2101 DSS is a relatively new grade of DSS with reduced chromium, nickel and molybdenum content as compared to the commonly used grade S32205. The effect of heat treatment on the microstructure of this grade of DSS has not been studied before. Hence, heat treatment was performed on 2101 DSS to study how the microstructure of this steel is affected by various annealing and aging temperatures and how the various microstructures may play a role in general corrosion and SCC initiation due to localized corrosion. Ratio of ferrite to austenite phase was measured for each heat-treated S32101 DSS sample. There was a very small variation in the ferrite to austenite ratio for the heat treatments performed in this study, as shown in TABLE 4.3. For S32101 DSS the percentage ferrite in the heat-treated specimens ranged from 42% (for D1-1000) to 35% (for D1-1100-800). Nucleation of intermetallic precipitates was observed at the phase boundaries of S32101 samples annealed at 1000°C and aged at 800°C for 1 hour, as shown in Figure 4.10.

Samples aged at 800°C for a longer period of time (4hrs) showed a distinct lighter region at the ferrite/austenite interface, delimited from the austenite by the precipitates (Figure 4.11). Precipitates had nucleated at the interface of the austenite phase and this lighter region in samples aged at 800^{o}C. The lighter region at the ferrite/austenite interface was very prominent in the samples aged at 800°C for 4 hrs and increased with aging time to 8 hours (Figure 4.12). SEM micrograph of 2101 DSS aged at 800 ^{o}C for 8 hrs (Figure 4.13) also shows the presence of precipitates at the interface of the austenite phase and the lighter region. A similar behavior was observed for the samples annealed at

a higher temperature (1100°C) and then aged at 800°C for 4hrs and 8hrs, as shown in Figure 4.14 and Figure 4.15 respectively. No visible precipitates were found in the unaged samples or samples aged at 475°C (Figure 4.16 and Figure 4.17 respectively). The ferrite values listed in TABLE 4.3 indicates that aging at 800 °C did not produce a significant loss in ferrite content for the S32101 DSS samples. Whereas a similar aging treatment of 2205 DSS at 800 °C resulted in a reduction in the ferrite number of the steel from 54% (solution annealed at 1000 °C) to 38% (solution annealed at 1000 °C and aged at 800 °C) (TABLE 4.6). In a previous study conducted by Truman.et.al on DSS containing 26% Cr and 1.45 % Mo, specimens aged at 800 °C for 4hours showed a ferrite content of about 12.5% in the steel [11]. They reported severe intermetallic precipitation in the above-mentioned duplex stainless steels with higher chromium content. Similar precipitates were also found in the present study for low chromium S32101 DSS. The loss in ferrite volume fraction in the higher chromium alloys 2205 and 2507 DSSs during 800^{o}C aging treatments was attributed to the formation of the sigma phase. The amount of intermetallic precipitation in the 2205 DSS was much more than in 2101 DSS samples aged at 800 °C for the same aging time [12]. Our heat treatment results and previous published data show that the alloy composition, and heat treatment, plays a major role in the formation and distribution of phases in DSS which in turn may affect the corrosion and SCC susceptibility of the steel.

TABLE 4.3. HEAT TREATMENTS GIVEN TO S32101 DUPLEX STAINLESS STEEL SAMPLES

Annealing Temp	Aging Temp	Aging Time (hr)	Sample Code	% Ferrite (using Feritscope)	% Ferrite (using image analysis)
1000°C	-		D1-1000	42	47
1000°C	475°C	4	D1-1000- 475	41	45
1000°C	600°C	4	D1-1000- 600	40	41
1000°C	800°C	1	D1-1000- 800	36	40
1100°C	-	-	D1-1100	41	44
1100°C	475°C	4	D1-1100- 475	42	43
1100°C	600°C	4	D1-1100- 600	36.5	42
1100°C	800°C	1	D1-1100-800	35	34

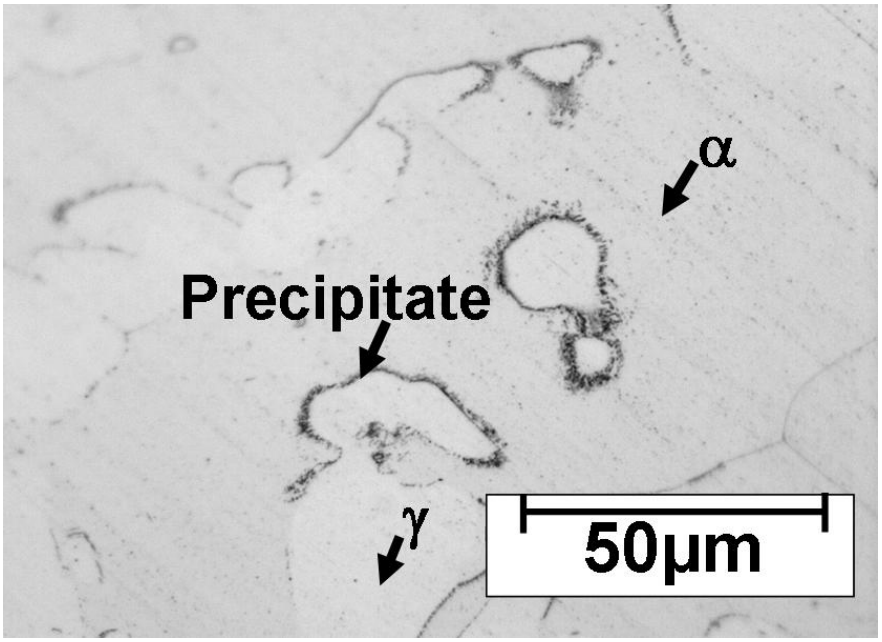

Figure 4.10. 2101 DSS annealed at 1000 °C and aged at 800 °C (1hr) and etched by Grosbeck solution showing intermetallic precipitates at phase boundaries using optical microscope

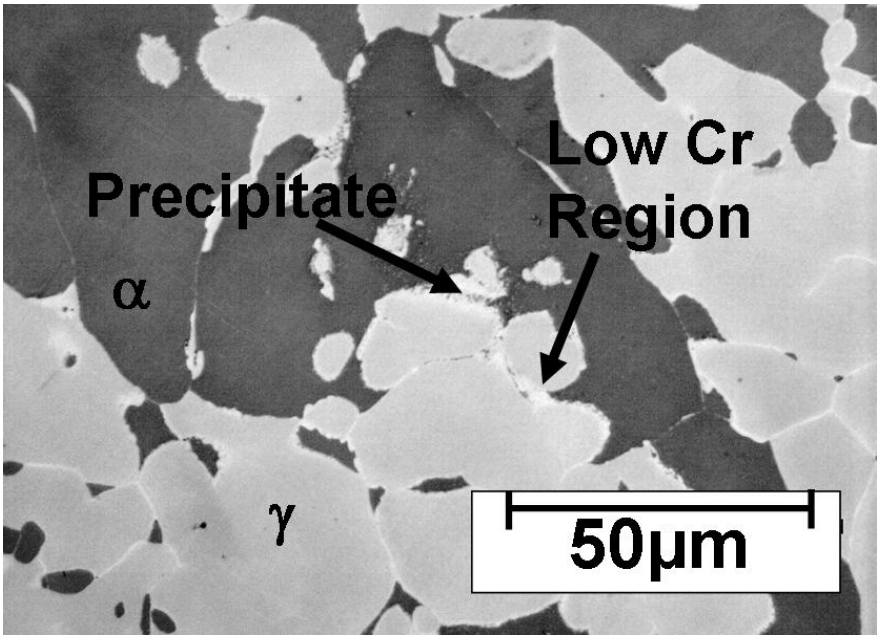

Figure 4.11. 2101 DSS annealed at 1000 °C, aged at 800 °C showing intermetallic precipitation and low chromium lighter region at α/γ interface with 4hrs of aging

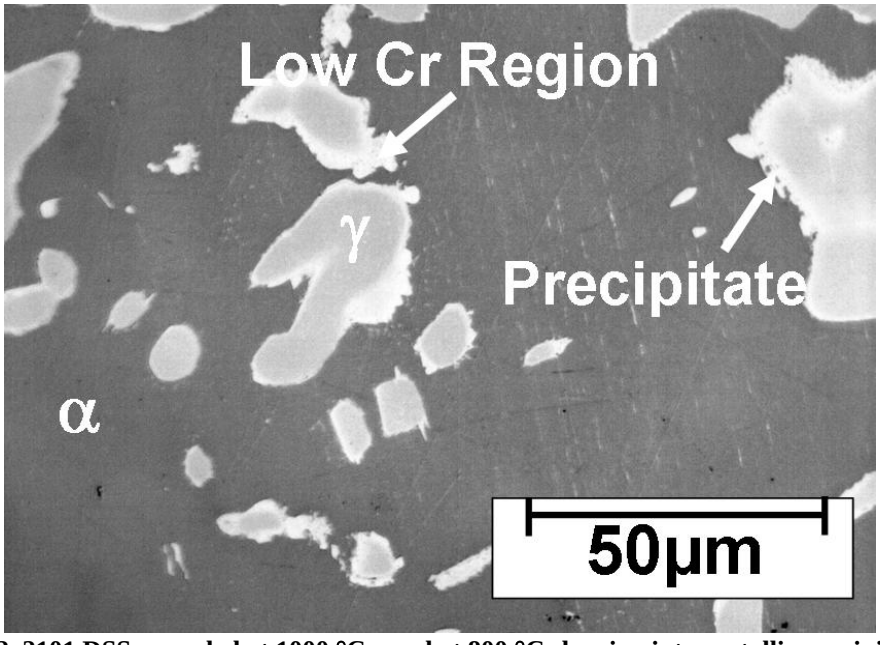

Figure 4.12. 2101 DSS annealed at 1000 °C, aged at 800 °C showing intermetallic precipitation and low chromium lighter region at α/γ interface with 8hrs of aging

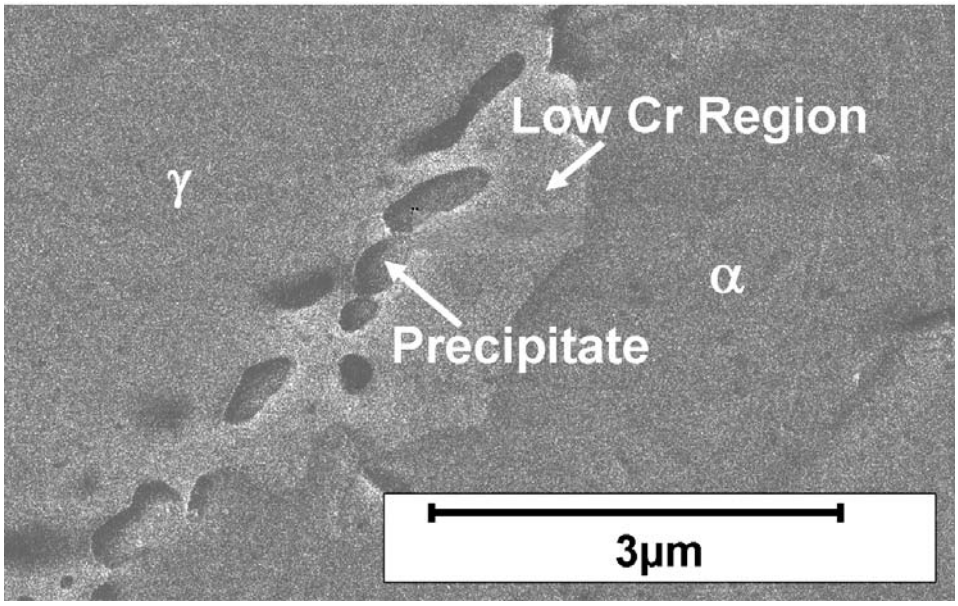

Figure 4.13. 2101 DSS annealed at 1000 °C and aged at 800 °C (8hrs) showing precipitates under SEM (secondary electron image)

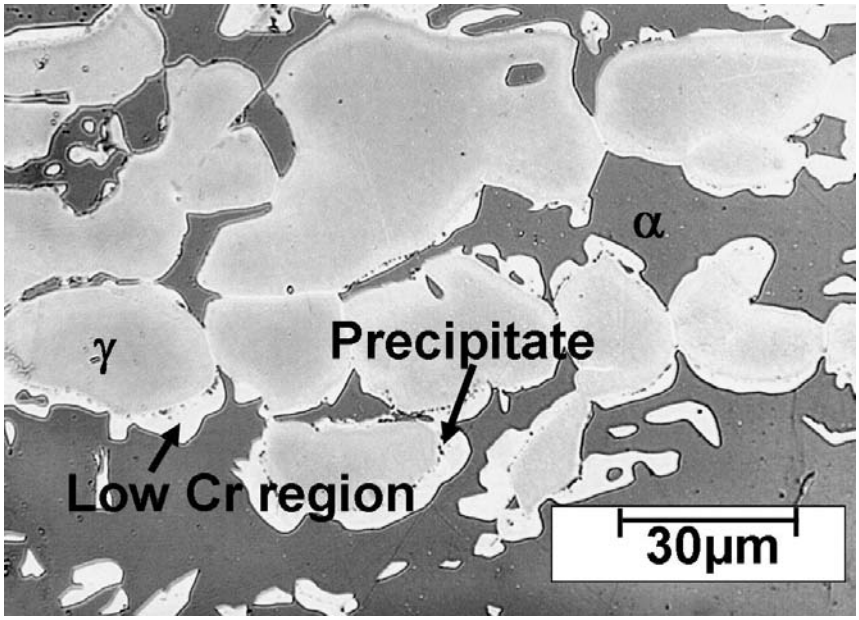

Figure 4.14. 2101 DSS annealed at 1100 °C, aged at 800 °C showing intermetallic precipitation and low chromium lighter region at α/γ interface with 4hrs of aging

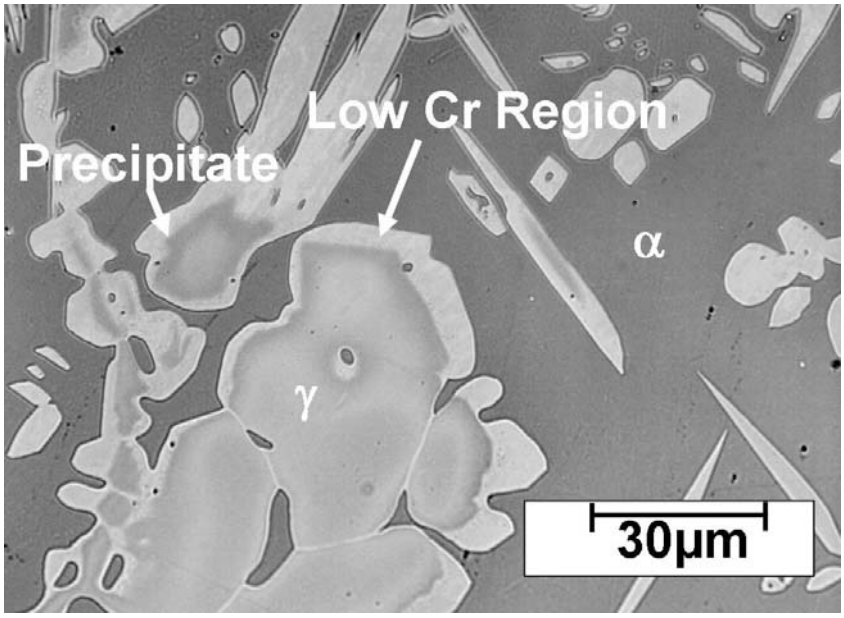

Figure 4.15. 2101 DSS annealed at 1100 °C, aged at 800 °C showing intermetallic precipitation and low chromium lighter region at α/γ interface with 8hrs of aging

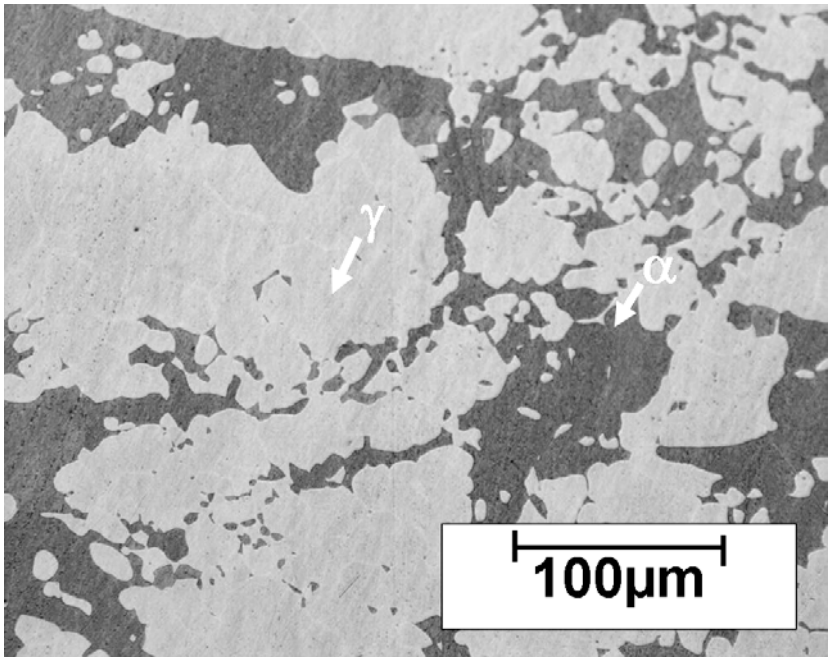

Figure 4.16. 2101 DSS annealed at 1100 °C and water quenched

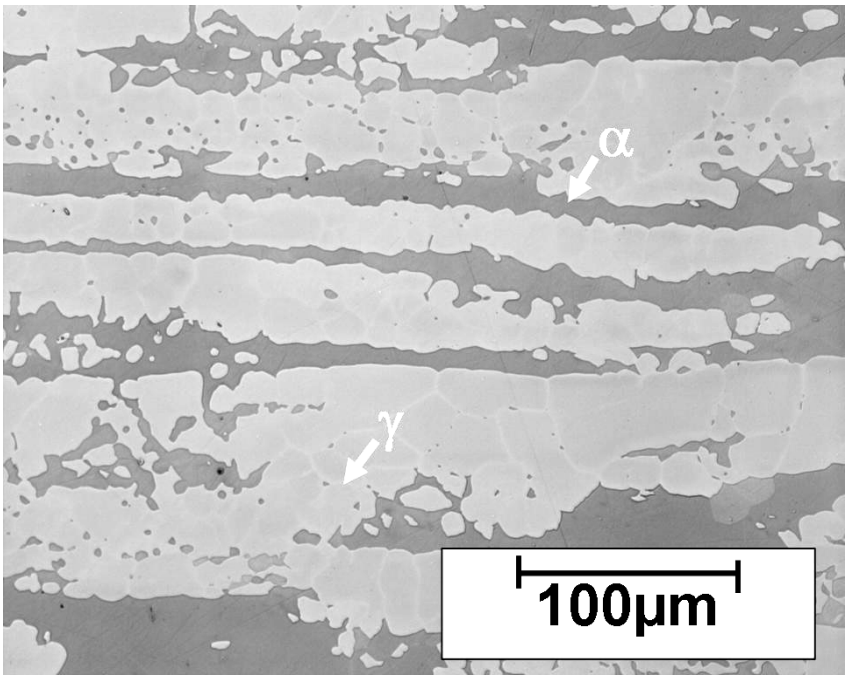

Figure 4.17. 2101 DSS annealed at 1100 °C, water quenched and aged at 475 °C

4.3.1.2. Chemical Analysis of DSS Phases in 2101 DSS

EDS was used for chemical analysis of the different phases in DSS samples after each heat treatment. To check the reproducibility of chemical analysis, fifteen different areas each of ferrite phase, austenite phase and the lighter region at the interface were analyzed. Forty precipitates were also analyzed for their composition. Figure 4.18 shows the SEM micrograph of precipitates formed after aging treatment at 800°C for 8hrs. Shape of these precipitates varies from round to ellipsoidal, with some precipitates showing a curved structure. EDS spectra corresponding to one of the precipitates in Figure 4.18 is shown in Figure 4.19 while the average composition of the precipitates, based on analysis from forty precipitates, is given in TABLE 4.4. From the micrographs and the EDS results, it can be inferred that the precipitates formed in the parent austenite phase of S32101 sample aged at 800°C had high chromium content (33.35 wt.%) as compared to the ferrite and austenite phases. Chemical composition of the lighter region near the

precipitates showed lower chromium (18.48 wt. %) and molybdenum (0.37 wt. %) content as compared to the precipitates. The chromium content in the lighter regions was even lower than that of the parent austenite. Low standard deviation in the chemical compositions in TABLE 2 indicates that the phase compositions were similar throughout the sample. XRD was used to characterize different phases and precipitates on this specimen and to determine if the sigma phase was present in these samples after 800°C aging. The XRD pattern from these samples was compared with the values in the literature [13][14]. The XRD pattern did not show any sigma peaks. However, in a similar study performed by Berner et al., the precipitates formed in S32101, aged at 800 °C, were identified as $M_{23}C_6$ by using transmission electron microscopy and selected area diffraction (TEM/SAD) [15]. Chromium depleted regions delimited from the austenite phase by precipitates, similar to the ones identified in this study, were also reported by Berner et al. and they identified this phase as secondary austenite γ_2. Hence, from our results and published work, it can be inferred that the high chromium containing precipitates formed in this study may be chromium carbides, which also result in the formation of low chromium containing secondary austenite, which appears as a lighter region around the precipitates.

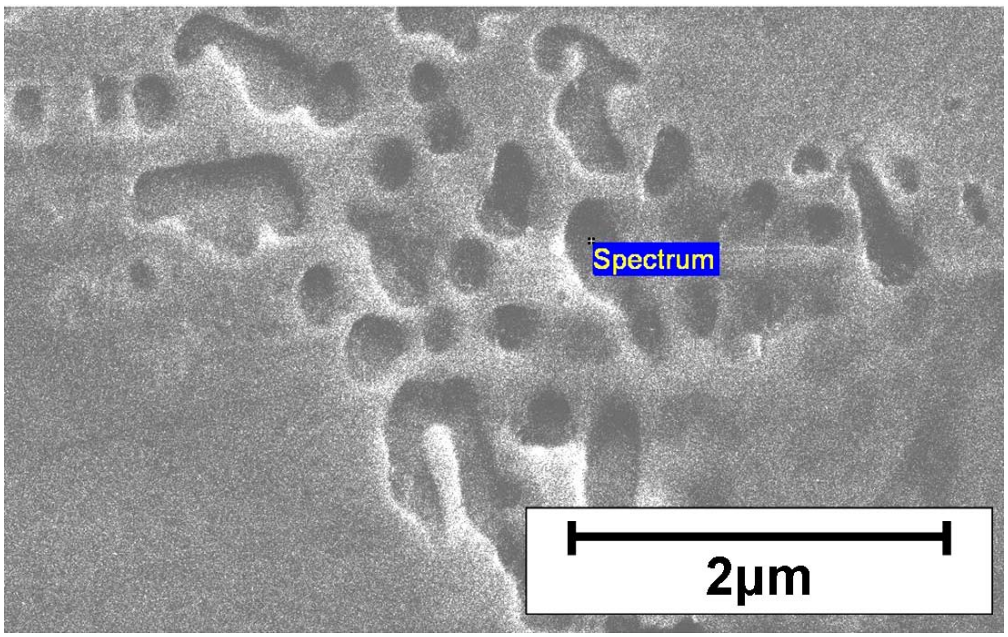

Figure 4.18. Secondary electron image showing precipitates in 2101 DSS aged at 800 °C

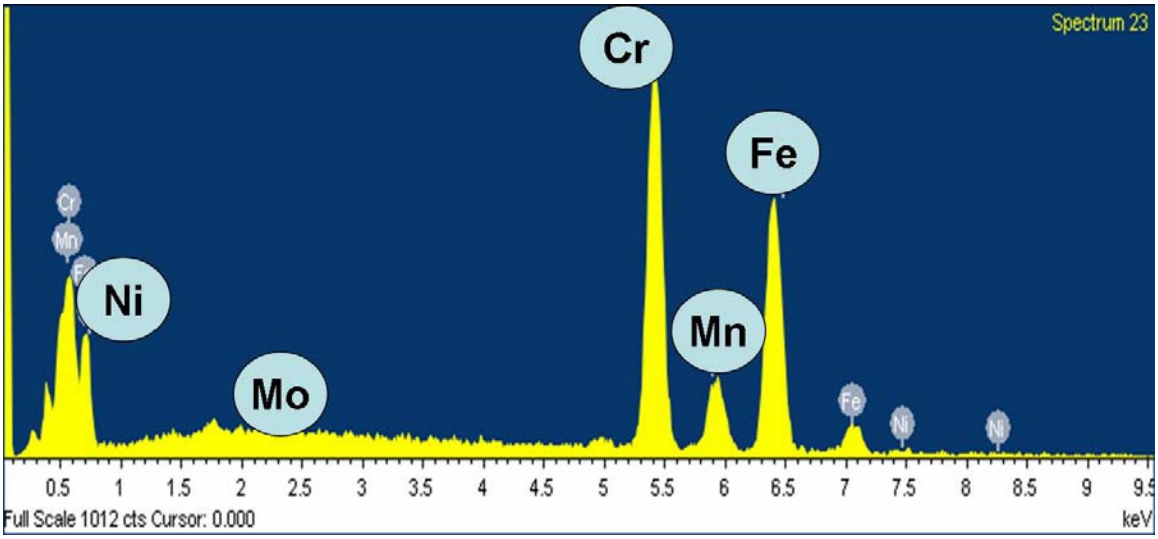

Figure 4.19. EDS spectra of intermetallic precipitate in Figure 4.18 showing high chromium content with presence of manganese and iron.

4.3.1.3. Partition coefficient of alloying elements in 2101 DSS

The partition coefficient of alloying elements in S32101 DSS was determined by microanalysis using EDS. The partition coefficients were calculated by taking the ratio of concentration of each element in the ferrite phase to that in the austenite phase. Calculated partition coefficients for Fe, Ni, Cr, Mn, and Mo are given in TABLE 4.4. The coefficients for Cr, Ni, Mo and Mn in S32101 were found to be 1.14, 0.57, 1.8 and 0.84 respectively. These values indicate that the ferrite phase is enriched in Cr and Mo and the austenite phase is enriched in elements such as Ni and Mn, which is as expected and in agreement with the values in literature [16]. Partition coefficients in 2205 DSS have been reported to be 1.2 for Cr, 0.58 for Ni and 1.72 for Mo [17]. Partition coefficients for S32101 and 2205 were found to be very similar.

TABLE 4.4. AVERAGE CHEMICAL COMPOSITION OF DIFFERENT PHASES PRESENT IN S32101 DSS AGED AT 800 °C

Phases	**Average Chemical Composition, in wt. %, *(Standard Deviation)***				
	Cr	**Fe**	**Ni**	**Mn**	**Mo**
Ferrite	23.42,*(0.29)*	70.05 *(0.58)*	1.16,*(0.4)*	4.89,*(0.25)*	0.48,*(0.19)*
Austenite	20.64 *(0.24)*	71.25 *(0.39)*	2.02,*(0.26)*	5.82,*(0.34)*	0.27,*(0.16)*
Depleted zone at α/γ interface (B)	18.48, *(0.62)*	72.58, *(0.61)*	2.24,*(0.24)*	6.34,*(0.24)*	0.37,*(0.16)*
Precipitate (A)	33.35, *(6.16)*	60, *(5.65)*	1.12,*(0.38)*	5.25,*(0.67)*	0.40,*(0.17)*

TABLE 4.5. PARTITION COEFFICIENT BETWEEN FERRITE AND AUSTENITE FOR DIFFERENT ELEMENTS

Grade	**Partition coefficient**				
	Cr	**Fe**	**Ni**	**Mn**	**Mo**
S32101	1.14	0.98	0.57	0.84	1.8

TABLE 4.6. S32205 WITH DIFFERENT HEAT TREATMENTS

Code for 2205 Samples	Annealing Temperature °C	Cooling	Aging Temperature °C	Aging time (hrs)	% Ferrite
D5-as received	1040	water quench	-	-	58
D5-1000-WQ	1000	water quench	-	-	54
D5-1000-WQ-475	1000	water quench	475	4	52
D5-1000-WQ-600	1000	water quench	600	4	49
D5-1000-WQ-800	1000	water quench	800	1	38
D5-1150-WQ	1150	water quench	-	-	59.5
D5-1150-WQ-475	1150	water quench	475	4	63
D5-1150-WQ-600	1150	water quench	600	4	60
D5-1150-WQ-800	1150	water quench	800	1	51.8

4.3.2. Microstructure of Heat treatment S32205 DSS

2205 DSS is the commonly used grade for pulp mill equipments. Hence, it is important to characterize the changes in microstructure due to various heat treatments, which might affect the corrosion and SCC susceptibility of the steel in caustic environment. To study this effect, 2205 steel samples with compositions listed Table 2.1 (Chapter 2) were subjected to selected heat treatments. Two different annealing treatments given to the DSS S32205 samples in this study involved heating the samples at 1000°C or 1150°C for one hour followed by water quenching. After annealing treatments, the 2205 DSS samples were aged at three different aging temperatures, similar to ones used for S32101 i.e.475°C (for 4 hrs), 600°C (for 4 hrs), and 800°C (for 1hr). TABLE 4.6 summarizes the different heat treatments given to the S32205 samples and the sample codes for each heat-treated sample used in this study. In each sample-code, D5 represent 2205 DSS. 1000°C and 1150°C represents annealing temperatures. 475°C, 600°C and 800°C refers to the aging temperatures given to that particular sample.

The percentage ferrite for differently heat-treated samples, shown in TABLE 4.6, shows the difference in the phase ratios between the as received sample and the heat-treated samples. The effect of annealing temperatures on the phase ratio of the steel is evident from these results. The as-received sample was annealed at 1040°C and had a percentage ferrite of 58%. However, annealing the samples at lower temperatures (1000°C) had resulted in a decrease in the percentage ferrite of the steel and annealing at higher temperatures (1150°C) had resulted in a higher ferrite volume fraction of the steel. All the samples annealed at 1150°C showed a higher ferrite volume fraction as compared to samples annealed at 1000°C and subjected to similar aging temperatures. Prior work has shown that when duplex stainless steels are annealed above 1100 ºC, the austenite phase dissolves and its fraction decreases near the solidus temperature, depending upon the chemical composition of the alloy. This is also evident from Figure 4.20 which shows the pseudo-binary phase diagram of DSS containing 68% Fe. On cooling, retransformation of austenite takes place. Slow cooling favors more austenite retransformation. However, this austenite-to-ferrite transformation is suppressed if the cooling is rapid. Hence, annealing 2205 DSS to a higher temperature resulted in dissolution of austenite into δ-ferrite. Rapid cooling by water quenching did not allow enough retransformation of austenite to take place. Therefore, the resulting microstructures of 2205 DSS samples annealed at higher temperatures showed higher ferrite content. Moreover, samples aged at 800°C showed the lowest volume fraction of ferrite as compared to all other samples. At higher aging temperatures, some ferrite may have undergone eutectoid decomposition into the sigma phase, resulting in lower ferrite volume fraction in the matrix [1]. Micrographs in Figure 4.23 to Figure 4.29 also indicate

higher ferrite content of samples annealed at 1150°C compared to the ones annealed at lower temperatures.

Annealing at higher temperature had also produced a change in the phase morphology of duplex stainless steels. The phases in the as received rolled sample were elongated along the rolling direction (Figure 4.21) and were smaller in size. Although, annealing at 1000°C did not produce a significant change in the phase morphology of the steel (Figure 4.22) but annealing at a higher temperature of 1150°C produced more evenly distributed grains with a significant growth in the size of the two phases (Figure 4.23). This difference in the phase morphology of 2205 DSS annealed at 1000°C and 1150°C can also be seen in the aged samples (Figure 4.24 to Figure 4.29). There was appreciable growth in the size of the phases as diffusion rates are higher at higher temperatures resulting in the coarsening of grains and larger grain growth in the resulting microstructure.

The sample D5-1000-WQ-475 aged at 475°C had reduced ferrite content as compared to the solution-annealed sample. Micrographs of D5-1000-WQ-475 and D5-1150-WQ-475 are shown in Figure 4.24 and Figure 4.25 respectively. No visible precipitation was observed in these samples under the optical microscope. Similarly, the optical micrographs of samples D5-1000-WQ-600 and D5-1150-WQ-600 in Figure 4.26 and Figure 4.27 respectively did not show any visible precipitations. Aging of duplex stainless steels may produce various intermetallic precipitates depending upon the aging time and temperature, as shown in Figure 4.35. Aging treatment at 600 ºC did not show any visible precipitation under optical microscope or SEM because according to the time temperature transformation (TTT) curve for 2205 DSS at 600 ºC (Figure 4.36), the

kinetics of precipitation is very slow. Hence, 4 hours of aging treatment at 600 ºC may not be long enough to show any precipitation under optical microscope. However, both D5-1000-WQ-800 and D5-1150-WQ-800 aged at 800°C showed precipitation at the ferrite/austenite phase boundaries, as is evident from micrographs in Figure 4.28 and Figure 4.29 respectively. SEM images of D5-1000-WQ-800 shown in Figure 4.30 confirmed the presence of two types of precipitates, a lighter phase and a darker phase. These precipitates nucleated at the phase boundaries and had grown towards the ferrite phase. There was a distinct lighter region around the precipitates, as can be seen in Figure 4.31. Similar observation was also made for the sample annealed at 1150°C and aged at 800°C (D5-1150-WQ-800). In this case also, the precipitates had nucleated at the phase boundaries, as can be seen in Figure 4.32 and Figure 4.33. Higher magnification SEM images confirmed the presence of two types of precipitates and a lighter region around the precipitates (Figure 4.33). EDS was used to find the chemical composition of the precipitates and the results are summarized in TABLE 4.7. EDS results showed that these precipitates had higher chromium and molybdenum content as compared to the parent phase. EDX analysis of the lighter phase indicated that these precipitates were particularly enriched in molybdenum. Whereas the darker precipitate had very high chromium content and higher molybdenum as compared to the ferrite phase. The lighter region around the precipitates had lower chromium and molybdenum content as compared to the surrounding ferrite phase. X-ray diffraction of sample D5-1000-WQ-800 aged at 800°C for one hour was further used to identify precipitates. Figure 4.34 shows the X-ray diffraction spectrum of D5-1000-WQ-800 and as-received 2205 DSS. The X-ray diffraction data of D5-1000-WQ-800 confirmed the presence of sigma phase. Sigma

peaks identified in previous studies were used to identify sigma in this study [18]. XRD of the as-received sample (Figure 4.34) did not show any sigma peaks. According to the TTT curve of 2205 DSS (Figure 4.35 and Figure 4.36), aging at 800 ºC can produce χ and σ precipitations. Prior work has shown that the χ phase is enriched in molybdenum and the σ phase is enriched in chromium and molybdenum [19]. Hence, comparing the EDX results in TABLE 4.7 with previously established data, it can be inferred that the lighter precipitates were χ and the darker precipitates were σ phase. Lighter region was also observed around the precipitates, which had low chromium and molybdenum content. Sigma phase formation takes place due to the eutectoid decomposition of the ferrite according to the reaction: ferrite → sigma + secondary austenite [1]. During sigma phase formation, the surrounding regions may be depleted in chromium and molybdenum due to the formation of this secondary austenite [20]. Hence, the lighter region around the precipitate was secondary austenite. The lowering of ferrite in the samples aged at 800 ºC was due to the decomposition of ferrite into sigma and secondary austenite.

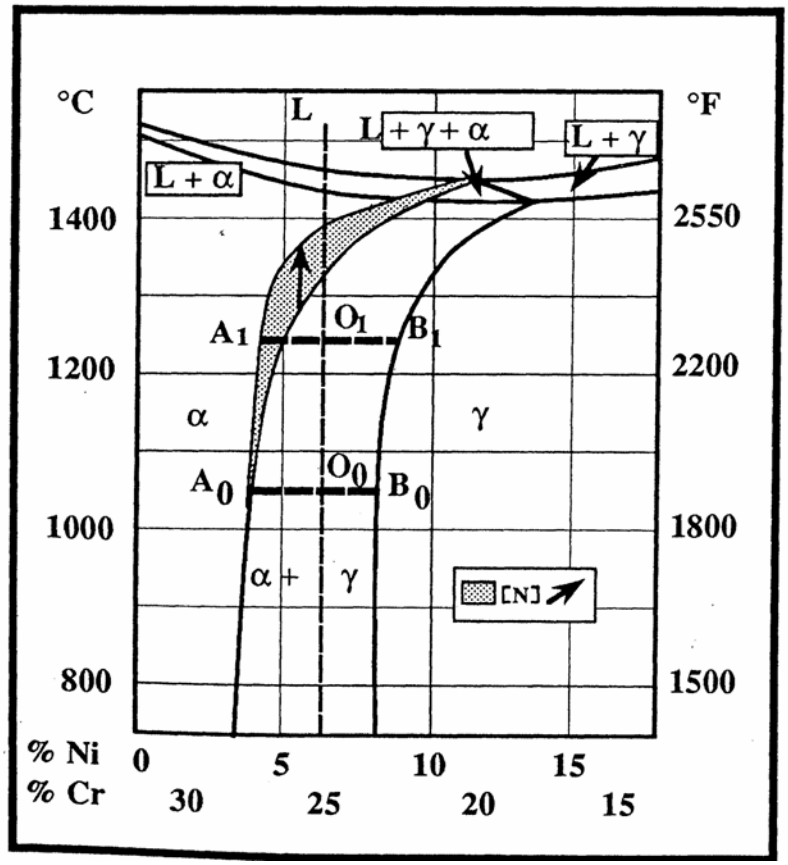

Figure 4.20. Pseudo-binary Cr-Ni-68Fe phase diagram [1]

Results from different heat treatments, as shown by the micrographs in Figure 4.22-Figure 4.33 clearly show that when duplex stainless steels are subjected to different thermal treatments (annealing, aging and cooling rates), these steels may undergo changes in the ferrite/austenite ratio, phase morphology, and produce intermetallic precipitations, depending on the heat-treatment given. All of these microstructural changes can influence the corrosion and SCC behavior of the DSS.

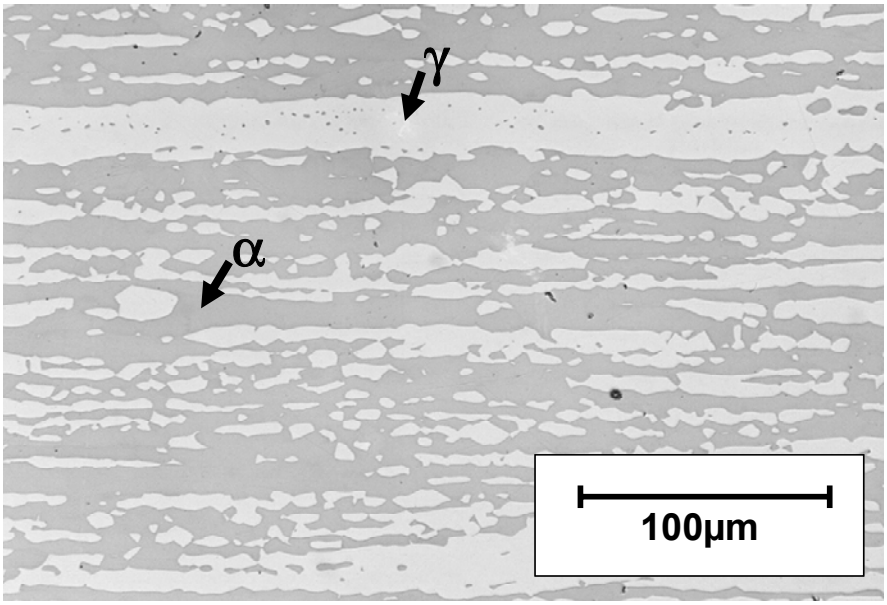

Figure 4.21. Optical micrograph of as received2205 DSS

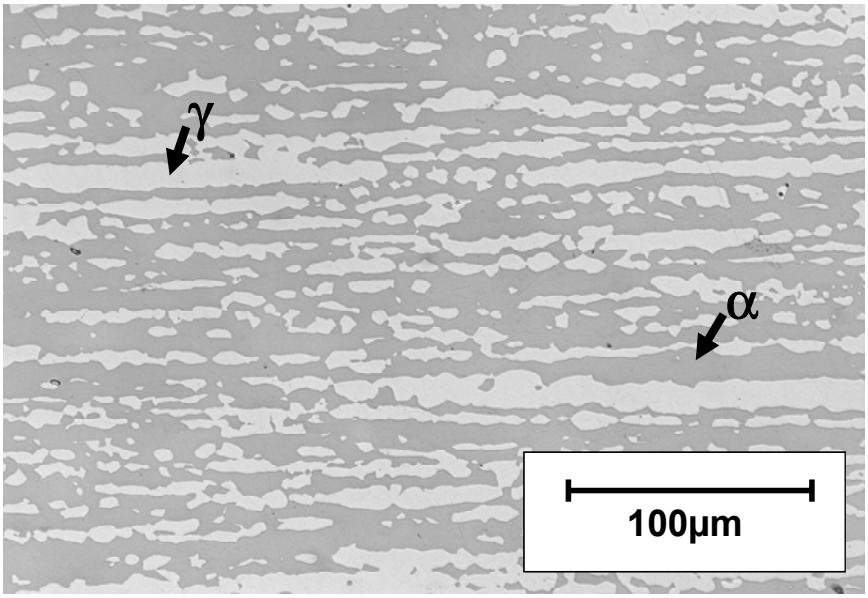

Figure 4.22. Optical micrograph of D5-1000-WQ

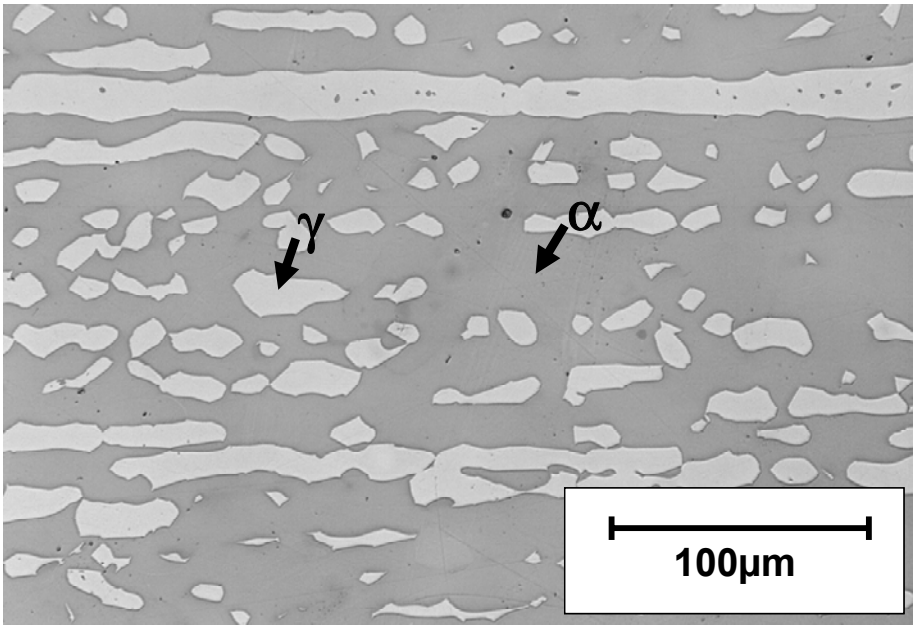

Figure 4.23. Optical micrograph of D5-1150-WQ

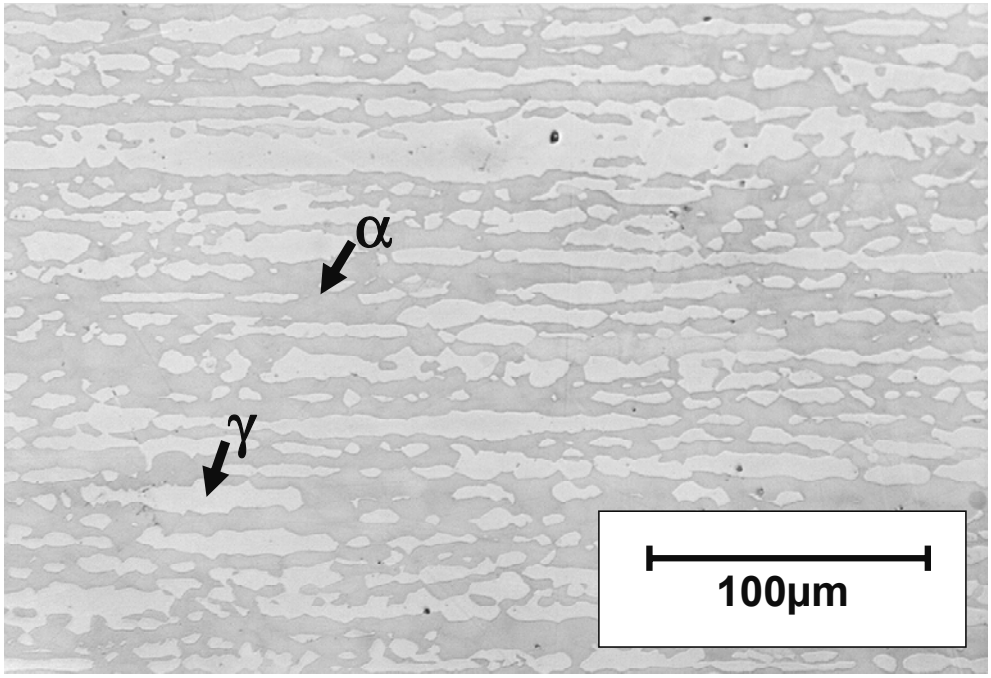

Figure 4.24. Optical micrograph of D5-1000-WQ-475

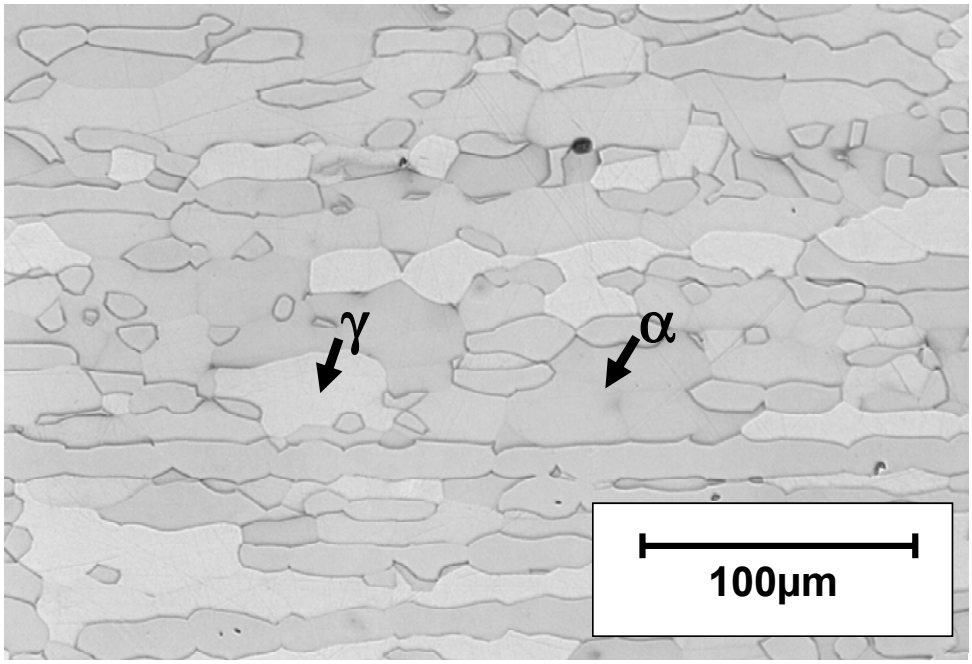

Figure 4.25. Optical micrograph of D5-1150-WQ-475

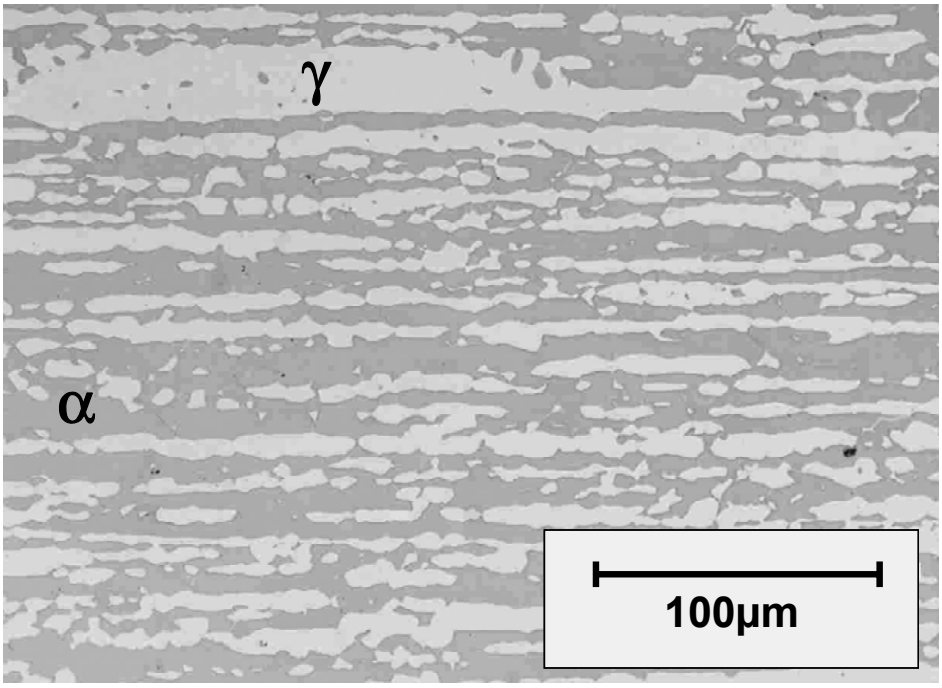

Figure 4.26. Optical micrograph of D5-1000-WQ-600

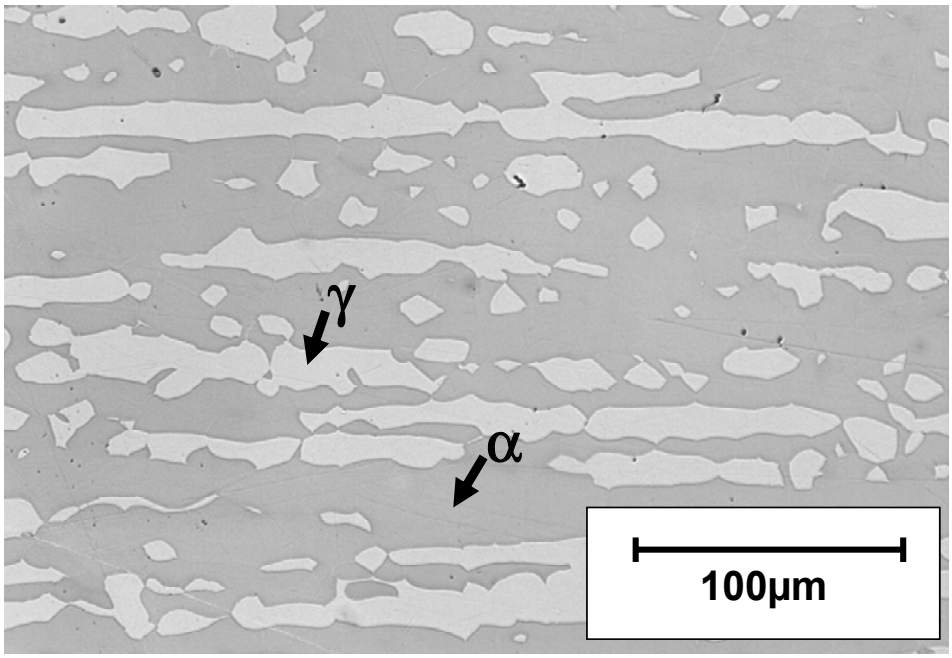

Figure 4.27. Optical micrograph of D5-1150-WQ-600

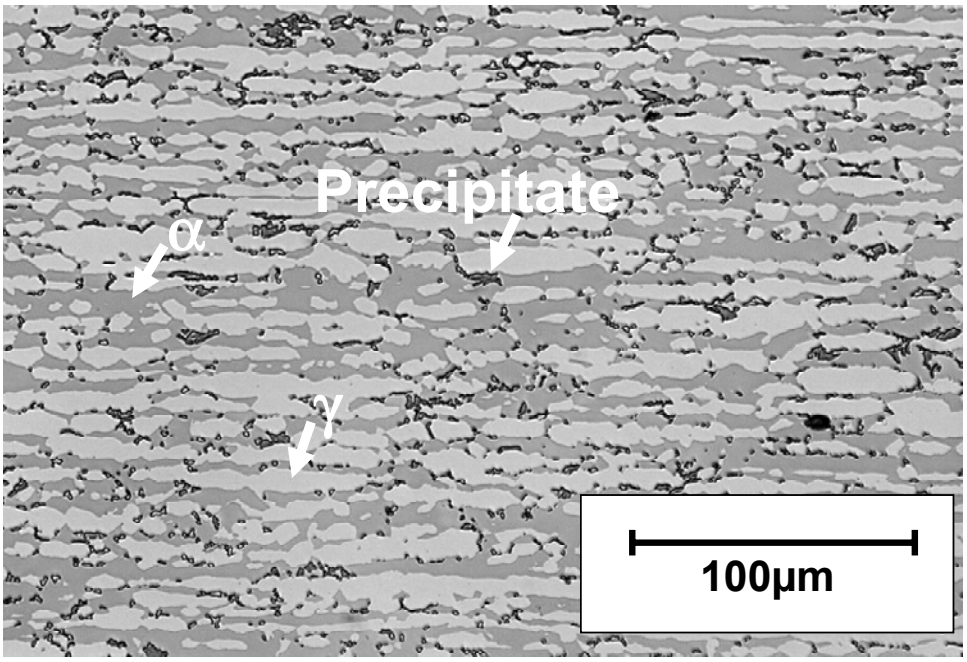

Figure 4.28. Optical micrograph of D5-1000-WQ-800

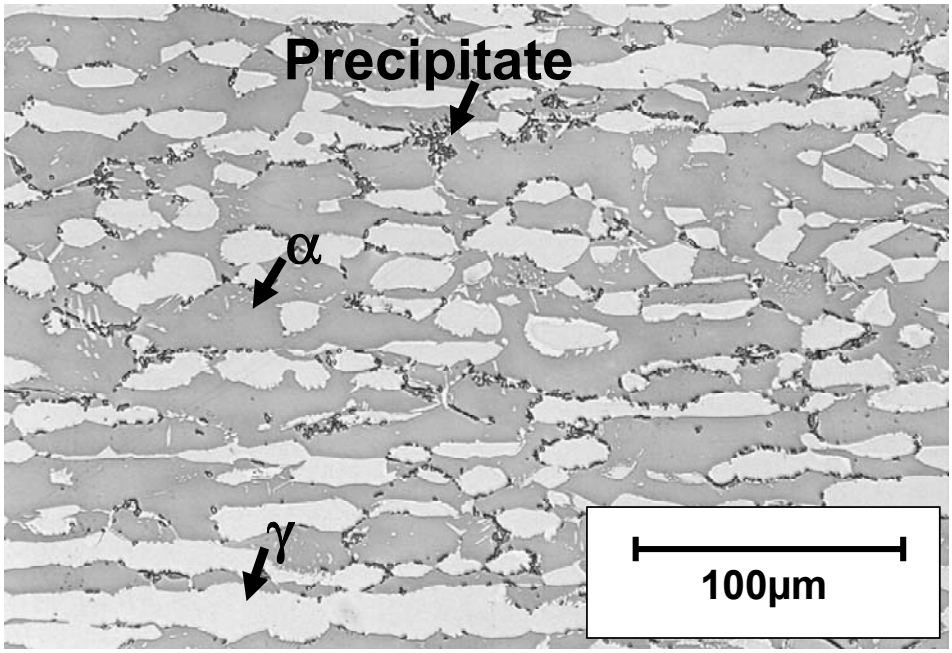

Figure 4.29. Optical micrograph of D5-1150-WQ-800

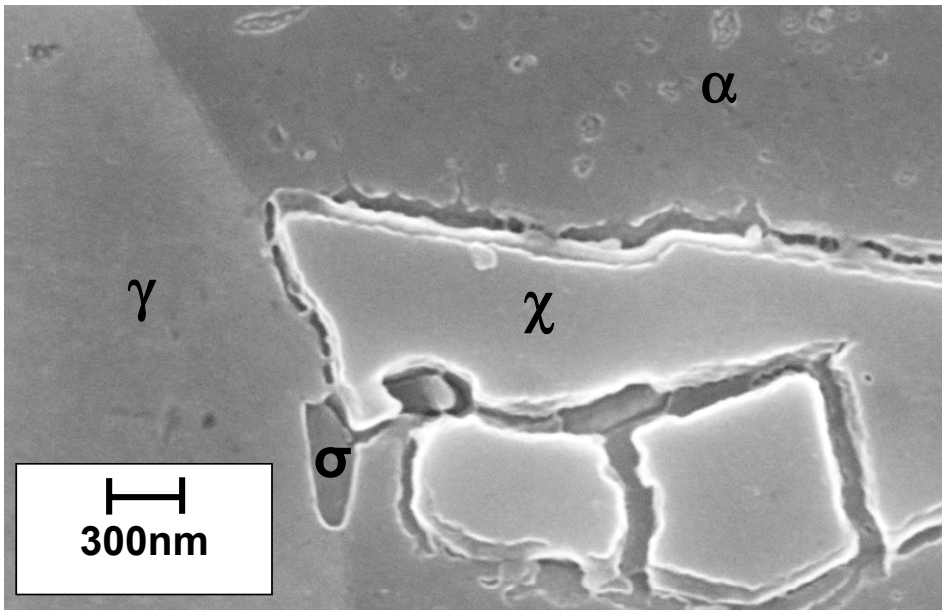

Figure 4.30. SEM image of D5-1000-WQ-800 showing σ and χ precipitates

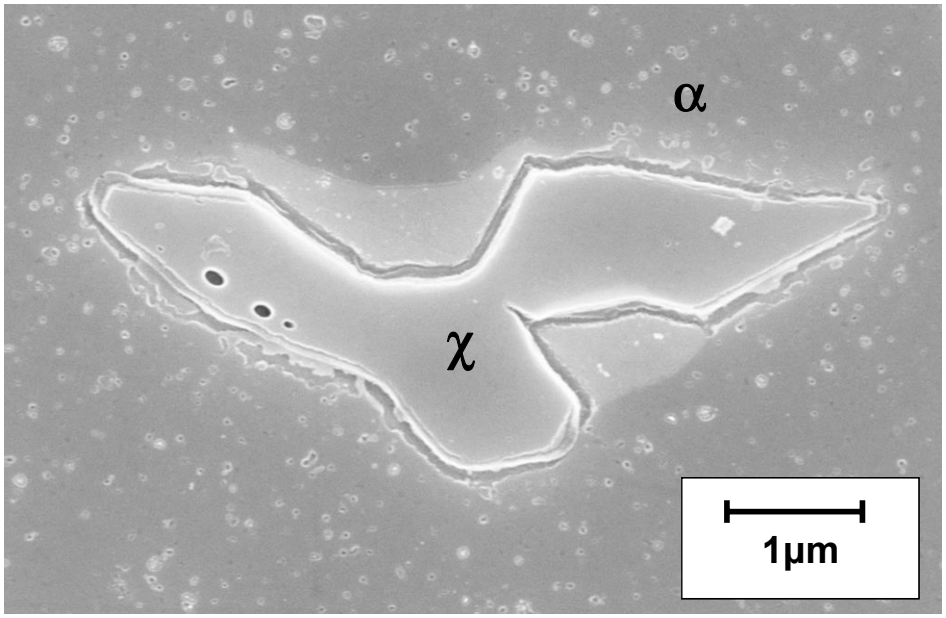

Figure 4.31. SEM image of D5-1000-WQ-800 showing lighter chromium and molybdenum depleted zone around χ phase

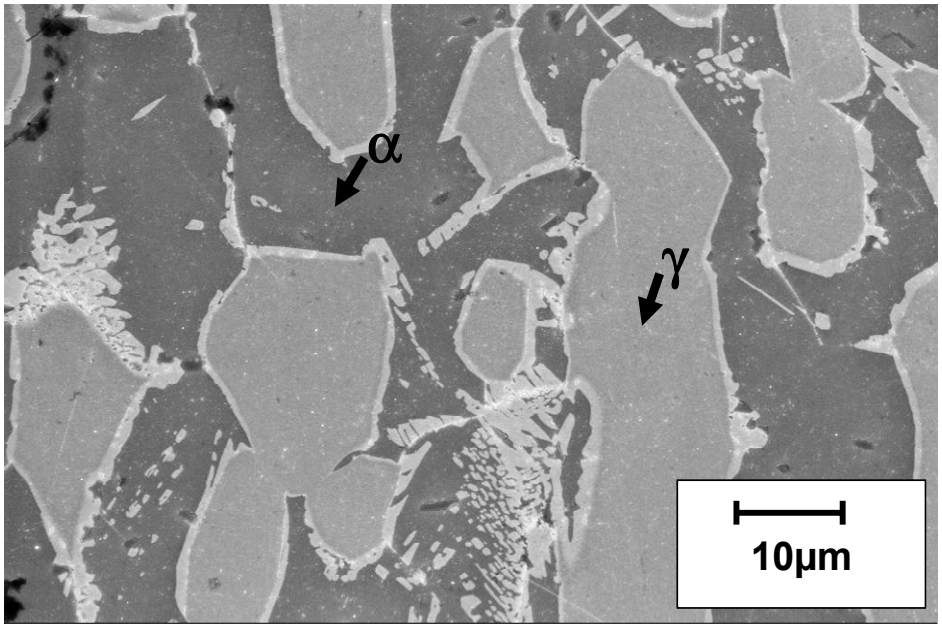

Figure 4.32. SEM image of D5-1150-WQ-800 showing lighter chromium and molybdenum depleted zone at the phase boundaries

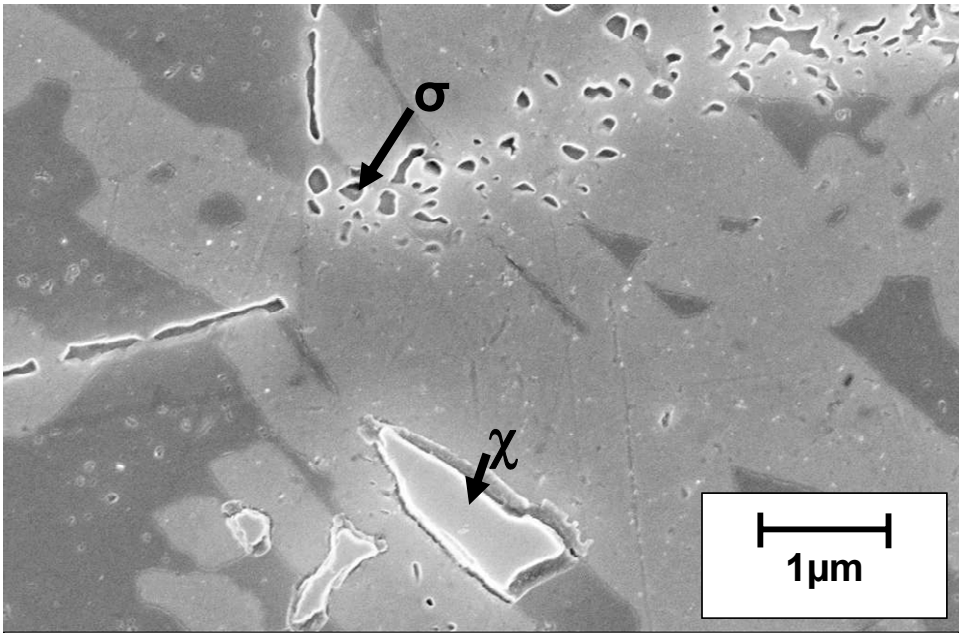

Figure 4.33. SEM image of D5-1150-WQ-800 showing σ and χ precipitates surrounded by depleted zone

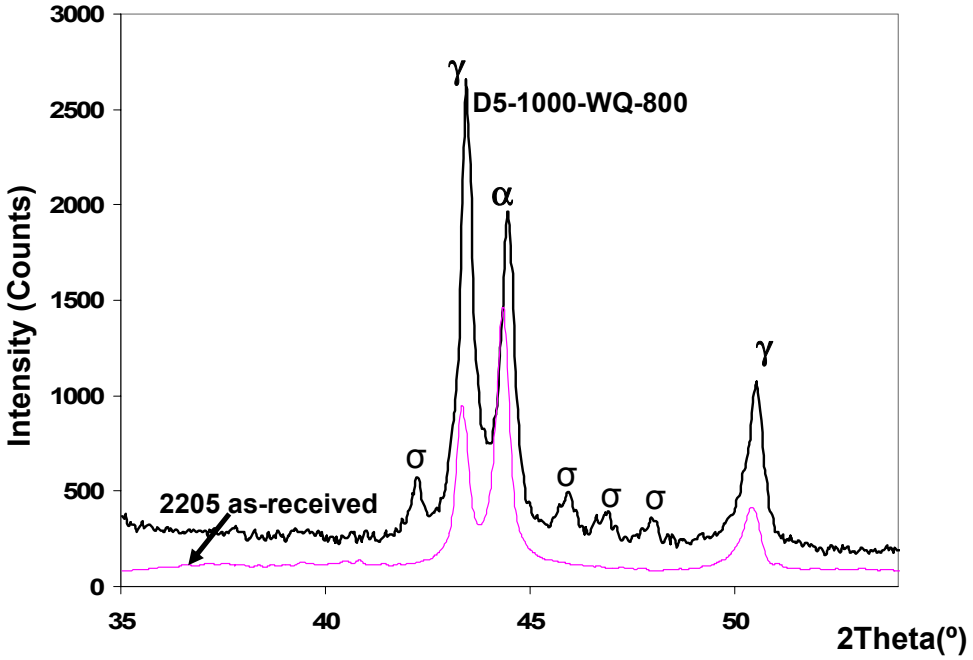

Figure 4.34. X-ray diffraction patterns of D5-1000-WQ-800 and as-received 2205 DSS

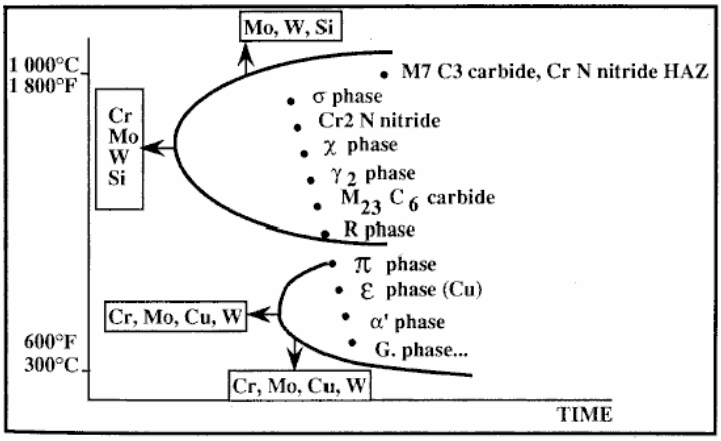

Figure 4.35. TTT curve for DSS showing possible precipitations in DSS [17]

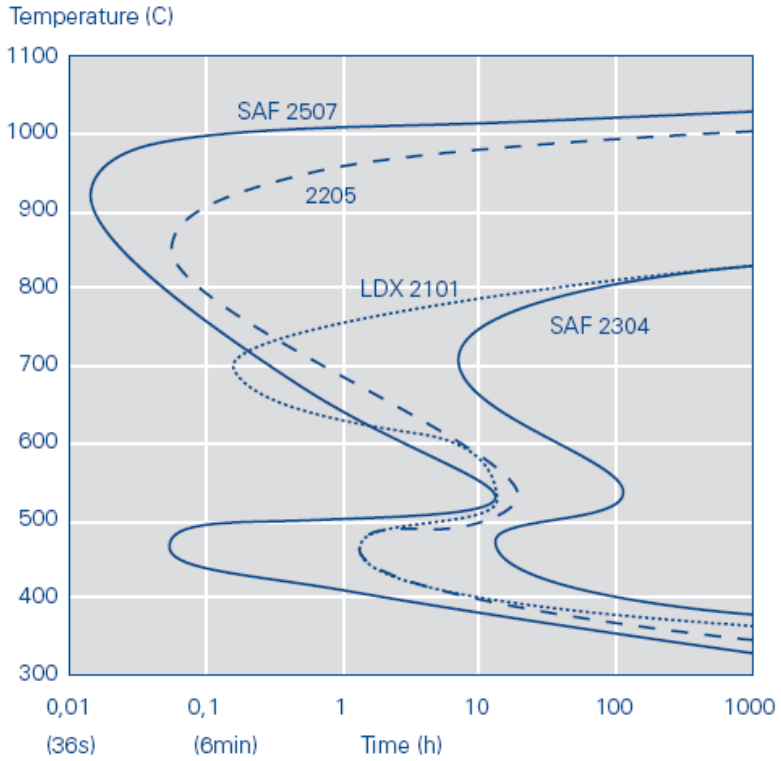

Figure 4.36. TTT curves for various duplex stainless steel grades showing relation between time and temperature that leads to formation of various intermetallic phases. [21]

TABLE 4.7. AVERAGE CHEMICAL COMPOSITION OF DIFFERENT PHASES PRESENT IN S32205 AGED AT 800°C AS DETERMINED BY EDX

Phases	Cr	Fe	Ni	Mo
Ferrite	26	66.4	3.7	4
Austenite	22.2	68.4	6.8	2.6
Sigma (σ)	40.5	46.5	3.6	9.4
Chi (χ)	25	61.7	2.6	16.8
Lighter region around precipitates	18.9	70.8	8.1	2.4

The results of the heat treatments performed on 2101 and 2205 DSS indicated that identical annealing and aging treatments given to the two grades of DSS did not seem to produce similar microstructures (phase ratio, precipitates). This difference in the behavior of the steels can be attributed to the difference in composition of both the grades of DSS. For S32101 DSS the percentage ferrite in the heat-treated specimens annealed at 1000ºC ranged from 42% (for D1-1000) to 36% (for D1-1000-800). Precipitates formed at 800 ºC did not produce a considerable reduction in the ferrite content of the steel. On the other hand, for S32205 DSS, the % ferrite decreased from 54% (for D5-1000) to 38% (for D5-1000-800). This significant decrease in ferrite content could be attributed to the sigma precipitates formed in S32205 due to the eutectoid decomposition of the ferrite phase. No sigma was detected in 2101 DSS. The composition of the precipitates formed at 800 ºC was also different for 2101 and 2205 DSS. Whereas precipitates formed in 2101 DSS aged at 800 ºC showed high chromium and manganese content due to the presence of manganese in the steel, 2205 DSS had produced precipitates (sigma and chi precipitates) containing high chromium and molybdenum content and were devoid of manganese. The amount of molybdenum in the precipitates of S32101 was also low due to the overall low Mo content of the steel. Precipitates formed in 2101 DSS had grown into the austenite

phase whereas precipitates found in 2205 DSS had grown into the ferrite phase. However, in both the grades of DSS, secondary austenite phase depleted in chromium were found around the precipitates. This comparative study on the effect of heat treatment on two grades of DSS differing in alloy composition clearly indicate that composition of DSS plays an important role in the evolution of microstructure during heat treatments.

4.3.2.1. Mechanical properties of ferrite and austenite phased in heat treated 2205 DSS

Various thermo-mechanical treatments may change the hardness of the ferrite and austenite phases of DSS, which will, in turn, affect the steel's overall mechanical behavior and SCC susceptibility. For example, ά precipitates formed during '475 embrittlement' of DSS cause immobilization of dislocations in the ferrite phase resulting in an increase in the hardness and in severe embrittlement of the ferrite phase [22]. To find out the effect of heat treatment (annealing and aging temperatures) on the hardness of the two phases of 2205 DSS, nanoindentations and Vickers hardness tests were performed on the ferrite and austenite phases of five DSS samples as listed in TABLE 4.8. The heat treatment procedure for the as-received DSS grade was according to ASTM A 480/A 480M – 06b. Although the annealing temperatures of the as-received and solution annealed samples were almost similar but the results showed that the overall hardness of the as-received DSS samples was higher as compared to the solution annealed samples. This indicates that sufficient strain hardening had occurred in DSS during thermo-mechanical treatments, rolling, of the as-received steel plates. The strain hardening of the as-received DSS is also evident from the stress-strain curves in Figure 4.43 and Figure 4.44. The hardness of the ferrite phase was found to slightly higher as

compared to the austenite phase. Solution annealing at both 1000°C and 1150°C has resulted in a decrease in the hardness values of the two phases, which shows that the solution annealing had decreased some of the strain hardening effects of the as-received DSS. The greater toughness of the solution-annealed specimens, D5-1000-WQ and D5-1150-WQ as shown by the area under the stress strain curve in Figure 4.43 and Figure 4.44, further shows that annealing had resulted in an increase in toughness of DSS as compared to the as-received structure. Vicker's microhardness results of D5-1000-WQ-475 showed an increase in the hardness of the ferrite phase (326.7) as compared to the specimens annealed at 1000 °C (279.8) without aging, but the nanoindentation results did not indicate this embrittlement effect in D5-1000-WQ-475. However, specimen annealed at 1150°C and aged at 475°C showed a significant increase in the hardness of the ferrite phase as compared to the austenite phase from the solution annealed specimen (D5-1150-WQ-475), which may be due to ά precipitates formed at that temperature, as shown by the hardness data in TABLE 4.8.

TABLE 4.8. NANO-HARDNESS AND VICKERS HARDNESS OF THE FERRITE AND AUSTENITE PHASES OF HEAT-TREATED 2205 DSS

Code for 2205 Samples	**Nano-hardness (GPa)**		**Vickers Hardness**	
	Ferrite	**Austenite**	**Ferrite**	**Austenite**
D5-as received	4.411	4.39	412	382
D5-1000-WQ	3.91	3.86	279.8	279.1
D5-1150-WQ	4.322	4.11	295.8	289.5
D5-1000-WQ-475	3.81	4.158	326.7	312.9
D5-1150-WQ-475	5.169	4.505	419	294.3

4.4. ROLE OF MICROSTRUCTURE ON THE GENERAL AND LOCALIZED CORROSION SUSCEPTIBILITY OF DSS

Microstructure plays a vital role in the general and localized corrosion susceptibility of materials. In order to find out how different microstructures produced during different heat treatments affect the general and localized corrosion susceptibility of DSS in sulfide-containing caustic solutions, the heat-treated DSS samples were exposed to high pH caustic environments. Similarly heat-treated DSS samples were further exposed to corrosion tests in low pH chloride environment to compare the corrosion behavior of DSS in the two different environments.

4.4.1. Corrosion susceptibility of 2101 DSS in acidic chloride solution

Corrosion tests were performed to evaluate the general and localized corrosion susceptibility of differently heat-treated S32101 in acidic ferric-chloride solution (pH~0.54). Serrated crevice washers were used in these tests to simulate local crevice conditions. Results in TABLE 4.9 show a significant effect of heat treatment and resulting microstructure on general and localized corrosion behavior of S32101. The samples D1-1000-800 and D1-1100-800 aged at 800 °C and tested in acidic chloride solution showed a significant decrease in weight, which was predominately due to the pitting and crevice corrosion on test samples, as shown in Figure 4.37. Similar corrosion behavior was also seen for the S32101 samples aged at 600 °C, which also showed significant weight loss and pitting (Figure 4.38). However, the pit size and the pit density were much higher for the sample aged at 800 °C as compared to the sample aged at 600 °C. The solution annealed unaged specimens (D1-1000 and D1-1100) and the specimens aged at 475 °C (D1-1000-475 and D1-1100-475) had lower weight loss and very few or

no pits after exposure to the ferric chloride solution at 25 ºC. Optical micrographs in Figure 4.39 and Figure 4.40 show the pit initiation sites in S32101 DSS specimens annealed at 1100ºC and aged at 800 ºC and 600 ºC respectively. Pitting had initiated near the ferrite/austenite phase boundaries in the specimen aged at 800 ºC, as shown in Figure 4.39. Pit initiation could be a result of the selective dissolution of one phase versus another. The micro-galvanic cells formed between the noble and active phases might have resulted in the selective dissolution of the less noble phase along the phase boundaries and initiated corrosion pits on S32101 DSS in acidic chloride solution. Chromium depletion in the secondary austenite phase at the ferrite/austenite phase boundary could also have resulted in an unstable passive film formation and pit initiation. Once initiated, the pits propagated through the ferrite phase, as is evident from Figure 4.39, indicating that the ferrite phase is more susceptible to dissolution and localized corrosion in low pH chloride environment. Pitting was also found in S32101 specimens aged at 600 °C. Optical micrograph of these specimens (Figure 4.40) suggest that pit initiation was also along the ferrite/austenite interface and these pits have grown in the ferrite phase. Although no visible precipitation was observed under optical microscope or SEM for samples aged at 600 °C, intermetallic precipitation is likely to occur in DSSs at temperatures between 600 °C and 1000 °C [23]. However, according to the TTT curve for S32101, shown in Figure 4.36, the growth kinetics for precipitates at 600 °C is very slow as compared to that at 800°C. Hence, the precipitates may be too small to be detected by optical microscopy or SEM and further TEM investigation may be required for their detection. It is likely that the pit initiation in S32101 specimens aged at 600 °C

may also be due to selective dissolution of precipitates formed at ferrite/austenite interface.

For precipitation in S32101 DSS in the temperature range of 350 °C to 525 °C, the nose of the TTT curve is at 475 °C, indicating the temperature at which maximum precipitation could occur. However, the specimens aged at 475 °C for 4hours did not show any significant pitting. This may be due lack of sufficient precipitation for the localized corrosion to occur. Previous work has shown that the formation kinetics of α' phase is very slow and localized corrosion resistance of 24.6 Cr, 6.6 Ni DSS in chloride solution decreases after 100 hours of aging [24].

TABLE 4.9. WEIGHT LOSS DUE TO GENERAL AND LOCALIZED CORROSION OF HEAT TREATED S32101 DSS IN 6% $FECL_3$ SOLUTION AT 27^OC FOR 4 DAYS

Heat treated sample	Weight Loss ($mg/dm^2/day$)*	Localized Corrosion	
		Pitting	Crevice
D1-1000	254.4	*Pitting*	*Yes*
D1-1000- 475	876.84	*No*	*Yes*
D1-1000- 600	1661.10	*pitting*	*Yes*
D1-1000- 800	2374.23	*pitting*	*Yes*
D1-1100	298.53	*No*	*Yes*
D1-1100- 475	423.33	*No*	*Yes*
D1-1100- 600	2811.14	*pitting*	*Yes*
D1-1100-800	1299.40	*pitting*	*Yes*

***S32101 DSS samples had localized corrosion attack on the surface so general corrosion rates could not be calculated from the weight change in these tests.**

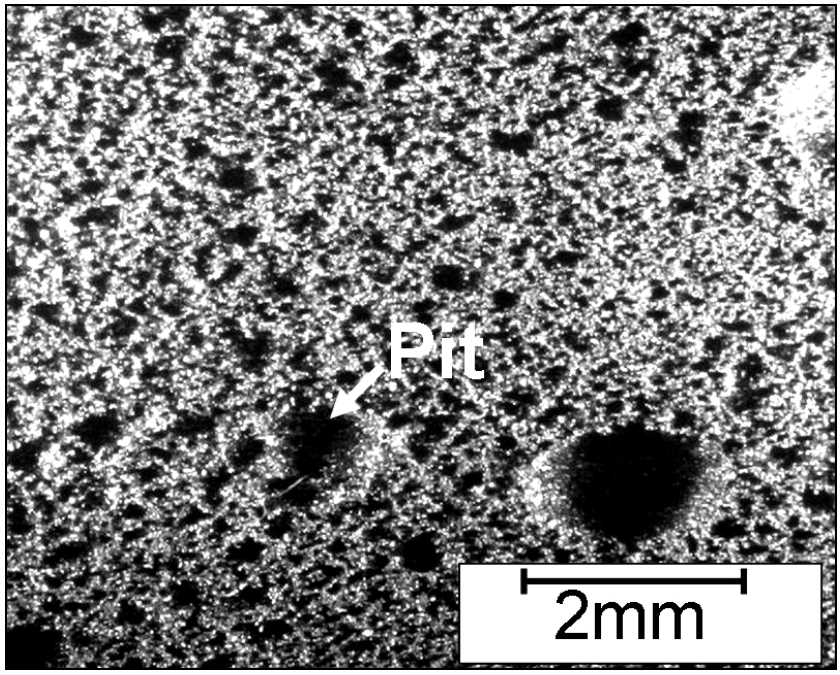

Figure 4.37. 2101 DSS showing pitting in chloride environment after annealing at 1100 °C and aging at 800 °C (1hr)

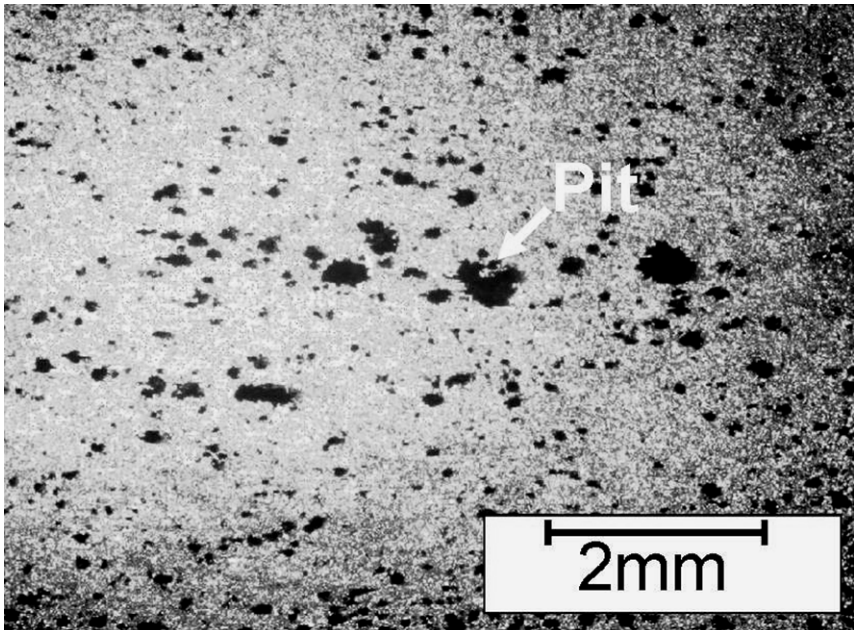

Figure 4.38. 2101 DSS showing pitting in chloride environment after annealing at 1100 °C and aging at 600 °C for 4hrs

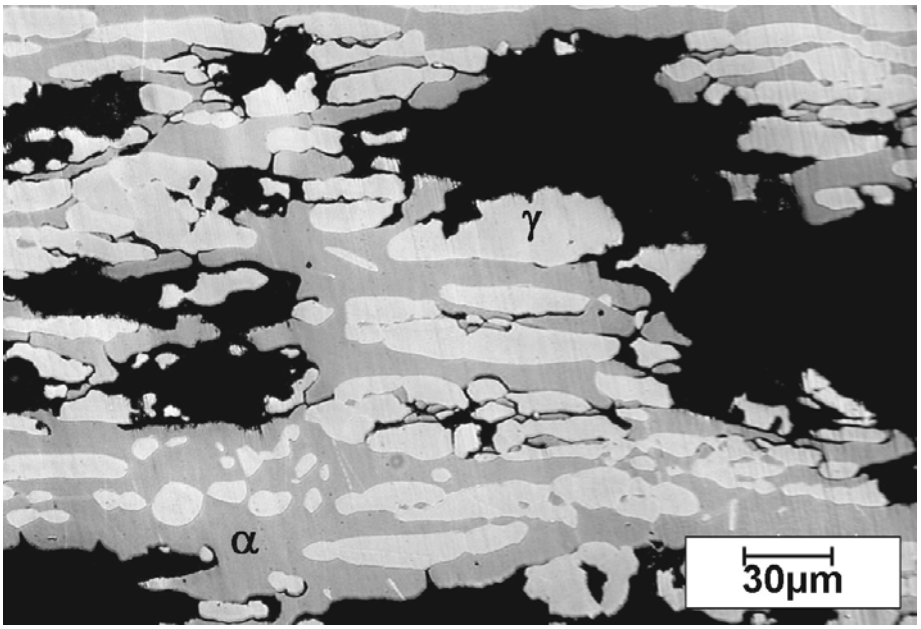

Figure 4.39. 2101 DSS showing selective dissolution of ferrite phase and pitting in chloride environment after annealing at 1100 °C and aging at 800 °C

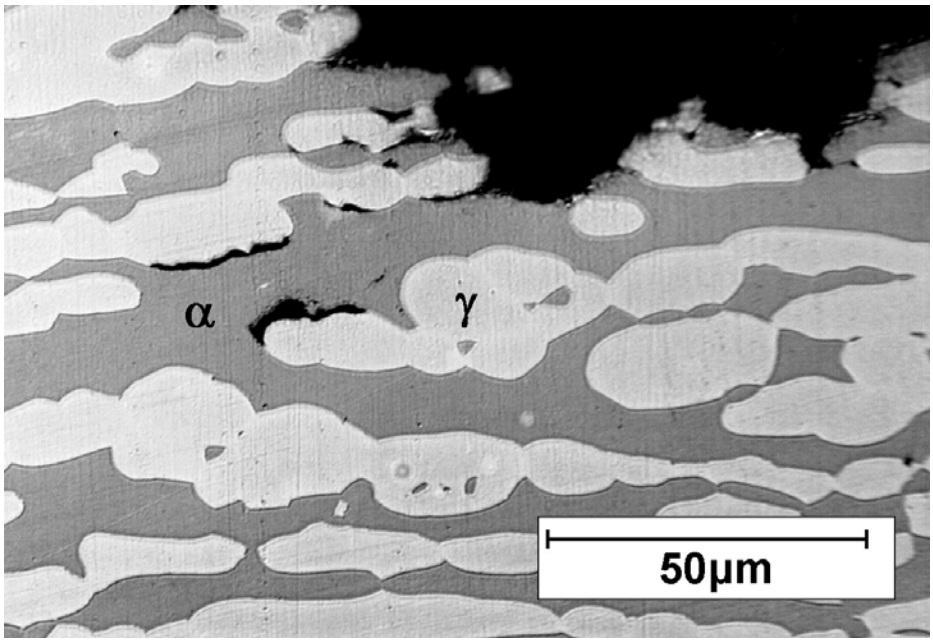

Figure 4.40. 2101 DSS showing selective dissolution of ferrite phase and pitting in chloride environment after annealing at 1100 °C and aging at 600 °C for 4hrs

4.4.2. Corrosion susceptibility of 2101 in sulfide-containing caustic solution

General and localized corrosion tests were performed in sulfide-containing caustic solution with high pH (~12.5), similar to the white liquor typically used in pulping kraft process. White liquors are considered to be the most corrosive in terms of general and localized corrosion as compared to other environments in a typical pulp mill. Sulfide in high pH sulfide-containing caustic solutions (white liquor) exists mainly as hydrated (HS^-) but also in the forms of sulfide (S^{2-}) and polysulfides [25]. Corrosion behavior of DSS alloys was very different in sulfide-containing caustic solutions compared to that in the acidic ferric chloride solution (TABLE 4.10). In sulfide-containing caustic solution, the general corrosion rates for S32101 was very low for all heat-treated samples. Weight changes for D1-1100-600 and D1-1100-800 in chlorides were 2811.14 mpy and 1299.40 mpy respectively (TABLE 4.9), significantly more than that in the caustic solutions (TABLE 4.10). No pitting or crevice corrosion was found on any of the heat treated S32101 samples tested in caustic environment. The specimens (aged at 800 °C and 600 °C) susceptible to localized corrosion in chloride solution were resistant to pitting or crevice corrosion in caustic environment.

Corrosion results show that the intermetallic precipitation, in samples aged at 800 °C, which has an adverse effect on the localized corrosion behavior of 2101DSS in acidic chloride solution had no effect on the corrosion behavior when tested in the sulfide-containing caustic solution at 170°C for 15 days. Microstructural features (ferrite/austenite ratio and intermetallic precipitates) formed due to the different heat treatments did not play a significant role in the general and localized corrosion behavior of the steel in sulfide-containing caustic solutions. This also indicates that the

microstructural changes in 2101 DSS due to welding or other thermomechanical fabrication process may not be as critical in high pH solutions like white liquors or other kraft pulping liquor in terms of corrosion susceptibility. These results are only applicable under static or low velocity flow conditions where the S32101 DSS does not have significant tensile stresses, whether applied or residual.

TABLE 4.10. CORROSION RATES AND LOCALIZED CORROSION SUSCEPTIBILITY OF HEAT TREATED S32101 DSS IN CAUSTIC SOLUTIONS AT 170°C FOR 15 DAYS

Heat treated sample	Corrosion Rate. ($mg/dm^2/day$)	Corrosion Rate. (mm/year)	Localized Corrosion.	
			Pitting	Crevice
D1-1000	36.51	0.17	*No*	*No*
D1-1000- 475	33.56	0.15	*No*	*No*
D1-1000- 600	36.85	0.17	*No*	*No*
D1-1000- 800	40.71	0.19	*No*	*No*
D1-1100	43.16	0.20	*No*	*No*
D1-1100- 475	49.3	0.18	*No*	*No*
D1-1100- 600	38.44	0.18	*No*	*No*
D1-1100- 800	40.44	0.18	*No*	*No*

4.4.3. Corrosion susceptibility of 2205 DSS in acidic chloride solution

Differently heat-treated S32205 was also tested for general and localized corrosion susceptibility in acidic ferric-chloride solution (pH~0.54). Results from the corrosion tests are shown in TABLE 4.11. Corrosion test results from these tests showed a significant effect of heat treatment and resulting microstructure on general and localized corrosion behavior of S32205, as was observed in case of 2101 DSS in chloride environment. The samples D5-1000-800 and D5-1150-800 aged at 800 °C and tested in

acidic chloride solution showed a significant decrease in weight which was predominately due to the pitting and crevice corrosion on test samples. Figure 4.41 shows cross section of pits formed in D5-1000-800 annealed at 1000°C and aged at 800°C. These pits formed in DSS in chloride environment can act as stress concentrators and precursor sites for SCC initiation. Micrograph of D5-1000-800 exposed to chloride environment indicates that the pits have initiated due to selective dissolution of the precipitates and have propagated into the ferrite phase (Figure 4.42). Prior work has shown that sigma phase precipitates makes the DSS alloys susceptible to localized corrosion in chloride environments. The ferrite phase is found to be susceptible to pitting in chloride environment.

TABLE 4.11. WEIGHT LOSS DUE TO GENERAL AND LOCALIZED CORROSION OF HEAT-TREATED S32205 DSS IN 6% FECL3 SOLUTION AT 27^{O}C FOR 4 DAYS

Heat treated sample	Weight Loss ($mg/dm^2/day$)	Localized Corrosion	
		Pitting	Crevice
D5-1000-WQ	0	*No*	*No*
D5-1000-WQ-475	2139	*Yes*	*Yes*
D5-1000-WQ-600	0	*No*	*No*
D5-1000-WQ-800	3220	*Yes*	*Yes*
D5-1150-WQ	0	*No*	*No*
D5-1150-WQ-475	1.34	*No*	*No*
D5-1150-WQ-600	1079	*No*	*Yes*
D5-1150-WQ-800	2096	*Yes*	*Yes*

***S32205 DSS samples had localized corrosion attack on the surface so general corrosion rates could not be calculated from the weight change in these tests.**

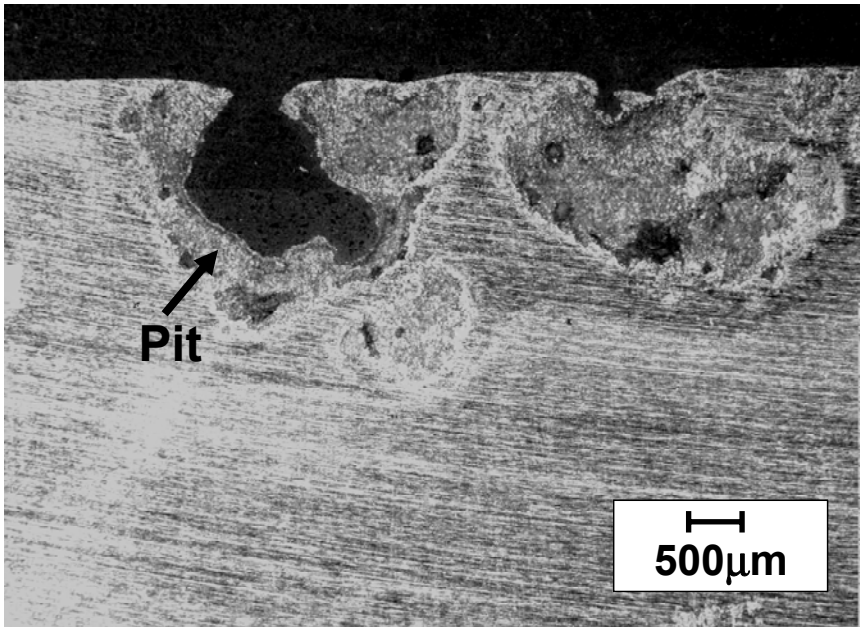

Figure 4.41. Micrograph showing cross section of pits in 2205 DSS exposed to chloride environment after annealing at 1000 °C and aging at 800 °C for 1hr

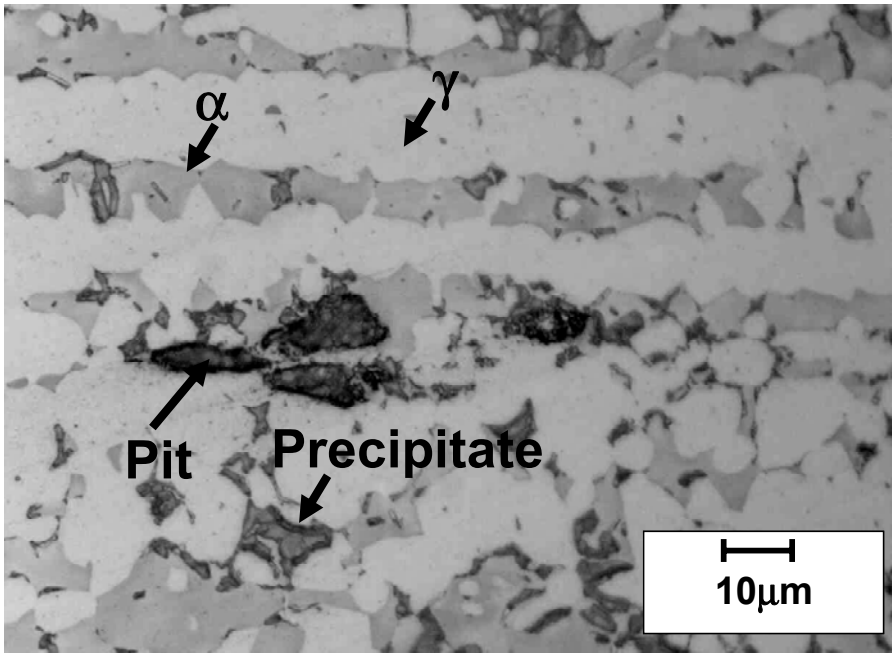

Figure 4.42. 2205 DSS showing selective dissolution of precipitates and pitting in chloride environment after annealing at 1000 °C and aging at 800 °C for 1hr

4.4.4. Corrosion susceptibility of 2205 in sulfide-containing caustic solution

Similarly heat treated 2205 DSS samples were exposed to sulfide-containing caustic solution (150g/L NaOH + 50g/L of Na_2S) for general and localized corrosion tests. The results of the tests are summarized in TABLE 4.12.

Heat treatments of 2205 DSS did have any significant effect on their general corrosion rates in sulfide-containing caustic environments. General corrosion rates for some 2205 samples in caustic environment were found to be less than 0.28mm/year. Different ferrite/austenite ratio and precipitation of second phase particles did not seem to have much effect on the general corrosion and corrosion pit initiation in 2205 DSS tested in caustic environment. These results are very different from that in chloride environment where the microstructure was found to have a significant effect on the general and localized corrosion susceptibility of duplex stainless steels [26].

Results from the corrosion exposure tests in caustic environment at 170°C indicate that the duplex stainless steel 2205 in as-received condition or under tested aging treatments are not susceptible to pitting or crevice corrosion in sulfide-containing caustic solutions. Heat treatments may cause changes in the microstructures of 2101 and 2205 DSS, but will not have any effect on the general and localized corrosion resistance of DSS in sulfide-containing caustic solution. Sigma, chi and secondary austenite precipitation did not cause localized corrosion of the steel in caustic environment. This behavior of DSS is very different from that in the acidic chloride environments, where the intermetallic precipitates such as sigma and chi are known to initiate pitting by selective dissolution of the chromium and molybdenum depleted regions around these precipitates [27]. In this study, in both 2101 and 2205 DSS, aging treatments at 600°C and 800°C were found to

affect their pitting and crevice corrosion susceptibilities adversely in chloride environment. Since corrosion pits can act as initiation sites for the stress corrosion cracks [6], absence of pits in the caustic solution indicates that the SCC initiation in DSS in this medium is not due to pitting and is different from the one for the chloride environments.

TABLE 4.12. GENERAL AND LOCALIZED CORROSION SUSCEPTIBILITY OF S32205 IN SULFIDE-CONTAINING CAUSTIC SOLUTION

Heat treated sample	Corrosion Rate. ($mg/dm^2/day$)	Corrosion Rate. (mm/year)	Localized Corrosion.	
			Pitting	Crevice
D5-1000-WQ	50.41	0.23	*No*	*No*
D5-1000-WQ-475	49.1	0.23	*No*	*No*
D5-1000-WQ-600	54.93	0.25	*No*	*No*
D5-1000-WQ-800	49.78	0.23	*No*	*No*
D5-1150-WQ	49.2	0.23	*No*	*No*
D5-1150-WQ-475	40.03	0.18	*No*	*No*
D5-1150-WQ-600	59.92	0.27	*No*	*No*
D5-1150-WQ-800	61.54	0.28	*No*	*No*

4.5. ROLE OF MICROSTRUCTURE ON THE STRESS CORROSION CRACKING SUSCEPTIBILITY OF DSS

Stress corrosion cracking susceptibility of duplex stainless steels in caustic solutions was the main drive for the present study. To understand the effect of microstructure and environmental parameters on SCC susceptibility of different DSS grades, tests were carried out on differently heat-treated samples. As-received as well as the heat-treated 2205 DSS tensile samples were tested by slow strain rate test method in sulfide-containing caustic solution. The results of the slow strain rate tests are summarized in TABLE 4.13. Results show that although microstructural differences in differently heat-treated DSS samples did not have much effect on the general and localized corrosion

behavior of 2205 DSS (TABLE 4.12), these differences had a significant affected on the SCC susceptibility of the steels in caustic environment.

TABLE 4.13. SCC SUSCEPTIBILITY OF S32205 IN SULFIDE-CONTAINING CAUSTIC SOLUTION

Code for 2205 Samples	% Ferrite	SCC Susceptibility	% Elongation	% Reduction in area	Linear Roughness Index
D5-as received	58	Yes	12.3	52.23	1.888
D5-1000-WQ	54	No	23.25	87.85	1.431
D5-1000-WQ-475	52	Yes	22.1	65.93	1.519
D5-1000-WQ-600	49	No	25.25	69.81	1.423
D5-1000-WQ-800	38	No	19.95	56.94	1.69
D5-1150-WQ	59.5	No	22.35	82.42	1.141
D5-1150-WQ-475	63	Yes	18.9	68.94	1.656
D5-1150-WQ-600	60	No	22.45	79.54	1.486
D5-1150-WQ-800	51.8	No	22	59	1.456

SCC was found in the as-received samples as well as in the samples aged at 475°C. However, no cracking was found in 2205 DSS samples annealed at 1000°C and 1150°C or the samples aged at 600°C or 800° C. Stress corrosion cracking susceptibility, in the slow strain rate tests, can be detected by the signs of embrittlement in the stress vs strain curve for the tested sample. The lower % elongation and % reduction in area for an alloy sample tested in an environment, compared to an equivalent sample tested without that environment, typically indicates the SCC susceptibility of that alloy in the under test conditions. The lower ductility of the as-received sample as compared to other heat-treated samples in sulfide-containing caustic solution is indicated by the stress-strain curves in Figure 4.43 and Figure 4.44. Stress strain curves from the slow strain rate tests also indicate that different ferrite/austenite ratios in 2205 DSS also affect its mechanical properties. D5-1000-WQ and D5-1150-WQ samples without aging had higher %

elongation and % reduction in area, indicating that significant necking had occurred before the final failure, which is indicative of a ductile mode of failure. 475°C and 800°C aged samples had suffered a brittle mode of failure as compared to the annealed samples without aging. Both samples D5-1000-WQ-475 and D5-1150-WQ-475aged at 475°C showed significant strain hardening and a higher ultimate tensile strength. Higher values of linear roughness index of fractured samples in TABLE 4.13 indicated more tortuous fracture path for these samples.

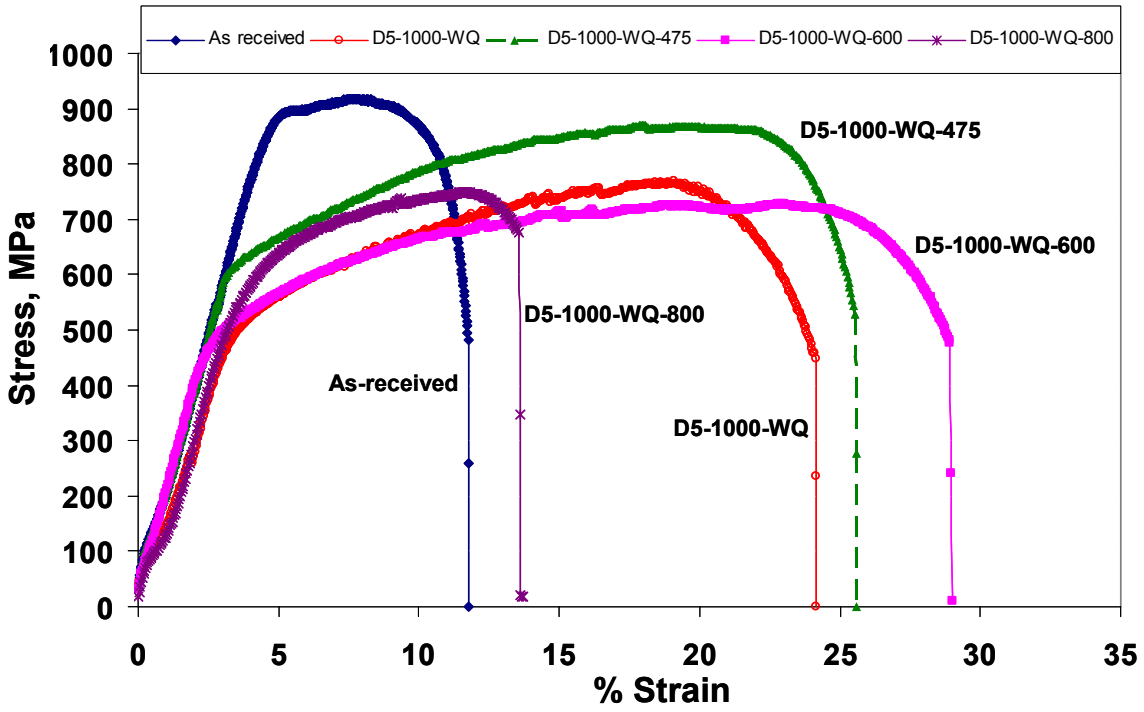

Figure 4.43. Stress strain curve for 2205 DSS annealed at 1000 ºC and subjected to 475ºC, 600ºC and 800ºC aging

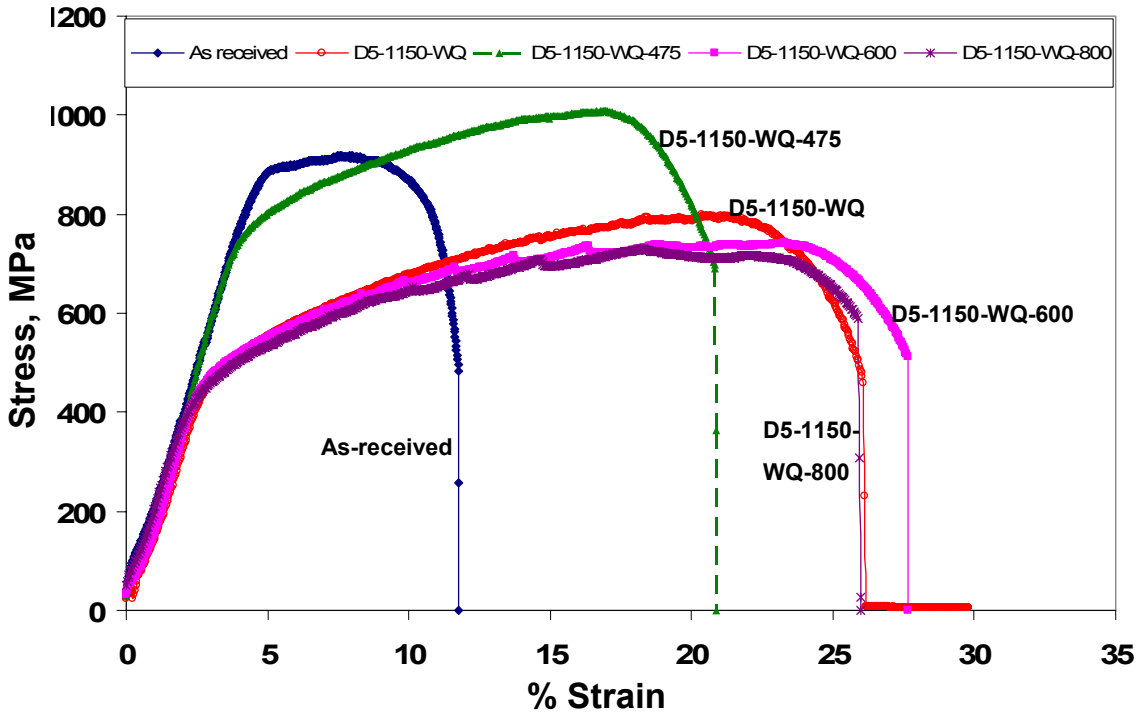

Figure 4.44. Stress strain curve for 2205 DSS annealed at 1150 ºC and subjected to 475ºC, 600ºC and 800ºC aging

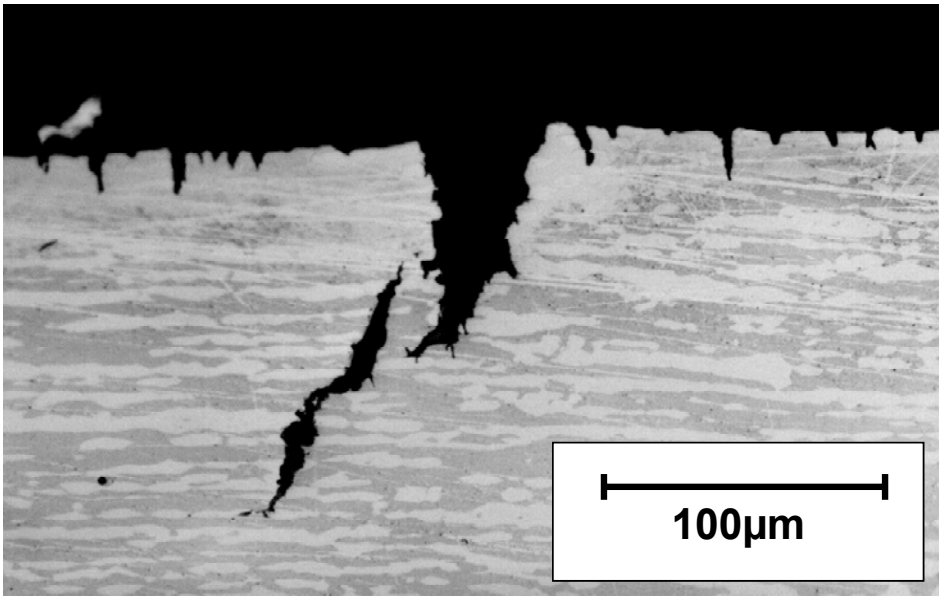

Figure 4.45. Optical micrograph of 2205 as received sample showing transgranular cracking

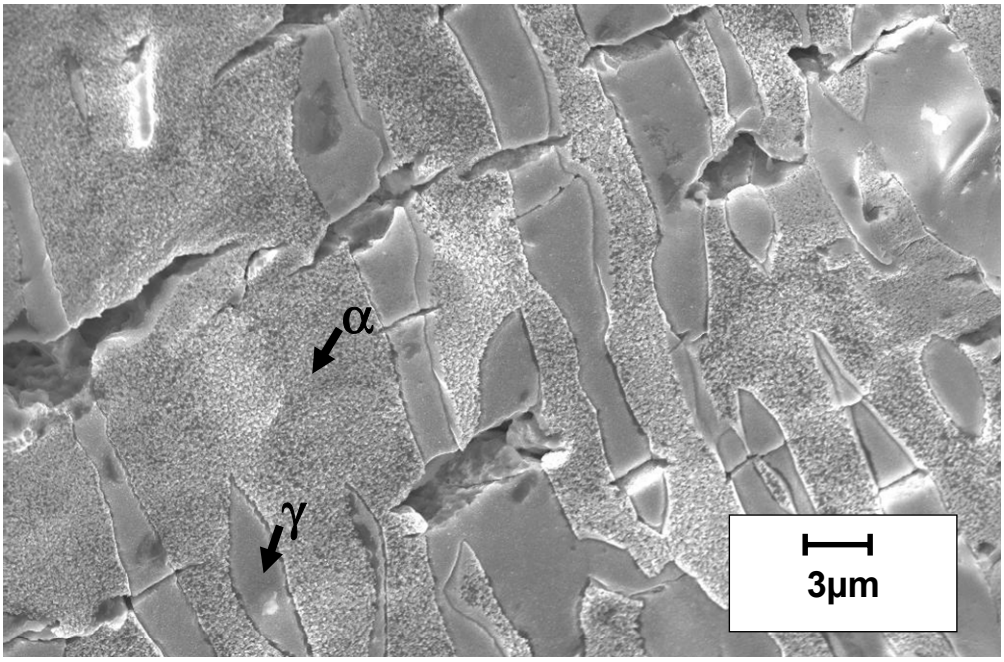

Figure 4.46. SEM image of 2205 as-received sample fracture surface showing crack initiation sites in the austenite phase

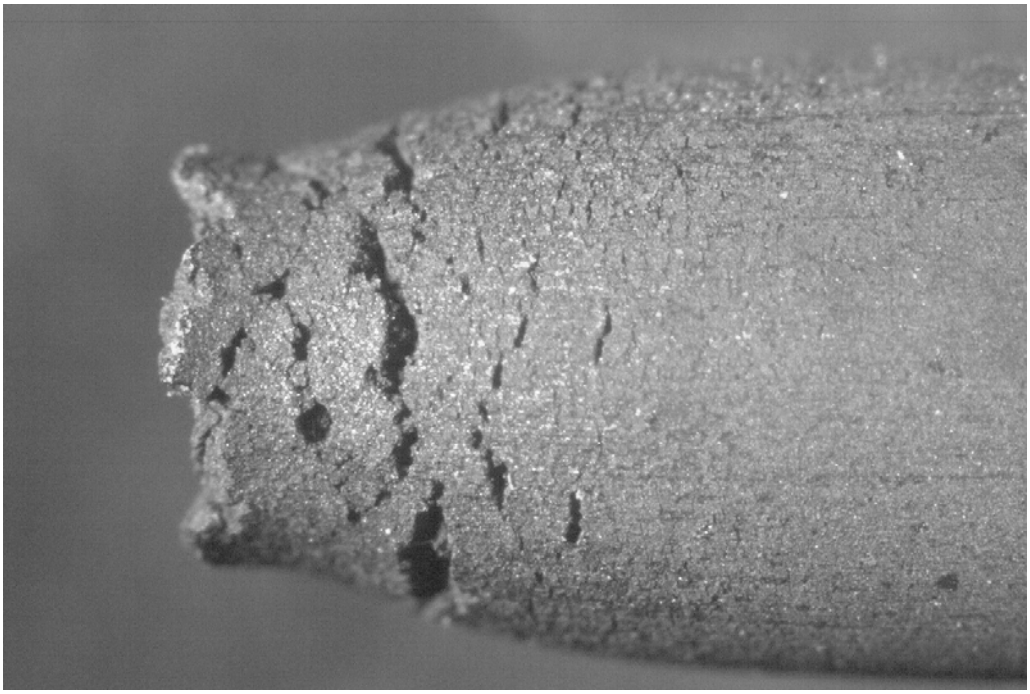

Figure 4.47. D5-1000-WQ-475 showing severe cracking on the surface

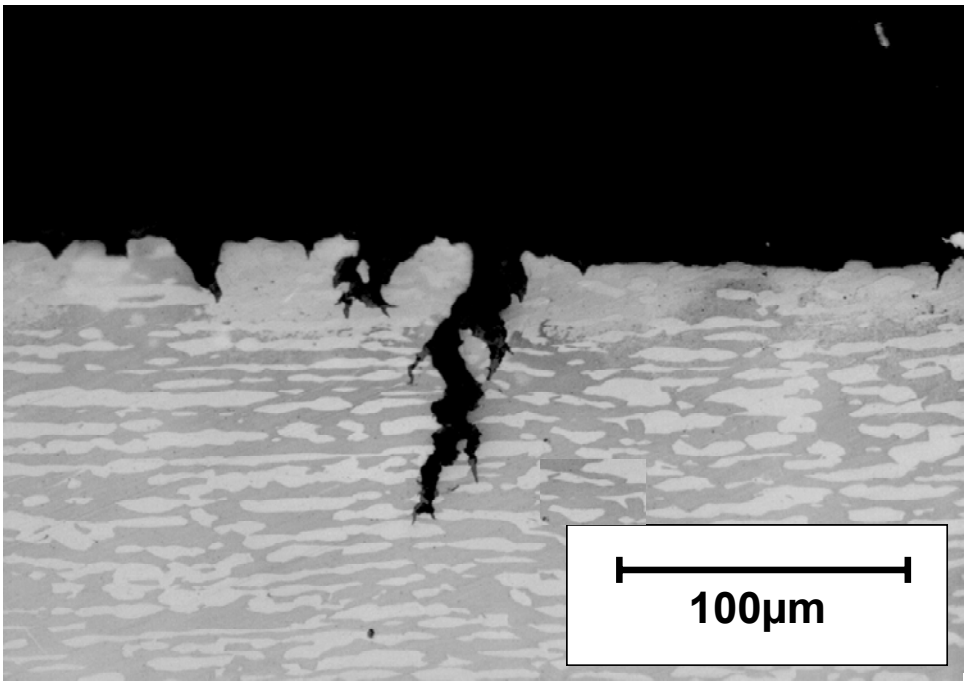

Figure 4.48. D5-1000-WQ-475 showing transgranular cracks across both the phases

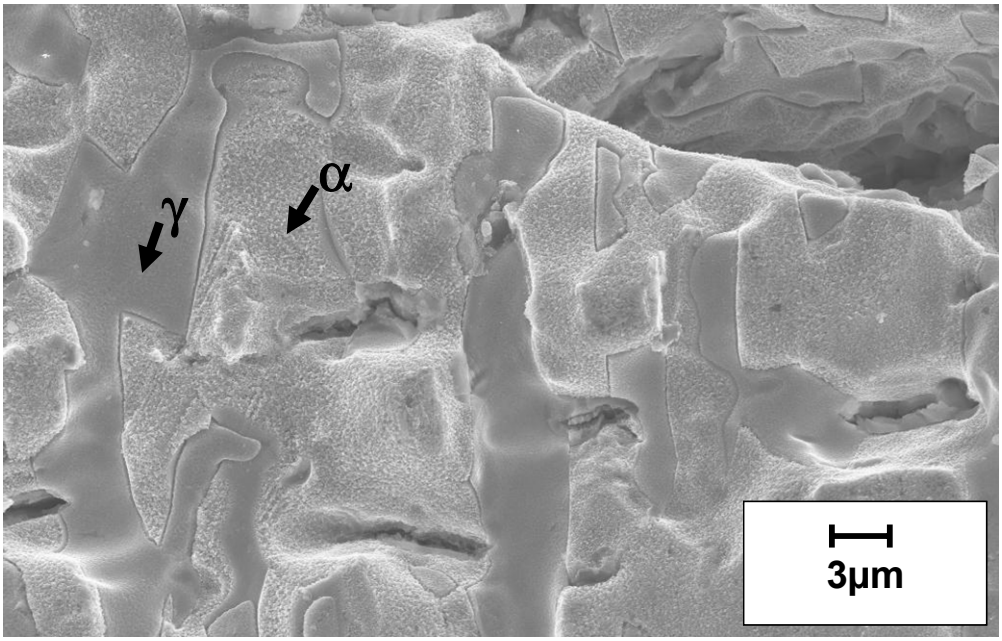

Figure 4.49. SEM micrograph of D5-1000-WQ-475 showing crack initiation sites in the ferrite phase

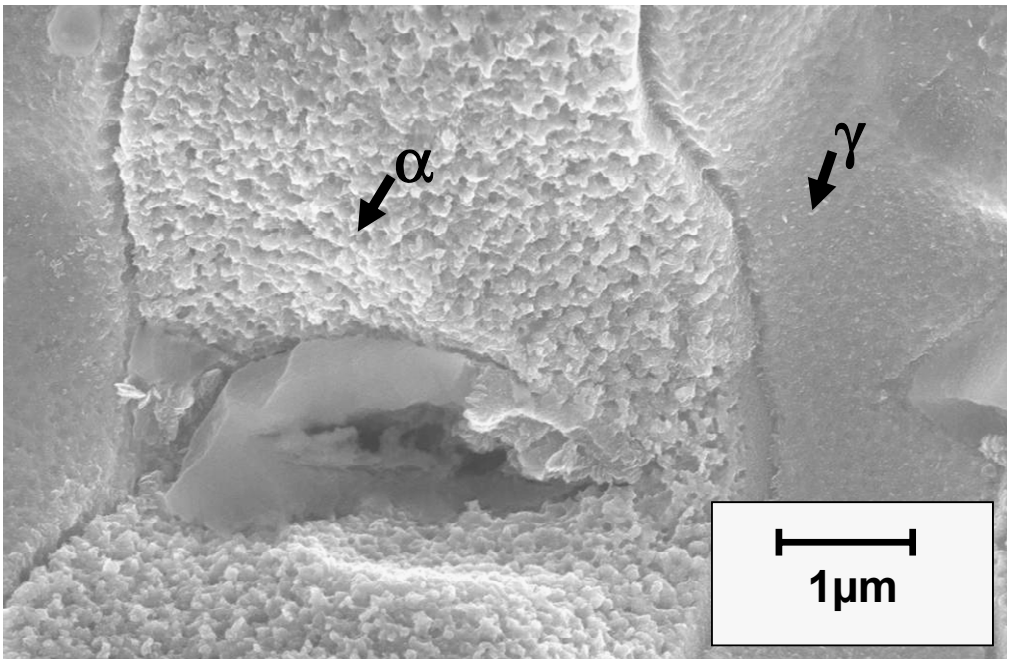

Figure 4.50. SEM micrograph of D5-1000-WQ-475 showing crack initiation sites in the ferrite phase

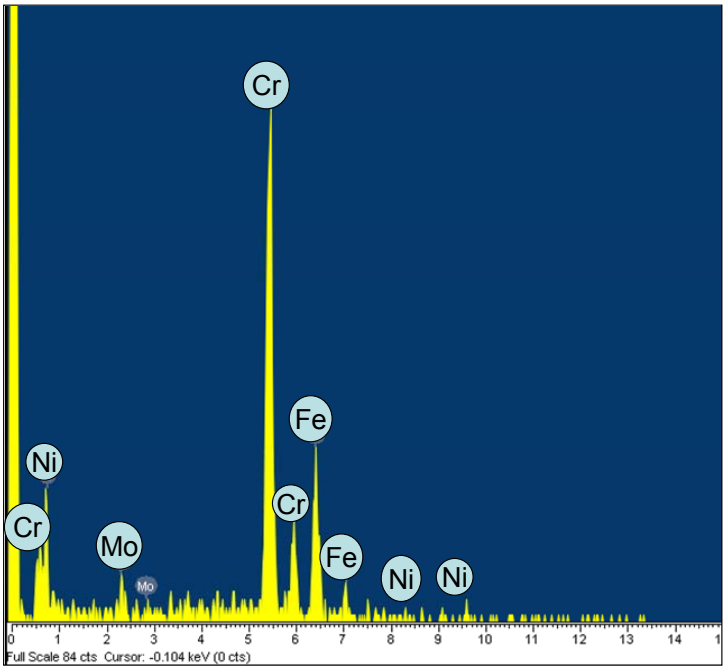

Figure 4.51. EDX analysis of the phase associated with crack initiation in D5-1000-WQ-475, as shown in Figure 4.50.

Optical micrograph in Figure 4.45 shows severe stress corrosion cracking in the as-received 2205 DSS sample. Multiple stress corrosion cracks had initiated at the surface. The cracks were found to be transgranular in nature. Side of the fractured tensile sample was further examined by scanning electron microscope (SEM), as shown in Figure 4.46. Cracks typically initiated in the austenite phase, as was confirmed by the EDX. Heat-treated sample D5-1000-WQ-475 aged at 475°C was also found to be susceptible to severe stress corrosion cracking, as shown by cracks in Figure 4.47. Cracks on the D5-1000-WQ-475 samples were also transgranular in nature (Figure 4.48). However, SEM metallography of the sides of the fractured sample confirmed that the crack initiation sites for D5-1000-WQ-475 samples were associated with precipitates in the ferrite phase, unlike those in the as-received sample, where cracks had initiated in the austenite phase (Figure 4.49 and Figure 4.50). EDX analysis of the areas associated with the crack initiation in the ferrite phase in Figure 4.50 showed the presence of very high chromium content. This is evident from the EDX spectrum in Figure 4.51. Prior work has shown that ά precipitates formed during '475 embrittlement' of DSS has a high level of chromium [28]. Mo partitioning also occurs in these precipitates. The composition of the precipitates found in D5-1000-WQ-475 was very similar to the composition of ά in DSS. However, further investigation using transmission electron microscopy is required to characterize the precipitates formed in D5-1000-WQ-475.

The sample annealed at 1150°C and aged at 475°C showed intergranular stress corrosion cracks in the sulfide-containing caustic solution. Optical micrograph of sample D5-1150-WQ-475 in Figure 4.52 shows stress corrosion cracks along the grain boundaries. Figure 4.53 and Figure 4.54 shows SEM micrograph of the sides of the

fractured tensile sample with stress corrosion cracks initiating along the grain boundaries. The crack initiation seems to be associated with the precipitates along the grain boundary, as shown in Figure 4.54. Corrosion product was also found near the crack initiation sites as shown in Figure 4.54. EDX analysis of the precipitates at the boundary (Figure 4.55 and Figure 4.56) showed enrichment of chromium, molybdenum and nickel as compared to the surrounding phases. The results also showed a considerable lowering of iron in the precipitates.

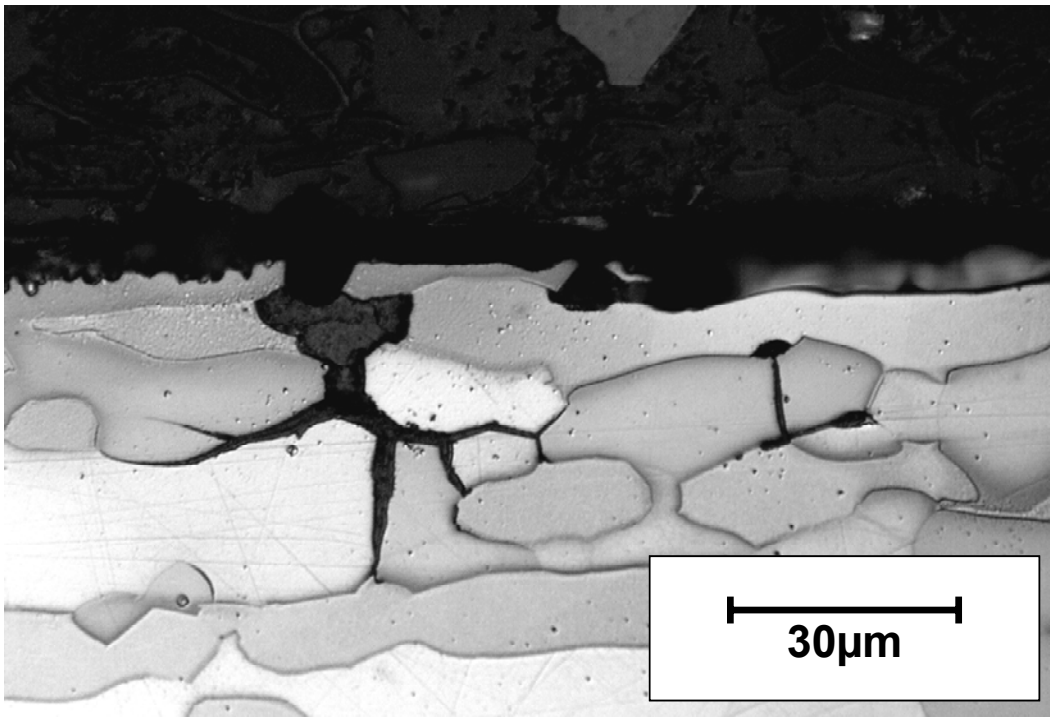

Figure 4.52. Optical micrograph of sample D5-1150-WQ-475 showing intergranular stress corrosion cracking

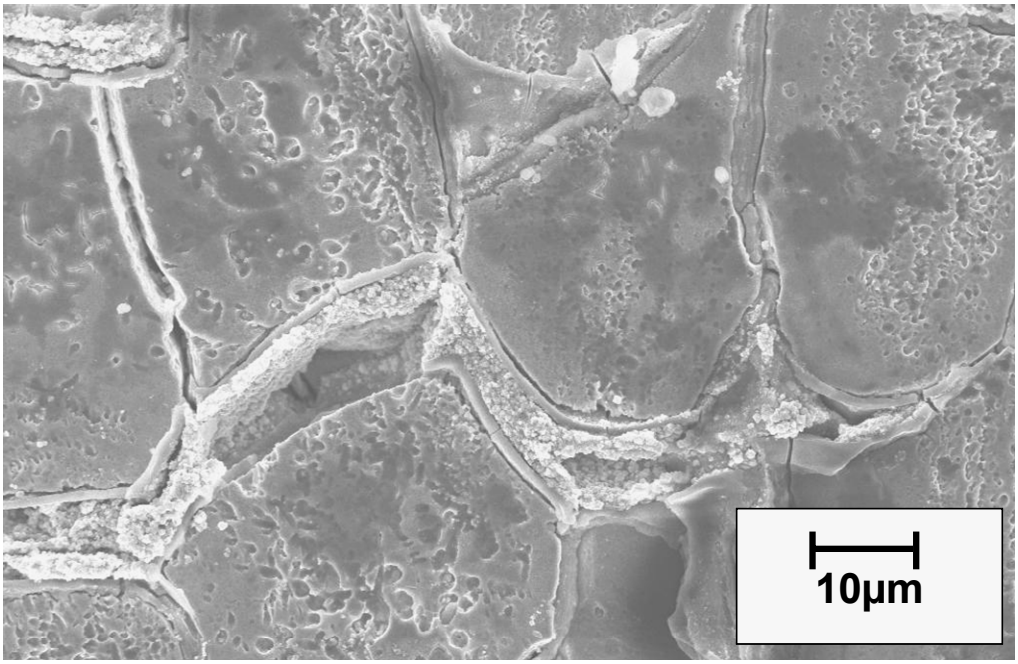

Figure 4.53. SEM micrographs of the sides of the fractured sample D5-1150-WQ-475 showing crack initiation sites along grain boundaries.

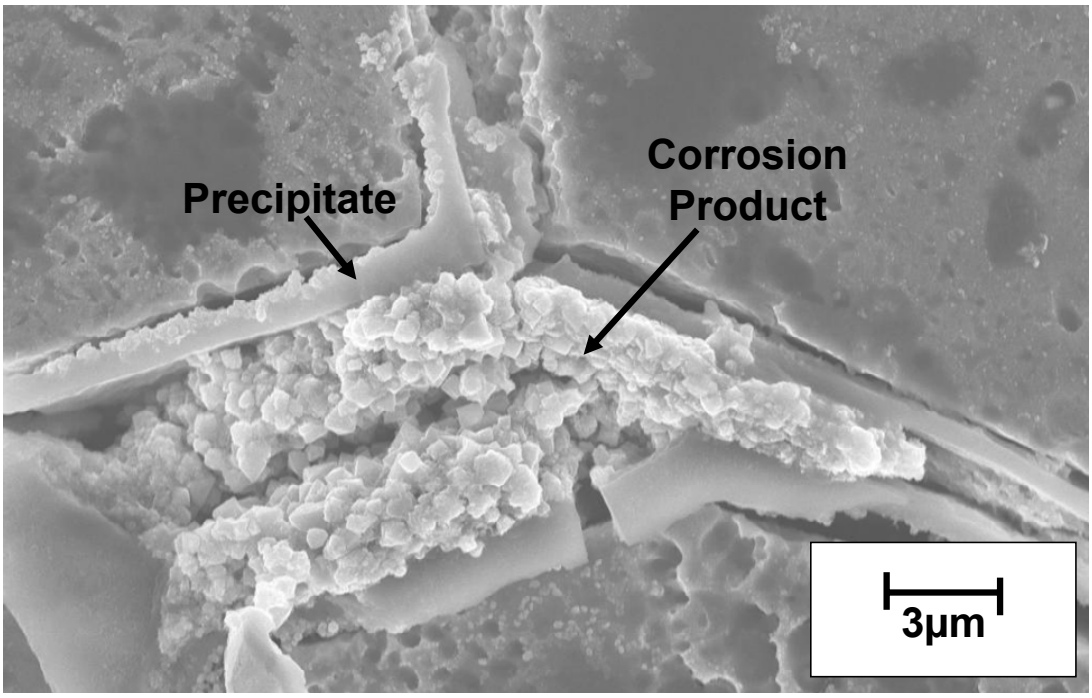

Figure 4.54. SEM micrographs of the sides of the fractured sample D5-1150-WQ-475, showing corrosion product in the crack initiation sites along grain boundaries.

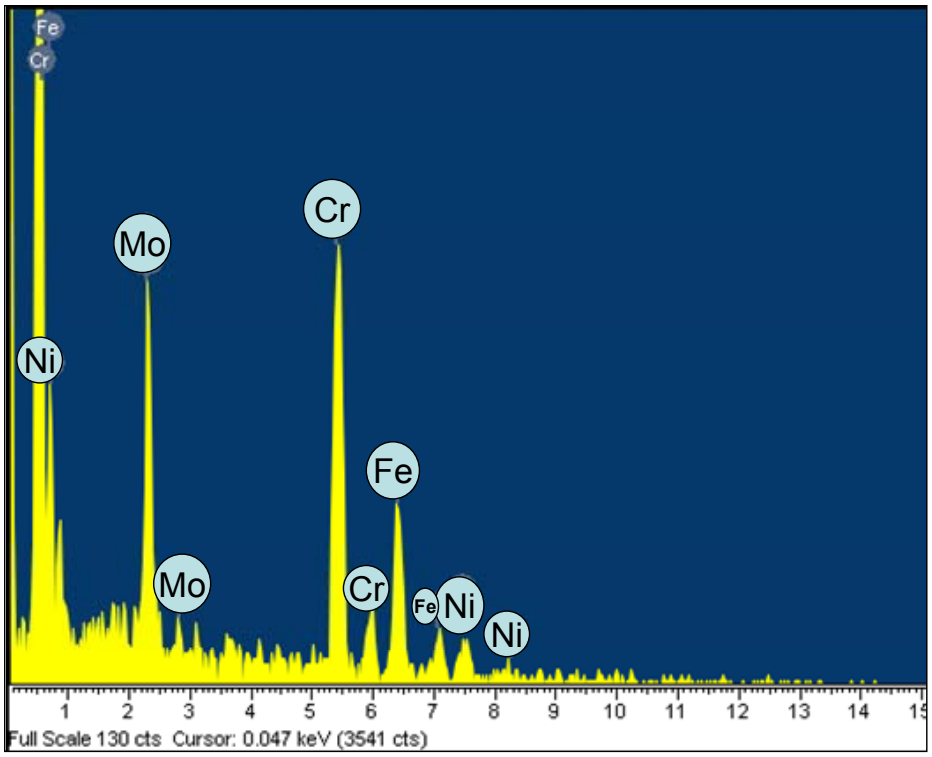

Figure 4.55. EDX spectra of the grain boundary precipitate at the crack initiation site of sample D5-1150-WQ-475

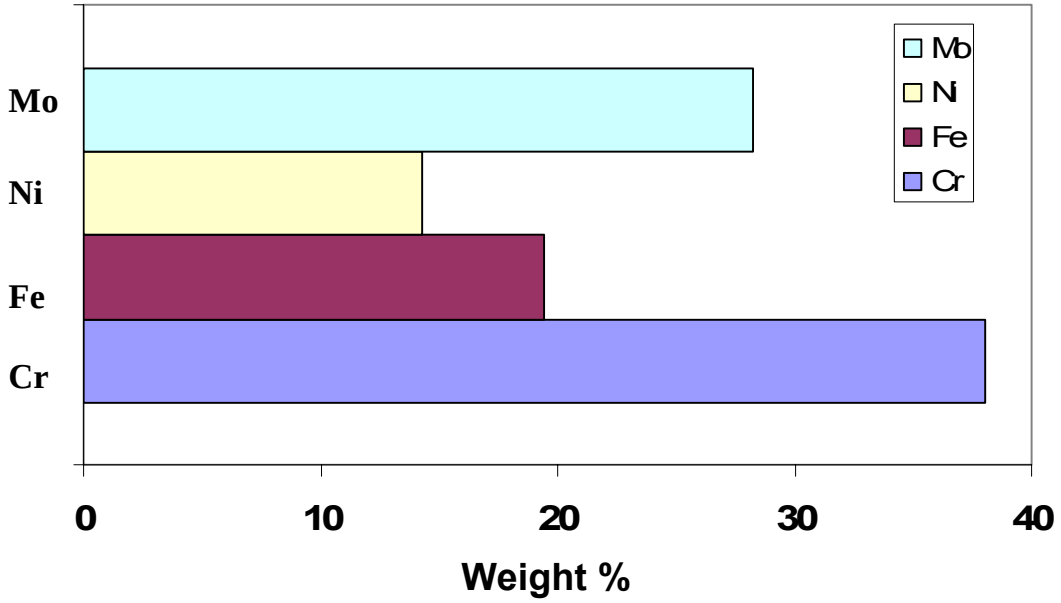

Figure 4.56. Bar graph showing chemical composition of the grain boundary precipitate at the crack initiation site of sample D5-1150-WQ-475

4.5.1. Discussion of Slow-strain Rate Test Results

Results from the slow strain rate tests for differently heat treated 2205 DSS revealed that the as-received tensile samples, as well as samples aged at 475 ºC were susceptible to the stress corrosion cracking. Cracking in the as-received sample may also be affected by the localized residual stresses in the material. Previous study has shown that the austenite phase in 2205 DSS is in tension whereas the ferrite phase is in compression [29]. This may further contribute to the preferential crack initiation in the austenite phase of an as-received DSS sample. Samples annealed and aged at 600 ºC also did not show SCC susceptibility in the sulfide-containing caustic environments. Similarly, the samples aged at 800 ºC and containing sigma and chi precipitates showed a brittle mode of failure but did not show any susceptibility to SCC in sulfide-containing caustic solution. Pitting corrosion was shown to assist crack initiation in the acidic chloride environment and was one of the precursors to the stress corrosion cracking [6]. However, the presence of deleterious secondary phases in 2205 DSS aged at 800 ºC did not show any influence on the general, localized corrosion, or SCC initiation in the caustic solutions tested.

Aging at 475 ºC was found to play a significant role in the SCC susceptibility of 2205 DSS in caustic solutions. 475 ºC aging is known to produce '475 embrittlement' which can induce a progressive hardening and reduction in the material toughness [30]. '475 embrittlement' occurs in the ferrite phase and is associated with the spinodal decomposition of the ferrite phase into Cr rich α' and Cr poor α phase. The aging at 475 ºC produces changes in the dislocation structure of the ferrite phase as studied by TEM [28]. The Cr rich α' precipitates lower the mobility of the dislocations and create micro-void near them in the ferrite matrix [24]. The samples annealed at 1000 ºC and 1150 ºC

and aged at 475 ºC showed an increase in the strength as compared to other heat-treated DSS samples in sulfide-containing caustic solution. This is evident from the high σ_{UTS} and σ_{YS} values in the stress-strain curves in Figure 4.43 and Figure 4.44. This is due to the resistance to the dislocation motion because of precipitation. A similar behavior of duplex stainless steel 2205 aged at 475 ºC was reported by Girones et al [31]. Crack initiation in the ferrite phase in the sample D5-1000-WQ-475 can be attributed to the preferential crack initiation at the chromium depleted region around the precipitates as well as due to the general embrittlement of the ferrite phase. D5-1150-WQ-475 annealed at a higher temperature and aged at 475 ºC showed a much higher ferrite volume fraction. During aging at 475 ºC, the hardness of the ferrite increases significantly but the hardness of the austenite remains essentially constant [22]. Hence, a larger volume fraction of the hard ferrite phase increases the strength and decreases the toughness of the 475 ºC aged specimens (Figure 4.44). Precipitates were found along the grain boundaries in sample D5-1150-WQ-475. Intergranular cracking in D5-1150-WQ-475 is associated with this grain boundary precipitation, shown clearly in Figure 4.53.

4.6. CONCLUSION

Different grades of as-received DSS were tested under similar environmental conditions to study effect of alloy composition and thermo-mechanical treatments on their SCC susceptibilities in sulfide-containing caustic solution. 2101 and 2205 DSS were further heat treated to study the effect of different microstructures on the general and localized corrosion susceptibility of the steels in sulfide-containing caustic solutions. Similar specimens were also exposed to corrosion tests in chloride environment to study

the difference in corrosion behavior (pitting corrosion, SCC) of DSS in the two different environments. The following conclusions were arrived at:

1. Different alloy composition and thermo-mechanical treatments affected the SCC susceptibilities of various grades of DSS differently. Higher chromium containing 2304 DSS was found to be immune to SCC in caustic environment.
2. Aging treatment of both 2205 DSS and lean DSS S32101 at 800 °C produced intermetallic precipitations, but these precipitates differed in composition due to the difference in alloy composition. 2101 DSS produced precipitates containing high chromium as compared to the ferrite and austenite phases. Due to the manganese content of the alloy, considerable amount of manganese was also found in these precipitates. On the other hand, S32205 DSS samples aged at 800°C produced sigma and chi precipitates, which did not contain manganese.
3. In both the grades of DSS, chromium and molybdenum depleted regions were found around the precipitates and at the ferrite/austenite interface adjacent to the precipitates, which were identified as secondary austenite. Width of this chromium depleted region increased with an increase in aging time, due to the partitioning of chromium in the precipitates.
4. DSS samples aged at 800°C and 600°C showed very high weight loss and pitting in acidic chloride environment as compared to annealed and unaged samples or samples aged at 475°C.
5. Pit initiation in 2101 DSS was found to be along ferrite/austenite phase boundaries due to selective dissolution of the less noble phase. Once initiated,

these pits grew into the ferrite phase. In 2205 DSS, pit initiation was in the ferrite phase.

6. The general corrosion rates of 2205 DSS was found to be slightly higher as compared to 2101 DSS in sulfide-containing caustic solution due to the higher molybdenum content of the steel.
7. Changes in the duplex stainless steel microstructures as a result of different heat treatments used in this study made the steel susceptible to corrosion in chloride environment but did not show any significant effect on the general and localized corrosion behavior of the steel in sulfide-containing caustic solution. General corrosion rates in caustic solution were very low and no pitting or crevice attack was found on DSS samples even at 170°C.
8. As received 2205 DSS was found to be susceptible to stress corrosion cracking in sulfide-containing caustic solution. Cracking in as-received DSS in sulfide-containing caustic solution was found to be transgranular in nature. SEM and EDS studies showed that crack initiation was mostly in the austenite phase.
9. Microstructural difference in DSS due to various heat treatments did not have any effect on the general and pitting corrosion resistance of the steels in sulfide-containing caustic solutions, but had significant effect on their SCC susceptibility in caustic environment.
10. DSS samples aged at 800°C and containing sigma and chi precipitates did not show any susceptibility to stress corrosion cracking, indicating that sigma and chi precipitates do not affect crack initiation or propagation in caustic environments.

11. Sample annealed at 1000ºC and aged at 475ºC showed severe stress corrosion cracking. Crack initiation sites showed very high chromium content as compared to the surrounding ferrite phase. Crack initiation was associated with precipitates in the ferrite phase, which was different from the as received sample. This may suggest that "475ºC embrittlement" can have a deleterious effect on the stress corrosion cracking susceptibility of 2205 DSS in caustic environments.
12. Sample annealed at 1150ºC and aged at 475ºC showed severe intergranular stress corrosion cracking. The cracking in this case was associated with precipitates at ferrite/austenite interphase and grain boundaries.

The overall results indicate that heat treating DSS may produce microstructures which may change the mode of crack initiation and propagation in sulfide-containing caustic solution as compared to the as-received DSS sample.

REFERENCES

[1] J.CHARLES, "The Duplex Stainless Steels: Materials to Meet Your Needs", Duplex Stainless Steels, Vol. 1, 1991, pp. 3-48.

[2] H.D.SOLOMON, "Age hardening in a duplex stainless steel", Duplex stainless steels, ASTM conference proceedings, Edited by R.A.Lula, pp.41-69.

[3] S. ATAMERT, J.E.KING, "Elemental partitioning and microstructural development in duplex stainless steel weld metal," Acta metal. Mater, 1991, 39, pp.273-285.

[4] D.Y. KOBAYASHI, S. WOLYNEC, "Evaluation of the low corrosion resistant phase formed during the sigma phase precipitation in duplex stainless steels", Materials Research 2 (1999): p. 239.

[5] Z.CVIJOVIC, G.RADENKOVIC, “Microstructure and pitting corrosion resistance of annealed duplex stainless steel,” Corrosion Science, 2006, 48, pp.3887-3906.

[6] WEN-TA TSAI, MING-SHAN CHEN, “Stress corrosion cracking behavior of 2205 duplex stainless steel in concentrated NaCl solution,” Corrosion Science , 42, pp.545-559, 2000

[7] V. MUTHUPANDI, P.BALA SRINIVASAN, S.K.SESHADRI, S.SUNDARESAN, “Effect of weld metal chemistry and heat input on the structure and properties of duplex stainless steel welds,” Materials Science and Engineering A358, pp.9-16, 2003.

[8] ANANYA BHATTACHARYA, PREET.M.SINGH, H.T.LEINONEN, JAMSHAD MAHMOOD, NACE Corrosion 2006, Paper No. 06497, March 12-16, San Diego, CA, USA, (2006)

[9] ASTM A 480/A 480M – 06b, “Standard Specification for General Requirements for Flat-Rolled Stainless and Heat-Resisting Steel Plate, Sheet, and Strip”.

[10] H.T.LEINONEN, "Corrosion Resistance of Duplex Stainless Steel and its Welds in Modern Kraft Batch Cooking," 11th International Symposium on Corrosion in Pulp and Paper Industry, pp. 55-66, June 2004.

[11] J. E. TRUMAN AND K. R. PIRT, Duplex Stainless Steels, Proceedings of the American Society for Metals Conference (ASM, Metals Park, Ohio), USA, p.113, (1983).

[12] ANANYA BHATTACHARYA, PREET M. SINGH, "Corrosion and stress corrosion cracking of duplex stainless steels in pulping liquor", NACE Corrosion Conference and Expo., Paper#07206, Nashville, Tennessee, (2007).

[13] J.A. JIMENEZ, M.CARSI, O.A. RUANO, Journal of Materials Science 35 (2000) p. 907.

[14] I.F. MACHADO, M.CARSI, A. F. PADILHA, ISIJ International 40 (2000) p. 719.

[15] M. BERNER, H.P. LIU, C. O. A. OLSSON, 14th Nordic Corrosion Congress (NKM-14), Copenhagen, Denmark, 13th-15th May, (2007).

[16] S.ATAMERT, J.E.KING, Acta metal.mater 39 (1991) p. 273.

[17] J. CHARLES, Duplex stainless steels '91, Volume 1, Les editions de physique, France, pp. 3-48.

[18] J.A.JIMENEZ, M.CARSI, O.A.RUANO, "Characterization of a f/a DSS," Journal of Materials Science, 35, pp.907-915, 2000

[19] T.H.CHEN, K.L.WENG, J.R.YANG, "The effect of high-temperature exposure on the microstructural stability and toughness property in a 2205 duplex stainless steel," Materials Science and Engineering A, 338, pp.259-270, 2002

[20] S.S.M. TAVARES, M.R.DA SILVA, J.M.NETO, "Magnetic property changes during embrittlement of a duplex stainless steel," Journal of Alloys and Compounds, 313, pp.168-173, 2000

[21] http://www.outokumpu.com/36719.epibrw Last accessed on June 2005

[22] K.L.WENG, H.R.CHEN, J.R.YANG, " The low-temperature aging embrittlement in a 2205 duplex stainless steel," Materials Science and Engineering A, 379, pp.119-132, 2004.

[23] ZUCATO, M. C. MOREIRA, I. F. MACHADO, S. M. G. LEBRAO, Materials Research 5 (2002) p. 385.

[24] CHAN-JIN PARK, HYUK-SANG KWON, Materials Chemistry and Physics 91 (2005): p.355.

[25] J.RAMO, M.SILLANPAA, A.KUJALA, O.HYOKYVIRTA, S.PELTONEN, "Interactions of sulphur anions and stainless steels at kraft pulp digesting temperature," Materials and Corrosion, Volume 52, (2001), pp. 531-539.

[26] ANANYA BHATTACHARYA, PREET M SINGH, "Role of microstructure on the corrosion susceptibility of UNSS32101 Duplex Stainless Steel," Corrosion, 64(6), 2008.

[27] R.MAGNABOSCO, N.ALONSO-FALLEIROS, "Pit morphology and its relation to microstructure of 850 ºC aged duplex stainless steel," Corrosion, 61, 2005, pp.130-136.

[28] K.L.Weng, H.R.Chen, J.R.Yang, "The low-temperature aging embrittlement in a 2205 duplex stainless steel," Materials Science and Engineering A, 379, pp.119-132, 2004

[29] H.T.LEINONEN, P.POHJANNE, "Stress corrosion cracking susceptibility of duplex stainless steels and their welds in simulated cooking environments," *NACE Corrosion 2006*, Paper No. 06244, March 12-16, San Diego, CA, USA, 2006.

[30] S.S.M.TAVARES, R.F.DENORONHA, M.R.DASILVA, J.M.NETO, S.PAIRIS, "475C embrittlement in a duplex stainless steel UNS S31803," Materials Research, 4(4) , pp.237-240, 2001

[31] A.GIRONES, L.LIANES, M.ANGLADA, A.MATEO, "Dynamic strain aging effects on superduplex stainless steels at intermediate temperatures," Materials Science and Engineering, 367, pp.322-328, 2004.

CHAPTER 5

ROLE OF ENVIRONMENT ON GENERAL CORROSION AND SCC SUSCEPTIBILITY OF DSS

5.1. INTRODUCTION

Stress corrosion cracking susceptibility of materials depends on the solution composition (pH, dissolved ions) and temperature [1]. For example, carbon steels may undergo SCC in solutions of anodic inhibitors such as hydroxides and carbonates while magnesium-based alloys are susceptible to SCC in the presence of a mixture of CrO_4^{2-} and Cl^- ions, but not with either of these species alone [2]. A number of research groups have investigated the effect of environmental parameters on the SCC susceptibility of DSS in low-pH chloride environments. However, the effects of these environmental parameters on the general and localized corrosion susceptibility of DSS in high-pH caustic or sulfide-containing caustic environment have not been studied. Hence, temperature effects and role of ionic species on SCC susceptibility of DSS in high-pH environments needs to be explored to understand the basic mechanisms of SCC operating in these systems

In this chapter, effect of temperature and role of hydroxide and sulfide addition on the corrosion and SCC susceptibilities of DSS in sulfide-containing caustic environment has been discussed.

5.2. EFFECT OF TEMPERATURE AND IONIC SPECIES ON GENERAL CORROSION SUSCEPTIBILITY OF DSS

5.2.1. Corrosion performance of DSS in 3.75M NaOH solution

Samples of S32205, S32101 and S32304 DSS were exposed to 150g/l NaOH (3.75M NaOH) solution at different temperatures to study temperature effect on the corrosion rates for these alloys. The pH of the caustic solution was measured to be 12.5. Figure 5.1 shows the corrosion rates of the three grades of DSS in 3.75M NaOH solution at 40ºC, 60ºC, 90ºC and 170ºC. The overall corrosion rates of DSS were found to be low, less than 0.2mm/year even at 170ºC. Previous studies have also shown that the better corrosion resistance of DSS can be attributed to the higher chromium content and controlled, intermediate nickel content in the steel [3]. Results further showed the detrimental effect of temperature on the corrosion performance of DSS as the corrosion rate of the DSS samples increased with an increase in the test temperature. The corrosion rates of difference grades of DSS were found to differ for similar test conditions. The corrosion rate of S32205 was lower compared to the other two grades of DSS tested in 3.75 M caustic solution at high temperatures. Results in Chapter 4 have shown that alloy composition plays an important role in the corrosion resistance of DSS. Hence these results are in agreement with the findings of Chapter 4.

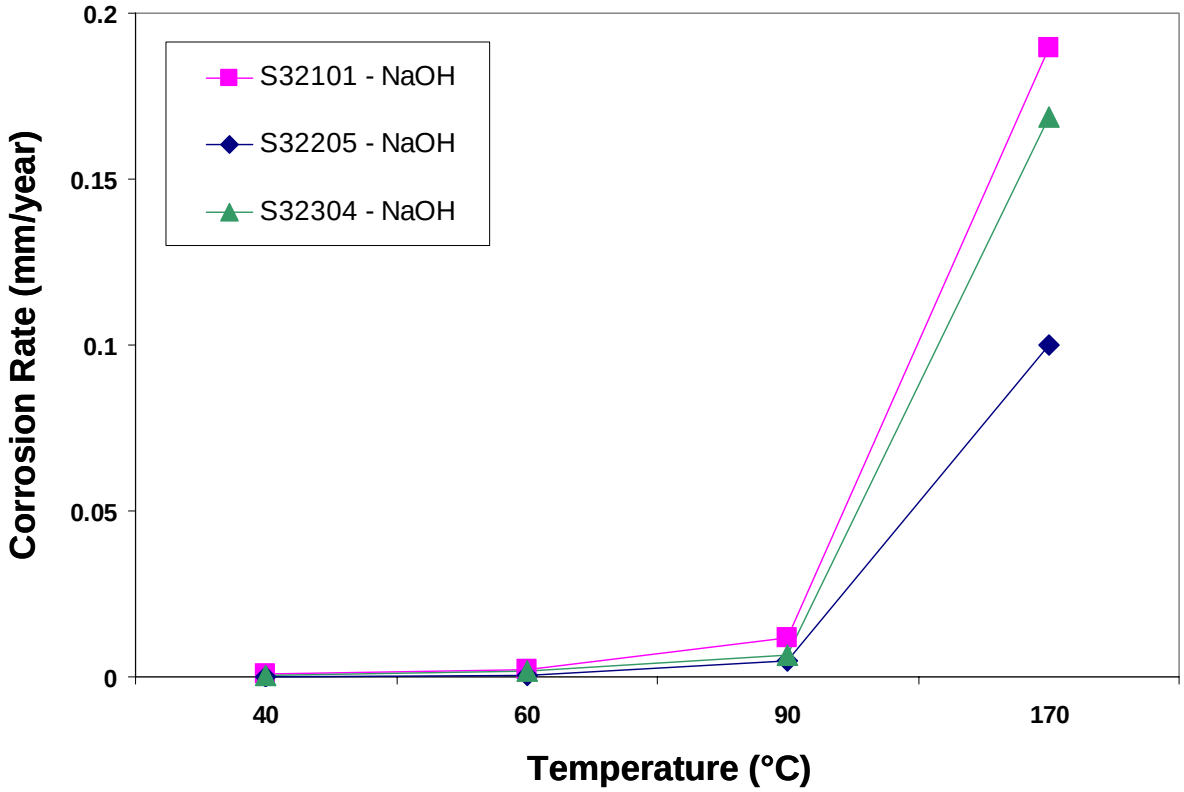

Figure 5.1. Corrosion rates of S32205, S32101 and S32304 in 3.75M NaOH solution at 40ºC, 60ºC, 90ºC and 170ºC.

5.2.2. Corrosion performance of DSS in 3.75M NaOH + 0.64M Na_2S solution

S32205, S32101 and S32304 grades of DSS were exposed for corrosion tests in caustic environment with the addition of sulfide ions to find out the role of sulfide addition on the general corrosion rates of the steels. The solution used was 150g/l NaOH + 50g/l Na_2S solution (3.75M NaOH + 0.64M Na_2S) which is the typical white liquor (WL) composition used in pulp mills and the test temperatures were 40 ºC, 60 ºC, 90 ºC and 170 ºC . The results were compared with the corrosion susceptibility of DSS in 3.75M NaOH solution. These tests also helped to find the localized corrosion susceptibility of the steels in sulfide-containing caustic environment. The three grades of DSS did not show any localized corrosion such as pitting or crevice corrosion. Figure 5.2 shows the general corrosion rates of duplex stainless steels in sulfide-containing caustic solution as

a function of temperature. From the figure, it is evident that the corrosion rates of the steels increased with rise in temperature. The general corrosion rates of S32205, S32101 and S32304 were different (Figure 5.2). The difference in corrosion rates was more at higher temperature (170 ºC). S32205 was found to be more susceptible to general corrosion as compared to S32101 and S32304, which was different from that in pure caustic environment (Figure 5.2). S32304 had the lowest corrosion rates at all tested temperatures. The difference in corrosion rates could be attributed to the difference in the alloy composition of the steel. Alloying elements play a vital role in the corrosion resistance of materials.

The test results further showed the detrimental effect of sulfide addition on the corrosion resistance of DSS. Figure 5.3 compares the corrosion rates of S32205, S32101 and S32304 in caustic environment with and without sulfide addition. The results indicate an increase in the corrosion rates of the steel with sulfide addition to caustic solution. Prior work has shown that sulfide addition will favor formation of metal-sulfur compounds. Such metal-sulfur compounds are non-adherent or may hydrolyze in water easily, exposing the metal to further attack [4]. Hence, the increased corrosion rates in sulfide-containing caustic environment are due to the formation of various metal-sulfur compounds on DSS and are further discussed in CHAPTER 6.

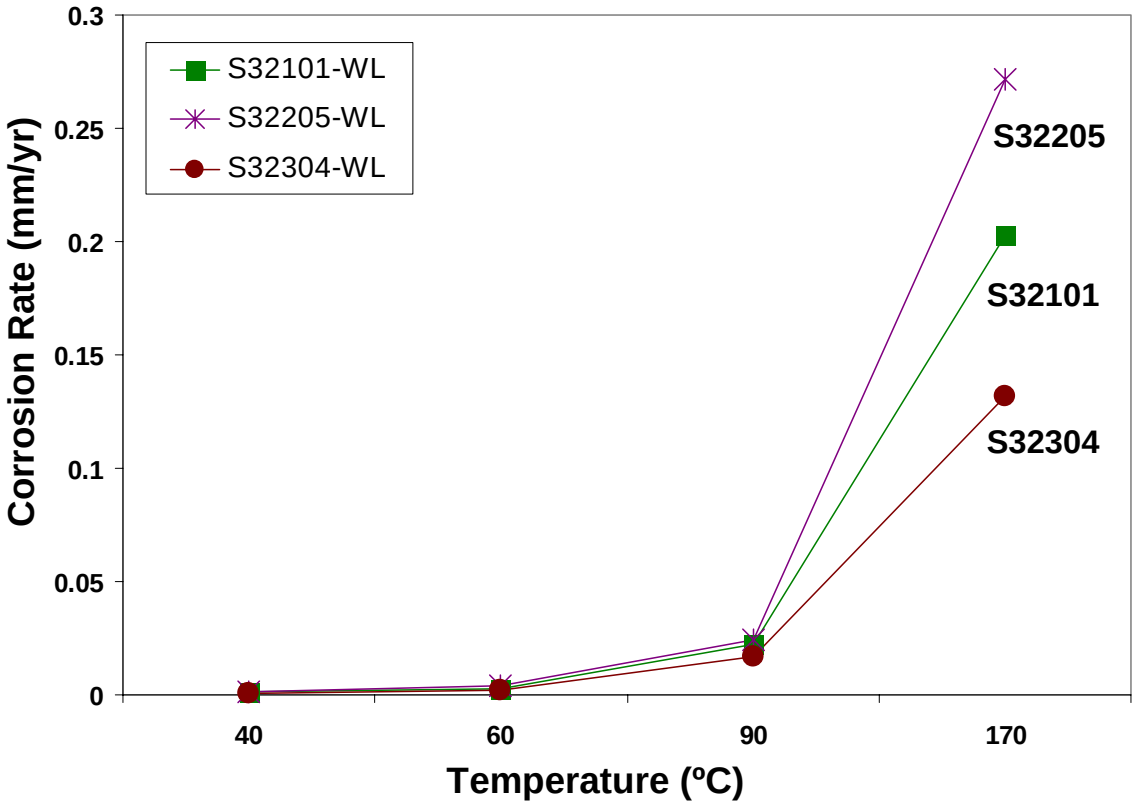

Figure 5.2. Corrosion rates of S32205, S32101 and S32304 in 3.75M NaOH + 0.64M Na_2S solution at 40 ºC, 60 ºC, 90 ºC and 170 ºC

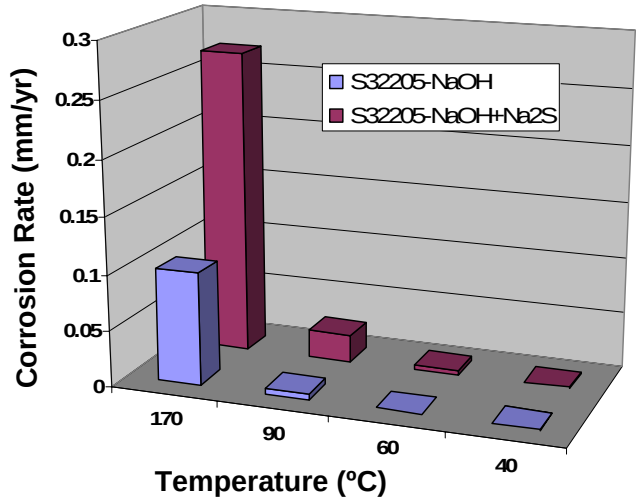

(a)

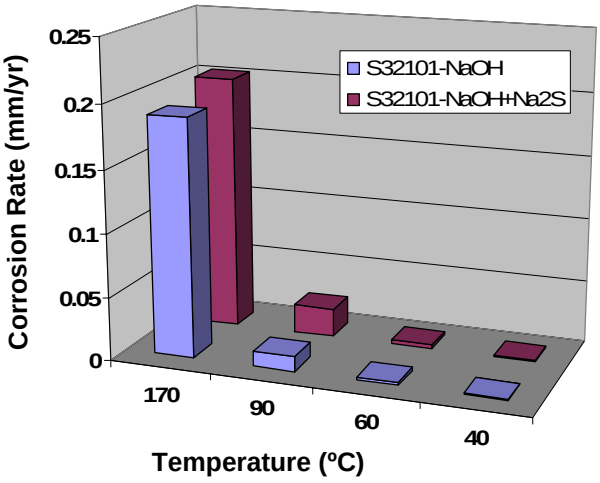

(b)

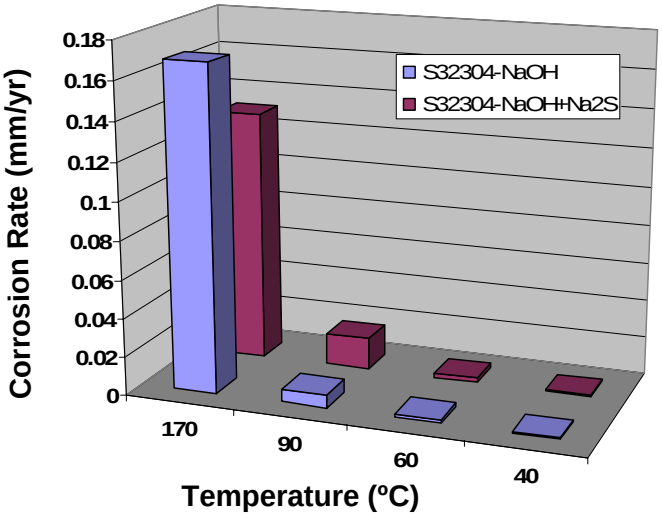

(c)

Figure 5.3. Bar graphs comparing corrosion rates of (a) S32205 (b) S32101 (c) S32304 in caustic environment with and without sulfide addition as a function of temperature

5.2.3. Corrosion performance of DSS in caustic environment with varying OH^- and S^- concentrations

The effect of ionic concentration (concentration of OH^- and S^- species) on the corrosion resistance of DSS was further studied by exposing as-received DSS samples of S32205, S32304, and S32101 for general corrosion tests in environment containing different combinations of sodium hydroxide and sodium sulfide. The compositions of the sulfide-containing caustic solutions, as listed in TABLE 5.1, were chosen to simulate the commonly used caustic environments in various pulp mills. These different sulfide-containing caustic environments represent the range of sulfidity and alkalinity that is typically used in the industry. The results of the 170^oC exposure tests, shown in TABLE 5.2, indicate that the corrosion rates of DSS specimens generally increased with an increase in sodium sulfide concentration. The test results corroborate the results of Section 5.2.2 and further point towards the fact that sulfide ions in caustic solution adversely affect the corrosion resistance of all the grades of DSS. There was no sign of localized corrosion such as pits or crevice corrosion on any of the DSS samples tested in different sulfide-containing caustic solutions in this study. The corrosion rates for DSS samples were significantly lower than the equivalent corrosion rates for carbon steel samples tested under identical conditions [5]-[6]. Carbon steel (516-Gr70) samples were found to corrode at rates ranging from 250 to 150 mils per year (mpy) in previous studies [5]-[8]. However, the corrosion rates of DSS coupons tested in sulfide-containing caustic environment in this study ranged from 12 mpy to 0.1 mpy, depending upon the composition of the environment. S32205 DSS specimens showed somewhat higher corrosion rate than S32304 or S32101 DSS samples in all environments tested. Previous

studies have shown that the presence of molybdenum in the austenitic and duplex stainless steels can be detrimental for the general corrosion resistance in sulfide containing caustic solutions at high temperatures. Therefore, a higher general corrosion susceptibility of 2205 DSS in caustic environment at 170^{o}C may be attributed to its higher Mo content. S32304 DSS with higher chromium and low molybdenum content had the least amount of corrosion in sulfide-containing caustic environments under the conditions tested.

TABLE 5.1. COMPOSITION OF SULFIDE-CONTAINING CAUSTIC SOLUTIONS USED IN THIS STUDY

Environment	Composition (per liter)
Environment 1	NaOH 150gm + Na_2S 50gm
Environment 2	NaOH 100gm + Na_2S 55gm
Environment 3	NaOH 125gm + Na_2S 75gm

TABLE 5.2. GENERAL CORROSION RATES FOR DIFFERENT GRADES OF DSS IN DIFFERENT CAUSTIC ENVIRONMENTS, TESTED AT 170°C FOR 7 DAYS

Environment	DSS Grade	Corrosion Rate (mpy)
NaOH 150gm + Na_2S 50gm	S32101	0.34
	S32205	0.86
	S32304	0.13
NaOH 100gm + Na_2S 55gm	S32101	4.72
	S32205	5.03
	S32304	4.95
NaOH 125gm + Na_2S 75gm	S32101	5.43
	S32205	11.38
	S32304	9.43

TABLE 5.3. EFFECT OF DISSOLVED IONIC SPECIES AND TEMPERATURE ON CRACK LENGTH, CRACK VELOCITY AND CORROSION RATE OF S32101 DSS SAMPLES (TESTED BY SLOW STRAIN RATE METHOD)

Environment	Temp (°C)	Crack Length (μm)	Crack Velocity mm/sec	Corrosion Rate (mpy)	Stress Corrosion Susceptibility
NaOH 150gm + Na_2S 50gm	170	62.71	3.27E-7	21.07	SCC
	140	52.64	2.66E-7	9.003	SCC
	120	0.00	0	7.59	No SCC
NaOH 100gm + Na_2S 55gm	170	110.6	6.19E-7	17.73	SCC
	140	0	0	5.35	No SCC
NaOH 125gm + Na_2S 75gm	170	92.33	5.03E-7	31.22	SCC
	140	93.17	4.77E-7	10.29	SCC
	120	0.00	0	0.65	No SCC

5.3. EFFECT OF TEMPERATURE AND IONIC SPECIES ON SCC SUSCEPTIBILITY OF DSS

As environment plays a key role in the SCC of different materials, the main aim of this study is to understand how environmental parameters such as ionic species (OH^- and S^- species concentrations) and temperature affects the SCC susceptibility of DSS in alkaline solutions. S32101 DSS was tested by slow strain rate tests in environment containing different combinations of sodium hydroxide and sodium sulfide, as shown in TABLE 5.1. Slow strain rate tests were also carried out at different temperatures to study temperature effects as well. TABLE 5.3 summarizes the SCC test results for S32101 where the crack length and crack velocity for samples tested in different sulfide-containing caustic environment (white liquor, WL) at different temperatures are compared. The results show that with decreasing hydroxide concentration and increasing sodium sulfide, the susceptibility of S32101 to general corrosion and SCC increased. The severity of cracking was also found to increase with increasing temperature. At 120^oC, there was no

sign of stress corrosion cracking in tested white liquors. As the temperature was increased to 140^{o}C, the cracks started to initiate in the DSS. The length of the cracks or crack velocity increased as the test temperature was increased to 170^{o}C.

5.4. EFFECT OF STRAINING ON GENERAL CORROSION OF DSS

Data shown in TABLE 5.2 shows that the corrosion rates for different grades of DSS in different sulfide containing caustic solutions were generally low. However, high corrosion rates have been reported in localized areas of DSS equipments such as in pipes, evaporators and other areas with high flow rates. Tensile samples were used to evaluate the effect of passive film disruption, due to the turbulent flow conditions, on the corrosion behavior of these alloys. Tensile samples were strained at a constant strain rate where the passive film is continuously disrupted during exposure. Comparison of the corrosion rates of coupon testing to the corrosion rate of specimens from the slow strain rate testing tested under similar conditions showed that the corrosion rates of the tensile specimens (TABLE 5.3) were significantly higher than the corrosion rates for the coupons (TABLE 5.2). These alloys rely on a stable passive film on their surface to resist corrosion. If that film is frequently damaged, either by straining or by the erosive action of fast flowing liquids, the corrosion rates in those local areas can be significantly higher. These effects may be localized in areas where the passive film is prone to frequent damage.

5.5. CONCLUSIONS

This study was aimed at investigating the effect of environmental parameters such as temperature and dissolved ionic species on the general corrosion and stress corrosion

cracking susceptibility of various grades of DSS in sulfide-containing caustic solutions. The following conclusions can be drawn from these results.

1. The overall corrosion rates for DSS alloys are less than 0.3mm/year, even at 170ºC in caustic and sulfide-containing caustic solution. At lower temperatures than 90ºC, rates are almost an order of magnitude lower.
2. Increase in corrosion rates of duplex stainless steels with sulfide addition show the detrimental effect of sulfur on the corrosion susceptibility of DSS. The increased corrosion rates in sulfide-containing caustic environment are due to the formation of various metal-sulfur compounds on DSS.
3. Molybdenum containing DSS S32205 had a slightly higher corrosion rate in sulfide-containing caustic solution as compared to low-Mo grades like S32304 or S32101.
4. Highly alloyed 2304 DSS with higher chromium content was found to be immune to SCC in caustic environment which shows the importance of alloying elements in the corrosion performance of DSS.
5. DSS were found to be susceptible to stress corrosion cracking in sulfide-containing caustic solutions at temperatures of 140^{o}C and above and the severity of SCC in simulated pulping environments increases with increase in temperature.
6. The corrosion rate of DSS may increase in situations where the passive film is disrupted either by mechanical or chemical action.

Electrochemical behavior of alloys determines their corrosion, passivation and SCC susceptibilities. Hence it is necessary to find out the electrochemical properties of different DSS grades and their alloying elements in caustic solution under various

environmental conditions for better understanding of the corrosion properties of the steel. Chapter 6 relates the electrochemical properties and passive films formed on DSS to the results in this Chapter.

REFERENCES

[1] J.H.PAYER, W.E.BERRY, W.K.BOYD, “Evaluation of slow strain-rate stress corrosion tests results”, ASTM, Toronto, Canada, May 2-4, 1977.

[2] L.L.SHREIR,R.A.JARMAN,G.T.BURSTEIN, "Corrosion 1, Metal/Environment Reactions," Third Edition, 1994.

[3] TRUMAN J E, PIRT K R (1983) Duplex Stainless Steel, ed. Lula, R.A. ASM, Metals Park, OH, USA, pp. 113-142.

[4] G.H.THEUS, R.W.STAEHLE, “Review of stress corrosion cracking and hydrogen embrittlement in the austenitic Fe-Cr-Ni alloys,” NACE Corrosion Conference, Unieux-Firminy, France, June 12-16, (1973).

[5] PREET M. SINGH, ADOLFO ANAYA, Effect of Wood Species on Corrosion Behavior of Carbon Steel and Stainless Steels in Black Liquors, Corrosion Science, 49, No.2, pp. 497-509, 2007.

[6] PREET M. SINGH, ADOLFO ANAYA, KATIE FREY, AND JAMSHAD MAHMOOD, Corrosivity of Black Liquors - Role of Wood Species Pulped, Proceedings of the 10th International Symposium on Corrosion in the Pulp and Paper Industry, Helsinki, Finland. August 21-24, 2001

[7] PATRICK E. HAZLEWOOD, PREET M. SINGH AND JEFFERY S. HSIEH, The Role of Wood Extractives in Black Liquor Corrosivity, Corrosion, 62, No.10, pp911-917, Oct. 2006.

[8] ERC Project Report, Institute of Paper Science and Technology at Georgia Tech, August 2006.

[9] ANANYA BHATTACHARYA, PREET.M.SINGH, H.T.LEINONEN, JAMSHAD MAHMOOD, NACE Corrosion 2006, Paper No. 06497, March 12-16, San Diego, CA, USA, (2006)

CHAPTER 6

ELECTROCHEMICAL BEHAVIOR OF DUPLEX STAINLESS STEELS IN CAUSTIC ENVIRONMENTS

6.1. INTRODUCTION

The corrosion resistance of an alloy in a particular environment depends on its electrochemical behavior, which in-turn depends on the environmental and material related parameters such as temperature, composition of environment, and alloy composition [1]. Although environmental factors affect the electrochemical behavior of a given alloy, the alloy composition is very important in determining the overall corrosion behavior in a given environment. It is important to understand the role of alloying elements in the corrosion and passivation behavior of a particular alloy in a specific environment.

Caustic corrosion and stress corrosion cracking has been a major concern in the chemical process industries such as hydroxide manufacturing, pulp and paper industries, oil refineries, alumina processing and other processes that use or produce caustic environments at high temperatures [2]-[3]. Studies have been carried out to optimize the material composition for use in hot sodium hydroxide aqueous solutions [4]-[5]. Prior work has shown that by increasing the chromium content in austenitic stainless steels, the critical current density for achieving passivity is markedly reduced and the passivation potential of the steel shifts towards more electropositive direction in alkaline solutions

[6]. Another study compared the polarization behavior of austenitic stainless steels with individual polarization behavior of its alloying elements in hot lithium hydroxide and showed that the primary passivation of the steel in this environment was mainly due to the formation of chromium oxide or hydroxide compounds [7].

Although research has been done to study the corrosion and electrochemical behavior of austenitic stainless steels in high pH caustic solutions [8]-[11], very few studies were aimed at understanding the role of alloying elements and environmental parameters in the corrosion susceptibility of duplex stainless steels (DSS) in alkaline environments, with or without the presence of sulfides. Chemical compositions and microstructure of different DSS grades influence the corrosion behavior of duplex stainless steels. The differences in the corrosion resistance can be attributed to the changes in the electrochemical behavior of steels due to the presence of alloying elements. Work in this chapter systematically investigates the corrosion and electrochemical behavior of different grades of duplex stainless steels (2304, 2205 and 2101), with varying chemical composition and microstructure in high pH caustic solution at different temperatures. The present study investigated the role of individual alloying elements to explain the corrosion and passivation behavior of different DSS in caustic and sulfide-containing caustic solutions.

6.2. TEMPERATURE EFFECT ON THE ELECTROCHEMICAL BEHAVIOR OF DSS AND THEIR ALLOYING ELEMENTS

6.2.1. Electrochemical Behavior in Caustic Solution

Corrosion and passivation behavior of DSS 2205 (UNSS32205), 2304 (UNSS32304) and 2101 (UNSS32101) was evaluated by using potentiodynamic polarization method. The nominal compositions of materials tested in this study are shown in Table 2.1

(Chapter 2). The changes in the polarization behavior of the three grades of DSS (S32205, S32304 and S32101) were studied as a function of temperature through a series of potentiodynamic polarization tests at 40ºC, 60ºC, 90ºC and 170ºC. Initial polarization tests were carried out in 3.75M NaOH solution at selected temperatures. Since alloying elements play an important role in the electrochemical behavior of alloys, four major alloying elements of DSS (Fe, Cr, Ni and Mo) were also tested in this environment at different temperatures.

Polarization behavior of selected DSS in caustic solution (3.75 M NaOH) shows a significant change when the test temperature was increased from 40^{o}C to 170^{o}C, as shown in Figure 6.1 to Figure 6.3. With an increase in temperature, there was a decrease in the corrosion potential and, in general, an increase in the current densities at a given potential for all tested DSSs. The critical current densities of the DSS specimens increased from ~10^{-5}A/cm^2 to ~10^{-4}A/cm^2 with an increase in temperature from 40ºC to 170ºC.

The polarization behavior of individual DSS alloying elements in caustic solution, at selected temperatures, is shown in Figure 6.4 to Figure 6.7. Temperature had a similar effect on the individual polarization behavior of alloying elements. With an increase in the test temperature from 40^{o}C up to 170ºC, there was a decrease in the corrosion potential for Cr, Fe, Ni and Mo, as is evident from Figure 6.4, Figure 6.5, Figure 6.6 and Figure 6.7, respectively. An overall increase in the current densities of the elements was also observed with increase in temperature, as is expected due to increased reaction rates at higher temperatures. This indicates that due to the change in the polarization and

passivation behavior of the alloying elements with change in temperature, the steel may become more susceptible to general corrosion at higher temperatures.

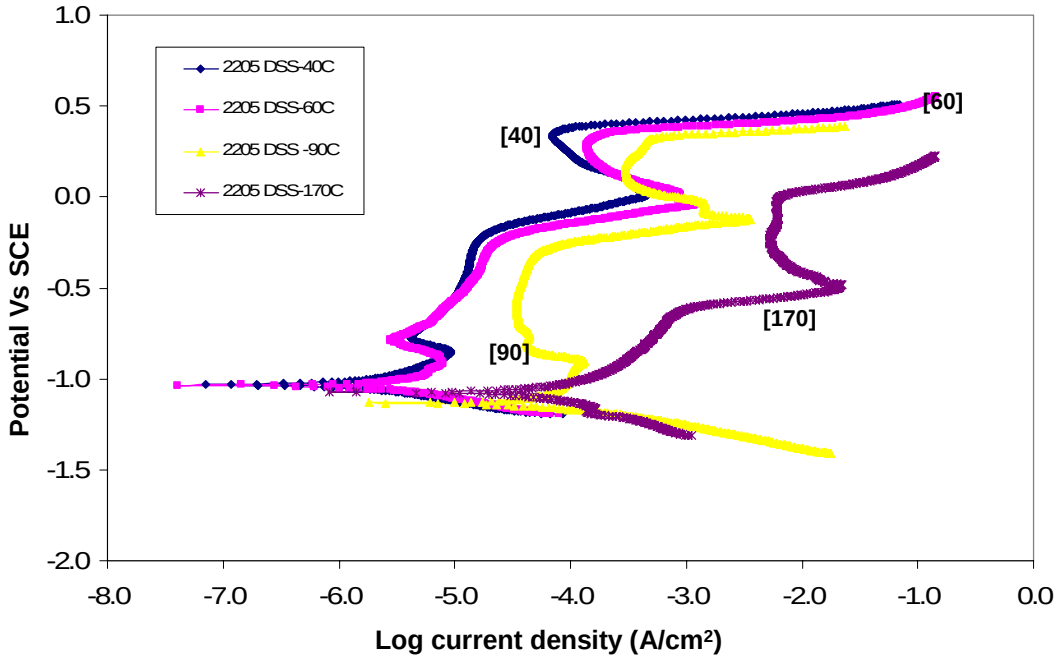

Figure 6.1. Effect of Temperature on the Polarization Behavior of S32205 in Caustic Solution

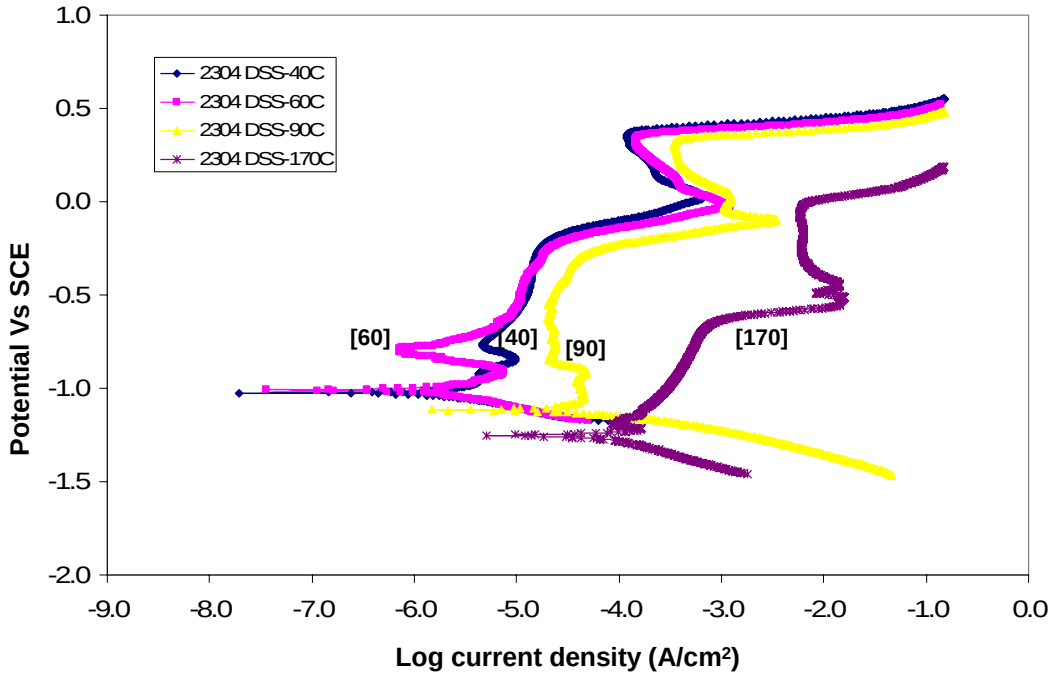

Figure 6.2. Effect of Temperature on the Polarization Behavior of S32304 in Caustic Solution

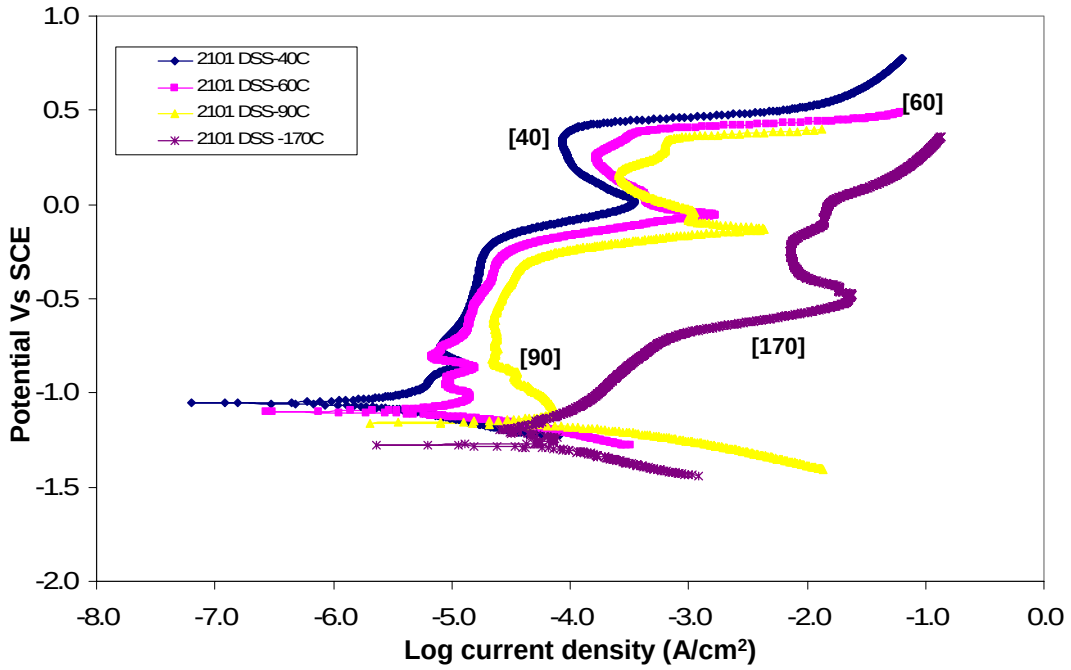

Figure 6.3. Effect of Temperature on the Polarization Behavior of S32101 in Caustic Solution

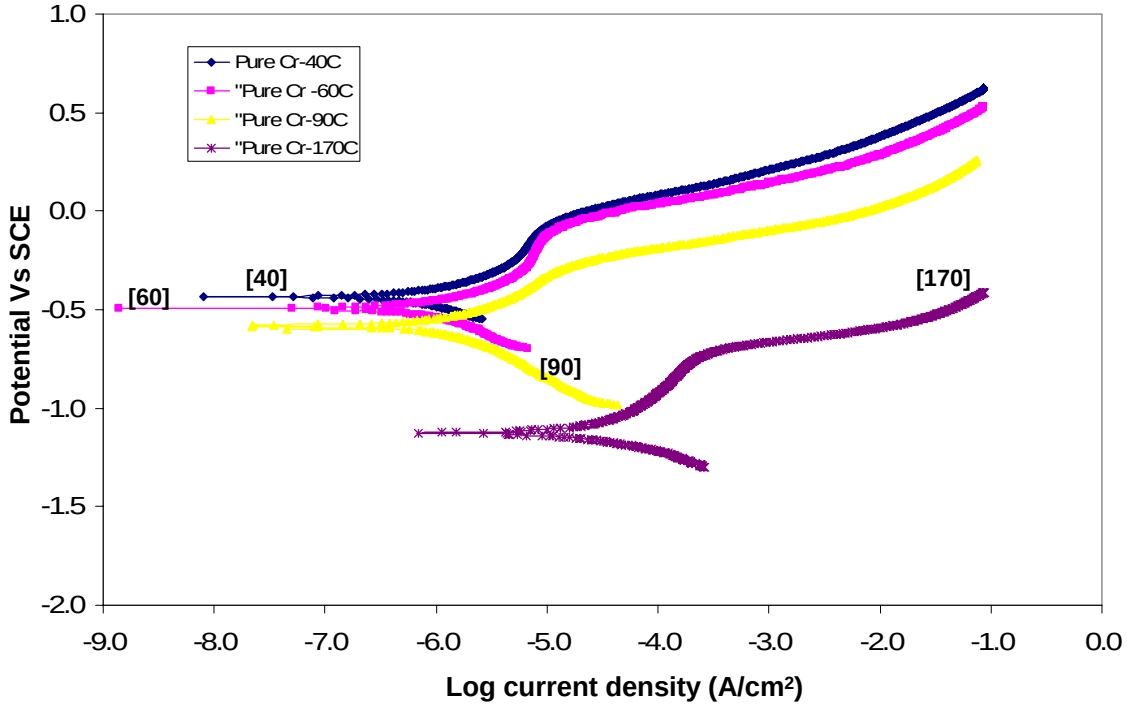

Figure 6.4. Effect of Temperature on the Polarization Behavior of Pure Cr in Caustic Solution

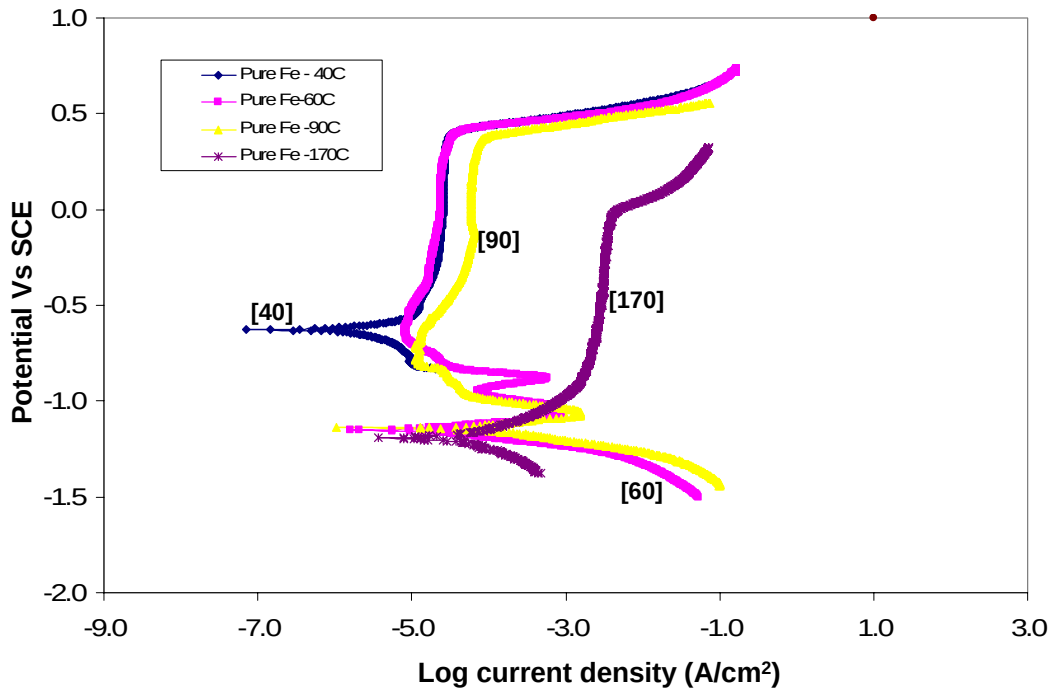

Figure 6.5. Effect of Temperature on the Polarization Behavior of Pure Fe in Caustic Solution

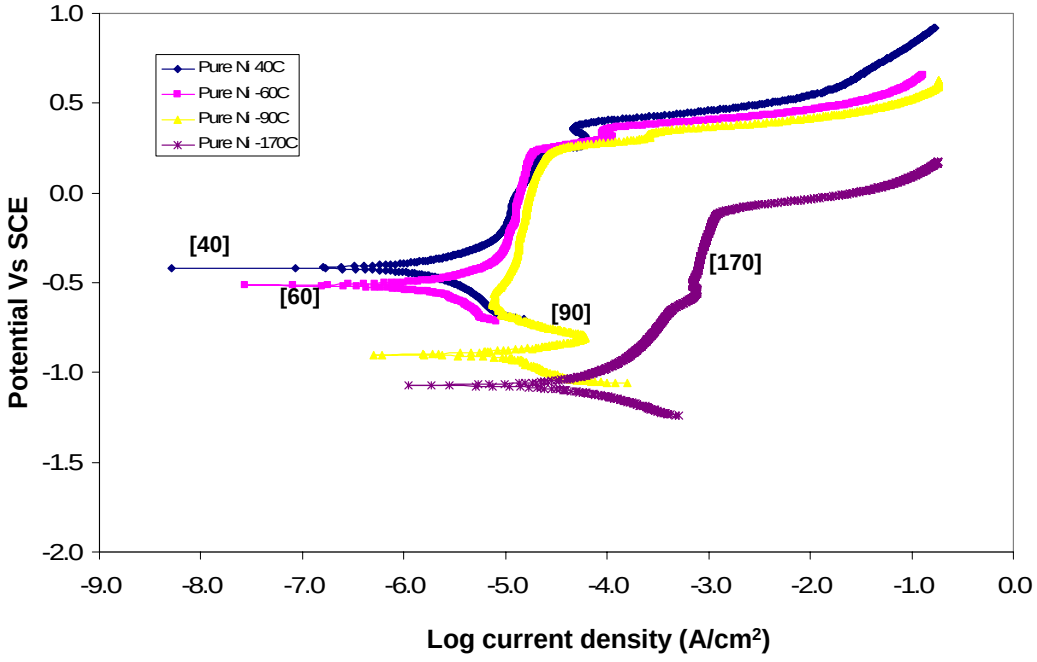

Figure 6.6. Effect of Temperature on the Polarization Behavior of Pure Ni in Caustic Solution

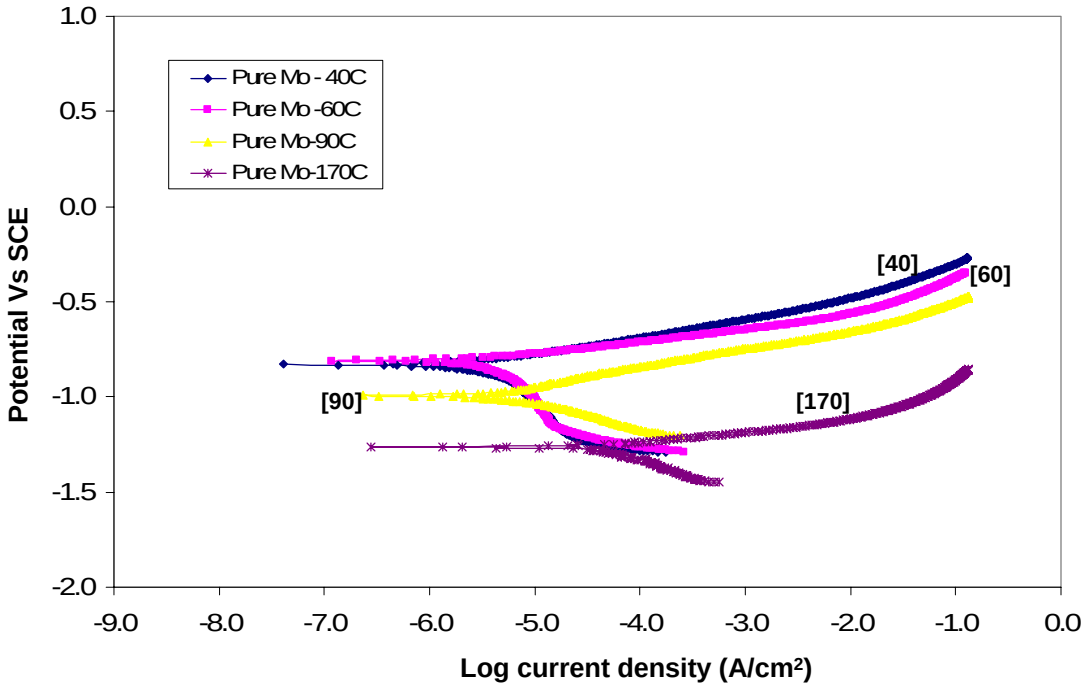

Figure 6.7. Effect of Temperature on the Polarization Behavior of Pure Mo in Caustic Solution

Chromium shows passivity beyond its open circuit potential at all temperatures in caustic solution mainly due to the formation of various oxides and hydroxides of Cr (Figure 6.4). Iron also shows passivity at all tested temperatures due to the formation of magnetite (Fe_3O_4 and Fe_2O_3) at various oxidation potentials (Figure 6.5). Polarization of nickel (Figure 6.6) shows that it undergoes passivation due to the formation of nickel oxide (NiO). Molybdenum does to form any passive film and undergoes active dissolution at all temperatures due to the formation of molybdate ions (Figure 6.7). The various reactions corresponding to the polarization curves of DSS and their alloying elements are further explained in details in Section 6.6.1 of this Chapter.

6.2.2. Electrochemical Behavior in Sulfide-Containing Caustic Solution

Polarization behavior of DSS S32205, S32101, S32304 and pure Fe, Cr, Ni and Mo was also evaluated in the presence of sulfide ions in the caustic solution to see their effect on the overall corrosion behavior. Electrochemical tests were carried out in 150g/L of NaOH solution containing 50g/L of Na_2S (3.75M NaOH + 0.64M Na_2S), white liquor (WL),at 40ºC, 60ºC, 90ºC and 170ºC. The effect of temperature on the polarization behavior of DSS and their alloying elements in sulfide containing caustic environment (WL) are shown in Figure 6.8 to Figure 6.14. Polarization curves in sulfide containing solutions are different from the ones in the pure caustic solutions, mainly due to various possible redox reactions for the sulfur species present in the solution. However, the detrimental effect of temperature on the corrosion susceptibility in sulfide-containing caustic solution is evident from these results, which show a decrease in the corrosion potentials and an increase in the critical current densities with rise in temperature.

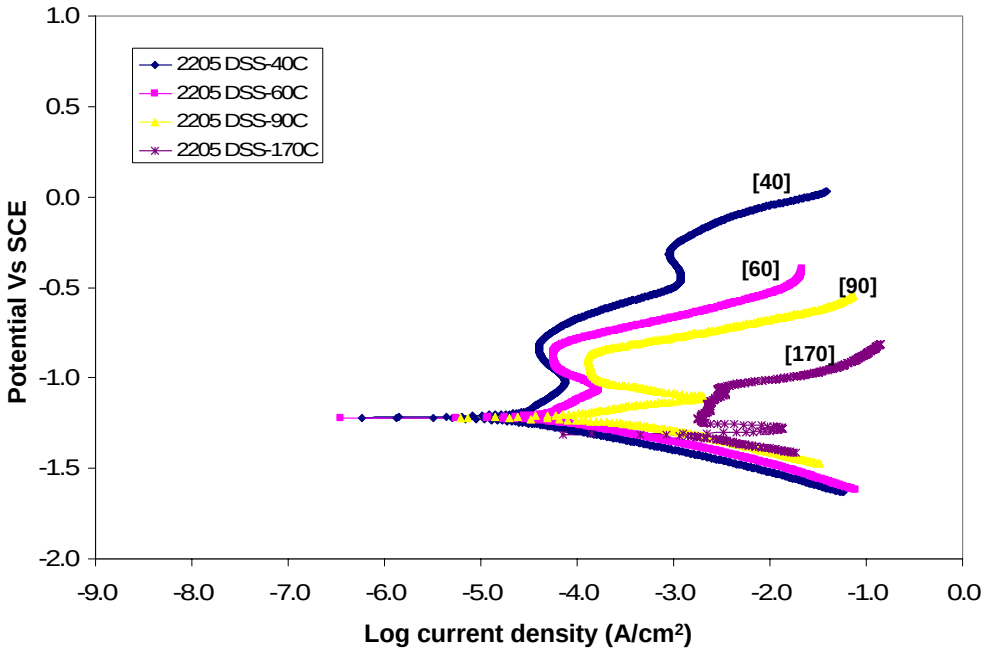

Figure 6.8. Effect of Temperature on the Polarization Behavior of S32205 in Sulfide-Containing Caustic Solution

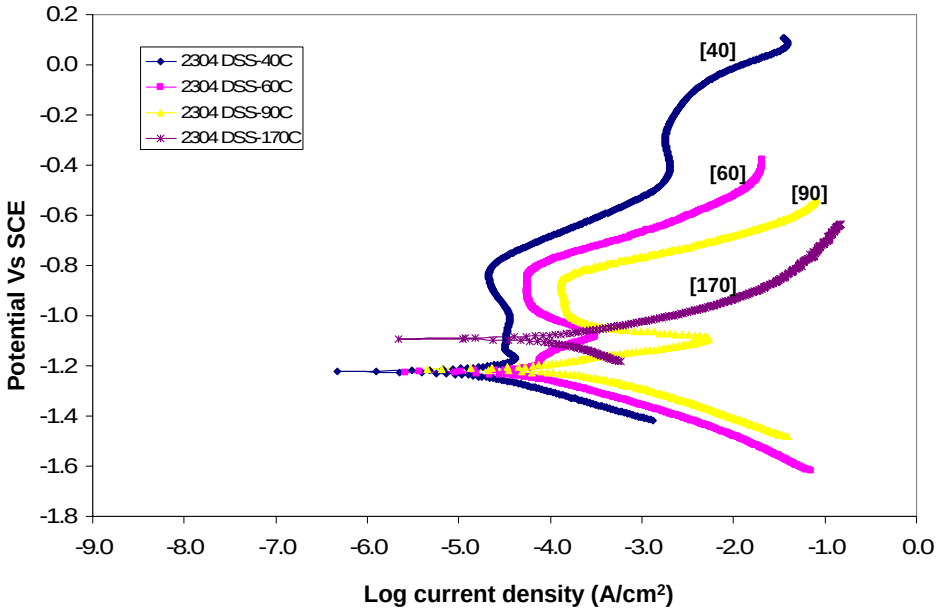

Figure6.9. Effect of Temperature on the Polarization Behavior of S32304 in Sulfide-Containing Caustic Solution

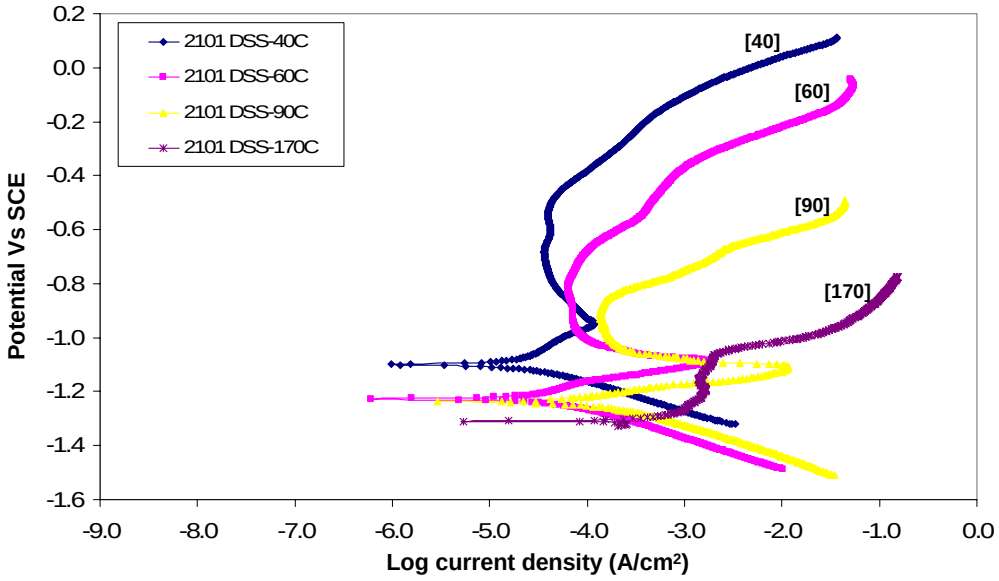

Figure 6.10. Effect of Temperature on the Polarization Behavior of S32101 in Sulfide-Containing Caustic Solution

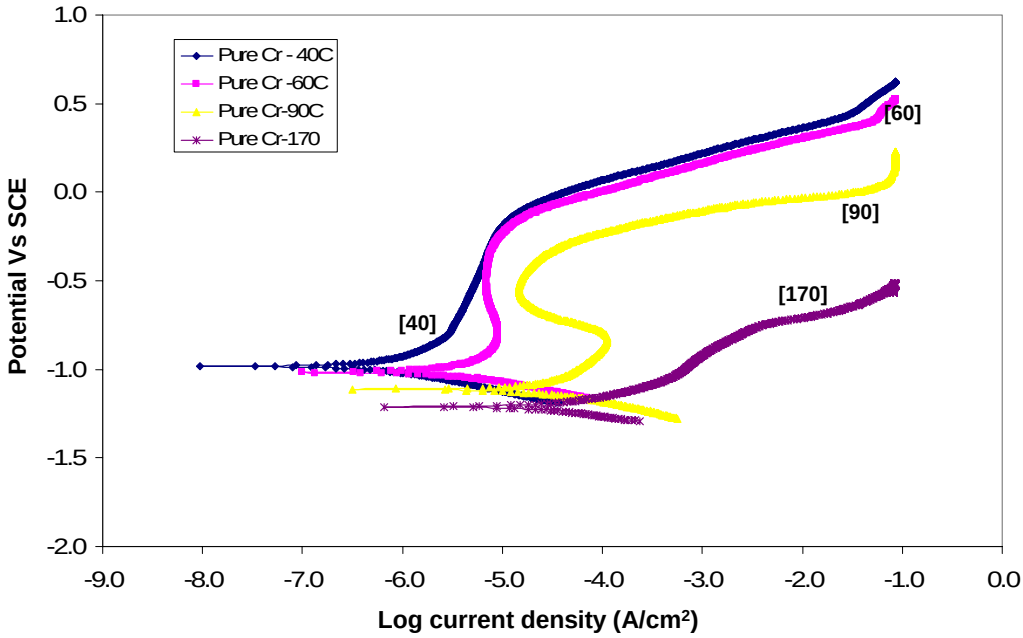

Figure 6.11. Effect of Temperature on the Polarization Behavior of Pure Cr in Sulfide-Containing Caustic Solution

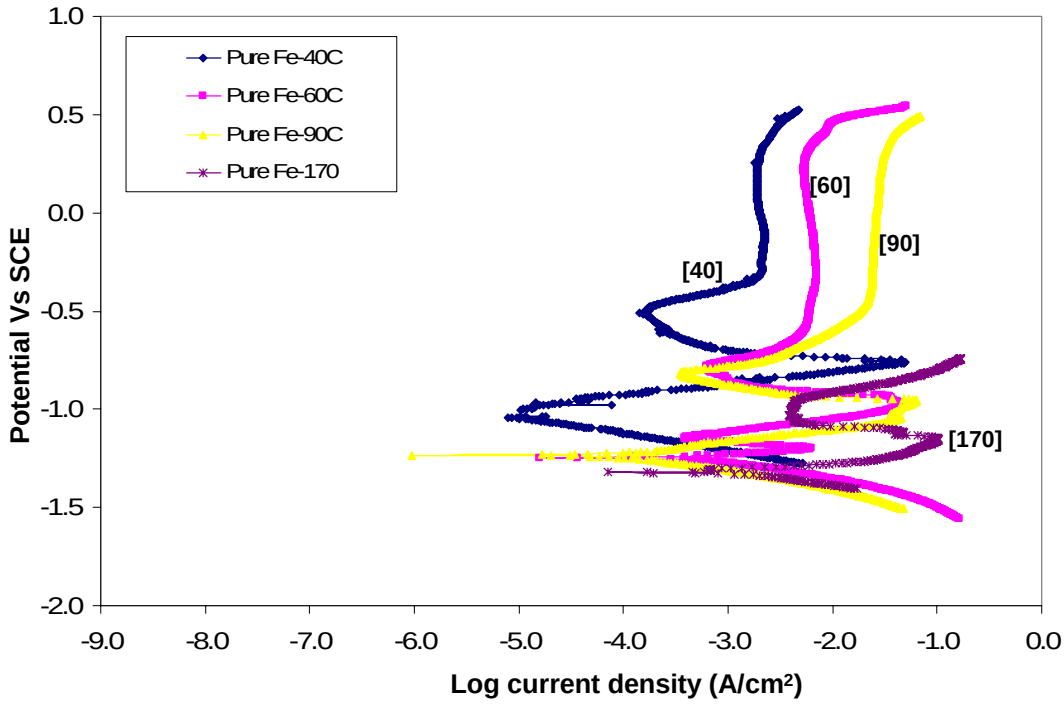

Figure 6.12. Effect of Temperature on the Polarization Behavior of Pure Fe in Sulfide-Containing Caustic Solution

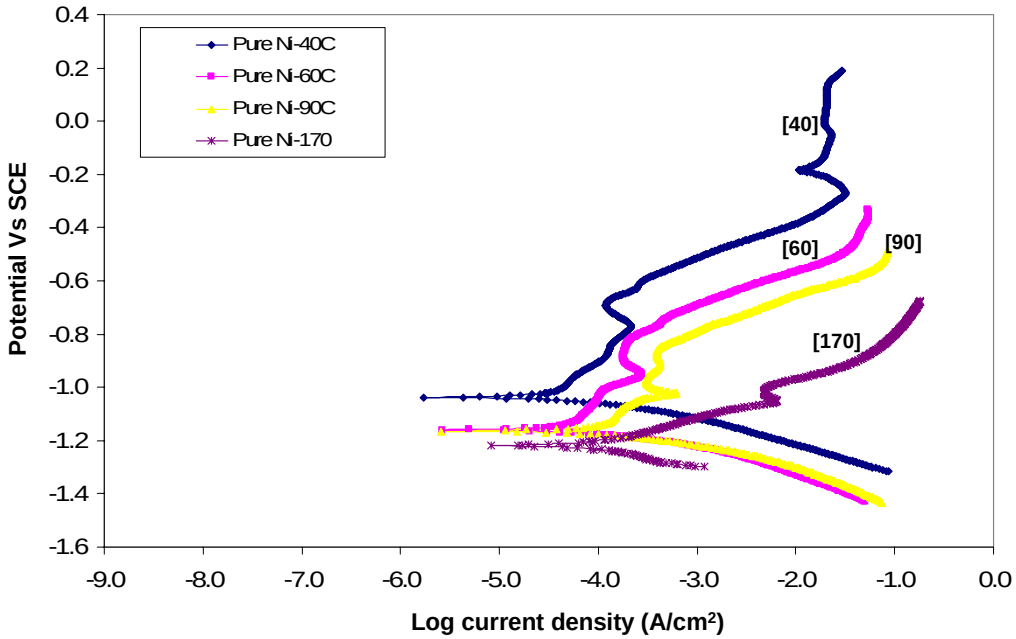

Figure 6.13. Effect of Temperature on the Polarization Behavior of Ni in Sulfide-Containing Caustic Solution

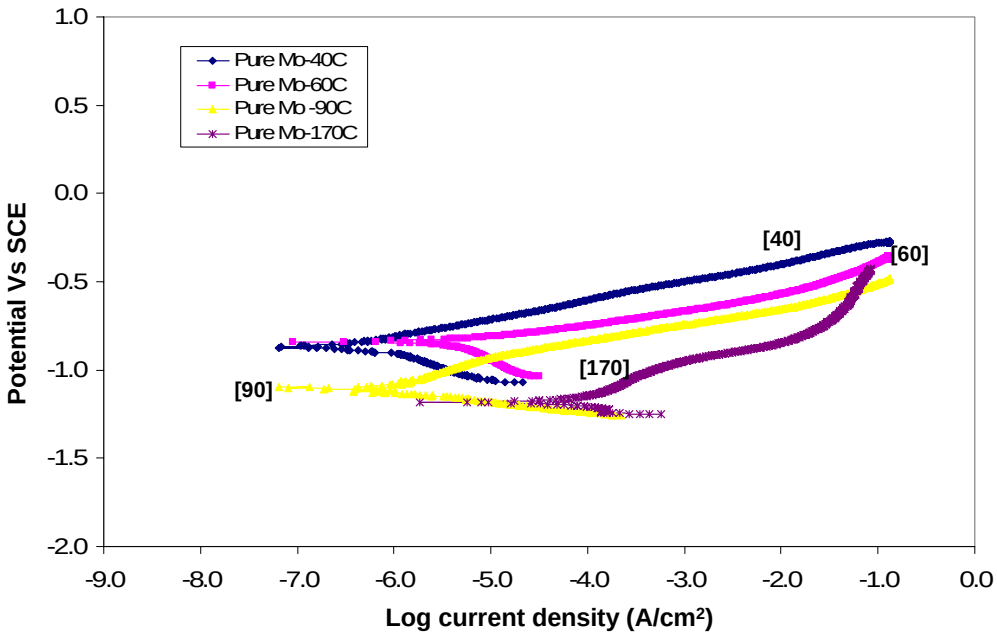

Figure 6.14. Effect of Temperature on the Polarization Behavior of Mo in Sulfide-Containing Caustic Solution

In the presence of sulfide ions, Fe and Ni formed various iron sulfide and nickel sulfide compounds. Molybdenum was found to undergo active dissolution in sulfide-containing caustic solution as well due to the formation of molybdate ions (Figure 6.14). Chromium showed passivity at all temperatures even with the addition of sulfide to caustic solution (Figure 6.11). The reactions of DSS and their alloying elements in sulfide-containing caustic solution have been explained further in Section 6.6.2 of this Chapter.

6.3. COMPARISON OF POLARIZATION BEHAVIOR OF DSS IN CAUSTIC SOLUTION

Results in Figure 6.15 to Figure 6.18 compare the polarization behavior of S32205, S32101 and S32304 in caustic solution (3.75M NaOH) at 40ºC. Results indicate that

under aerated conditions, the corrosion potential and anodic polarization behavior of S32205, S32101 and S32304 was very similar. The three selected grades of DSS exhibited a broad range of passivation and primary and secondary active-passive transition zones. Based on these results, the corrosion behavior of the three DSS grades are expected to be similar at 40ºC. Further electrochemical tests at higher temperatures showed that the general behavior of the three DSS grades was also similar for 60ºC and 90ºC, shown in Figure 6.16 and Figure 6.17 respectively. Further electrochemical tests at higher temperatures (170^{o}C) were done in the autoclave. Pressure balanced reference electrode was used to evaluate the polarization behavior of DSS samples in the caustic environment under these test conditions. Even at 170ºC, the polarization behaviors for all tested grades of DSSs were found to similar at higher oxidation potentials (Figure 6.17 and Figure 6.18 respectively). However, at 170ºC, 2205 DSS had the most noble corrosion potential and it went into passivation without showing active-passive transition. This ease of attaining passivation due to lower critical current density might increase the corrosion resistance of 2205 DSS as compared to the other grades of steel. Polarization behavior of S32101 in caustic environment showed that the critical current density for the lean DSS grade was higher at all tested temperatures as compared to S32205 and S32304, which affect the relative passivation of lean duplex stainless steel.

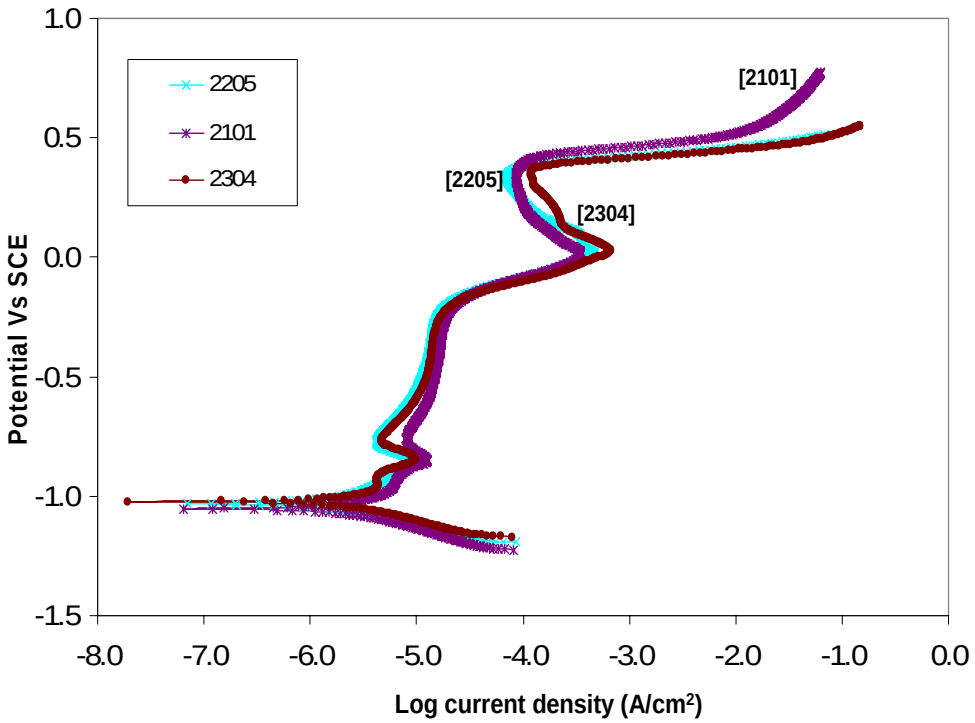

Figure 6.15. Potentiodynamic Polarization Curves for S32205, S32101 and S32304 DSS in 3.75M NaOH Solution at 40°C.

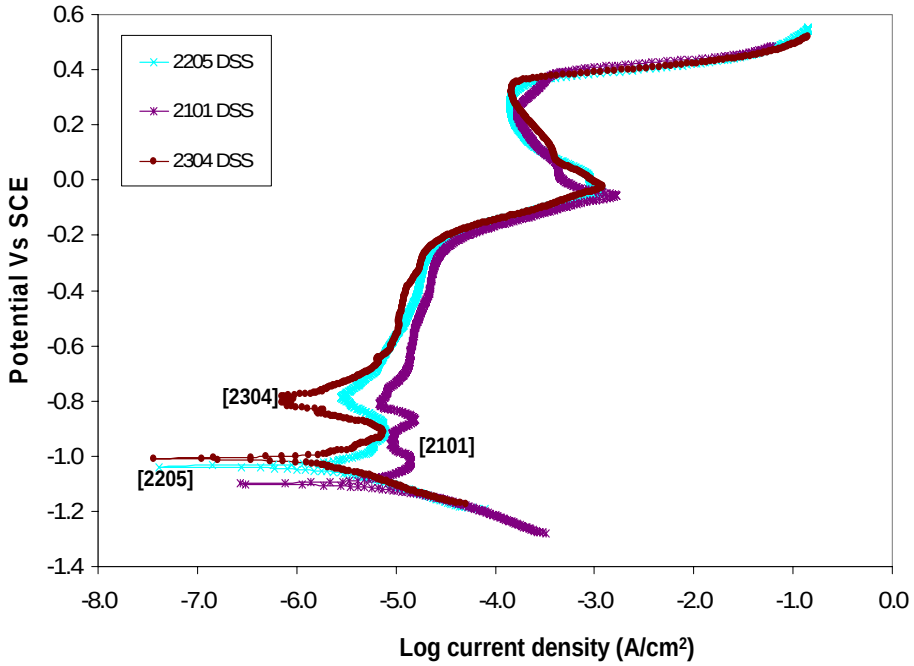

Figure 6.16. Potentiodynamic Polarization Curves for S32205, S32101 and S32304 DSS in 3.75M NaOH Solution at 60°C.

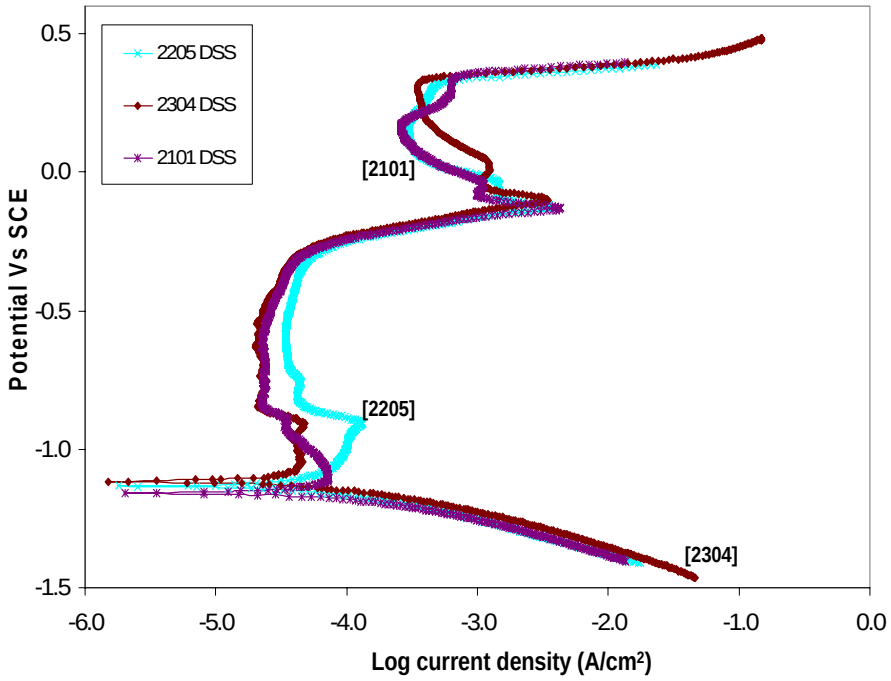

Figure 6.17.Potentiodynamic Polarization Curves for S32205, S32101 and S32304 DSS in 3.75M NaOH Solution at 90°C.

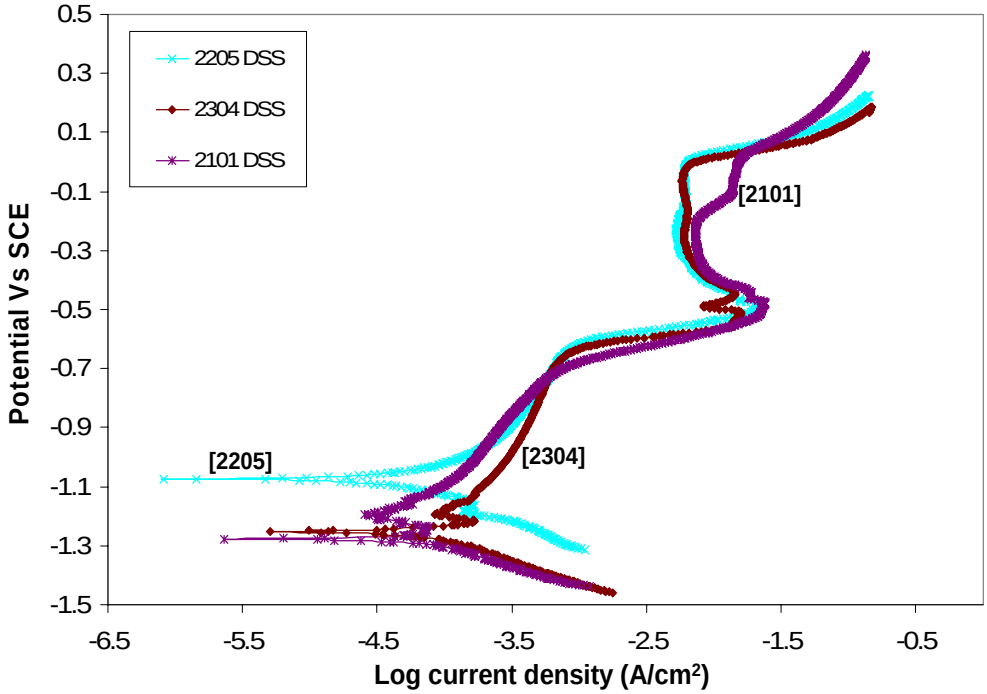

Figure 6.18.Potentiodynamic Polarization Curves for S32205, S32101 and S32304 DSS in 3.75M NaOH Solution at 170°C.

6.4. COMPARISON OF POLARIZATION BEHAVIOR OF DSS IN SULFIDE-CONTAINING CAUSTIC SOLUTION

The corrosion properties of DSS may change depending upon their alloy composition. To evaluate the electrochemical behavior of, S32205, S32304 and S32101 DSS in caustic environments, in the presence of sulfide ions, polarization test were carried out in sulfide-containing caustic solution (3.75M NaOH + 0.64M Na_2S) at 40ºC, 60ºC, 90ºC and 170ºC. Figure 6.19, Figure 6.20, Figure 6.21 and Figure 6.22 shows the polarization behavior of the three grades of DSSs at 40ºC, 60ºC, 90ºC and 170ºC respectively. At 40^{o}C and 60^{o}C, the polarization behavior of S32101 samples was different from that of S32304 and S32205 DSS samples. S32101 showed higher critical current densities as compared to other two DSS grades up to 90ºC.

At 90ºC, the polarization curves for all three grades of DSS were very similar. However, at 170ºC, the polarization of 2205, 2304 and 2101 DSS in sulfide-containing caustic solutions exhibited different behavior. The polarization behavior of S32304 DSS changed considerably with rise in temperature from 90ºC to 170ºC. The corrosion potential of this grade of DSS became noble as compared to 2205 and 2101 DSS. Polarization characteristics also include an absence of active-passive transition zone, unlike the two other grades, which showed distinct active-passive transition region, as shown in Figure 6.22. These results indicate that the test sample of DSS S32304 was already in the passive state under test conditions, which is reflected by the more noble open circuit potential and the lack of active-passive transition peak. The critical current density of 2205 DSS was the highest at 170ºC (almost $10^{-1.88}$mA/cm^2).

The effect of temperature on the polarization behavior of DSS and their alloying elements can also be perceived from the polarization curves in Figure 6.19, Figure 6.20, Figure 6.21 and Figure 6.22. The detrimental effect of temperature on the corrosion susceptibility in sulfide-containing caustic solution is evident from these results, which show a decrease in the corrosion potentials and an increase in the critical current densities with rise in temperatures.

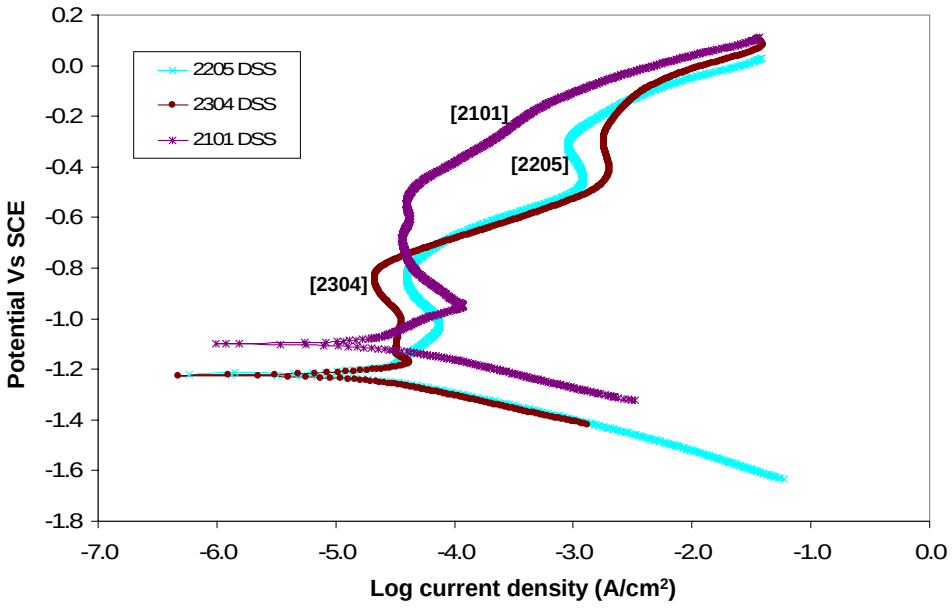

Figure 6.19.Potentiodynamic Polarization Curve for S32205, S32101 and S32304 DSS in 3.75M NaOH + 0.64M Na_2S Solution at 40°C

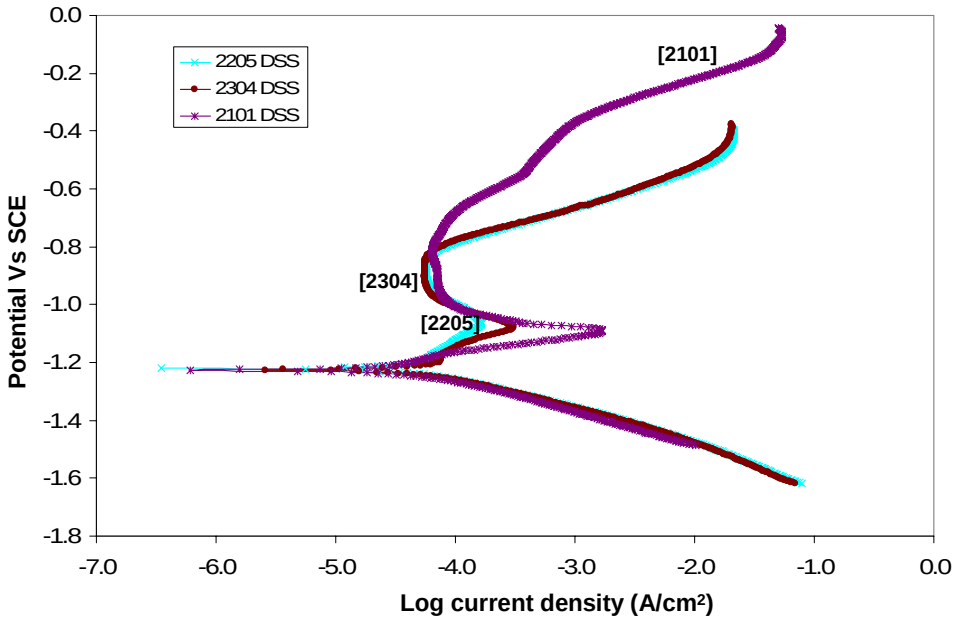

Figure 6.20. Potentiodynamic Polarization Curve for S32205, S32101 and S32304 DSS in 3.75M NaOH + 0.64M Na_2S Solution at 60°C

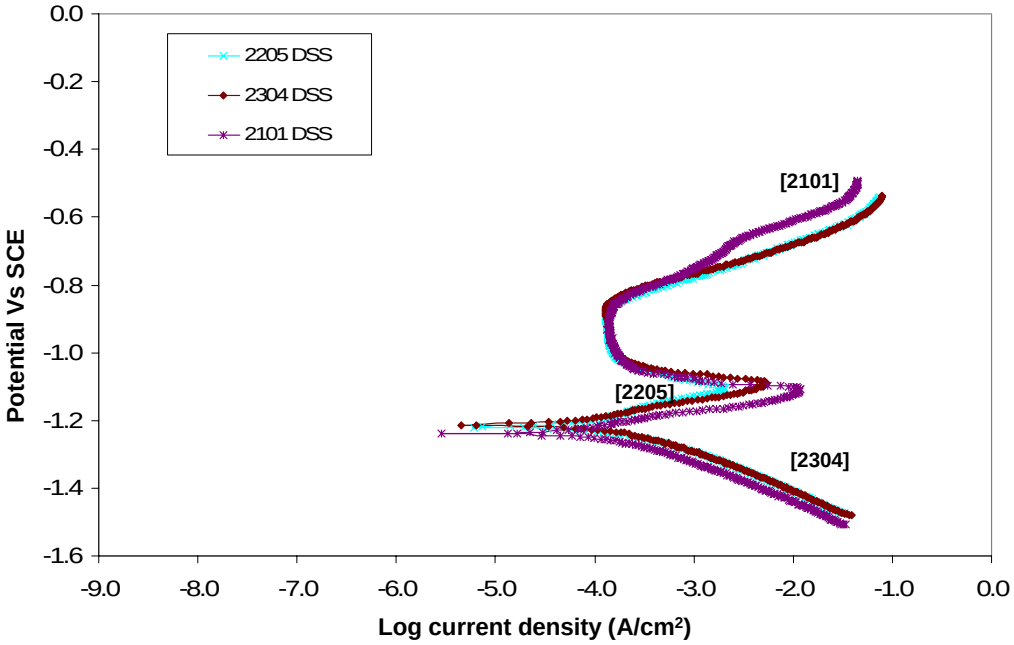

Figure 6.21. Potentiodynamic Polarization Curve for S32205, S32101 and S32304 DSS in 3.75M NaOH + 0.64M Na_2S Solution at 90°C

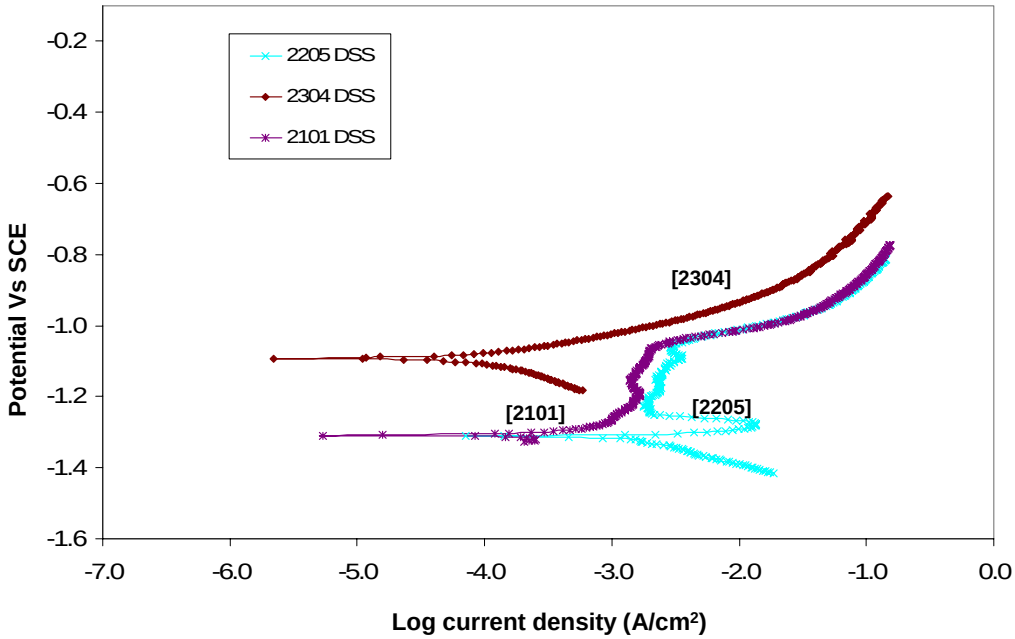

Figure 6.22. Potentiodynamic Polarization Curve for S32205, S32101 and S32304 DSS in 3.75M NaOH + 0.64M Na_2S Solution at 170°C

6.5. EFFECT OF SULFIDE ADDITION ON THE POLARIZATION BEHAVIOR OF DUPLEX STAINLESS STEELS

Results in Figure 6.23 compare the polarization behavior of 2205 DSS in caustic and sulfide-containing caustic solutions at 90ºC. All three grades of duplex stainless steels exhibited similar polarization behavior at 90ºC in both test environments so the polarization behavior of only one grade (S32205) is compared here. From the figure, it can be clearly noticed that on addition of sulfide ions (Na_2S) to the caustic solution at 90ºC, the corrosion potential, $E_{i=0,}$ of S32205 specimen dropped from -1130mV to -1220mV. There was not only a decrease in the corrosion potential of the steel in the presence of sulfide ions, but also an increase in the critical current density of 2205 DSS. Increase in the critical current density due to sulfide addition may affect passive film

formation for these steels. Hence, increase in the magnitude of the critical current density of DSS in sulfide-containing caustic solution reflects difficulty in attaining passivation in these solutions. Current densities of all three grades of DSS were higher in the presence of sulfide in the caustic solutions as compared to that in the pure caustic solution. A similar kind of behavior of S31803 DSS has been reported by Rondelli et al. in caustic and sulfide-containing caustic solutions [1]. This indicates that the presence of sulfides to the caustic solution can have an adverse effect on the passivation behavior under certain conditions and may affect the corrosion resistance of duplex stainless steels.

Polarization behavior of S32205 in pure caustic solution and sulfide-containing caustic solution, white liquor (WL), at 170ºC is shown in Figure 6.24. S32205 in caustic solution did not show any active-passive transition. This was because the steel was already passivated in caustic environment at 170ºC due to the formation of magnetite (Fe_3O_4) and nickel oxide (NiO) [32]. By comparing this with the polarization behavior of S32205 in sulfide-containing caustic solution, it was found that the steel showed an active-passive transition and the current density of the steel was high at all potentials as compared to that in caustic environment. Sulfide addition had also lowered the corrosion potential of the steel. S32205 did not show any secondary passivation in sulfide-containing caustic environment unlike that in pure caustic environment and its current density increased beyond the passive region. This increase in current density was not due to the trans-passive dissolution and corrosion of the steel but due to the redox reactions for the sulfur species. This is because the potential at which current density increased corresponded to the S^{-2}/SO_4^{-2} equilibrium. Sulfide ions got oxidized to sulfate ions, releasing electrons that had resulted in increase in the current density of the steel. A similar difference in

behavior was observed for S32101 in caustic environment with and without sulfide addition. But in this case, the lowering of corrosion potential due to sulfide addition was less as compared to S32205 (Figure 6.25). S32304 showed a completely different behavior in sulfide-containing caustic solution at 170ºC as compared to the other two grades of DSS (Figure 6.26). Sulfide addition did not lower the corrosion potential of the steel.

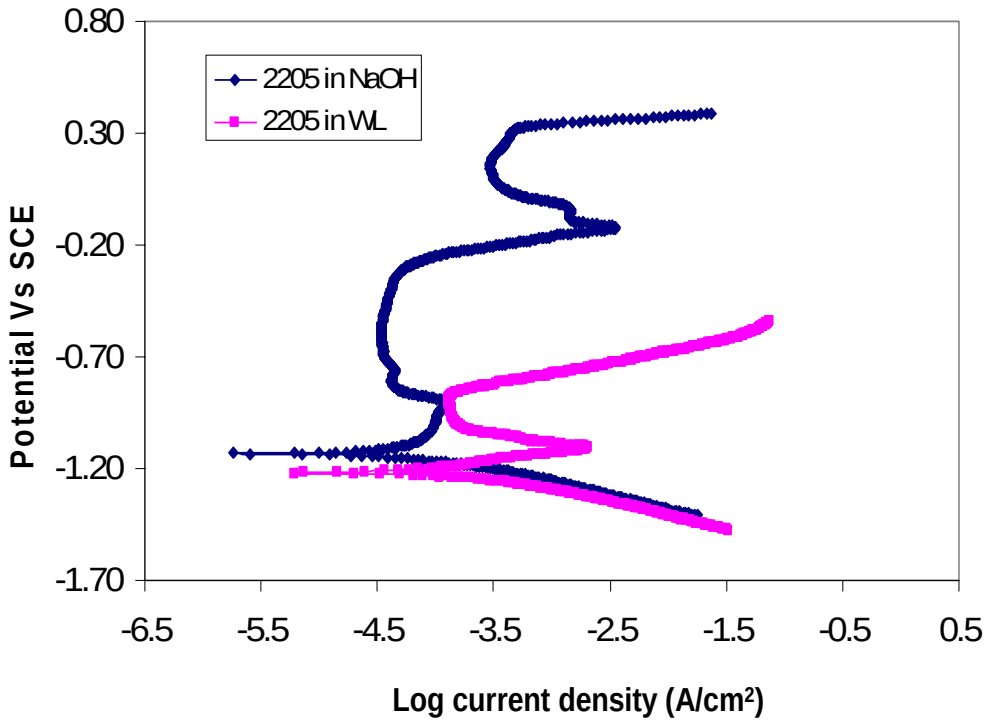

Figure 6.23. Potentiodynamic Polarization Curve for S32205 DSS in 3.75M NaOH Solution With and Without Sulfide Addition at 90ºC

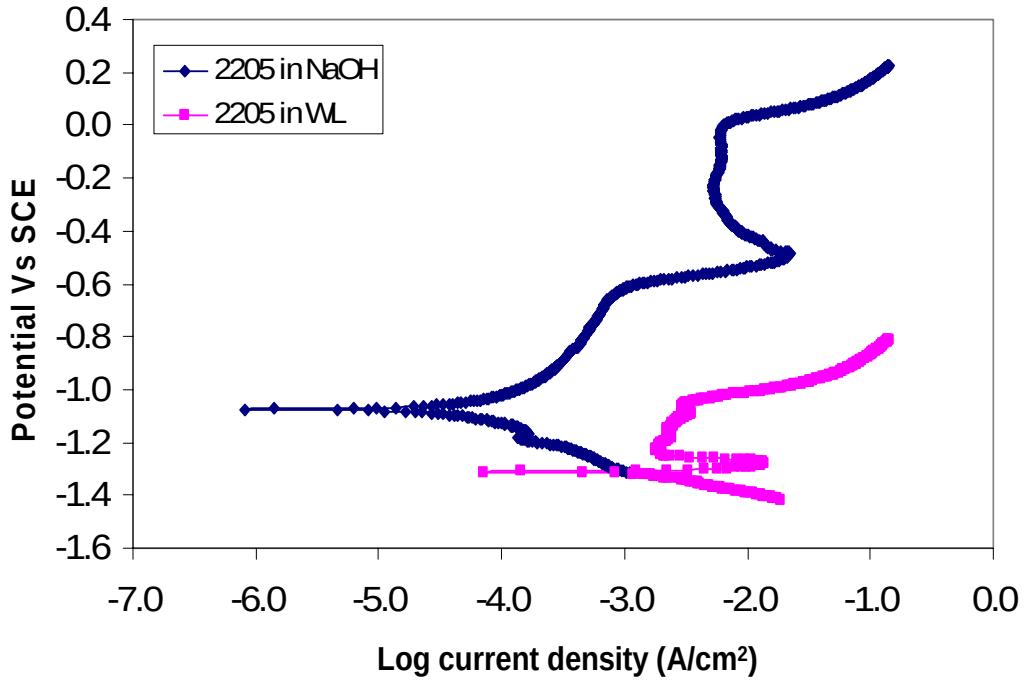

Figure 6.24. Potentiodynamic Polarization Curve for S32205 DSS in 3.75M NaOH Solution With and Without Sulfide Addition at 170°C

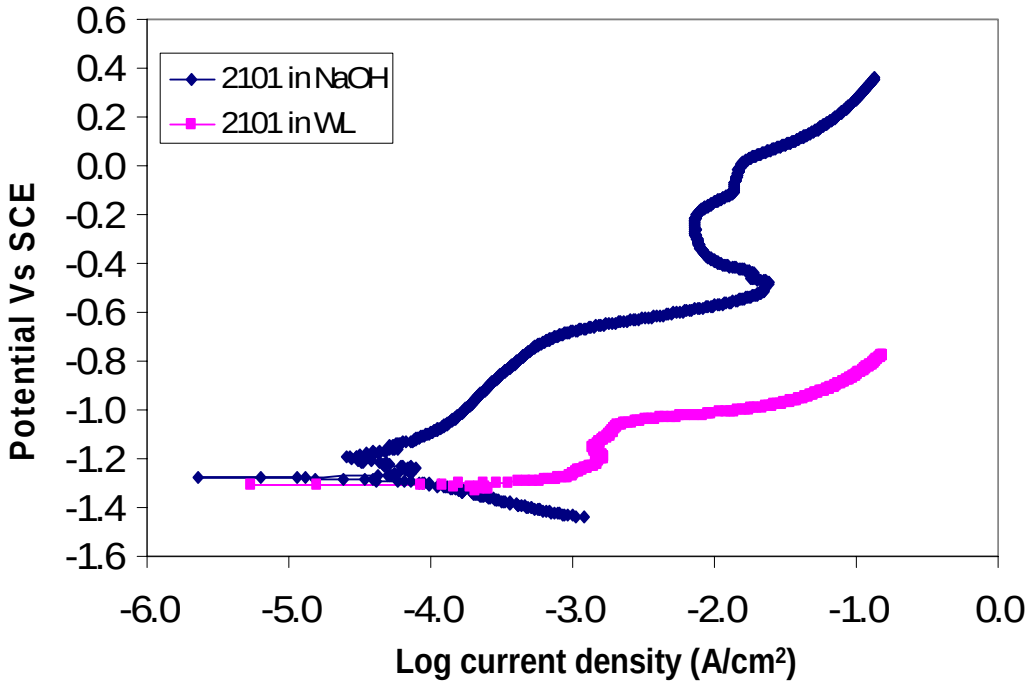

Figure 6.25. Potentiodynamic Polarization Curve for S32101 DSS in 3.75M NaOH With and Without Sulfide Addition at 170°C

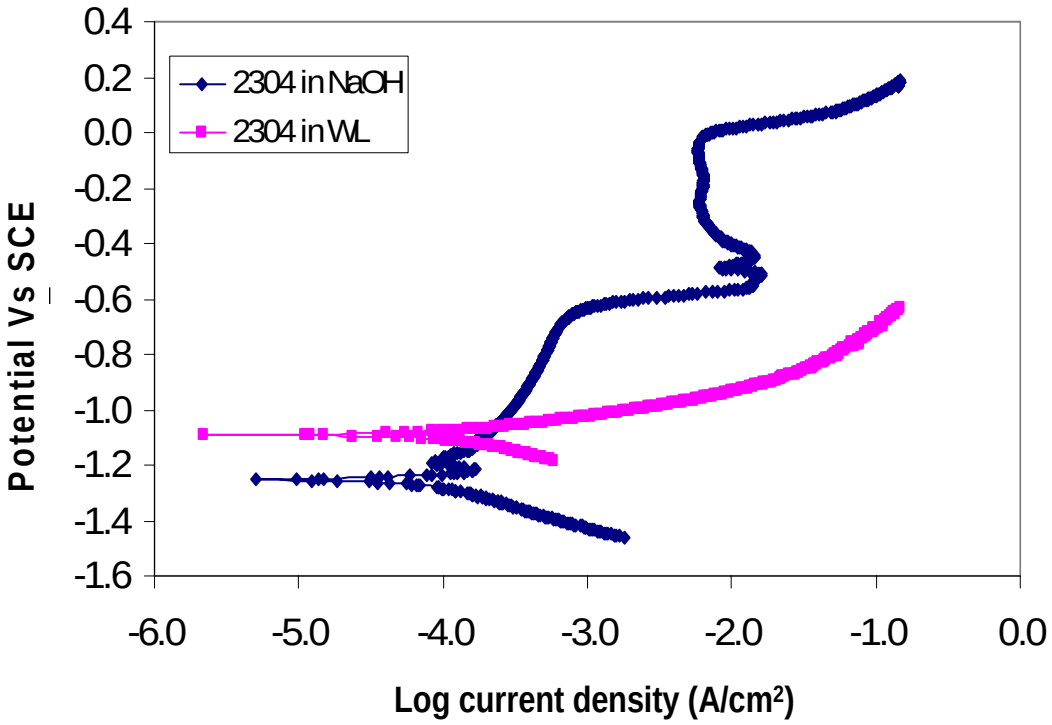

Figure 6.26. Potentiodynamic Polarization Curve for S32304 DSS in 3.75M NaOH Solution With and Without Sulfide Addition at 170°C

6.6. ROLE OF ALLOYING ELEMENTS IN ELECTROCHEMICAL BEHAVIOR OF DSS IN CAUSTIC ENVIRONMENTS

Alloying elements play a key role in the electrochemical behavior of stainless steels. Depending upon the electrochemical properties of the alloying elements in a particular environment, DSS may undergo passivation or active corrosion. The role of alloying elements in the polarization behavior of DSS has not been studied before. Hence, systematic work was carried out to study the effect of alloying elements in the polarization and corrosion behavior of DSS in caustic environment.

6.6.1. Reactions Responsible For the Polarization Behavior of DSS and Their Alloying Elements in Caustic Environment

6.6.1.1. Reactions at 90ºC

The anodic polarization behavior of major alloying elements (Fe, Cr, Ni and Mo) in DSSs was compared with that of 2205 DSS in caustic solution at 90ºC. The polarization curves of these elements are shown in Figure 6.27.

The corrosion potential of pure Fe in NaOH solution at 90ºC was at -898mV_{SHE}. According to the potential-pH diagram for Fe-H_2O system at 90ºC [18], the corrosion potential of iron (-898mV_{SHE}) at pH of 12.5 was in the region of Fe/$HFeO_2^-$ equilibrium potential. A similar behavior of pure iron in NaOH solution at 90ºC has been reported by Agarwal et al [19]. Following the corrosion potential, there was a sharp increase in the current density of Fe in caustic solution (Peak1) and Fe underwent an active-passive transition. Increase in the current density at potentials beyond the corrosion potential corresponds to the active dissolution of iron into dihypoferrite (Fe/$HFeO_2^-$) ion. The critical current density of Fe was higher than the other alloying elements in DSS. Calculated Pourbaix diagram (E-pH diagram) for iron [18] at 90ºC shows that Fe_3O_4 was the stable phase at potentials nobler than the active-passive transition potential in the polarization curve of Fe, shown in Figure 6.27. The reactions and potentials, which correspond to the formation of Fe_3O_4 and Fe_2O_3 [20], are shown below:

$$Fe_3O_4 + 2H_2O + 2e^- = 3\,HFeO_2^- + H^+ \quad (1)$$

$$E_{Fe3O4/\,HFeO2-} = -1.74 + 0.037pH - 0.037\log [HFeO_2^-]^3,\ V_{SHE} \quad (2)$$

$$3Fe_2O_3 + 2H^+ + 2e^- = 2Fe_3O_4 + H_2O \quad (3)$$

$$E_{Fe2O3/Fe3O4} = +0.261 - 0.074pH,\ V_{SHE} \quad (4)$$

This suggests that Fe_3O_4 may be formed during active-passive transition and results into the passivation of iron in the caustic solution. Wensley et al. has also reported the formation of Fe_3O_4 on mild steel in NaOH solutions at 90^oC [21]. However, the passivity observed at higher oxidation potentials is due to the formation of Fe_2O_3 from Fe_3O_4. At potentials beyond +310mV_{SCE}, current density increased due to oxygen evolution.

The corrosion potential of pure nickel was -662mV_{SHE} in 3.75M NaOH at 90^oC. Ni also had lower current density than iron at all potentials, as is evident from Figure 6.27. The critical current density of Ni was almost an order of magnitude lower as compared to that of iron. According to the high temperature potential pH diagram for Ni-H_2O system, the corrosion potential and the primary current peak (Peak1) in nickel occurred in the region defined by Ni/$HNiO_2^-$ equilibrium [22]. A similar behavior of pure Ni in sodium hydroxide solution has been reported by Agarwal et al [19]. Following the primary active-passive transition region, there was a decrease in current density of Ni and a primary passivation region. The passive region of Ni indicates that despite the broad range of stability of $HNiO_2^-$, a protective film forms beyond the active-passive transition region of Ni and extends for several hundred millivolts. As the potential was increased in the anodic direction, there was a sharp increase in the anodic current (+220mV_{SCE}) due to oxygen evolution reaction.

The corrosion potential of pure chromium was -340mV_{SHE}, which was more noble than that of Fe and Ni. Cr did not show any active-passive transition. Previous work by Zheng and Bogaerts on the polarization behavior of pure chromium in caustic solution has also shown similar behavior [9]. As can be seen in the figure, there was a sharp increase in the anodic current density at -300mV_{SCE}, probably due to the formation of CrO_4^{--} ions from

$Cr(OH)_3$. Agarwal et al have also reported a similar behavior of pure Cr in NaOH solution [19]. The reaction showing the formation of CrO_4^{--} ions from $Cr(OH)_3$ in the transpassive region of the polarization curve is given below:

$$Cr(OH)_3 + H_2O = CrO_4^{2-} + 5H^+ + 2e \quad (5)$$

The corrosion potential of pure molybdenum was more noble as compared to iron, but active to nickel and chromium. Molybdenum did not show passivation behavior in caustic solution. Therefore, an increase in potential beyond the corrosion potential for Mo resulted into a sharp increase in the anodic current. This active behavior of molybdenum is likely due to the formation of MoO_4^{--} or molybdate ions formed in this potential range according to the reaction:

$$MoO_2 + 2H_2O = MoO_4^{--} + 4H^+ + 2e^- \quad (6)$$

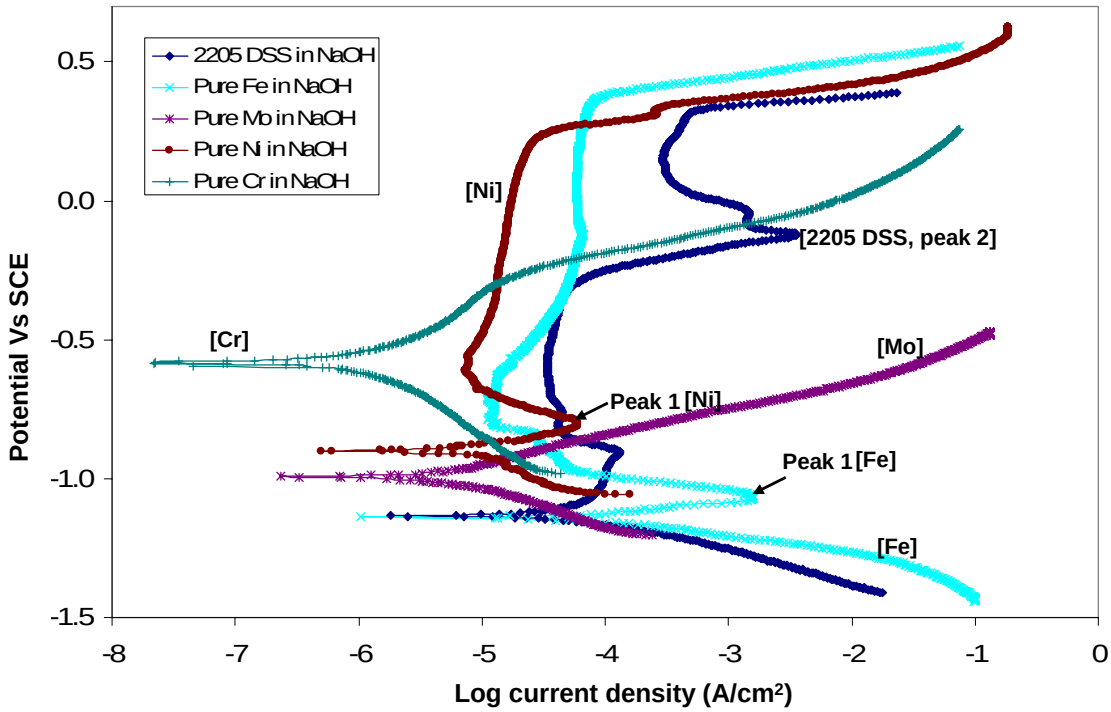

Figure 6.27. Potentiodynamic Polarization Curve for S32205 and Pure Fe, Ni, Mo and Cr in 3.75M NaOH Solution at 90°C

The polarization curves of pure Fe, Ni, Mo and Cr was compared with that of 2205 DSS (Figure 6.27) to understand the role of each alloying element in the corrosion and passivation of DSSs. Since the polarization behavior of the three grades of DSS was similar, the polarization curve of only one grade, S32205, was chosen for comparison. It is evident from polarization results shown in Figure 6.27 that the current peak of 2205 DSS prior to primary passivation was due to the combined effect of Fe and Ni behavior in this potential regime. Moreover, Fe, Ni and Cr contribute to the primary passivation of DSSs. With an increase in the anodic potential, current density also increased for DSSs (peak 2), followed by the secondary active-passive transition. The current peak in the secondary active-passive transition of DSS corresponds to the transpassive dissolution of Cr in the form of CrO_4^{2-} ions. Beyond the secondary active-passive transition, a

secondary passivation region was shown which corresponds to the passive region for the iron and the continuing passivation of nickel. Transpassive region of DSS (above +325mV vs SCE) corresponds to the oxygen evolution reaction. Presence of molybdenum is not expected to help with passive film formation, as the molybdate ions are stable in the potential range above the passivation potential of DSS in caustic solution with pH of 12.5.

6.6.1.2. Reactions at 170ºC

Polarization behavior of Fe, Ni, Cr and Mo in 3.75 NaOH solution at 170ºC are shown in Figure 6.28. Comparison of polarization curves in Figure 6.27 and Figure 6.28 show that with increase in temperature, the corrosion potential of the alloying elements of DSSs moves to negative values. Comparing the polarization curves at 90ºC with that at 170ºC, it can be observed that Mo had the most active corrosion potential at 90ºC. On increasing the potential beyond the corrosion potential, Mo underwent active dissolution due to dissolution of MoO_4^{--} or molybdate ions in caustic solution according to equation (6).

Fe had more noble corrosion potential (-952mV_{SHE}) as compared to Mo and it did not show any active-passive transition at 170ºC. Comparing its corrosion potential with the high temperature potential-pH diagram for iron water system [23], the corrosion potential was found to lie in the region where Fe_3O_4 was the stable phase. So the absence of active-passive transition suggest that Fe was already passivated in NaOH solution at 170ºC due to the formation of Fe_3O_4 and the continuing passivation of Fe at higher oxidation potentials was due to the formation of Fe_2O_3 from Fe_3O_4 according to reaction (7).

$$4\ Fe_3O_4 + O_2 = 6\ Fe_2O_3 \qquad (7)$$

Cr also did not show any active-passive transition at 170ºC and at a potential of -467mV vs. SHE, there was a sharp increase in the current density of Cr, corresponding to the oxidation of CrO_3^{3-} to CrO_4^{2-} and dissolution as CrO_4^{2-} ion in the solution. This is evident from the high temperature potential-pH diagram for the Cr-H_2O system at 150ºC [22]. Unlike the polarization behavior at 90ºC, Ni also did not show active-passive transition peak at 170ºC. The corrosion potential of Ni was -834mV_{SHE}, which according to the E-pH diagram was above the Ni/$HNiO_2^-$ equilibrium [22] but showed passivation at potentials beyond the corrosion potential of the element due to the formation of a protective film of nickel oxide (NiO_2).

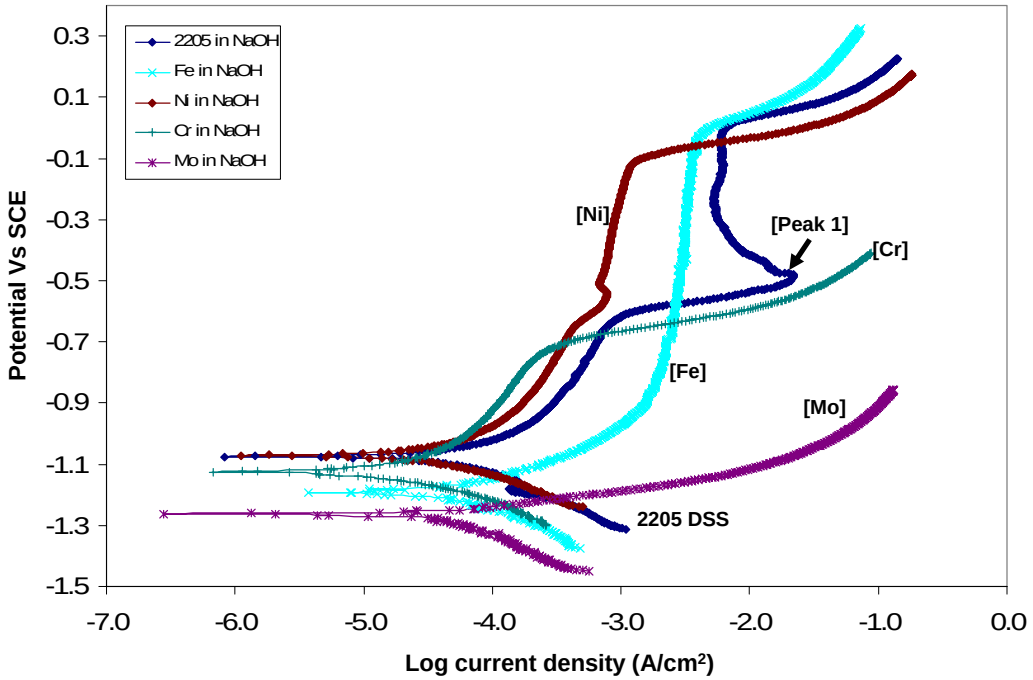

Figure 6.28. Potentiodynamic Polarization Curve for Pure Fe, Ni, Mo, Cr and 2205 in 3.75M NaOH Solution at 170°C

The polarization curves for the four alloying elements at 170ºC were compared with the polarization curve of DSS. The corrosion potentials of DSS S32205, S32101 and S32304 at 170ºC were different but the overall polarization behavior of the three grades of DSS were very similar at higher oxidation potentials (Figure 6.18). Hence, 2205 DSS was used for comparison, as shown in Figure 6.28. The corrosion potential of S32205 was very similar to that of nickel. The corrosion potential of S32101 and S32304 were below the corrosion potential of iron, nickel and chromium. It is evident from the results that the primary passivation of the steels could be due to the combined effect of Fe, Ni and Cr. The breakdown of the primary passivation of DSS (peak 1) could be attributed to the dissolution of Cr in the form of CrO_4^{--} ions. Nevertheless, DSS showed secondary passivation due to the continuing passivation of both Ni and Fe. However, Mo did not contribute to the passive film formation of the DSSs and hence can considered to be detrimental to general corrosion behavior of DSS alloys in caustic solutions. Prior work has shown the negative influence of molybdenum in the corrosion resistance of stainless steel in caustic environment [25].

6.6.2. Reactions Responsible for the Polarization Behavior of DSS and Their Alloying Elements in Sulfide-Containing Caustic Environment

6.6.2.1. Reactions at 90ºC

Polarization behavior of duplex stainless steels was compared with its alloying elements to understand the role of alloying elements in the corrosion and passivation behavior of the steel (Figure 6.31). Tests at higher temperatures (90ºC) were chosen for comparison, as the rates of corrosion at higher temperatures are higher. Since the

polarization behavior of all three grades of DSS at 90ºC was similar, the polarization curve of only one grade (S32205) was chosen for comparison.

Upon polarization, pure iron sample showed a significant rise in anodic current as the potential was raised above its free corrosion potential of -994mV_{SHE}. According to the E-pH diagram of iron-water-sulfur system at high temperature (Figure 6.29), the corrosion potential of iron lies in the S^{2-}/FeS equilibrium region [23]. The pH-potential calculations showed that at the corrosion potential, the stable dissolved species are likely to be S^{2-} and Fe dissolved as $HFeO_2^-$. Increase in the current density of iron beyond its corrosion potential followed by a subsequent decrease in the current density corresponded to the oxidation of Fe to form $HFeO_2^-$ and the $HFeO_2^-$, S^{2-} interaction to form iron sulfide (FeS) respectively according to reaction (8).

$$HFeO_2^- + S^{2-} + 3H^+ = FeS + 2H_2O \quad (8)$$

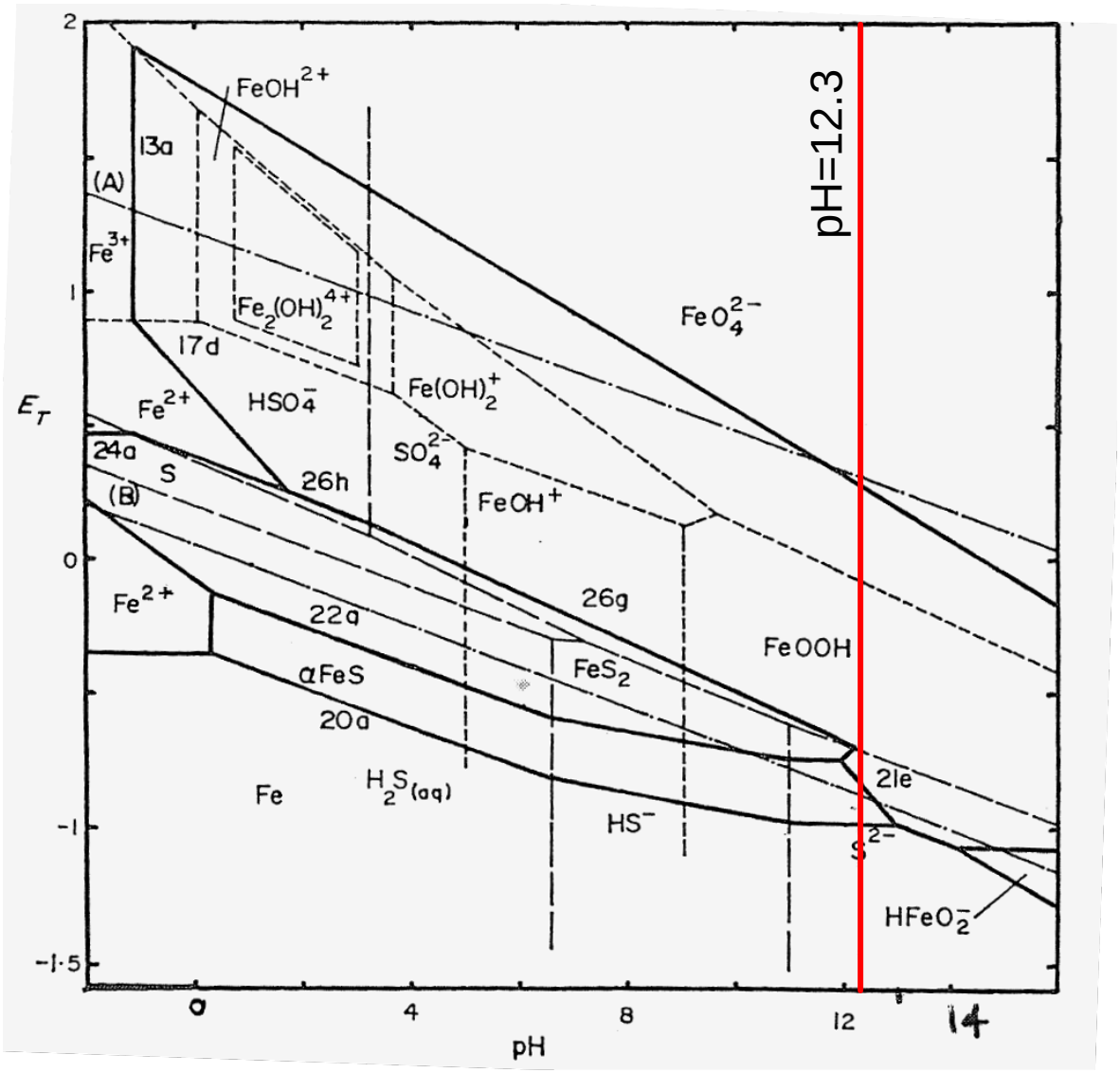

Figure 6.29. Potential/pH diagram for Fe-H_2O-S system at 100 ºC [23]

Prior work has shown that the sulfide addition will favor formation of FeS [28]. Such metal-sulfur compounds are non-adherent or may hydrolyze in water easily, exposing the metal to further attack. Tromans [29] has also suggested that the sulfide addition to the caustic solution favors a poorly protective film consisting of iron oxide and iron sulfide on carbon steels. This $Fe_3O_{4-x}S_x$ film formed on the metal surface is less stable as compared to the magnetite (Fe_3O_4) film formed in pure caustic solutions. In another study, Shoesmith et al. had studied the electrochemical behavior of iron in strongly alkaline (pH≥12) sulfide solution [30]. The results showed that in alkaline sulfide solution there was a growth of mackinawite film preceded by the formation of an oxide film. Mackinawite film formed does not completely passivate the surface. Hence, the reduced corrosion resistance of pure iron in sulfide-containing caustic solution in this study could be due to the unstable iron sulfide compounds formed on the metal surface or due to machinawite film formation.

The corrosion potential of other alloying elements like Mo, Ni and Cr were also shifted in cathodic direction. In the caustic solution, open circuit potential of Ni was found to be more noble as compared to Mo [31], but the situation was reversed in the sulfide-containing caustic solution where the Ni became more active as compared to Mo. Cr was found to have the most noble corrosion potential among all the alloying elements, which also indicates that the surface of chromium may have been in the passive state under these test conditions. The corrosion potential of Ni was -923mV_{SHE}, which according to the E-pH diagram of Ni in sulfide solution [32] is in the region where nickel sulfide (NiS_2) is the stable phase. Mo did not show any active-passive transition or passivity. The corrosion potential of Mo was -857mV_{SHE}, which according to the E-pH diagram of

Mo at 90 ^{o}C corresponded to the region of stability of soluble molybdate (MoO_4^{-2}) ions. Hence, with increase in potential beyond open circuit potential, Mo was found to undergo active corrosion according to equation (9).

$$MoO_2 + 2H_2O = MoO_4^{--} + 4H^+ + 2e^- \quad (9)$$

The increase in the current density during the anodic polarization of pure platinum in sulfide-containing caustic solution (Figure 6.31) at higher oxidation potentials was due to the oxidation of sulfur species and corresponded to the S^{-2}/SO_4^{-2} equilibrium according to reaction (10), (Figure 6.30) [33]. The potentials for transpassive region for Fe, Ni and Mo samples tested in WL coincided with the potential at which S^{-2}/SO_4^{-2} oxidation is expected to take place. Hence it can be deduced from these results that oxidation of sulfur species at the electrode surface in each pure-element polarization in the WL was the dominant reaction at higher anodic potentials. The polarization behavior of Fe, Ni and Mo were masked by this sulfur oxidation reaction at the electrode surface. From the polarization graphs in Figure 6.31, no further information could be obtained about the continuing passivation of Fe, Ni and Mo beyond the oxidation potential of SO_4^{-2}. In sulfide containing caustic solution, Cr showed passivation beyond its corrosion potential. Passivation current density for Cr was almost two orders of magnitude better than that for the Fe and Ni in sulfide containing caustic solutions at 90^{o}C.

$$S^{2-} + 4H_2O = SO_4^{2-} + 8H^+ + 8e^- \quad (10)$$

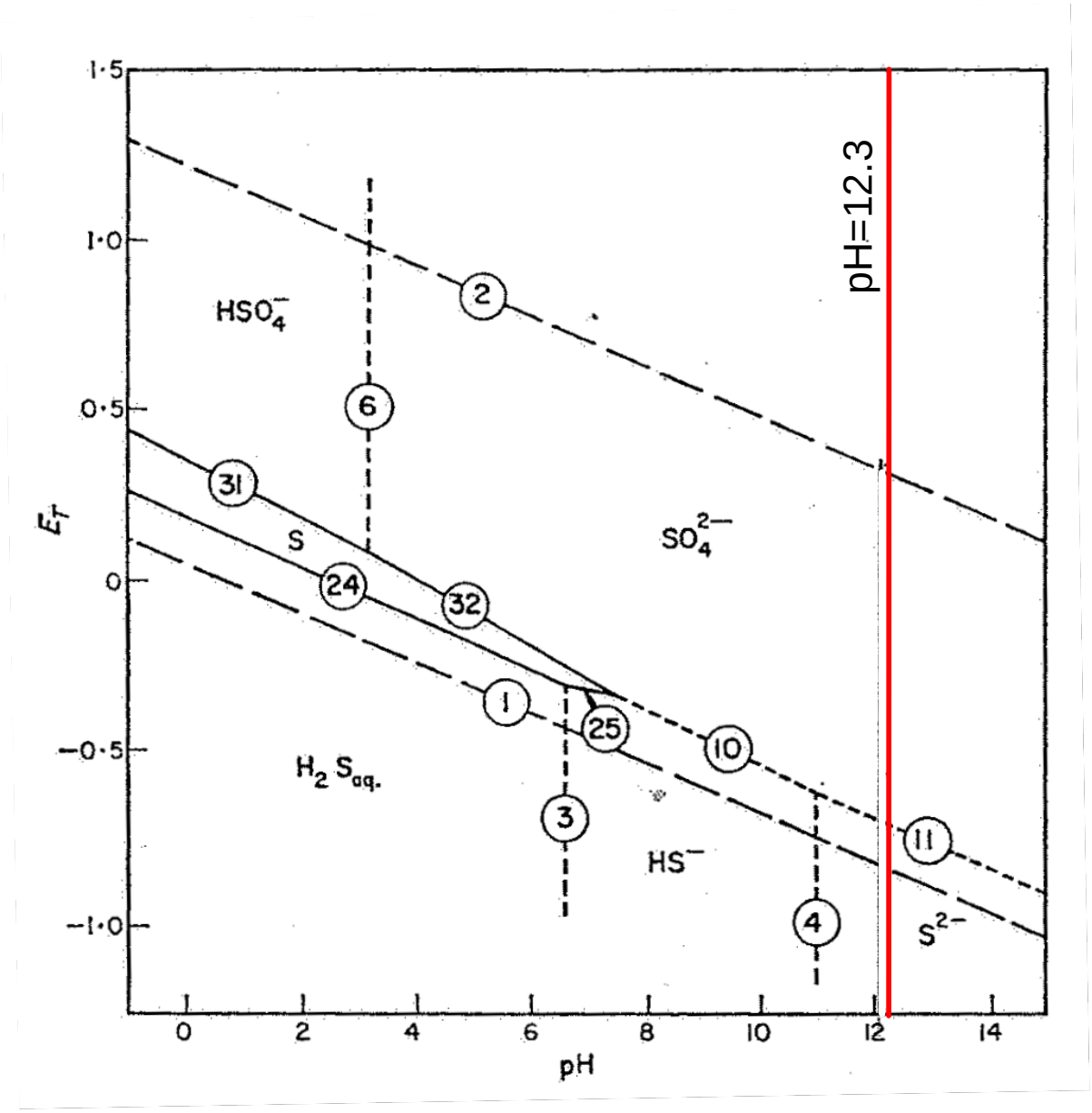

Figure 6.30. Potential/pH diagram at 100 ºC and unit activity of dissolved sulfur species (as revised from Biernat and Robins) [33]

Comparing the polarization behavior of pure Fe, Ni, Mo and Cr with that of 2205 DSS in sulfide-containing caustic solution, it is clear that the polarization behavior of duplex stainless steel near the open circuit potential is affected by the polarization behavior of Fe and Ni. The increase in the current density beyond the corrosion potential of S32205 is due to the dissolution of Fe. However, the dissolution of S32205 and further increase in current density of the alloy is prevented owing to the passivation of nickel. Due to the formation of nickel sulfide, DSS showed primary passivation in sulfide-containing caustic solutions. Mo did not seem to provide any help with the passivation of the steel. Prior work has shown the negative influence of molybdenum in the corrosion resistance of stainless steel in white liquor [25]. In this study, it was clear that the molybdenum had high dissolution rate in the form of MoO_4^{--} or molybdate ion, so the molybdenum would not provide any protection against corrosion for duplex stainless steels in caustic or sulfide containing sulfide solutions. Increase in the current density beyond the primary passivation region of 2205 DSS was due to the oxidation of sulfur species (S^{-2}/SO_4^{-2} oxidation reaction).

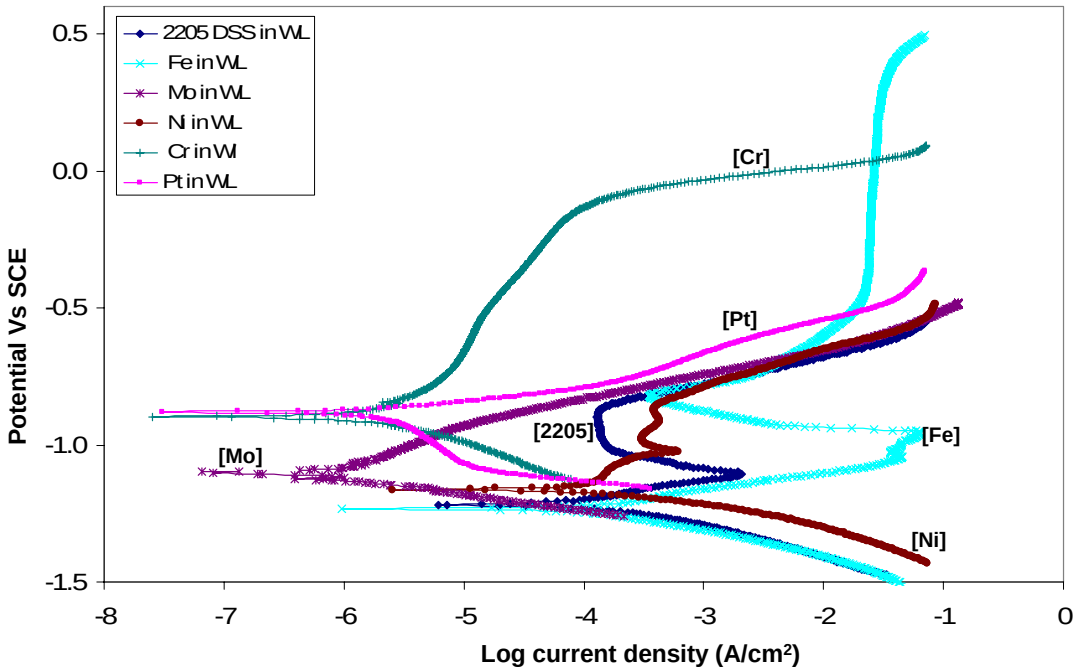

Figure 6.31. Potentiodynamic Polarization Curve for 2205 DSS and Pure Pt, Fe, Ni, Mo and Cr in 3.75M NaOH + 0.64M Na_2S Solution at 90°C

6.6.2.2. Reactions at 170°C

The operating temperatures in pulp and paper mills are around 170°C. Hence, polarization tests were performed at 170°C on the three grades of duplex stainless steels and their alloying elements to understand the corrosion and passivation behavior of the steels. Tests at 170 °C showed a significant lowering of the corrosion potentials of Fe, Ni, Cr and Mo as compared to that at 90°C (Figure 6.32). Fe in this case also had the most active corrosion potential as compared to other alloying elements. Comparison of the corrosion potential of iron with the high temperature potential/pH diagrams for iron-water-sulfur system [23] showed that the potential corresponded to the $HFeO^{2-}/Fe_3O_4$ equilibrium potential (equation 11). Hence, the increase in current density in the active-

passive region was due to the oxidation of iron to Fe_3O_4, which was followed by a lowering of current and passivation.

$$3\ HFeO_2^- + H^+ = Fe_3O_4 + 2H_2O + 2e^- \quad (11)$$

The corrosion potential of Ni (-979mV_{SHE}) was more noble as compared to Fe. The corrosion potential of Ni was in the region where nickel sulfide (NiS_2) is the stable phase [32]. The current density of Ni was lower by several magnitudes in the active-passive region as compared to that of iron. Cr had a corrosion potential of -970mV_{SHE}, which was in the region of stability of chromium sulfide (Cr_2S_3) [32]. The lower current density and passivation of chromium could be attributed to the formation of Cr_2S_3. From these results, it can be deduced that the higher dissolution rate of Fe was compensated by the lower current density of Ni and Cr near the corrosion potential and active-passive transition region. These results indicate that alloying Fe with Cr and Ni helps to raise the corrosion potential and lower critical current density of the alloy. The presence of Ni and Cr in duplex stainless steels proved beneficial in terms of its passivation behavior as the steels showed more noble corrosion potential as compared to if Fe alone was present. Cr and Ni had also lowered the current densities in the active-passive transition region (Figure 6.32), making it easier for the alloy to attain passivation.

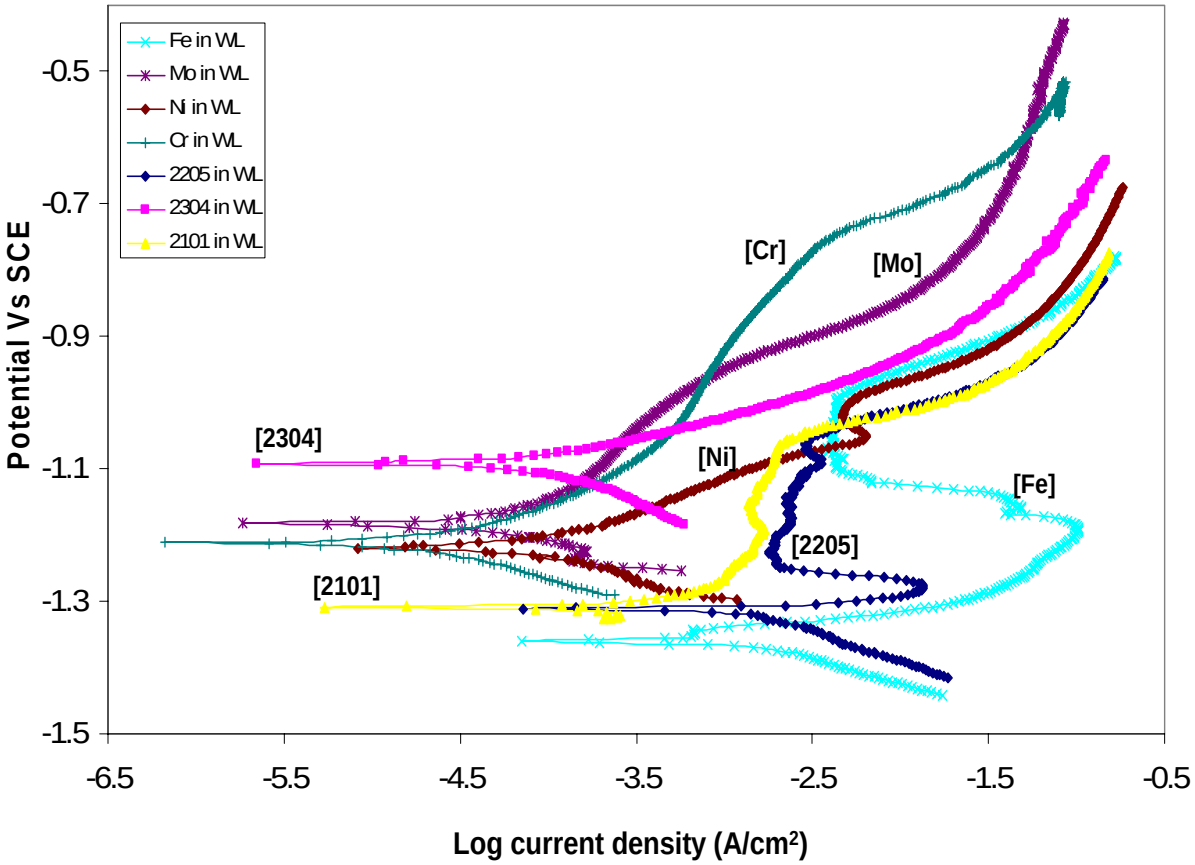

Figure 6.32. Potentiodynamic Polarization Curve for S32205, S32101, S32304 and Pure Fe, Ni, Mo and Cr in 150g/L NaOH + 50g/L Na_2S Solution at 170°C

6.7. CHARACTERIZATION OF CORROSION FILM FORMED ON DUPLEX STAINLESS STEELS BY X-RAY DIFFRACTION

Duplex stainless steels exposed to caustic and sulfide-containing caustic environments at 170°C react with the environment to form product film on their surfaces. The film composition on the DSS surface may vary from one grade to another depending upon the alloy composition. The corrosion and SCC resistance of DSS depends upon the stability of these films in the surrounding environment. Hence, it is important to characterize the

composition and nature of the passive films formed on DSS in alkaline environment. X-ray diffraction was used to study the films formed on DSS in caustic and sulfide-containing solutions at 170ºC.

6.7.1. Passive Film on DSS Samples in Caustic Environment

DSS samples, S32205, S32101 and S32304, were exposed to 3.75M NaOH to study the corrosion products formed on their surface. The DSS samples were exposed to caustic environment at 170ºC under open circuit potential for 15days. Surface film formed on DSS samples after exposure to the caustic solution was characterized using x-ray diffraction method to identify the phases formed at the surface. X-ray diffraction patterns of unexposed DSS grades S32205, S32101 and S32304 are shown in Figure 6.36. XRD pattern for the unexposed DSS samples predominately show austenite and ferrite peaks. Figure 6.37 shows XRD peaks for the DSS samples exposed to caustic environment at 170ºC for 15 days. Comparison of unexposed DSS sample pattern with equivalent sample exposed to caustic solution at 170ºC indicate various peaks corresponding to the corrosion product film at the steel surface. Comparing peak positions of S32205, S32101 and S32304 DSS with the peak positions of nickel iron oxide ($Ni_{0.4}Fe_{2.6}O_4$), chromite ($FeCr_2O_4$) and magnetite (Fe_3O_4) in Figure 6.37, it is evident that the corrosion film of DSS mainly consists of spinel oxides. High temperature Pourbaix diagrams for iron species in the Fe-Cr-Ni system have shown that nickel iron oxides have the largest stability area of the spinels existing in a wide potential range and are the dominant species formed in high pH alkaline environments (Figure 6.33) [26]. Pourbaix diagrams of Fe, Cr and Ni species also indicate that more than one solid phase can be stable at a given potential/ pH coordinate and nickel iron oxide can be stable with chromite (Figure

6.33-Figure 6.35). Hence, test results and prior work indicate that a combination of nickel iron oxide, chromite and magnetite (spinel oxides) may simultaneously exist in the corrosion films of DSS in alkaline NaOH solution at 170ºC. Polarization tests of DSS and their alloying elements at 170ºC have shown that the polarization and passivation behavior of DSS is affected by the polarization behavior of pure Fe and Ni, though chromium plays a role in passivation too. This is further evident from the spinel oxides of iron, nickel and chromium on the metal surface, as detected by x-ray diffraction. Surface energies of spinels are high and their solubilities are very low, providing a good corrosion resistance to steels [26]. The overall better corrosion performance of DSS as compared to the other grades of steels in caustic environment can be attributed to the presence of spinel oxides on the metal surface. Absence of molybdenum in the corrosion films on the DSS samples with Mo, may be due to active dissolution of molybdate ions in caustic environment. This is in agreement with the polarization behavior of molybdenum in caustic environment.

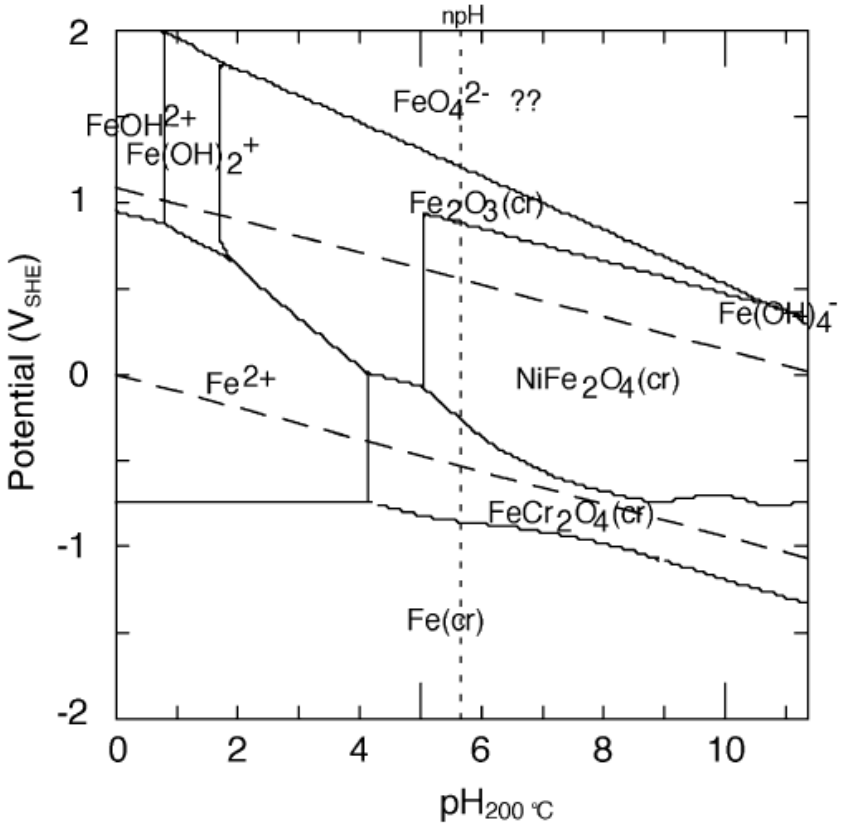

Figure 6.33. Pourbaix diagram for Fe species in the ternary system of Fe-Cr-Ni at 200°C. [26]

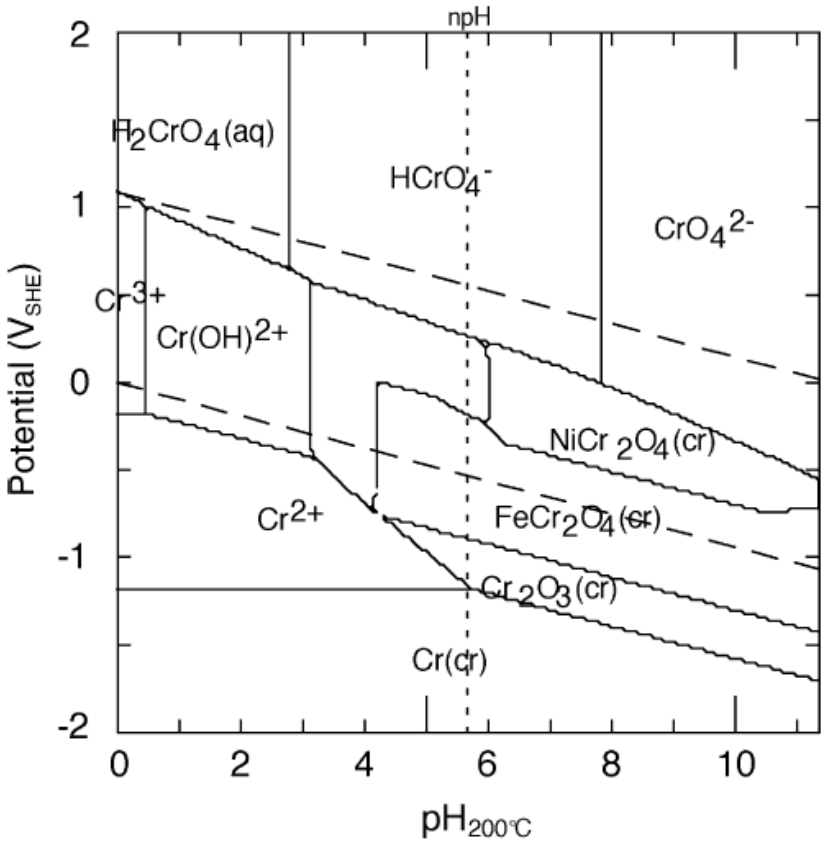

Figure 6.34. Pourbaix diagram for Cr species in the ternary system of Fe-Cr-Ni at 200°C. [26]

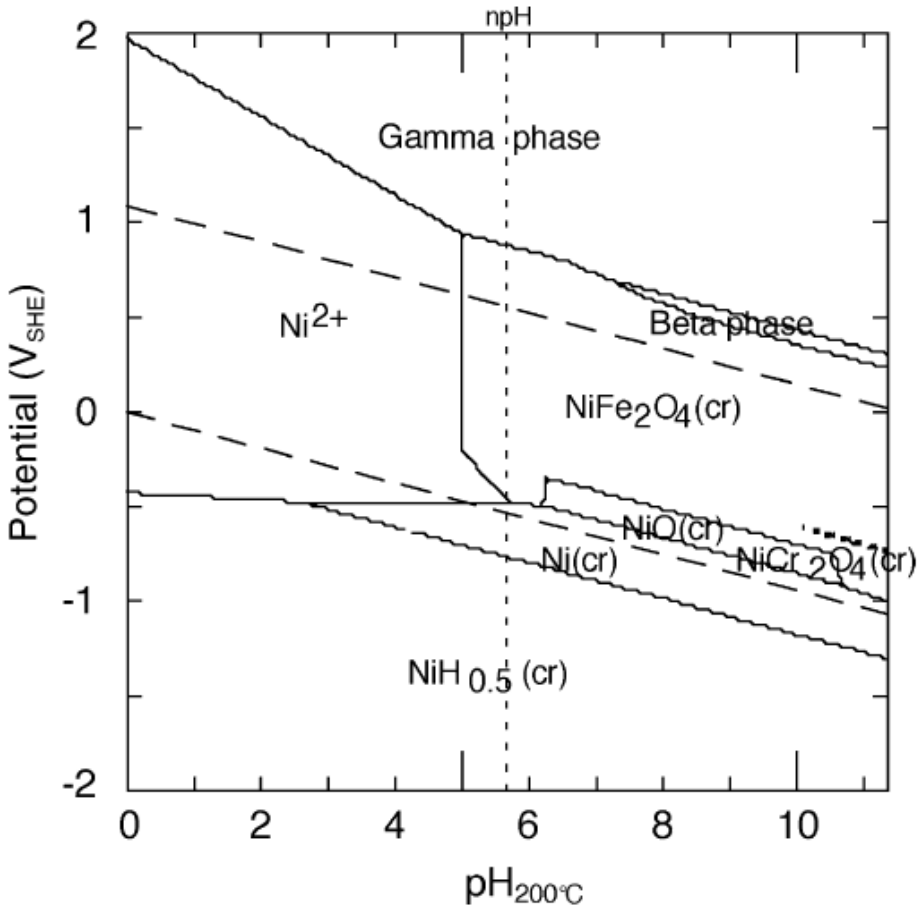

Figure 6.35. Pourbaix diagram for Ni species in the ternary system of Fe-Cr-Ni at 200°C. [26]

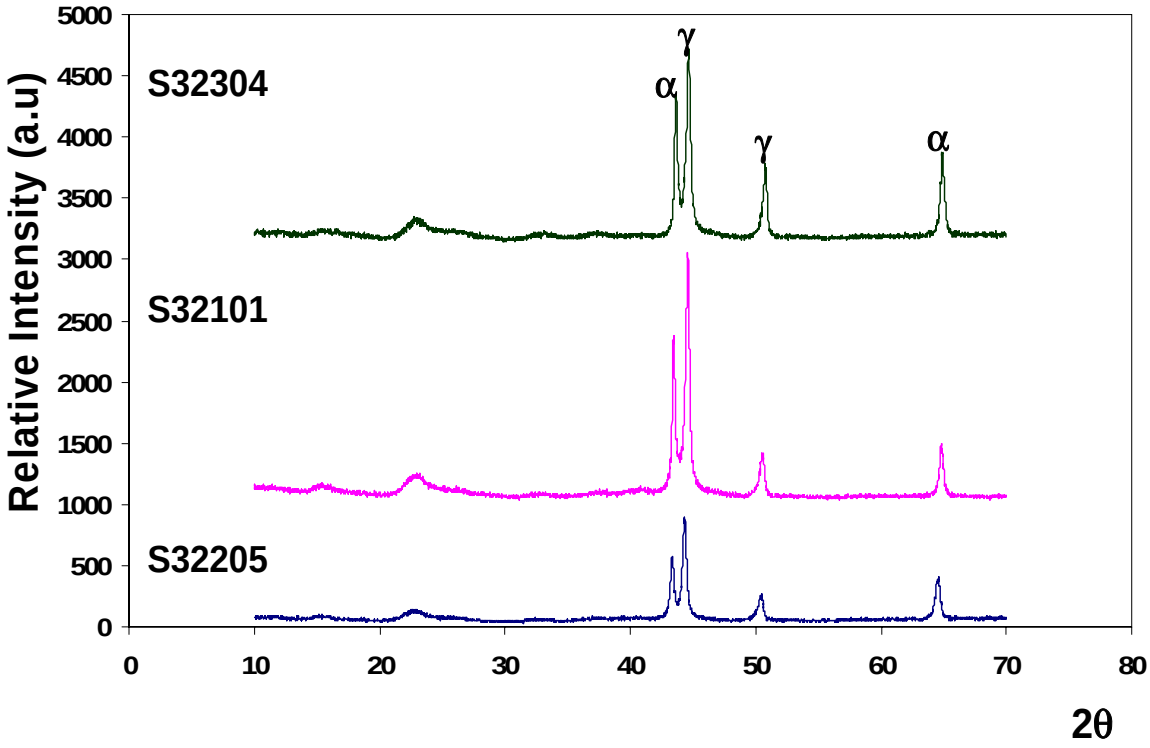

Figure 6.36. XRD pattern of S32205, S32304 and S32101 base metal, α- ferrite phase, γ- austenite phase

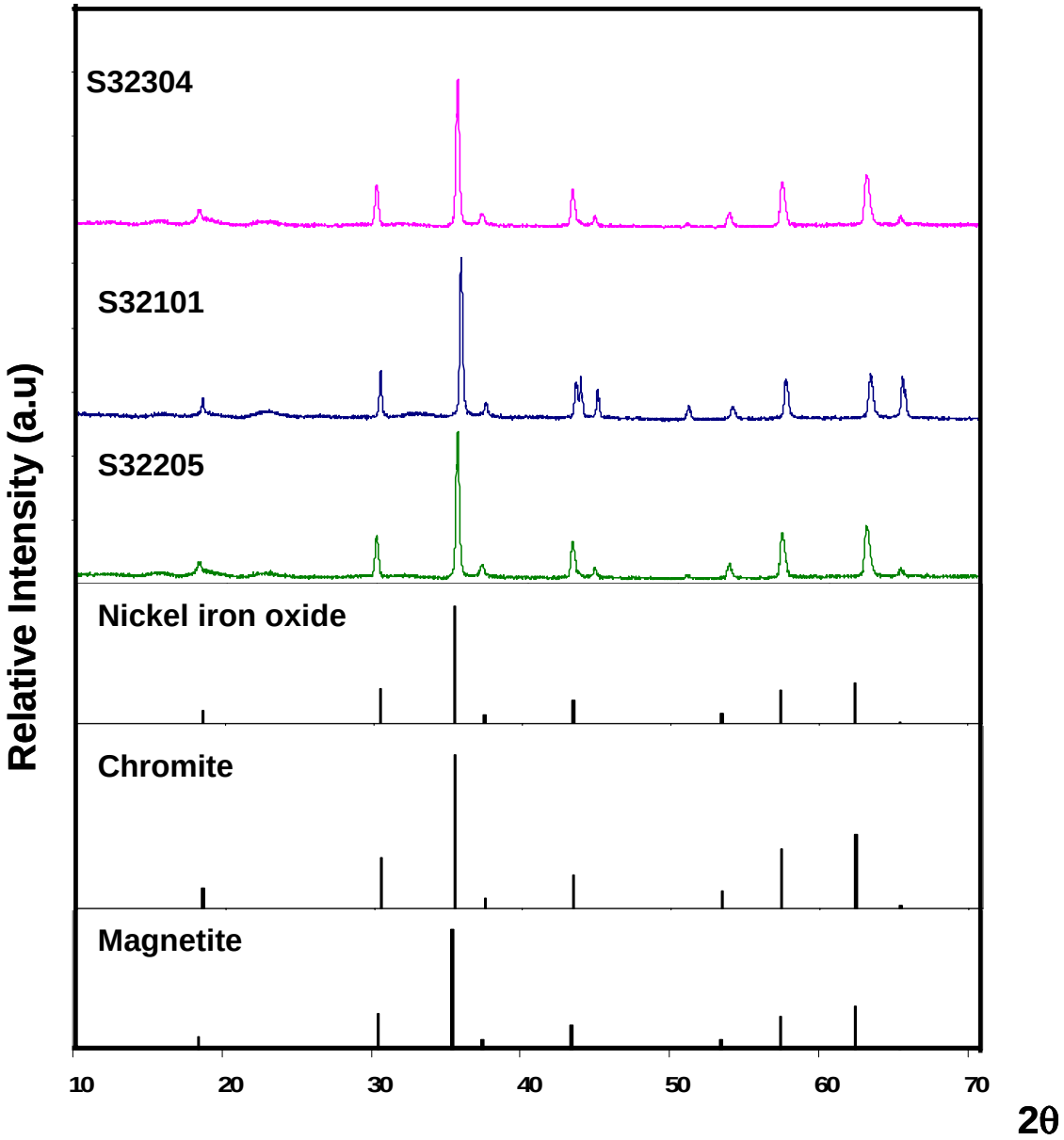

Figure 6.37. XRD patterns comparing corrosion product peaks of S32205, S32101 and S32304 exposed to 3.75M NaOH solution at 170ºC with peak positions of nickel iron oxide (ref.pattern: 01-087-2336), chromite (ref.pattern: 01-089-2618) and magnetite (ref.pattern: 01-086-1358)

6.7.2. Passive Film on DSS Samples in Sulfide-Containing Caustic Environment

X-ray diffraction was used to characterize the films formed on S32205, S32101 and S32304 exposed to sulfide-containing caustic solution at 170ºC. The results are shown in Figure 6.38, Figure 6.39 and Figure 6.40. From the results, it is evident that the corrosion films formed on the three grades of duplex stainless steels was different. The film formed on S32205 in sulfide-containing caustic solution mainly consisted of magnetite (Fe_3O_4) but certain amount of nickel sulfide (NiS_2) was also present in the film (Figure 6.38). XRD pattern of S32101 showed the presence of magnetite, which formed the main constituent of the film. However, apart from magnetite, some chromium sulfide (Cr_5S_8) and iron sulfide (FeS) were also present (Figure 6.39). Prior work has shown that sulfide addition will favor formation of FeS [28]. Passive film of S32304 consisted mainly of awaruite ($FeNi_3$). Magnetite and small amount of chromium sulfide (Cr_2S_3) were also present (Figure 6.40). The chromium sulfide films formed on S32101 and S32304 were of different stoichiometry. As is evident from these results, the major elements contributing to the passive film formed on the duplex stainless steel grades are Fe, Cr and Ni. Hence, the XRD results are in agreement with the polarization curves obtained for DSS and their alloying elements, where Fe, Cr and Ni seem to be contributing to the corrosion products or passive films formed on the DSS (Figure 6.32). According to Figure 6.32, the formation of magnetite (Fe_3O_4) is the dominant reaction of iron, and all three grades of DSS have corrosion films consisting of magnetite as one of the corrosion products.

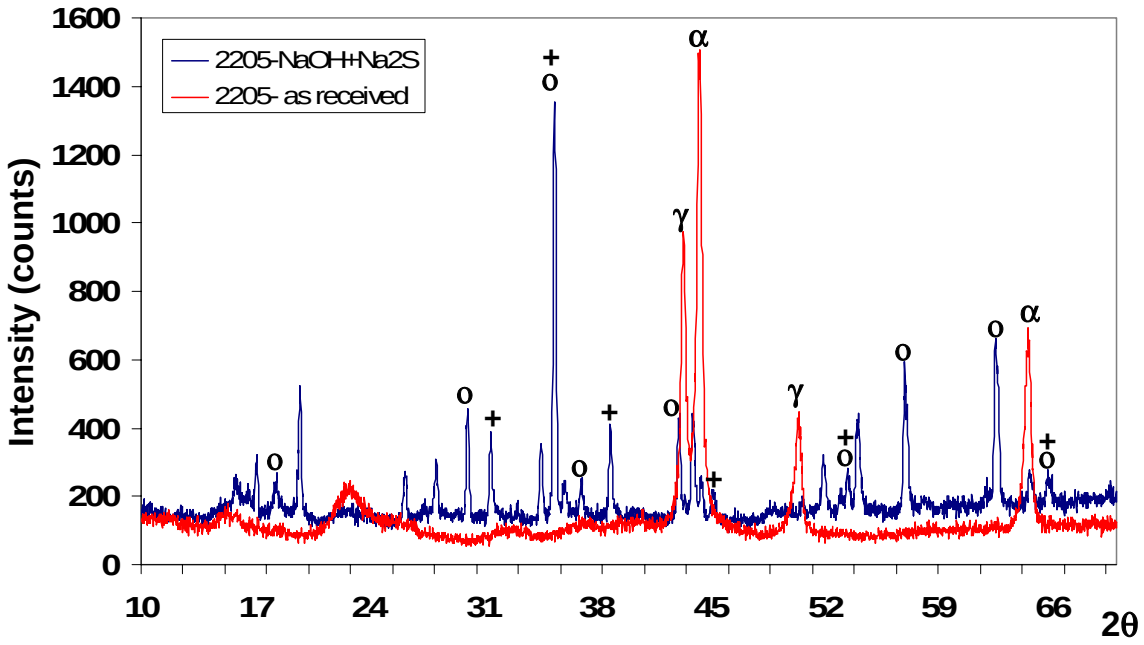

Figure 6.38. XRD pattern of passive film on S32205 exposed to sulfide-containing caustic solution at 170 ºC (o-Magnetite; +-Nickel sulfide; γ-Austenite; α-Ferrite)

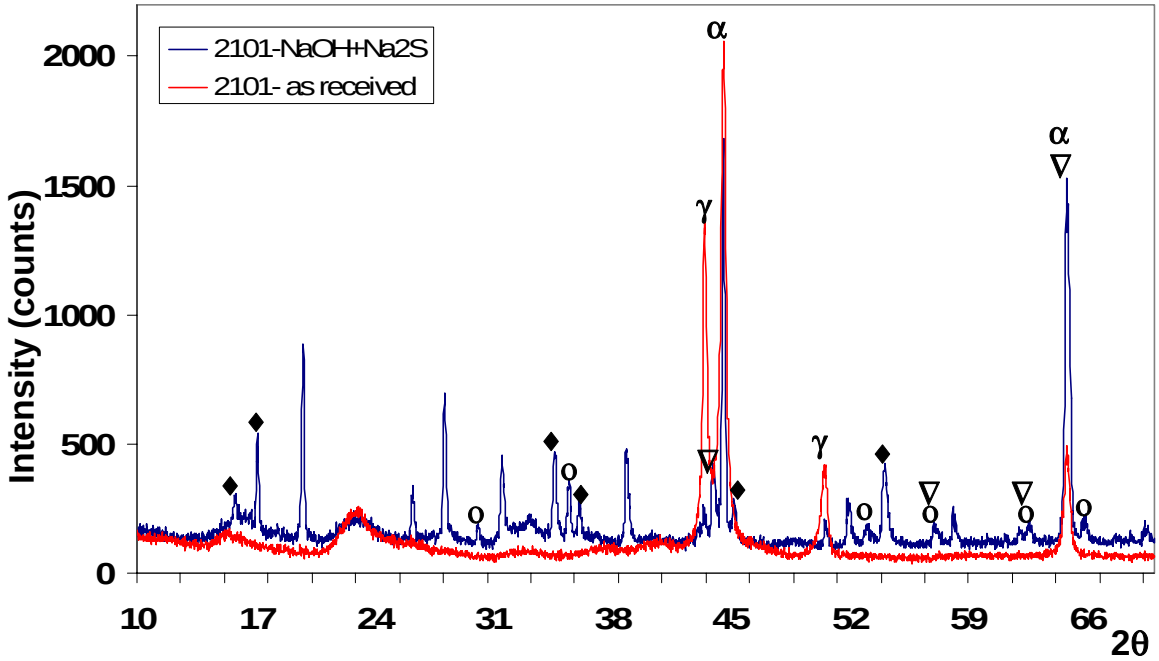

Figure 6.39. XRD pattern of passive film on S32101 exposed to sulfide-containing caustic solution at 170 ºC (o-Magnetite; ♦-Chromium sulfide; ∇-Iron sulfide; γ-Austenite; α-Ferrite)

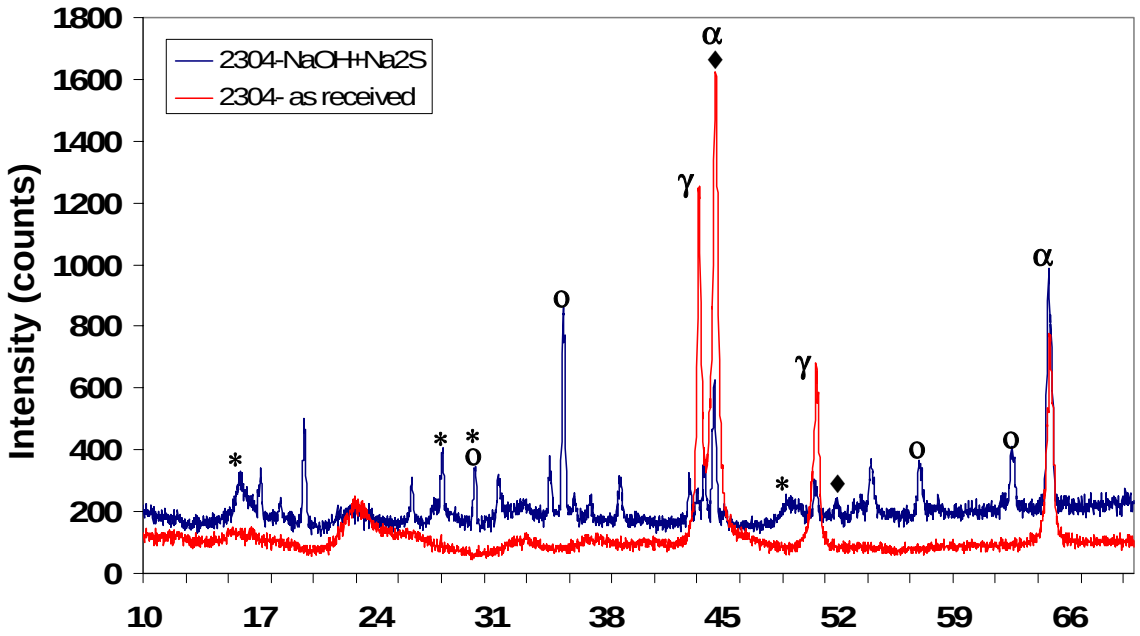

Figure 6.40. XRD pattern of passive film on S32304 exposed to sulfide-containing caustic solution at 170 ºC (o-Magnetite; ♦-Awaruite; *-Chromium sulfide; γ-Austenite; α-Ferrite)

6.8. CHARACTERIZATION OF CORROSION FILM FORMED ON DSS BY X-RAY PHOTOELECTRON SPECTROSCOPY

X-ray photoelectron spectroscopy (XPS) study was used to find out the chemical composition of the corrosion film formed on one of the DSS grades (2205) exposed to sulfide-containing caustic solution at 170ºC for 15 days. The results were further compared with the XRD data in Section 6.7.2 in this Chapter. Figure 6.41 presents the complete XPS spectrum of the film formed on S32205 exposed to sulfide-containing caustic environment, white liquor, at 170^{o}C. Signals corresponding to elements such as Fe, Cr, S, O and Ni show that the corrosion film is enriched in oxides or sulfides of Fe, Cr or Ni. Atomic percentages of the elements present in the film (TABLE 6.1) further indicate that there was sufficient amount of oxygen and iron present in the corrosion film

at the surface. These results are in agreement with the XRD data, which has shown the presence of iron oxide in the surface films formed on DSS in these environments. Significant amount of sulfur was also found to be present (TABLE 6.1), which indicates that metal sulfides may also be present along with the predominant oxides in the corrosion film. XRD study of 2205 DSS in Section 6.7.2 has shown the presence of metal sulfides in the corrosion films. Prior work by Tromans [29] has shown that the sulfide addition to the caustic solution favors a poorly protective film consisting of iron oxide and iron sulfide on carbon steels which is less stable as compared to the magnetite (Fe_3O_4) film formed in pure caustic solutions. Hence, the degradation of corrosion properties of DSS seems to be due to the presence of these metal sulfide compounds in the films.

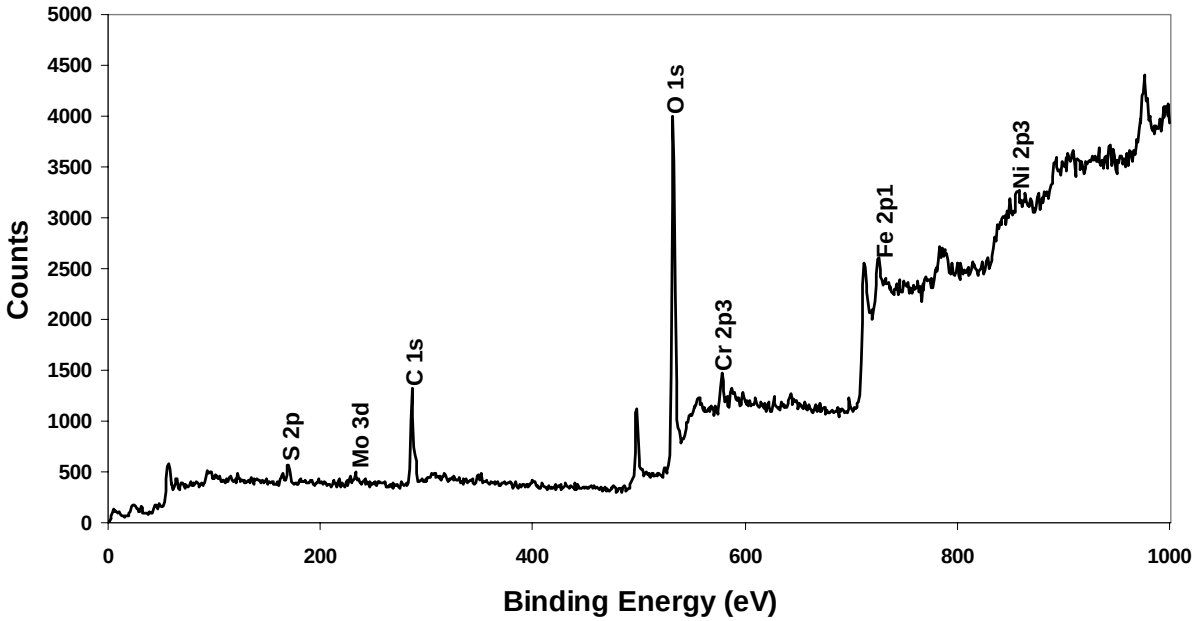

Figure 6.41. Representative XPS spectrum of the film formed on 2205 DSS exposed to sulfide-containing caustic solution at 170 ºC for 15 days

TABLE 6.1. CHEMICAL COMPOSITION (ATOMIC %) OF ELEMENTS PRESENT IN THE CORROSION FILM OF 2205 DSS EXPOSED TO SULFIDE-CONTAINING CAUSTIC SOLUTION AT 170ºC

XPS Line	Binding Energy (eV)	Atomic %
S 2p	169.454	2.709
Mo 3d	233.163	0.601
C 1s	286.035	35.734
O 1s	532.155	53.779
Cr 2p3	578.130	1.637
Fe 2p1	724.796	4.515
Ni 2p3	856.461	1.025

6.9. DISCUSSION

Polarization curves of DSS in caustic and sulfide-containing caustic environment have shown that with increase in temperature, the corrosion potential of the steels decrease and the critical current density increases. Increase in the magnitude of the critical current density of DSS with rise in temperature reflects greater difficulty in attaining passivation in these solutions. Section 5.2.1 and 5.2.2 of Chapter V has shown that with rise in temperature, the corrosion rates of DSS increases. Hence, the detrimental effect of temperature on the general corrosion susceptibility of DSS in caustic environment is obvious from both polarization curves and exposure tests. The difference in corrosion rates of DSS could be attributed to the difference in the alloy composition of the steel. As results have shown in this chapter, different alloying elements can lead to a difference in polarization behavior and variation in the passive film composition, which in turn will affect the corrosion resistance of DSS differently. The corrosion rates of all DSS grades

were low in caustic solution and increased with sulfide addition. XRD of DSS exposed to 3.75M NaOH solution at 170ºC showed the presence of spinel oxides of Fe, Cr and Ni. This dense microstructure of spinel oxides with very low solubility formed an adherent film on the metal surface, which helped to lower its corrosion rate in caustic solution. XRD of DSS samples exposed to sulfide-containing caustic environment showed the presence of various metal-sulfur compounds. Metal-sulfur compounds have been found to deteriorate the corrosion properties of steels [28]. Hence, the increased corrosion rates of DSS in sulfide-containing caustic environment are due to the lower corrosion potential and the formation of various metal-sulfur compounds on DSS. 2304 DSS showed better corrosion resistance in sulfide-containing caustic environment (Section 5.2.2 of Chapter V). XRD of this steel showed the presence of magnetite and awaruite ($FeNi_3$), which helped to form a more stable passive film in S32304 resulting in a lower corrosion rate. The higher corrosion rate of 2205 DSS in WL could be attributed to the presence of greater weight % of molybdenum in the steel. Molybdenum undergoes active dissolution and does not help in the passivity of the steel, as is evident from Figure 6.14 above.

6.10. CONCLUSION

The present study helped to provide vital information regarding the electrochemical and corrosion properties of DSS. The following conclusions can be drawn from this study:

1. Polarization behavior of DSS S32205, S32101 and S32304 were very similar in pure caustic solution but differed in sulfide-containing caustic environment.

2. The corrosion potentials of S32205, S32101 and S32304 were significantly lowered with sulfide addition to caustic solution. There was also an increase in the critical current densities of the DSS specimens with sulfide addition. These results suggest that sulfide addition to caustic environment has a detrimental effect on the passivation behavior of the steel.
3. Temperature increased current densities and the corrosion rates of DSS were found to increase with rise in temperature in both caustic and sulfide-containing caustic solution. Corrosion rates and polarization curves indicate that the general corrosion susceptibility of duplex stainless steels increase with rise in temperature.
4. Comparison of polarization curve of DSS with that of the alloying elements (Fe, Cr, Ni and Mo) in 3.75M NaOH solution at 90ºC shows that the polarization behavior of the steel at lower potentials was affected by all Fe, Ni and Cr, which played a role in the passivation of the steel. Tests at 170ºC indicate that the polarization and passivation behavior of DSS is governed by the polarization behavior of pure Fe and Ni. Chromium shows transpassive dissolution at -300mV_{SCE}, which affects polarization behavior of DSS alloys.
5. Comparing polarization curve of duplex stainless steels with that of the alloying elements (Fe, Cr, Ni and Mo) in sulfide-containing caustic environment, it is evident that alloying Fe with Cr and Ni helps to raise the corrosion potential and lower critical current density of the alloy, thus improving corrosion resistance of the steel.

6. Molybdenum seemed to undergo active dissolution in both caustic and sulfide-containing caustic solution at all tested temperatures and did not help in passivation of DSS. Hence, polarization results indicate that presence of molybdenum in duplex stainless steels may be detrimental to its corrosion resistance in slightly oxidizing high pH environments.
7. XRD data of S32205, S32101 and S32304 exposed to caustic environment at 170ºC indicated that the corrosion films of DSS alloys consisted of spinel oxides of Fe, Ni and Cr, with possibly a combination of nickel iron oxide, chromite and magnetite. The superior general corrosion properties of DSS in caustic solution can be attributed to the formation of these adherent spinel oxides on the metal surface.
8. S32205 was found to be most susceptible to general corrosion and S32304 had the lowest corrosion rates in sulfide-containing caustic environment. Magnetite and awaruite ($FeNi_3$) helped to form a more stable passive film in S32304 resulting in lower corrosion rates.

REFERENCES

[1] Shreir L L, Jarman R A, Burstein G T, (1994) Corrosion 1, 6 pp. 1:55-1:117.

[2] TRETHEWEY K R, KEENAM J S, (1992), Computer Modeling in Corrosion, ASTM STP 1154, R.S. Munn Ed., American Society for Testing and Materials, Philadelphia pp. 113-125.

[3] Rondelli G, Vincentini B, Sivieri E (1997) Corrosion Science 39:1037.

[4] KAJIYAMA Y, AWAYA H (1976) Boshoku-Gijutsu 25:149.

[5] HINE F, OKUBO M (1976) Boshoku-Gijutsu 25:509.

[6] HONDA M, KOBAYASHI Y, TAMADA A (1992) Corrosion 48:822.

[7] ZHENG J H, BOGAERTS W F, BRABERS M J (1992) Corrosion 48: 320.

[8] DEAKIN J, DONG Z, LYNCH B, NEWMAN R C (2004) Corrosion Science 46:2117.

[9] ZHENG J H, BOGAERTS W F, (1997) Proc. Eurocorr 1996, 2nd International Conference on Corrosion-Deformation Interactions in Conjunction , 1997 , Nice, France , ed. Thierry Magnin , The Institute of Materials 104

[10] HONDA M, TAMADA A, KATO K (1991) Corrosion 91, NACE, March 11-15 Cincinnati,Ohio.

[11] SINGH P M, IGE O, MAHMOOD J (2003) Corrosion Science 59:843.

[12] GOROG M (2006) Engineering, Pulping and Environmental Conference, Atlanta, GA, USA, November 5-8.

[13] Bhattacharya A, Singh P M (2008) Corrosion 64.

[14] BHATTACHARYA A, SINGH P M, (2007) NACE Corrosion Conference and Expo., Paper#07206, Nashville, Tennessee.

[15] BHATTACHARYA A, SINGH P M (2007) Journal of Failure Analysis and Prevention 7:371.

[16] LEINONEN H T, POHJANNE P (2006) NACE Corrosion 2006, Paper No. 06244, March 12-16, San Diego, CA, USA.

[17] REID C, (1999) 1999 TAPPI Engineering/Process and Product Quality Conference, Anaheim, CA, USA, September 12-16.

[18] ASHWORTH V, BODEN P J (1970) Corrosion Science 10:709.

[19] Agarwal A K, Sheth K G, Poteet K, Staehle R W (1972) J. Electrochem. Soc. 119:1637.

[20] TROMANS D J. (1980) Electrochem. Soc 127:1253.

[21] WENSLEY D A, CHARLTON R S (1980) Corrosion 36: 385.

[22] BROOKS P A (1972) Corrosion Science 12:297.

[23] BIERNAT R J, ROBINS R G (1972) Electrochemical Acta 17:1261.

[24] POURBAIX M (1995) Lectures on electrochemical corrosion NACE International, Houston.

[25] TROSELIUS L (2004) 11th International Pulp and Paper Industry Corrosion in the Pulp and Paper Industry, Charleston, South Carolina.

[26] Beverskog B, Puigdomenech I (1999) Corrosion 55:1077.

[27] TRUMAN J E, PIRT K R (1983) Duplex Stainless Steel, ed. Lula, R.A. ASM, Metals Park, OH, USA, pp. 113-142.

[28] G.H.THEUS, R.W.STAEHLE, “Review of stress corrosion cracking and hydrogen embrittlement in the austenitic Fe-Cr-Ni alloys,” NACE Corrosion Conference, Unieux-Firminy, France, June 12-16, (1973).

[29] D.TROMANS, J. Electrochem. Soc, Volume 127, (1980), pp.1253.

[30] D.W.SHOESMITH, M.G.BAILEY, B.IKEDA, "Electrochemical formation of mackinawite in alkaline sulfide solutions," Electrochemical Acta, Volume 23, (1978), pp. 1329-1339.

[31] A. BHATTACHARYA, P.M. SINGH, “Corrosion of duplex stainless steels in high pH caustic solution”, NACE Corrosion 2008, Paper No. 08194, March 16-20, 2008, New Orleans, Louisiana, USA.

[32] HSC Chemistry 5.11, Outokumpu Technology Engineering Research.

[33] R.J.BIERNAT, R.G.ROBINS, “High temperature potential/pH diagrams for the sulphur-water system,” Electrochemical Acta, Vol.14, pp.809-820, 1969.

CHAPTER 7

PROPOSED MECHANISM AND CONCLUSION

7.1. SUMMARY

Main objective of this study was to investigate the effect of composition, microstructure, and environmental parameters like solution composition and temperature on the corrosion and stress corrosion cracking of duplex stainless steels in caustic solutions. Ultimate motive of this study is to investigate the underlying mechanisms responsible for the SCC in this system. In this chapter, main results from this study have been summarized and discussed together and a mechanism of stress corrosion cracking in caustic solution has been proposed.

The influence of microstructure on SCC susceptibility was studied by performing tests on various heat treated and welded specimens, as described in Chapter III and Chapter IV. Metallographic examinations of the failed S32205 white liquor accumulator showed that the weld region and HAZ as well as DSS base metal were susceptible to stress corrosion cracking. Laboratory tests on simulated welded 2205 DSS specimens indicated that the weld composition and type of welding affects the microstructure (ferrite/ austenite ratio, phase morphology), which in turn effects the steel's susceptibility to SCC. Highly alloyed weld metal with higher chromium content had resulted in fewer cracks in the weld and HAZ. These results suggest that alloying DSS with higher chromium content will make the steel more resistant to stress corrosion cracking. Metallographic

examinations of failed samples indicated that the mode of cracking in as-received as well as welded DSS in sulfide-containing caustic solution is transgranular in nature. Initiation and propagation of cracks in the 2205 DSS weld region and base metal was found to be in the austenite phase, which indicated that the austenite phase in DSS is more susceptible to embrittlement and SCC in high pH sulfide-containing caustic solutions. This SCC behavior of DSS in the caustic environment is very different from that in low pH chloride environment, where the ferrite phase in DSS is more susceptible phase and the crack initiation typically occurs in the ferrite phase. The severity of stress corrosion cracking and degradation of mechanical properties due to SCC was found to increase with an increase in temperature.

The effect of microstructure on crack initiation in sulfide-containing caustic solution was further studied by changing the microstructure of a lean DSS S32101 and commonly used S32205 DSS through various annealing and aging treatments. Aging DSS at various temperatures (475ºC, 600ºC and 800ºC) has been found to produce precipitates, which affect the localized corrosion susceptibility of these steels in chloride environment [1]-[2]. Pits generated due to the selective dissolution of these precipitates act as precursor for SCC initiation in chloride solutions. The initiation of stress corrosion cracks from pits has been observed in a variety of systems and is usually taken as an indicative of the local environment within the pit being potent and different from that of the surrounding bulk environment [3]. Tests performed in the present study revealed that aging treatment of lean DSS S32101 at 800°C produced intermetallic precipitations along ferrite/austenite phase boundaries and in the austenite phase whereas S32205 DSS samples aged at 800°C showed intermetallic precipitations (formation of sigma 'σ' and chi 'χ' precipitates)

along ferrite/austenite phase boundaries and in the ferrite phase. Secondary austenite with low chromium and molybdenum were found around the precipitates in 2S3101 and S32205 DSS. Due to composition difference in the two grades of steel, the precipitate formed at 800°C for the same aging time differed in composition as well. DSS samples aged at 800°C and 600°C showed very high weight loss and pitting in acidic chloride environment as compared to annealed and unaged samples or samples aged at 475°C. Pit initiation in DSS was found to be along the ferrite/austenite phase boundaries due to selective dissolution of precipitates. These pits are likely to act as precursor sites for SCC initiation in DSS in chloride solution. Changes in the duplex microstructures, because of different heat treatments used in this study, made the steel susceptible to corrosion in chloride environment but did not show any significant effect on the general and localized corrosion behavior of the steel in sulfide-containing caustic solution. General corrosion rates in the caustic solution were very low and no pitting or crevice attack was found on DSS samples even at 170ºC. Results from this study indicate that unlike in chloride environment, SCC initiation in DSS in sulfide-containing caustic environment is not due to localized corrosion such as pitting or crevice corrosion but other crack initiation and propagation mechanism is responsible for the crack initiation in caustic environment.

The fact that the precipitates such as sigma and chi, that are formed due to aging at 800 ^{o}C, do not participate in localized corrosion and crack initiation in sulfide-containing caustic solution was further corroborated by tensile tests performed on heat-treated 2205 DSS samples aged at 800ºC. Samples aged at 800^{o}C did not show susceptibility to stress corrosion cracking, indicating that sigma and chi precipitates do not affect crack initiation or propagation in caustic environments. The present study also confirmed that the

changes in the microstructure of DSS due to various heat treatments could change cracking susceptibility and mode of cracking in DSS. As-received 2205 DSS was found to be susceptible to SCC in sulfide-containing caustic solution at 170^{o}C, with cracks initiating in the austenite phase. The same DSS annealed at 1000^{o}C or 1150^{o}C and tested under equivalent condition did not show any stress corrosion cracking. 2205 DSS annealed at 1000^{o}C or 1150^{o}C and aged at 600^{o}C did not show any cracking as well. However, 2205 DSS annealed and aged at 475^{o}C became susceptible to SCC. Heat treatments changed the mode of crack initiation and propagation. Samples annealed at 1000ºC and aged at 475ºC showed crack initiations in the ferrite phase. Crack initiation was associated with precipitates in the ferrite phase, which was different from the as received sample where the cracks preferentially started in the austenite phase. This may suggest that "475ºC embrittlement" can have a deleterious effect on the stress corrosion cracking susceptibility of 2205 DSS in caustic environments. Samples annealed at 1150ºC and aged at 475ºC showed severe intergranular stress corrosion cracking. The cracking in this case was associated with precipitates at ferrite/austenite inter-phase and grain boundaries. Hence, these results suggest that by performing heat treatments and changing the microstructure of DSS, the mode of stress corrosion cracking could be changed from transgranular to intergranular and one phase can be made more susceptible to crack initiation versus another.

Role of alloy composition and microstructure (ferrite/austenite ratio, phase morphology) on the stress corrosion cracking susceptibility of DSS was further tested by conducting slow strain rate tests on various grades of as-received DSS such as 2205, 2304, 2101 and 2003. Highly alloyed 2304 DSS did not show any cracking whereas

2205, and lean grades 2101 and 2003 with comparatively lower chromium content showed susceptibility to SCC. Test results showed that phase morphology in different grades of DSS played an important role in crack propagation. The mode of crack propagation was different for different grades of DSS. The thin lamellar ferrite phase between the thicker lamellae of austenite made it easier for the cracks to propagate in S32003. On the contrary, the discontinuous austenite phase in S32101 did not provide a continuous path for the crack propagation and the cracks were limited to the austenite phase and were arrested at the ferrite/austenite phase boundaries.

Effect of environmental parameters such as temperature and dissolved ionic species on general corrosion and SCC crack initiation and propagation in caustic environment was found out by testing duplex stainless steels at various temperatures and in white liquors containing different concentrations of hydroxides and sulfides. No cracking was found below 140^{o}C in sulfide-containing caustic solutions. Hence, 140^{o}C could be considered to be the critical temperature for cracking to occur under these environmental conditions. With an increase in temperature, corrosion rates and stress corrosion cracking susceptibility of DSSs was found to increase. Corrosion rates for DSS alloys in 3.75M NaOH solution without sulfide addition were less than 0.2mm/year, even at 170ºC. However, increase in corrosion rates of duplex stainless steels was observed with sulfide addition to the caustic environment. Crack velocity was also found to increase with increasing sodium sulfide concentrations. From the test results, it can be concluded that increase in temperature and sulfide addition to caustic solution has a detrimental effect on the corrosion and SCC susceptibility of DSS.

Corrosion is an electrochemical phenomenon and knowledge of polarization and passivation behavior of DSS has helped us further understand the results obtained through exposure tests and slow strain rate tests. Comparison of polarization curves of DSS in caustic environment with and without sulfide addition showed that the corrosion potentials of S32205, S32101 and S32304 were significantly lowered with sulfide addition to caustic solution. There was also an increase in the critical current densities of the DSS specimens with sulfide addition. These results suggest that the sulfide addition to caustic environment has a detrimental effect on the passivation behavior of the steel. Rise in the temperature increased current densities and resulted in lowering of the corrosion potentials of duplex stainless steels. Polarization curves indicated that the electrochemical behavior of duplex stainless steels is adversely affected by increase in temperature and sulfide addition. These results help to explain the increased corrosion and SCC susceptibility of the steel with rise in temperature and increase in sodium sulfide concentration.

Electrochemical studies also helped to find out how alloying elements contribute to the corrosion and passivation of duplex stainless steels. Comparison of polarization curve of DSS with that of the alloying elements (Fe, Cr, Ni and Mo) in pure caustic solution (3.75M NaOH solution) showed that the polarization behavior of the steel at lower potentials was affected by all Fe, Ni and Cr, which played a role in the passivation of the steel. Even with sulfide addition to caustic solution, it was found that alloying Fe with Cr and Ni helped to raise the corrosion potential and lower critical current density of the alloy, thus improving corrosion resistance of the steel. Molybdenum undergoes active dissolution in both caustic and sulfide-containing caustic solution at all tested

temperatures and did not help in passivation of DSS. Hence, the polarization results indicate that the presence of molybdenum in duplex stainless steels may be detrimental to its corrosion resistance in slightly oxidizing high pH environments. These results explain why molybdenum containing DSS S32205 has a slightly higher corrosion rate and higher crack velocity in sulfide-containing caustic solution as compared to low-Mo grades like S32304 or S32101. Duplex stainless steel grades such as S32304 with higher chromium content were found to be more resistant to SCC in sulfide-containing caustic environment as chromium helped in lowering current density and assisted in passivation of the steel, as is evident from polarization results.

XRD data of S32205, S32101 and S32304 exposed to caustic environment without sulfide addition at 170ºC indicated that the corrosion films of DSS alloys consisted of spinel oxides of Fe, Ni and Cr, with possibly a combination of nickel iron oxide, chromite and magnetite. The superior general corrosion properties of DSS in caustic solution as compared to carbon steel could be due to the formation of these adherent spinel oxides on the metal surface. DSS exposed to sulfide containing caustic solutions formed metal-sulfide films on the surface. XPS results of 2205 DSS exposed to sulfide-containing caustic solution also showed the presence of sulfur, probably metal-sulfide compounds, in the corrosion film of the steel. The increased corrosion susceptibility of DSS due to sulfide addition to caustic solution could further be attributed to these sulfide films, which hydrolyze in aqueous environments easily as compared to spinel oxides, exposing bare metal to the environment and assisting corrosion. The corrosion rate of 2304 DSS was the lowest as compared to 2101 and 2205 DSS in sulfide-containing caustic environment. Magnetite and awaruite ($FeNi_3$) helped to form a more stable passive film

in S32304 as compared to the iron sulfide and nickel sulfide films in S32101 and S32205 respectively, resulting in lower corrosion rates of 2304 DSS.

7.2. PROPOSED MECHANISM OF SCC OF DSS IN SULFIDE-CONTAINING CAUSTIC SOLUTION

The free corrosion potential of 2205 DSS was measured during slow strain rate tests in sulfide-containing caustic solution at 170ºC. The corrosion potential was found to be at -900mV_{SCE} throughout the test period as can be seen in Figure 7.1. Comparison of the corrosion potential of 2205 DSS with its potentiodynamic polarization curve under similar test conditions (Figure 7.2) revealed that 2205 DSS was passive in these test environments. The mechanism of transgranular SCC, which dominates under these conditions, is the slip dissolution model [4]. Prior work has shown that in transgranular SCC, especially in some face centered cubic (FCC) alloys such as copper-based alloys and austenitic stainless steels, the localization of dissolution is most often related to slip [3], [5]-[6]. These FCC alloys have low stacking fault energy and planar groups of dislocations are favored. SCC initiation in DSS in sulfide-containing caustic solution was found to be initiated in the austenite phase in this study. Austenite phase in DSS is face centered cubic in nature and in contrast to the ferrite phase (body centered cubic structure), has close packed slip planes. X-ray diffraction studies were performed by Leinonen et al. on S31803 to study stress state of the austenite and ferrite phases [7]. The results have shown that the austenite phase is in tension and the ferrite phase is in compression. This difference in the stress states is mainly due to the difference in the

coefficient of thermal expansions between the two phases (Chapter 1, Table 1.2) [8]. Hence, due to the more active slip system [9] and the residual tensile stress in the austenite phase of DSS, this phase undergoes plastic deformation more easily and at an applied stress far below the ferrite phase. This makes the austenite phase more susceptible to crack initiation and propagation. Under these conditions, slip dissolution mechanism might be the most favorable mechanism to initiate stress corrosion cracking in the austenite phase. The protective passive film on the metal surface is ruptured due to the emergence of slip steps during straining of the metal, exposing bare metal to the environment and leading to its dissolution and crack initiation [10]. Once initiated, crack tip propagation is governed by the oxidation of the bare metal surface as well as recurrence of film reformation and breakdown due to straining at the crack tip. Therefore, according to Faradays law, the average environmentally controlled crack propagation rate (V_t) is related to the oxidation charge density between oxide rupture events (Q_f) and the strain rate at the crack tip ($\dot{\varepsilon}_{ct}$) by:

$$\dot{V}_t = \frac{M}{z\rho F} \times \frac{Q_f}{\varepsilon_f} \times \dot{\varepsilon}_{ct} \qquad (1)$$

where M is the atomic weight and ρ is the atomic density of the crack tip metal, F is the Faraday's constant, z is the number of electrons involved in the oxidation of an atom of metal, and ε_f is the fracture strain of the oxide at the crack tip. The rate controlling steps that govern crack propagation by slip dissolution model are liquid diffusion of either water molecules or solvated cations to and from the crack tip region and the overall oxidation (dissolution and oxide re-growth) rate. Since both diffusion of ions and rate of dissolution and oxide re-growth increase with rise in temperature, the observed increased

susceptibility of DSS to SCC in sulfide-containing caustic solution and higher crack velocities at higher temperatures could be explained by the increased kinetics of the reactions. Further corroboration of this can be provided by the electrochemical results, which showed that the rate of oxidation and dissolution of metal increased with an increase in temperature. Corrosion rates of strained specimens in this study have also been found to be higher as compared to unstrained specimens. Therefore, due to the applied strain, disruption of passive film owing to slip step emergence may cause crack initiation and dissolution of bare metal and may lead to crack propagation, making the slip dissolution model to be the most favorable SCC mechanism under the tested conditions.

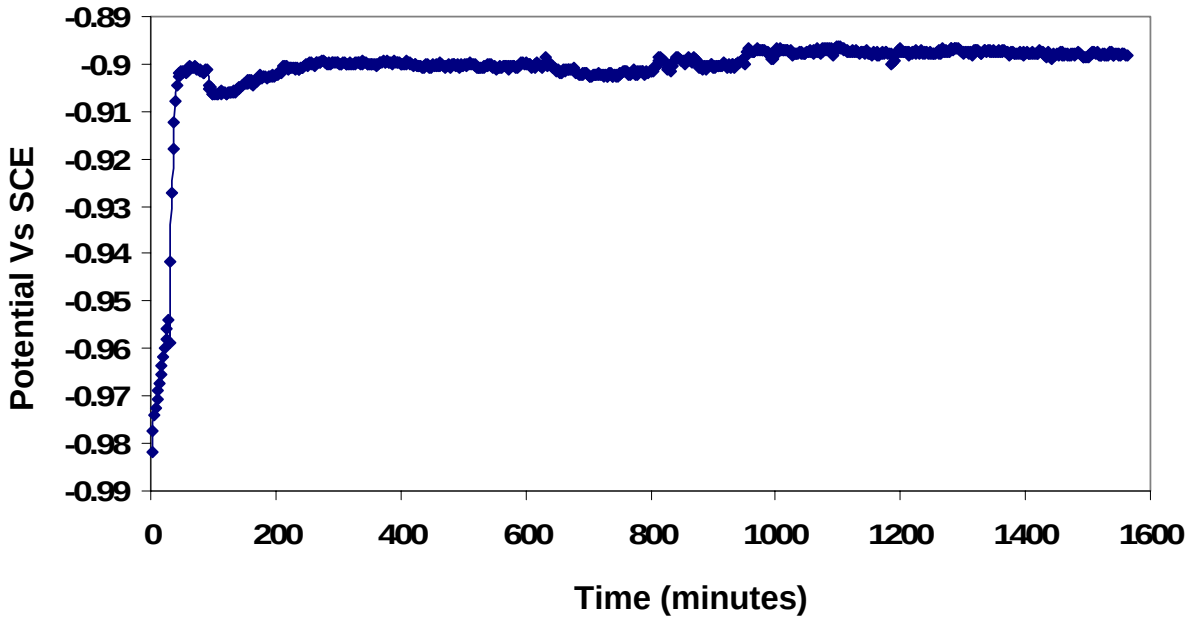

Figure 7.1. Corrosion potential of 2205 DSS in sulfide-containing caustic solution at 170°C during slow strain rate test

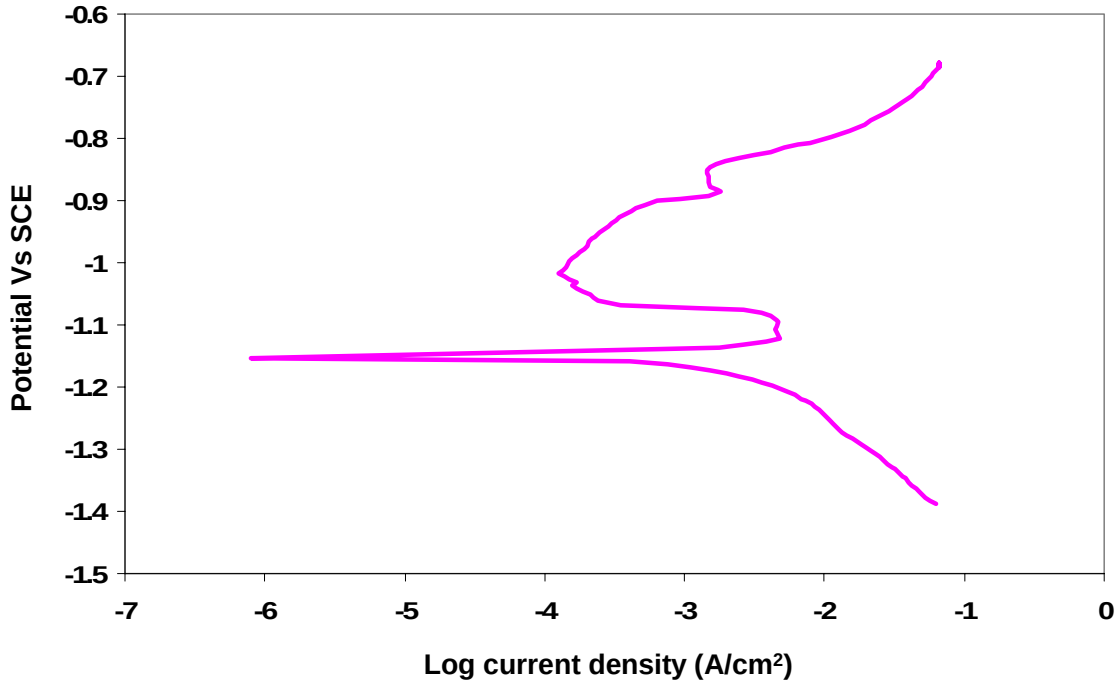

Figure 7.2. Potentiodynamic polarization curve of 2205 DSS in sulfide-containing caustic solution at 170°C

The mode of crack initiation and propagation in DSS in sulfide-containing caustic solution in this study due to slip dissolution can be explained by the following:

In all tested DSS samples in caustic environments, irrespective of the type of microstructure of the steel (as-received, welded or annealed and aged), stress corrosion cracking was found to be in the necking region of the tensile samples. This can be seen in Figure 7.3 (as-received DSS), Figure 7.4 (welded DSS) and Figure 7.5 (DSS annealed at 1000°C and aged at 475°C). No stress corrosion cracks were found beyond the necking region of these samples which indicates that the SCC did not initiate below the yield stress of sample, otherwise small SCC should be found throughout the gage of tensile samples. This indicates that plastic deformation is required for the SCC to initiate and propagate in this system. Plastic deformation will initiate dislocation movement in the austenite phase, which is more prone to cracking, as the phase is already in tension and

also has more favorable slip systems compared to the ferrite phase. The ferrite phase is less susceptible to SCC under these conditions as this phase is in compression in DSS alloys and also it is difficult for slip to occur in this BCC phase. The slip steps formed due to plastic deformation in the DSS is likely to rupture the unstable passive film on the metal surface. Film properties and repassivation behavior will play a major role in determining the SCC susceptibility of these alloys. Film properties depend on many factors, including the alloy composition, electrochemical conditions, composition of solution, other environmental factors like pH and temperature. In caustic solutions with sulfide, the surface film of DSS alloys consist of various metal-oxide-sulfide compounds, as is described in Chapter 6, Sections 6.7.2 and 6.8. A critical temperature is required for SCC to occur because once initiated, the cracks propagate only when the crack tip dissolution rate is higher as compared to the crack side dissolution rate. Hence at very low temperatures, due to the slow kinetics of reactions, dissolution of the crack tip is slow and may result in blunting of the cracks. Cracks initiated by the emergence of slip steps in DSS alloys will start propagating at the critical temperature which is the optimum temperature at which crack tip dissolves at a faster rate than the crack sides. In present system studied, SCC was not found to occur below 140^{o}C under all tested environments. Crack propagation will continue till the crack tip repassivates and will resume propagating when the passive film is ruptured again by another slip step emergence. If the film rupture does not reoccur (for example if the crack tip is in the less susceptible ferrite phase), crack propagation will stop and crack gets arrested at the ferrite/austenite phase boundaries. Cracks may also avoid the ferrite phase by traveling around the ferrite and continuing into the austenite phase (due to the three dimensional nature of the

cracks). This mechanism of cracking in DSS in caustic environment by slip dissolution can be further understood with the help of the schematic in Figure 7.6 a, b, c and d. In heat treated DSS samples (samples aged at 475^{o}C), where precipitates change the dislocation structure of the ferrite phase, the Cr rich α' precipitates lower the mobility of the dislocations and create micro-void near them in the ferrite matrix, which may act as initiation sites for cracks in caustic environment. Since the crack propagation mode is similar to that of the as-received DSS samples, slip dissolution may still be playing a role in crack propagation after the initiation of cracks

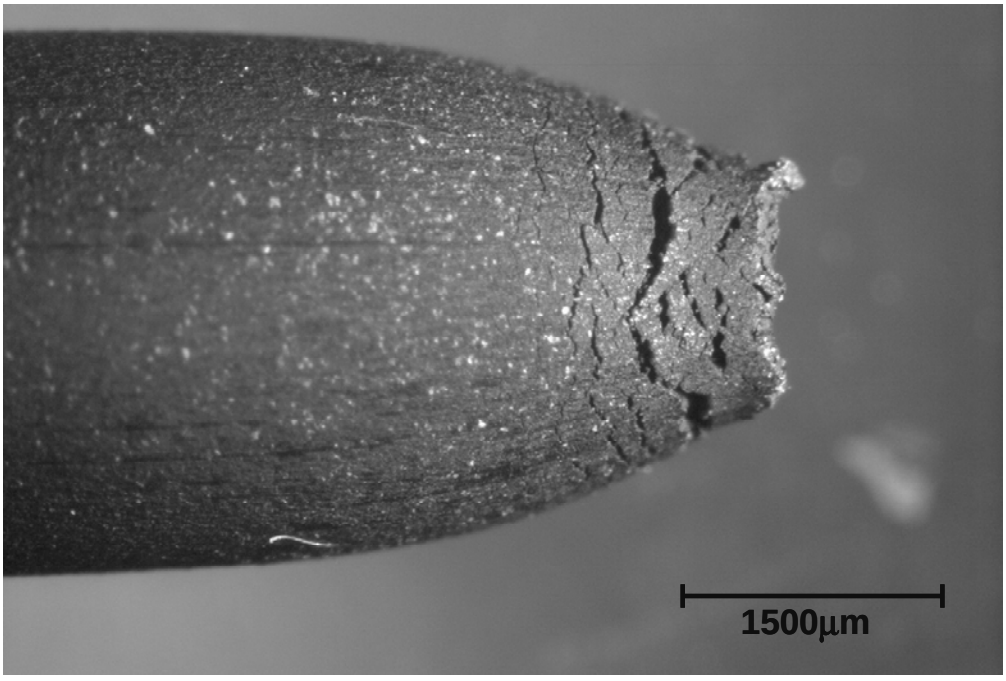

Figure 7.3. 2205 DSS sample tested in sulfide-containing caustic solution at 170°C

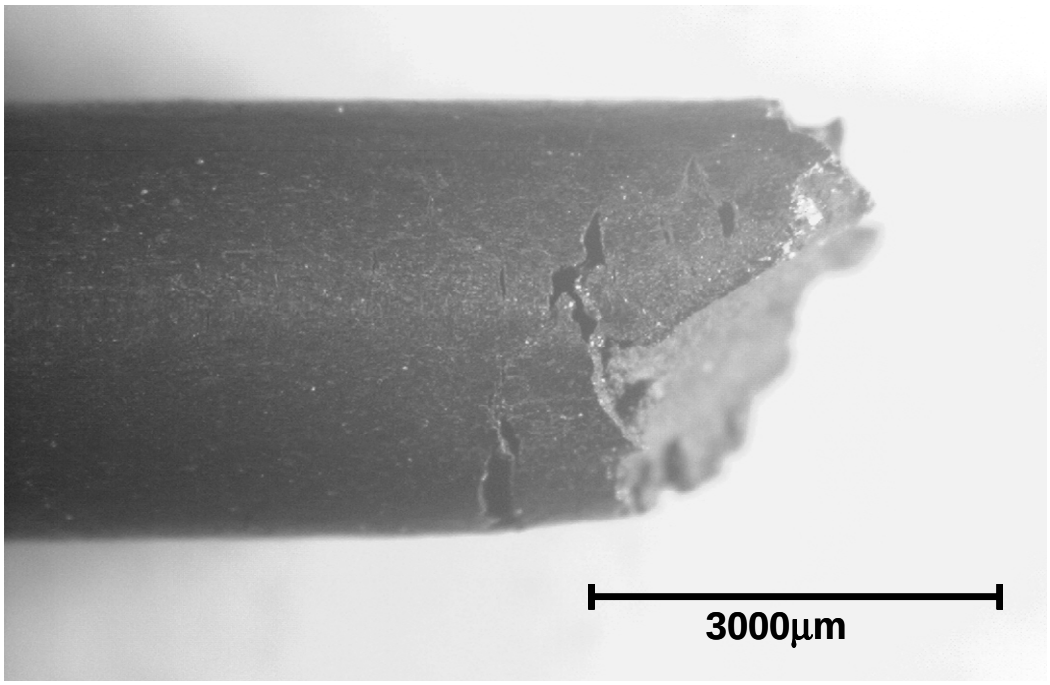

Figure 7.4. Welded 2205 DSS (2205-Lh) sample tested in sulfide-containing caustic solution at 170°C

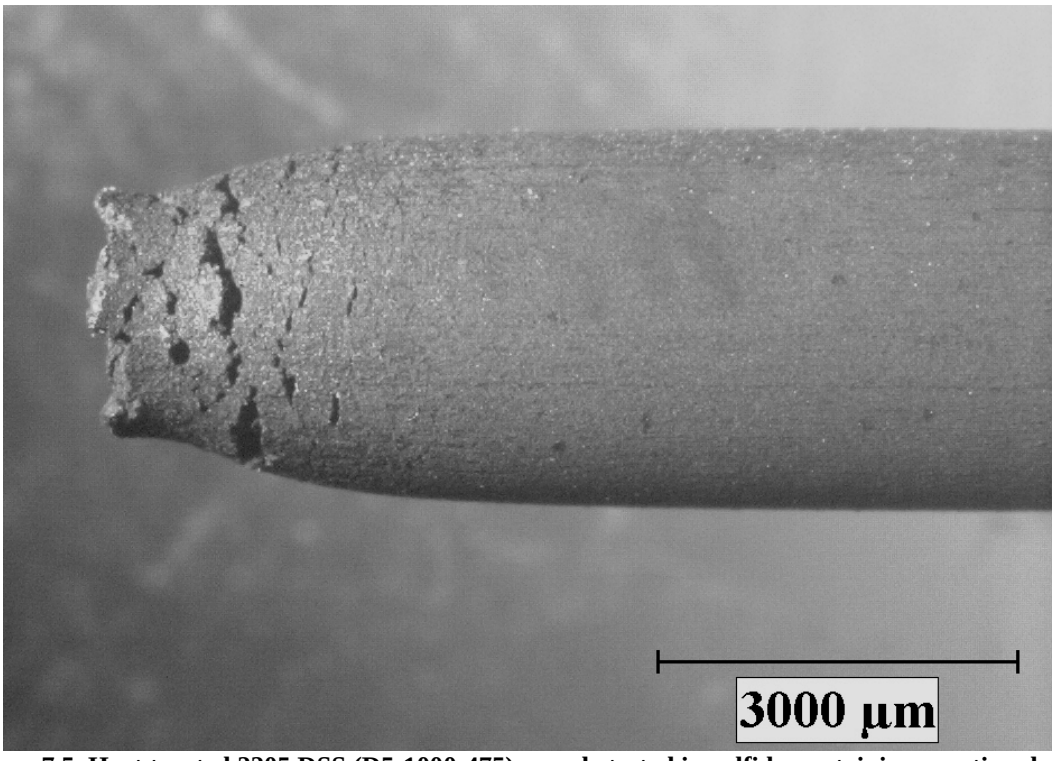

Figure 7.5. Heat treated 2205 DSS (D5-1000-475) sample tested in sulfide-containing caustic solution at 170°C

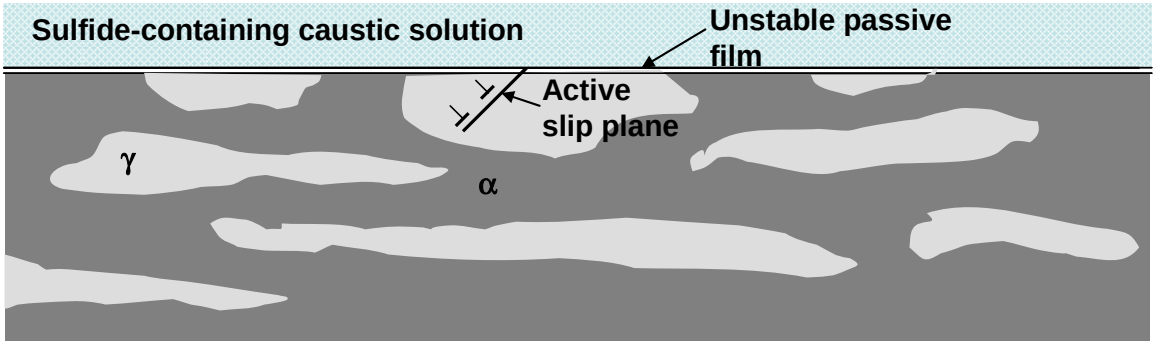

(a)

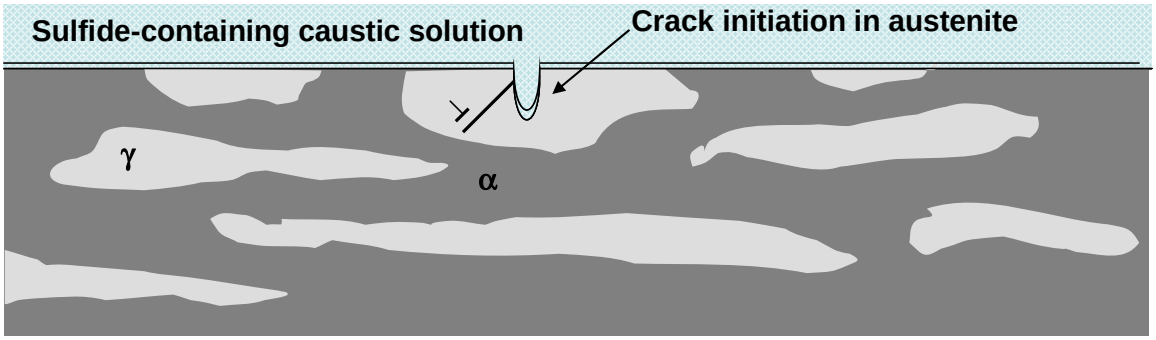

(b)

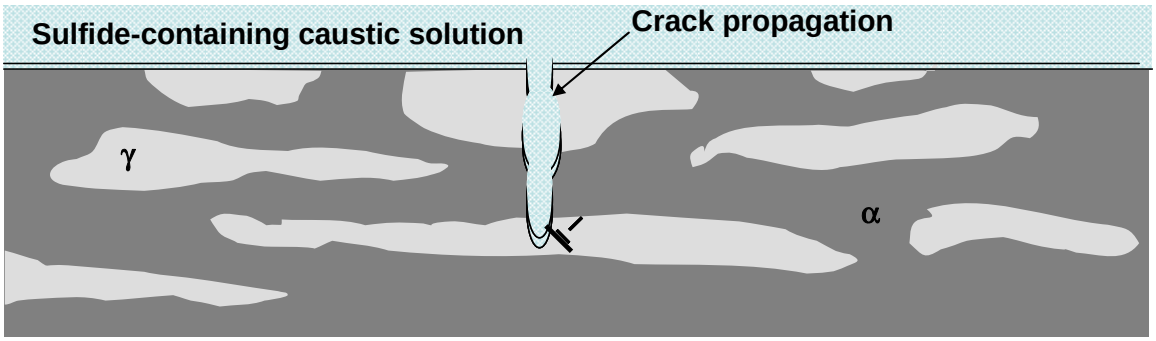

(c)

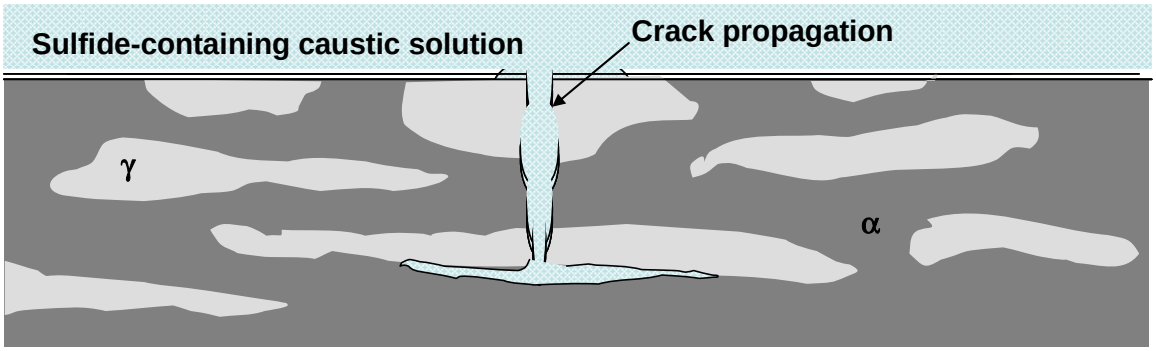

(d)

Figure 7.6. Schematic showing various steps of crack initiation and propagation in DSS by the slip dissolution model (a) slip step in the austenite phase intersecting unstable passive film (b) crack initiation due to breakdown of film and dissolution of metal in austenite (c) crack propagation (d) blunting of cracks at the ferrite phase boundaries

The effect of various material and environment related parameters on stress corrosion cracking of DSS in caustic environments and the underlying mechanism of SCC in these systems was not known before this study. This study helped us determine the effect of DSS microstructure and environmental parameters like temperature, pH, and dissolved ionic species on the cracking susceptibility of these steels in high pH alkaline solutions. Results from experiments and observations made in this study have helped us understand the mechanism of SCC under tested conditions.

7.3. FUTURE WORK

The present study has concentrated on the role of microstructure and environmental parameters on the corrosion and SCC susceptibility of DSS in caustic environment. Other aspects of this study which would help to understand the underlying mechanism of SCC of DSS in sulfide-containing caustic solution would be to study dislocation structure in the ferrite and austenite phases using transmission electron microscopy, perform micro-polarization on the austenite and ferrite phases in caustic environment to understand the electrochemical behavior of each phase in DSS and to measure residual stresses in the two phases in DSS.

REFERENCES

[1] D.Y. KOBAYASHI, S. WOLYNEC, “Evaluation of the low corrosion resistant phase formed during the sigma phase precipitation in duplex stainless steels”, Materials Research 2 (1999): p. 239.

[2] Z.CVIJOVIC, G.RADENKOVIC: “Microstructure and pitting corrosion resistance of annealed duplex stainless steel,” Corrosion Science, 2006, 48, pp.3887-3906.

[3] L.L.SHREIR,R.A.JARMAN,G.T.BURSTEIN, "Corrosion 1, Metal/Environment Reactions," Third Edition, 1994.

[4] J.DEAKIN, Z. DONG, B. LYNCH, R.C.NEWMAN, “De-alloying of type 316 stainless steel in hot, concentrated sodium hydroxide solution”, Corrosion Science, pp.2117-2133, 46, (2004).

[5] H.S.KHATAK, BALDEV RAJ, “Corrosion of Austenitic Stainless Steels, Mechanism, Mitigation and Monitoring”, ASM International.

[6] H.L.LOGAN, “The stress corrosion of metals”, National Bureau of Standards, Washington, D.C.

[7] H.T.LEINONEN, "Corrosion Resistance of Duplex Stainless Steel and its Welds in Modern Kraft Batch Cooking," 11th International Symposium on Corrosion in Pulp and Paper Industry, pp. 55-66, June 2004.

[8] J.JOHANSSON, M.ODEN, X.H.ZENG, Acta Mater. Volume 47, 9, pp. 2669-2684, 1999.

[9] J.P.SCHAFFER, A.SAXENA, S.D.ANTOLOVICH, T.H.SANDERS, JR, S.B.WARNER, “The science and design of engineering materials”, WCB McGraw-Hill Publication.

[10] F.P.FORD “The Crack-Tip System and Its relevance to the Prediction of Cracking in Aqueous Environments”, NACE 10, EICM Proccedings, pp.139-165.